INVESTIGATING STALAGMITES FROM NE NAMIBIA AND NW MADAGASCAR AS A KEY TO BETTER UNDERSTAND LOCAL PALEOENVIRONMENTAL CHANGES AND IMPLICATIONS FOR INTER-TROPICAL CONVERGENCE ZONE (ITCZ) DYNAMICS

by

NY RIAVO GILBERTINIE VOARINTSOA

(Under the Direction of LOREN BRUCE RAILSBACK)

ABSTRACT

While our understanding of climate systems continues to improve, it has also become clear that regional responses to global forcing, as well as the interaction of regional phenomena within global climate systems, are more complex than we have previously understood them to be. The complexity could be purely climatic, or it could be interfered with by anthropogenic influences. Climate reconstructions and simulations have suggested the need for more information from remote locations in the world, such as Africa and Madagascar, not only to complete gaps in our understanding of global atmospheric and oceanic circulation, but also to distinguish anthropogenic influences on climate from natural variability.

This dissertation research has been an investigation of past climate and vegetation changes in northeastern Namibia and in northwestern Madagascar using proxies from stalagmites. Stalagmites, which are upward growing, pillar-like, and convex-up shape cave deposits, can preserve various signatures ($\delta^{18}O$, $\delta^{13}C$, mineralogy, petrography, layer-specific width, macro-cavities distributions) that reflect environmental conditions at the time of their deposition. These proxies are powerful tools to reconstruct paleoclimate and paleoenvironmental changes.

The main research question has focused around the dynamics of the Inter-Tropical Convergence Zone (ITCZ) and the climatic responses in these regions during the last two millennia and during the Holocene. The stalagmite records have revealed linkage to the ITCZ in accord with climate simulations, which suggest that the ITCZ migrates latitudinally toward a warmer hemisphere. More specifically, the ITCZ migrates southward/northward during globally cooler/warmer conditions. This migration could determine the length of summer months in the ITCZ-visited regions. The records from northwestern Madagascar have also helped better understand the timing when humans started to leave significant imprints on the landscape, and they revealed that climate in Madagascar was also sensitive to abrupt climate changes, such as the 8.2 ka event. These new climatic data from northeastern Namibia and northwestern Madagascar are useful to refine our understanding of the global circulation. They can also be useful to test for climate models that could be used to predict changes in future climate.

INDEX WORDS: Paleoclimate, ITCZ, Monsoon, Namibia, Madagascar, Stalagmites, Multiple proxy, Stable isotopes, Mineralogy, Petrography

# INVESTIGATING STALAGMITES FROM NE NAMIBIA AND NW MADAGASCAR AS A KEY TO BETTER UNDERSTAND LOCAL PALEOENVIRONMENTAL CHANGES AND IMPLICATIONS FOR INTER-TROPICAL CONVERGENCE ZONE (ITCZ) DYNAMICS

by

NY RIAVO GILBERTINIE VOARINTSOA

BSc. Equivalent, University of Antananarivo, Madagascar, 2008

MSc. Equivalent, University of Antananarivo, Madagascar, 2012

A Dissertation Submitted to the Graduate Faculty of The University of Georgia in Partial Fulfillment of the Requirements for the Degree

DOCTOR OF PHILOSOPHY

ATHENS, GEORGIA

2017

© 2017

Ny Riavo Gilbertinie Voarintsoa

All Rights Reserved

# INVESTIGATING STALAGMITES FROM NE NAMIBIA AND NW MADAGASCAR AS A KEY TO BETTER UNDERSTAND LOCAL PALEOENVIRONMENTAL CHANGES AND IMPLICATIONS FOR INTER-TROPICAL CONVERGENCE ZONE (ITCZ) DYNAMICS

by

NY RIAVO GILBERTINIE VOARINTSOA

| | |
|---|---|
| Major Professor: | L. Bruce Railsback |
| Committee: | George A. Brook |
| | David F. Porinchu |
| | Douglas E. Crowe |
| | Hai Cheng |

Electronic Version Approved:

Suzanne Barbour
Dean of the Graduate School
The University of Georgia
May 2017

# DEDICATION

My dreams and my goals have pushed me to move forward, and my passion has encouraged me to achieve them.

I am dedicating my work and efforts to my very own country, Madagascar. I wish to bring something back home, soon or later, that would be beneficial to a community, a region, or possibly to the entire country.

I am also dedicating my work and efforts to inspire young women in pursuing academia and in pursuing STEM[1] education, and to inspire young generations that, regardless of our initial starting conditions, we could achieve our goals with determination and dedication.

"Learning is a process that never ends." – Carol Ann Tomlinson

"Develop a passion for learning, if you do, you will never cease to grow." – Anthony J. D'Angelo

"Aza mba manadino ny Tanindrazanao." (Never forget your home country.)—a Malagasy hymnal no. 760, v. 2.

[1] (Science, Technology, Engineering, and Math)

# ACKNOWLEDGEMENTS

Thank you, God, for giving me strength throughout my academic studies at the Department of Geology of the University of Georgia.

My gratitude goes to many other people who supported and encouraged me (here presented in chronological order) since my very first time in the USA. I would like to thank Dr. Rónadh Cox of the Department of Geosciences of Williams College in Williamstown, MA for giving me the opportunity to come to the USA to experience the US academic study and research. I would also like to thank Dr. Sandra Wyld, for giving me the opportunity to come study at the Department of Geology at UGA, as a Research Assistant. Without the financial supports from the University of Georgia, which were possible with the approval of our current Geology Department Head, Dr. Douglas E. Crowe, I would not have been able to finish my study, and I am very thankful. The Faculty and Staff at the Department of Geology at the University of Georgia, particularly Rachel Ashton, Ashley Arnold, and our former and current Graduate coordinator, have been very supportive too, and I thank them for all their hard work in making all the administrative processing smooth. I would also like to address a wholehearted gratitude towards my doctoral advisor, Dr. L. Bruce Railsback (and his wife, Dr. Celeste Condit), for the advice, mentorship, and support. Dr. Railsback has been critical and very constructive on the quality of my work, and these have allowed me to professionally and academically grow. I thank the other committee members,

including Dr. George A. Brook, Dr. Douglas E. Crowe, Dr. David F. Porinchu, and Dr. Hai Cheng for their support, guidance, advice, and their encouraging words. I'd like to thank my former lab mates, including Pete Akers and Lixin Wang, for discussing research and for words of encouragement. I also thank my co-authors in the published, accepted, and submitted papers for their collaboration. They include Brook G.A., Liang F., Marais E., Hardt B., Cheng H., Edwards, R.L. and Railsback, L.B. *for Chapter 2*; Wang L., Railsback L.B., Brook G.A., Liang F., Cheng H., Edwards R.L. *for Chapter 3*, and Railsback L.B., Brook G.A., Wang L., Kathayat G., Cheng H., Li X., Edwards R.L., Rakotondrazafy A.F.M., Madison Razanatseheno M.O. *for Chapter 4*. Each of these chapters also have specific acknowledgments that are further detailed below. Above all these, I'd like to thank the journal editors and the corresponding reviewers of each of the work submitted.

I also would like to thank all sources of financial support, direct or indirect, that have made this dissertation research possible. These include the National Science Foundation (NSF), the Natural Science Foundation of China (NSFC), the Schlumberger Foundation-Faculty for the Future Fellowship Award, the Geological Society of America-John Montagne Award, the Miriam Watts-Wheeler, the International Association of Sedimentologists Post-Graduate Research Grant, and the additional support from Dr. Railsback's lab account. Beyond funding, laboratory collaboration has helped my research to progress. With that regard, I thank Dr. Paul Schroeder, Dr. Sally Walker, Dr. Hai Cheng, and Dr. Lawrence Edwards for allowing me to work in their lab. I gained knowledge, I developed skills, and I made new friends from working in their lab.

Finally, I would like to thank my family and friends for their constant support and encouragement. I have been fighting my own battle, but they have cheered me up during moments of success and happiness, and they encouraged me during moments of failures and hardships. They understood that I am a “human”.

*Specific acknowledgment for Chapter 2*

Collection of Stalagmite DP1 was carried out with the permission of the Namibian Ministries of Environment and Tourism and Mining and Energy as well as that of Jurg-Reiner and Renate Otto. Funding was provided by the National Sciences Foundation Grant NSF 0002193 to George A. Brook and by Natural Sciences Foundation of China Grant NSFC 41230524 to Hai Cheng. X-ray diffraction analysis was conducted at the XRD lab of the department of Geology under the supervision of Paul A. Schroeder. Chris Fleisher of the Department of Geology also assisted with carbon-coating of the sample for SEM analysis.

*Specific acknowledgment for Chapter 3*

The completed research in Chapter 3 was supported by a grant from by the National Natural Sciences Foundation of China Grant (NSFC 41230524) to Hai Cheng and by a grant from NOAA to David Burney. We thank David Burney for organizing fieldwork at Anjohibe Cave in 1994, also supported by NOAA, that led to the collection of the stalagmites by Dr. Brook discussed in this paper. We thank Paul A. Schroeder, supervisor of the XRD lab of the department of Geology, for providing access to X-ray diffraction analysis. We also thank the government and people of Madagascar, particularly local guides in Anjohibe, for their

assistance in making this work possible. We thank the Cenozoic Research Group, a Malagasy-American collaboration sanctioned by the Service de Paléontologie and the Musée d'Art et d'Archéologie of the Université d'Antananarivo for fieldwork assistance and sample collection. We thank Dr. Rakotondrazafy Michel and Dr. Madison Razanatseheno from the Department of Geology of the University of Antananarivo Madagascar for helping acquiring useful documents that are only available at the libraries in Antananarivo. Similarly, we thank Mr. Bruno Rakotoarivelo, from the National Office of Environment (Office National pour l'Environment, ONE), in Antananarivo, Madagascar for his assistance in acquiring information about climate and vegetation of the Mariarano region. We also thank Dr. Stephen Burns of the Department of Geosciences of the University of Massachusetts for sharing the data of Burns et al. (2016) with us. Finally, we thank the Schlumberger Foundation, Faculty for the Future, and the University of Georgia for supporting N.R. Voarintsoa's research.

*Specific acknowledgment for Chapter 4*

The work completed in Chapter 4 was supported by grants from (1) the National Natural Science Foundation of China (NSFC 41230524, NBRP 2013CB955902, and NSFC 41472140) to Hai Cheng and Gayatri Kathayat, (2) the Geological Society of America Research Grant (GSA 11166-16) and John Montagne Fund Award, (3) the Miriam Watts-Wheeler Graduate Student Grant from the Department of Geology at UGA, and (4) the International Association of Sedimentology Post-Graduate Grant to N. Voarintsoa. We also thank the Schlumberger Foundation for providing additional support to N. Voarintsoa's

research. We thank the Department of Geology at the University of Antananarivo, in Madagascar, the Ministry of Energy and Mines, the local village and guides in Majunga for easing our research in Madagascar. We thank Pr. Paul Schroeder for giving us access to use the X-ray diffractometer of the Geology Department to conduct analysis on the mineralogy of the two stalagmites. We also thank Pr. Sally Walker for allowing us to use the microscope of the paleontology lab and for helping us photograph the stalagmites at very high resolution. We also thank Prof. John Chiang of the University of California in Berkeley, for sharing his thoughts and guiding us to useful literatures that are relevant to this work.

TABLE OF CONTENTS

Page

## LIST OF TABLES

Page

## LIST OF FIGURES

Page

# CHAPTER 1

# INTRODUCTION

## 1.1. Research motivation

While our understanding of climate systems continues to improve, it has also become clear that regional responses to global forcing, as well as the interaction of regional phenomena within global climate systems, are more complex than we have previously understood them to be. The complexity could be purely climatic, or it could be interfered with by anthropogenic influences. Climate reconstructions and simulations have suggested the need for more information from several remote locations in the world, such as Africa and Madagascar, not only to complete gaps in our understanding of the global circulation, such as understanding the dynamics of the Inter-Tropical Convergence Zone (ITCZ; Fig 1.1), but also to distinguish anthropogenic influences on climate from natural variability.

a

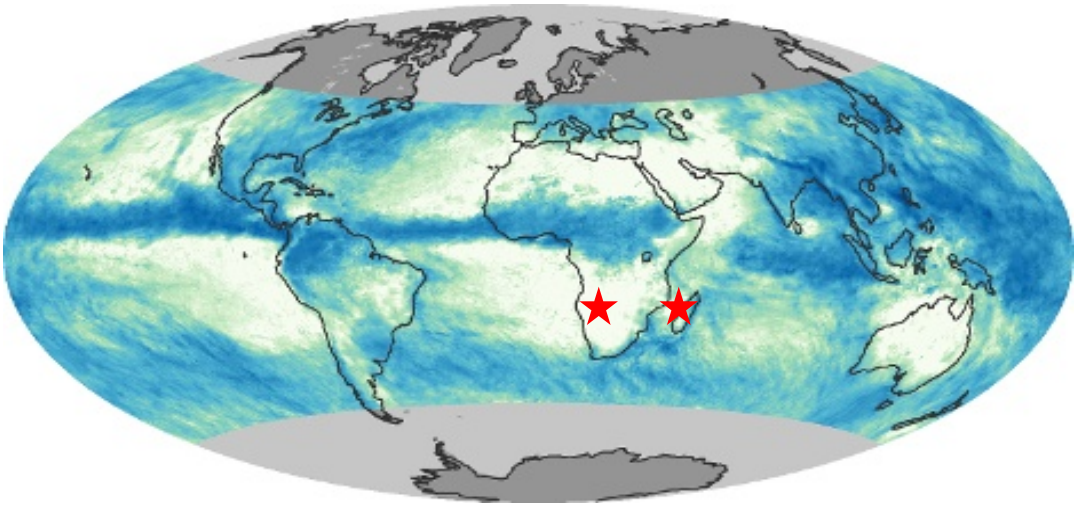

b

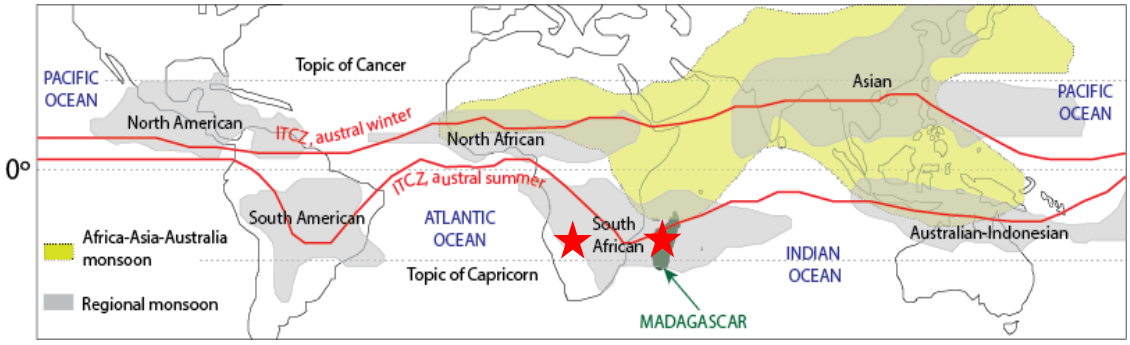
PACIFIC OCEAN
Topic of Cancer
North American
ITCZ, austral winter
North African
Asian
PACIFIC OCEAN
0°
ITCZ, austral summer
South American
ATLANTIC OCEAN
South African
Australian-Indonesian
Africa-Asia-Australia monsoon
Topic of Capricorn
INDIAN OCEAN
Regional monsoon
MADAGASCAR

**Figure 1.1.** Global map showing the geographic distribution of the Inter-Tropical Convergence Zone (ITCZ). (a) Rainfall map of July 2002 by NASA's Tropical Rainfall Measuring Mission (TRMM) satellite, available at http://earthobservatory.nasa.gov/GlobalMaps/view.php?d1=MOD_LSTAD_M&d2=TRMM_3B43M . Regions with highest rainfall are represented in dark blue, the ITCZ is the darkest blue shade near the equator. (b) Schematic representation of the ITCZ and Monsoons. Modified map from Wang (2009) and references therein. Red stars indicate study locations.

## 1.2. Project merit

The project is significant because we use stalagmites, secondary deposits in limestone caves (Figure 1.2), to reconstruct the climate history of Southern Africa, here northeastern Namibia, and northwestern Madagascar over the last millennium and during the Holocene. Few high-resolution paleoclimate archives have been produced from these locations, and even when available, additional data are still needed to improve the spatial and temporal resolution of paleoclimate information for the region.

Stalagmites have been very useful and reliable in paleoclimate reconstruction because they can be accurately dated using the U-Th techniques (e.g. Edwards et al., 1987). Additionally, stable isotope proxies have made them more valuable in producing very high-resolution temporal records. Furthermore, stalagmites have other proxies (Fairchild and Baker, 2012, p. 9-10), the combination of which has produced reliable and coherent paleoclimate information, specifically in regions where cave monitoring is almost unattainable due to the cost-effectiveness and the lack of experts to conduct the monitoring. The multiple proxy approach is performed in all stalagmite investigations reported in this dissertation.

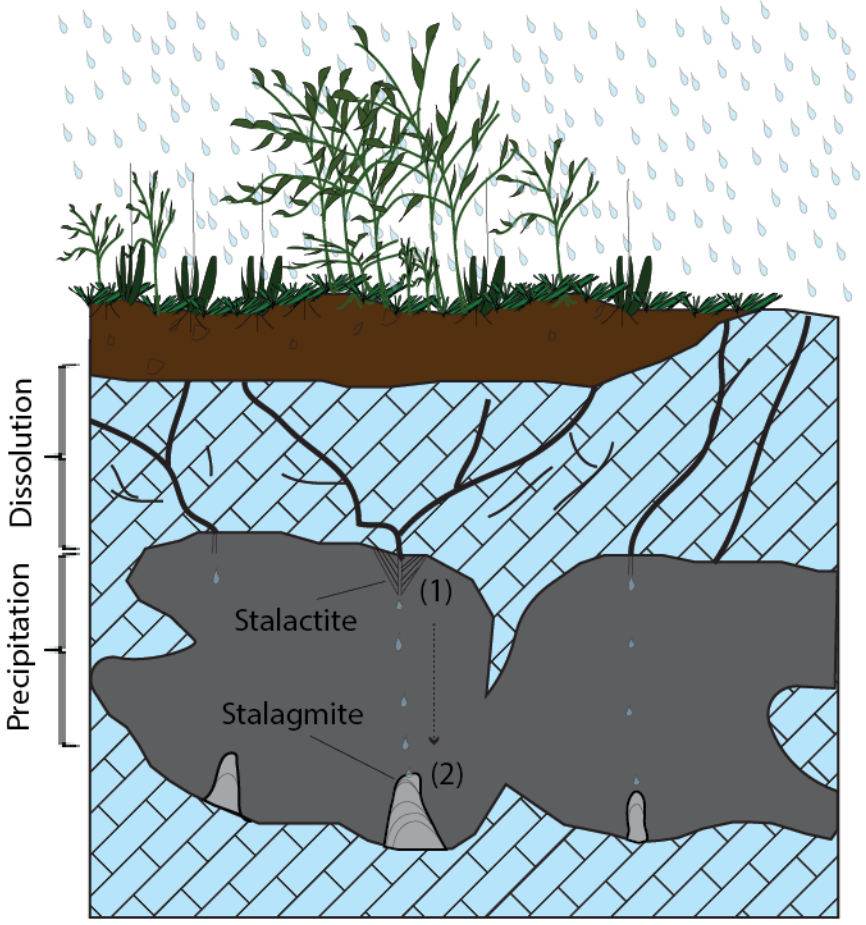


(1): Degassing (and/or evaporation) begins

: Saturation state increases

(2): $CaCO_3$ precipitation into stalagmite

**Figure 1.2.** Generalized sketch showing the processes of stalagmite formation (from dissolution, degassing and/or evaporation of the dripwater, to $CaCO_3$ precipitation to stalagmite), and the linkage between the cave system and the landscape above it. Stalactite and Stalagmite are examples of cave deposits.

### 1.3. Objective of the research

The overall objective is to develop multi-proxy records from stalagmites from northeastern Namibia and northwestern Madagascar to provide comprehensive data set to better understand paleoclimate of these regions over the last millennium and during the Holocene. The specific objective is to test the hypothesis pertaining to the dynamics of the Inter-Tropical Convergence Zone, or simply the ITCZ, in accord with the climate simulations of Chiang and Bitz (2005) and Broccoli et al. (2006). That is global cooling, with marked temperature gradient between the two hemispheres, where the Southern Hemisphere is warmer than the Northern Hemisphere, drives the ITCZ's mean position southward, bringing wetter conditions in austral summer regions. In contrast, global warming, where the Northern Hemisphere is warmer than the Southern Hemisphere, drives the ITCZ's mean position northward, leaving the austral summer regions in much drier conditions. This latitudinal migration of the ITCZ has been coeval with the weakening or strengthening of the monsoons. For example, a southward migration of the ITCZ weakened the northern hemisphere monsoon (e.g. Asian Monsoon and the East Asian Monsoon; Wang et al., 2005; Dykoski et al., 2005; Cheng et al., 2009; Liu et al., 2013) but strengthened the southern hemisphere monsoon (e.g. South American Summer Monsoon; Cheng et al, 2009). This climatic relationship is useful to test for climate models, to refine those models, and to improve prediction of climate changes in the near future.

## 1.4. Climate overview of the study locations

Study locations include Dante Cave, in Namibia (Africa), and Anjohibe and Anjokipoty Caves, in Majunga (Madagascar). These caves are located within the zone visited by the ITCZ (Figs. 1.1 and 1.3.a). The ITCZ brings rainfall to these locations during austral summers. Although both regions receive rainfall during austral summers (i.e. from October to April) as part of the South African Monsoon and Malagasy Monsoon, northeastern Namibia's climate is relatively dry. It belongs to the "warm semi-arid climate (Bsh)" of the Köppen-Geiger climate classification. Northwestern Madagascar is warmer and wetter than northeastern Namibia, and its climate belong to the tropical savanna climate (Aw) of Köppen-Geiger climate classification (Figure 1.3.b-c). Detailed environmental, climatic, and geologic settings of each locations can be found in the following Chapters (2–4).

## 1.5. The Inter-Tropical Convergence Zone (ITCZ)

The Inter-Tropical Convergence Zone (ITCZ), also known by sailors as the "doldrums", is a zone of low pressure near the equator, where two easterly trade winds originating from the northern hemisphere (NH) and southern hemisphere (SH) converge. The zone of convergence is characterized by a strong upward motion of air from its lower level, which diverges at its upper level to form clouds and precipitation. The ITCZ plays an important role in maintaining the Earth's climate (Zhang, 1993) at different timescales. It is the main driver of boreal and austral summers rainfall in the NH and SH, respectively.

a

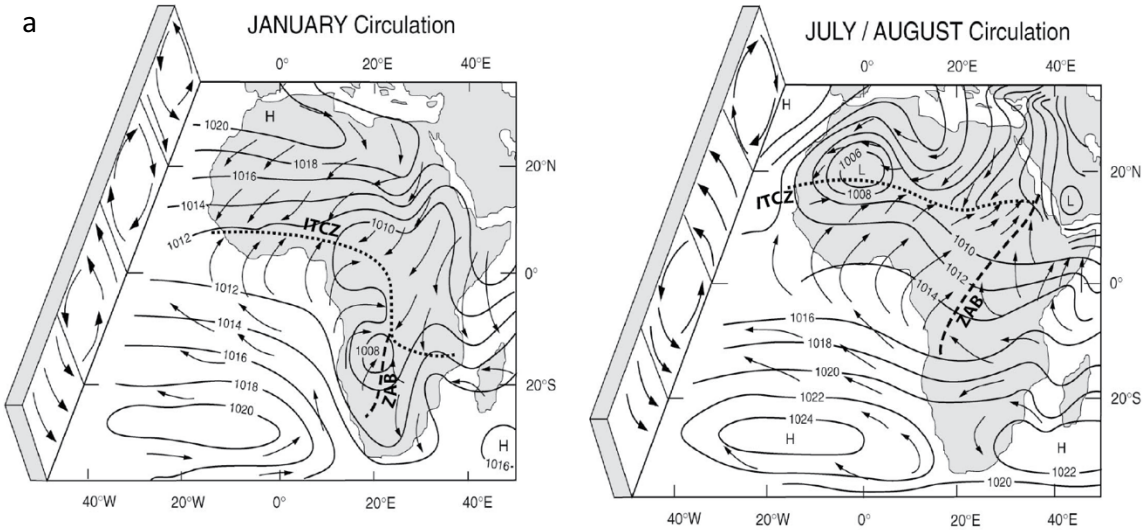


b

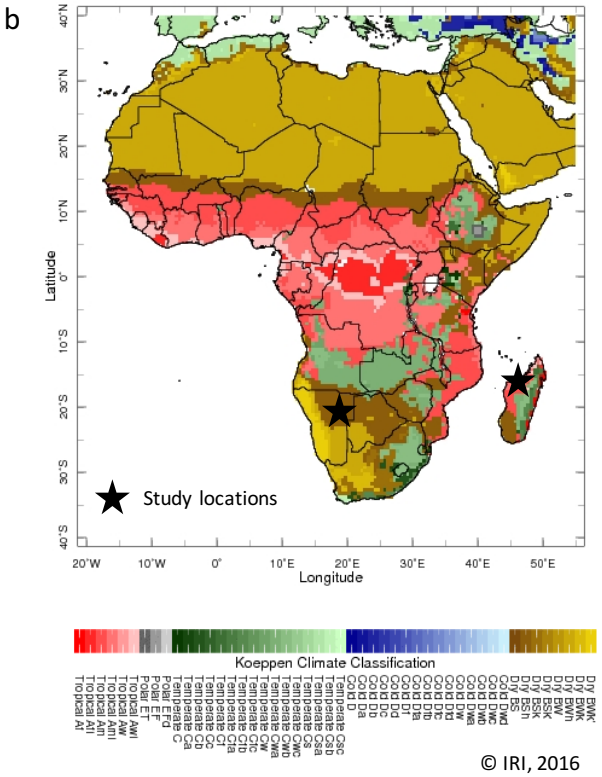


© IRI, 2016

c

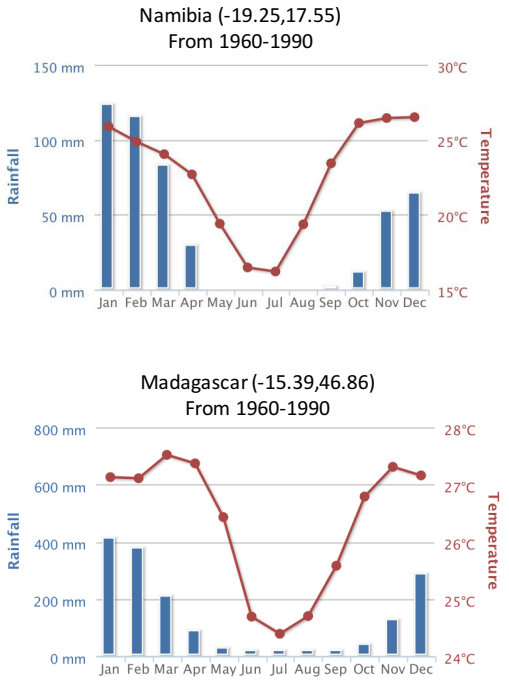


© The World Bank, 2016

Figure 1.3: Climatology of northeastern Namibia and northwestern Madagascar. a) General map showing the general patterns of winds and pressure over Africa. ITCZ: Inter-tropical Convergence Zone; ZAB: Zaire Air Boundary (or Congo Air Boundary). Source from Gasse (2000) but the figure was originally taken from Nicholson, 1996. b) Climate map of Africa based on the Köppen Climate Classification (IRI, 2016). c) Average monthly temperature and rainfall for northeastern Namibia and northwestern Madagascar from 1960-1990 (The World Bank, 2016, accessed Dec 05 2016).

Discrepancies in defining the ITCZ exist. Modern climate scientists and climate modelers realistically define the ITCZ as a belt of wind convergence near the equator. In contrast, because of the ITCZ's spatial complexity, paleoclimatologists, particularly those investigating terrestrial records to reconstruct past climate, use very simplified sketches to define the ITCZ, often using narrow lines as an estimate of the mean position of the ITCZ in the NH and the SH (see for example Wang, 2009). More fundamentally, because of the ITCZ's strong linkage to tropical and subtropical rainfall, paleoclimatologists often refer the ITCZ as a zone of seasonal rainfall near the equator, and paleoclimate data have been used to reconstruct paleo-precipitation in regions visited by the ITCZ. What makes it even more complicated is that the spatial extent of the ITCZ in the Pacific, in the Atlantic, and in the Indian Oceans is not uniform (see for example NASA Earth Observatory). It is very narrow in the Pacific region and it often splits into two narrow bands creating the "double ITCZ", often observed in modern animation of NASA's Tropical Rainfall Measuring Mission (TRMM) satellite around the months of March and April. This double-ITCZ has been problematic in most of the coupled general circulation models (CGCMs) (e.g. Lin, 2007). In the Atlantic region, the ITCZ is also narrow. However, it is very complicated in the Indian Ocean.

The ITCZ's complication in the Indian Ocean could be related to the large mass of lands (Africa to the West, Asia to the North, and Austral-Asia to the East) that bound it. With this regard, indeed, the ITCZ has been conceptually confused with the monsoon, which is another climate phenomenon that plays a key role in the climate of the tropics and subtropics. The monsoon, too, was defined inconsistently depending on the climatic

aspect being studied. Etymologically, the word “monsoons” comes from the Arabic word “mawsim” which means seasons (Berger, 2009), and it was defined as a seasonal reversal in wind direction of the near-surface wind (Trenberth et al., 2000; Wang, 2009). The term monsoon has therefore been incorrectly used to refer to heavy but short-term rains, although these rains meet the dictionary definition of monsoon (e.g. Wikipedia, 2017 and references therein). Although monsoons are driven by the thermal difference between continents (e.g. the Eurasian continent) and oceans (e.g. the Indo-Pacific Ocean), satellite and conventional observations suggest that the monsoon is a manifestation of seasonal migration of the ITCZ (Gadgil, 2003; Wang, 2009). Several regional monsoon systems are embedded within the global monsoon, leading Wang (2009) to conclude that the monsoon is not only global but also regional. Both the monsoon and the ITCZ play an important role for the majority of global atmospheric heat and moisture transport (e.g. Berger, 2009; Basha et al., 2015).

Understanding the monsoon strength is thus fundamental in understanding the dynamics of the ITCZ, and vice versa, and this is additionally crucial in understanding the atmospheric circulation at global scale. The ITCZ migrates seasonally, following the temperature gradient between the NH and the SH, which is one of the main driving factors of the ITCZ’s long-term migration (Chiang and Friedman, 2012). The long-term changes in the relative position of the ITCZ have been investigated via climate modeling and paleorecords. Climate modeling supports the migration of the ITCZ toward the warmer hemisphere (Broccoli et al., 2006; Chiang et al., 2003; Frierson and Hwang, 2012; Kang et

al., 2008; Koutavas and Lynch-Stieglitz, 2004; Schneider et al., 2014). Paleoclimate proxy data also support this interhemispheric difference in temperature in controlling the position of the ITCZ, when the ITCZ moves southward during extended cold periods such as the Last Glacial Maximum (Arbuszewski et al., 2013; Leech et al., 2013; McGee et al., 2014; Ziegler et al., 2008), the Heinrich stadials and the mid-Holocene (McGee et al., 2014). Beyond this latitudinal migration, researchers have also identified that in certain regions, such as the Pacific, the ITCZ did not only migrate north-south but instead it expanded and contracted over decadal to centennial timescales in response to external forcing (e.g. Yan et al., 2015; Denniston et al., 2016).

The latitudinal migration of the ITCZ has significantly impacted the monsoonal activities in the Asian regions (Fleitmann et al., 2007). The monsoon megadroughts of the last millennium reported in these regions are interpreted to have occurred at the onset of the Little Ice Age (Sinha et al., 2011), when the Northern Hemisphere was cooler than the Southern Hemisphere (see figure 2 of Neukom et al., 2014), favoring a southward migration of the ITCZ, and thus weakening the Indian Monsoon (Sinha et al., 2011). At an annual scale, a stronger monsoon year could be understood as a wet year, whereas a weaker monsoon year as a drier year. This understanding has been expanded beyond the instrumental records to improve our understanding of the monsoon and the position, structure, and migration of the ITCZ, because instrumental records are too short to capture the full variability of the climate system. Since the monsoon in our study location, NE Namibia and NW Madagascar, is synchronized with the seasonal migrations of the ITCZ, we simplified the ITCZ-monsoon relationship as follow: when the ITCZ is north, NH

monsoon is strong, and when the ITCZ is south, SH monsoon is strong, leading to an antiphase relationship between the NH and SH (Wang, 2009). On a paleoclimate perspective, monsoonal strength has been understood and reconstructed using geological records (e.g. Wang, 2009), such as speleothem $\delta^{18}O$. Negative speleothem $\delta^{18}O$ values are indicative of stronger monsoon in regions visited by the ITCZ, whereas positive speleothem $\delta^{18}O$ values are indicative of weaker monsoon when the ITCZ leaves those regions (e.g. Zhang et al., 2013; Cheng et al., 2009; Wang et al., 2001, 2005, 2008; Yuan et al., 2004; Dykoski et al., 2005; Cosford et al., 2008; Hu et al., 2008; Zhang et al., 2008; Yang et al., 2010; Sinha et al., 2011; Novello et al., 2016).

### 1.6. Broader impacts

Borrowing the uniformitarian principle, "the present is the key to the past" and "past could provide a key to better understand the future", understanding the changes of climate in the past in Northeastern Namibia and Madagascar could be useful to better predict the likely changes of climate in the future in these locations. Although the modern climate systems are impacted by concentration of greenhouse gases increasing today but effectively constant during the Holocene, this uniformitarian principle is used as a basis of our investigation of climate change in the past. Climate change is well known to significantly impact human life. In low and middle-income regions, such as Africa and Madagascar, climate change has greatly influenced the rate of human mortality, morbidity, and other health related issues (e.g. Hondula et al., 2012; Heath, 2010), and a slight increase (~0.2 to 0.8ºC) in temperature might negatively impact the agricultural activity in

some regions (e.g. Sarr, 2012). Extensive drought causes negative impacts on food production and human welfare (e.g. Cane et al., 1994) and decreases political stability (e.g. Benson and Clay, 1998). Humans are not the only ones affected by climate change, but also fauna and flora, particularly endemic species (e.g. Thuiller et al., 2006; Barrett et al., 2013), coral reefs (e.g. Bruggemann et al., 2012) and algal productivity in lakes (e.g. Castañeda et al., 2009), are significantly threatened by the change in their habitat and ecosystems. This suggests better prediction of future climate change, which mainly requires a better understanding of the past land-ocean-atmosphere interactions to help us better plan for a sustainable future. A better understanding of the land-ocean-atmosphere interaction, particularly the sensitivity of ocean circulation to past, present, and future perturbations, requires a combination of different approaches, including multiproxy paleoclimate reconstructions and modeling.

### 1.7. Dissertation outline

This dissertation is composed of *three chapters*:

*Chapter 2* examines Stalagmite DP1 collected from the Purgatory Chamber of Dante Cave, in northeastern Namibia. The study uses radiometric dating, stable isotopes of oxygen and carbon, mineralogy, and petrography to infer paleoenvironmental changes in northeastern Namibia. The findings from this investigation were published in *The Holocene* scientific journal, and thus the content of Chapter 2 identical to the content of that published article, with only minor editing to comply with the dissertation formatting.

*Chapter 3* uses three stalagmites, MA3, MA2, and ANJ94-5, from Anjohibe Cave, in northwestern Madagascar. The study has focused on U-series, $\delta^{18}O$, $\delta^{13}C$, layer-bounding surfaces, layer-specific width, mineralogy, and distribution of macroholes from Stalagmite MA3 to provide a detailed understanding of the paleoenvironmental changes in northwestern Madagascar between AD 370 and AD 1300. Attention has been paid to the anthropogenic influences on the landscape changes in the studied region. This work was accepted to the scholarly journal *Palaeogeography, Palaeoclimatology, Palaeoecology* (or Paleo 3). The content of Chapter 3 is identical to the content of the accepted version of that manuscript, with only minor editing to comply with the dissertation formatting.

*Chapter 4* examines two stalagmites, ANJB-2 and MAJ-5, collected from Anjohibe and Anjokipoty Caves respectively. The study used stable isotopes ($\delta^{18}O$ and $\delta^{13}C$), petrography, mineralogy, and variability of layer-specific width of the stalagmites to reconstruct paleoclimate in NW Madagascar during the Holocene, and use this information to investigate on the possible climatic drivers of tropical climate changes to draw a more comprehensive conclusion on the major factors controlling its hydrological cycle. This chapter was submitted to the *Climate of the Past* journal on 26 December 2016. Texts and figures in Chapter 4 are mostly identical to those of the submitted version, with changes and minor editing to comply with suggestions from advisory committee.

## REFERENCES


Arbuszewski, J. A., deMenocal, P. B., Cleroux, C., Bradtmiller, L., and Mix, A., 2013, Meridional shifts of the Atlantic intertropical convergence zone since the Last Glacial Maximum: Nature Geosci, v. 6, no. 11, p. 959-962.

Barrett, M. A., Brown, J. L., Junge, R. E., and Yoder, A. D., 2013, Climate change, predictive modeling and lemur health: Assessing impacts of changing climate on health and conservation in Madagascar: Biological Conservation, v. 157, p. 409-422.

Basha, G., Kishore, P., Venkat Ratnam, M., Ouarda, T. B. M. J., Velicogna, I., and Sutterley, T., 2015, Vertical and latitudinal variation of the intertropical convergence zone derived using GPS radio occultation measurements: Remote Sensing of Environment, v. 163, p. 262-269.

Benson, C., and Clay, E. 1998. The impact of droughts on sub- Saharan African economies. World Bank technical paper, 401, 80.

Berger, A., 2009, Monsoon and general circulation system: Chinese Science Bulletin, v. 54, no. 7, p. 1111-1112.

Broccoli, A. J., Dahl, K. A., and Stouffer, R. J., 2006, Response of the ITCZ to Northern Hemisphere cooling: Geophysical Research Letters, v. 33, no. 1.

Bruggemann, J. H., Rodier, M., Guillaume, M. M. M., Andrefouet, S., Arfi, R., Cinner, J. E., Pichon, M., Ramahatratra, F., Rasoamanendrika, F., Zinke, J., and McClanahan, T. R., 2012. Wicked Social-Ecological Problems Forcing Unprecedented Change on the Latitudinal Margins of Coral Reefs: the Case of Southwest Madagascar: Ecology and Society, v. 17, no. 4.

Cane, M. A., Eshel, G., and Buckland, R. W., 1994, Forecasting Zimbabwean Maize Yield Using Eastern Equatorial Pacific Sea-Surface Temperature: Nature, v. 370, no. 6486, p. 204-205.

Castañeda, I. S., Werne, J. P., and Johnson, T. C., 2009, Influence of climate change on algal community structure and primary productivity of Lake Malawi (East Africa) from the Last Glacial Maximum to present: Limnology and Oceanography, v. 54, no. 6, p. 2431-2447.

Cheng, H., Fleitmann, D., Edwards, R. L., Wang, X. F., Cruz, F. W., Auler, A. S., Mangini, A., Wang, Y. J., Kong, X. G., Burns, S. J., and Matter, A., 2009, Timing and structure of the 8.2 kyr BP event inferred from delta O-18 records of stalagmites from China, Oman, and Brazil: Geology, v. 37, no. 11, p. 1007-1010.

Cheng, H., Fleitmann, D., Edwards, R. L., Wang, X. F., Cruz, F. W., Auler, A. S., Mangini, A., Wang, Y. J., Kong, X. G., Burns, S. J., and Matter, A., 2009, Timing and structure of the 8.2 kyr BP event inferred from delta O-18 records of stalagmites from China, Oman, and Brazil: Geology, v. 37, no. 11, p. 1007-1010.

Chiang, J. C. H., and Bitz, C. M., 2005, Influence of high latitude ice cover on the marine Intertropical Convergence Zone: Climate Dynamics, v. 25, no. 5, p. 477-496.

Chiang, J. C. H., and Friedman, A. R., 2012, Extratropical Cooling, Interhemispheric Thermal Gradients, and Tropical Climate Change: Annual Review of Earth and Planetary Sciences, v. 40, p. 383-412.

Chiang, J. C. H., Biasutti, M., and Battisti, D. S., 2003, Sensitivity of the Atlantic Intertropical Convergence Zone to Last Glacial Maximum boundary conditions: Paleoceanography, v. 18, no. 4.

Cosford, J., Qing, H., Eglington, B., Mattey, D., Yuan, D., Zhang, M., Cheng, H., 2008. East Asian monsoon variability since the Mid-Holocene recorded in a high- resolution, absolute-dated aragonite speleothem from eastern China. Earth and Planetary Science Letters 275, 296–307.

Denniston, R. F., Ummenhofer, C. C., Wanamaker, A. D., Lachniet, M. S., Villarini, G., Asmerom, Y., Polyak, V. J., Passaro, K. J., Cugley, J., Woods, D., and Humphreys, W. F., 2016, Expansion and Contraction of the Indo-Pacific Tropical Rain Belt over the Last Three Millennia: Scientific Reports, p. 34485.

Dykoski, C. A., Edwards, R. L., Cheng, H., Yuan, D. X., Cai, Y. J., Zhang, M. L., Lin, Y. S., Qing, J. M., An, Z. S., and Revenaugh, J., 2005, A high-resolution, absolute-dated Holocene and deglacial Asian monsoon record from Dongge Cave, China: Earth and Planetary Science Letters, v. 233, no. 1-2, p. 71-86.

Dykoski, C.A., Edwards, R.L., Cheng, H., Yuan, D.X., Cai, Y.J., Zhang, M.L., Lin, Y.S., Qing, J.M., An, Z.S., Revenaugh, J., 2005. A high-resolution, absolute-dated Holocene and deglacial Asian monsoon record from Dongge Cave, China. Earth and Planetary Science Letters 233, 71–86.

Edwards, R. L., Chen, J. H., and Wasserburg, G. J., 1987, U-238 U-234-Th-230-Th-232 Systematics and the Precise Measurement of Time over the Past 500000 Years: Earth and Planetary Science Letters, v. 81, no. 2-3, p. 175-192.

Fairchild, I. J., and Baker, A., 2012, Speleothem Science: From Processes to Past Environments, Wiley-Blackwell.

Fleitmann, D., Burns, S. J., Mangini, A., Mudelsee, M., Kramers, J., Villa, I., Neff, U., Al-Subbary, A. A., Buettner, A., Hippler, D., and Matter, A., 2007, Holocene ITCZ and Indian monsoon dynamics recorded in stalagmites from Oman and Yemen (Socotra): Quaternary Science Reviews, v. 26, no. 1-2, p. 170-188.

Frierson, D. M. W., and Hwang, Y. T., 2012, Extratropical Influence on ITCZ Shifts in Slab Ocean Simulations of Global Warming: Journal of Climate, v. 25, no. 2, p. 720-733.

Gadgil, S., 2003, The Indian monsoon and its variability: Annual Review of Earth and Planetary Sciences, v. 31, no. 1, p. 429-467.

Gasse, F., 2000. Hydrological changes in the African tropics since the Last Glacial Maximum: Quaternary Science Reviews, v. 19, no. 1-5, p. 189-211.

Global Health Action, v. 5, p. 74-86.

Heath, T., 2010. Madagascar climate change briefing. Water & Sanitation for the Urban Poor, Cranfield University, 4p.

Hondula, D. M., Rocklov, J., and Sankoh, O. A., 2012, Past, present, and future climate at select INDEPTH member Health and Demographic Surveillance Systems in Africa and Asia:

Hu, C.Y., Henderson, G.M., Huang, J.H., Xie, S., Sun, Y., Johnson, K.R., 2008. Quantification of Holocene Asian monsoon rainfall from spatially separated cave records. Earth and Planetary Science Letters 266, 221–232.

IRI, 2016, IRI/LDEO Climate Data Library, IRI Climate and Society Map Room. Available at http://iridl.ldeo.columbia.edu. Accessed December 2016.

Kang, S. M., Held, I. M., Frierson, D. M. W., and Zhao, M., 2008, The response of the ITCZ to extratropical thermal forcing: Idealized slab-ocean experiments with a GCM: Journal of Climate, v. 21, no. 14, p. 3521-3532.

Koutavas, A., and Lynch-Stieglitz, J., 2004, Variability of the marine ITCZ over the eastern Pacific during the past 30,000 years - Regional perspective and global context: Hadley Circulation: Present, Past and Future, v. 21, p. 347-369.

Leech, P. J., Lynch-Stieglitz, J., and Zhang, R., 2013, Western Pacific thermocline structure and the Pacific marine Intertropical Convergence Zone during the Last Glacial Maximum: Earth and Planetary Science Letters, v. 363, p. 133-143.

Lin, J. L., 2007, The double-ITCZ problem in IPCC AR4 coupled GCMs: Ocean-atmosphere feedback analysis: Journal of Climate, v. 20, no. 18, p. 4497-4525.

Liu, Y. H., Henderson, G. M., Hu, C. Y., Mason, A. J., Charnley, N., Johnson, K. R., and Xie, S. C.: Links between the East Asian monsoon and North Atlantic climate during the 8,200 year event, Nat Geosci, 6, 117-120, 10.1038/Ngeo1708, 2013.

McGee, D., Donohoe, A., Marshall, J., and Ferreira, D., 2014, Changes in ITCZ location and cross-equatorial heat transport at the Last Glacial Maximum, Heinrich Stadial 1, and the mid-Holocene: Earth and Planetary Science Letters, v. 390, p. 69-79.

Neukom, R., Gergis, J., Karoly, D. J., Wanner, H., Curran, M., Elbert, J., Gonzalez-Rouco, F., Linsley, B. K., Moy, A. D., Mundo, I., Raible, C. C., Steig, E. J., van Ommen, T., Vance,

T., Villalba, R., Zinke, J., and Frank, D., 2014, Inter-hemispheric temperature variability over the past millennium: Nature Climate Change, v. 4, no. 5, p. 362-367.

Nicholson, S.E., 1996. A review of climate dynamics and climate variability in eastern Africa, in: Johnson, T.C., Odada, E. eds., The Limnology, Climatology and Paleoclimatology of the East African Lakes. Gordon & Breach, p. 25–56.

Novello, V.F., Vuille, M., Cruz, F.W., Stríkis, N.M., Saito de Paula, M., Edwards, R.L., Cheng, H., Karmann, I., Jaqueto, P.F., Trindade, R.I.F., Hartmann, G.A., Moquet, J.S., 2016. Centennial-scale solar forcing of the South American Monsoon System recorded in stalagmites. Sci. Report. 6:24762. http://dx.doi.org/10.1038/srep24762.

Sarr, B., 2012, Present and future climate change in the semi-arid region of West Africa: a crucial input for practical adaptation in agriculture: Atmospheric Science Letters, v. 13, no. 2, p. 108- 112.

Schneider, T., Bischoff, T., and Haug, G. H., 2014, Migrations and dynamics of the intertropical convergence zone: Nature, v. 513, no. 7516, p. 45-53.

Sinha, A., Stott, L., Berkelhammer, M., Cheng, H., Edwards, R. L., Buckley, B., Aldenderfer, M., and Mudelsee, M., 2011, A global context for megadroughts in monsoon Asia during the past millennium: Quaternary Science Reviews, v. 30, no. 1-2, p. 47-62.

The World bank, 2016, Climate Change Knowledge Portal, For Development Practitioners and Policy Makers. Available at: http://sdwebx.worldbank.org/climateportal/index.cfm?page=global_map_region&ThisMap=AF. Accessed December 2016.

Thuiller, W., Midgley, G. F., Hughes, G. O., Bomhard, B., Drew, G., Rutherford, M. C., and Woodward, F. I., 2006, Endemic species and ecosystem sensitivity to climate change in Namibia: Global Change Biology, v. 12, no. 5, p. 759-776.

Trenberth, K. E., Stepaniak, D. P., and Caron, J. M., 2000, The Global Monsoon as Seen through the Divergent Atmospheric Circulation: Journal of Climate, v. 13, no. 22, p. 3969-3993.

Wang, P. X., 2009, Global monsoon in a geological perspective: Chinese Science Bulletin, v. 54, no. 7, p. 1113-1136.

Wang, Y. J., Cheng, H., Edwards, R. L., He, Y. Q., Kong, X. G., An, Z. S., Wu, J. Y., Kelly, M. J., Dykoski, C. A., and Li, X. D.: The Holocene Asian monsoon: Links to solar changes and North Atlantic climate, Science, 308, 854-857, 10.1126/science.1106296, 2005.

Wang, Y.J., Cheng, H., Edwards, R.L., An, Z.S., Wu, J.Y., Shen, C.C., Dorale, J.A., 2001. A high-resolution absolute-dated Late Pleistocene monsoon record from Hulu Cave, China. Science 294, 2345–2348.

Wang, Y.J., Cheng, H., Edwards, R.L., He, Y., Kong, X., An, Z., Wu, J., Kelly, M.J., Dykoski, C.A., Li, X., 2005. The Holocene Asian monsoon: links to solar changes and North Atlantic climate. Science 308, 854.

Wang, Y.J., Cheng, H., Edwards, R.L., Kong, X.G., Shao, X.H., Chen, S.T., Wu, J.Y., Jiang, X.Y., Wang, X.F., An, Z.S., 2008. Millennial- and orbital-scale changes in the East Asian monsoon over the past 224,000 years. Nature 451, 1090– 1093.

Wikipedia, 2017, Monsoon. Available at https://en.wikipedia.org/wiki/Monsoon. Accessed 16 February 2017

Yan, H., Wei, W., Soon, W., An, Z., Zhou, W., Liu, Z., Wang, Y., and Carter, R. M., 2015, Dynamics of the intertropical convergence zone over the western Pacific during the Little Ice Age: Nature Geosci, v. 8, no. 4, p. 315-320.

Yang, Y., Yuan, D.X., Cheng, H., Zhang, M.L., Qin, J.M., Lin, Y.S., Zhu, X.Y., Edwards, R.L., 2010. Precise dating of abrupt shifts in the Asian Monsoon during the last deglaciation based on stalagmite data from Yamen Cave, Guizhou Province, China. Science China Earth Sciences 53, 633–641.

Yuan, D.X., Cheng, H., Edwards, R.L., Dykoski, C.A., Kelly, M.J., Zhang, M.L., Qing, J.M., Lin, Y.S., Wang, Y.J., Wu, J.Y., Dorale, J.A., An, Z.S., Cai, Y.J., 2004. Timing, duration, and transitions of the Last Interglacial Asian Monsoon. Science 304, 575–578.

Zhang, C., 1993, On the Annual Cycle in Highest, Coldest Clouds in the Tropics: Journal of Climate, v. 6, no. 10, p. 1987-1990.

Zhang, P., Cheng, H., Edwards, R.L., Chen, F., Wang, Y., Yang, X., Liu, J., Tan, M., Wang, X., 2008. A test of climate, sun, and culture relationships from an 1810-year Chinese cave record. Science 322, 940–942.

Ziegler, M., Lourens, L., Reichart, G. J., and Nürnberg, D., Late Pleistocene abrupt climate change –ITCZ, teleconnections and the impact of seasonality, in Proceedings Dutch Earth Science Conference (NAC 9), Veldhoven, The Netherlands., 2008.

# CHAPTER 2

## STALAGMITE MULTI-PROXY EVIDENCE OF WET AND DRY INTERVALS IN NORTHEASTERN NAMIBIA: LINKAGE TO LATITUDINAL SHIFTS OF THE INTER-TROPICAL CONVERGENCE ZONE AND CHANGING SOLAR ACTIVITY FROM AD 1400 TO 1950[2]

[2] Voarintsoa, N. R. G., Brook, G. A., Liang, F., Marais, E., Hardt, B., Cheng, H., Edwards, R. L., and Railsback, L. B. 2016. The Holocene, doi:10.1177/0959683616660170.

Reprinted here with permission of Publisher [SAGE Publications, 2017]

## ABSTRACT

Multiple proxies using variation in $\delta^{18}O$, $\delta^{13}C$, mineralogy, and petrography in a newly-generated high-resolution record of Stalagmite DP1 from Dante Cave indicate a linkage between changes in hydroclimate in northeastern Namibia and changes in solar activity and changes in global temperatures. The record suggests that during solar minima and globally cooler conditions (ca. 1660-1710 and ca.1790-1830), wetter periods (reflecting longer summer seasons) in northeastern Namibia were linked to advances of the Inter-Tropical Convergence Zone (ITCZ) and the Inter Ocean Convergence Zone (IOCZ) southwestward. A slight southward push of the Angola-Benguela Front (ABF) during such intervals could also be expected, bringing more rainfall inland. On the other hand, drier and warmer periods in northeastern Namibia, inferred from the increasing $\delta^{18}O$ trend in Stalagmite DP1 after AD. 1715, coincide with globally warmer conditions, and thus a northeastward migration of the ITCZ, specifically with more warming of the Northern Hemisphere (NH). This finding agrees with reducing precipitation observed in the summer rainfall zone of southern Africa since ca. 1900. Therefore, predictions of warming in high-latitude regions of the NH in the next century should suggest that the presently semi-arid climate of northern Namibia may become even drier.

## 2.1. Introduction

The Inter-Tropical Convergence (ITCZ) responds to changes in interhemispheric temperature contrast (e.g. Broccoli et al., 2006). For example, cooling in the NH pushed the ITCZ southward, and this resulted in wetter conditions in the Southern Hemisphere (e.g. Schefuß et al., 2011; Sachs et al., 2009). This hypothesis was supported by paleoclimatological analyses (Koutavas and Lynch-Stieglitz, 2004; Russell and Johnson, 2005; Brown and Johnson, 2005; Sinha et al., 2011; Leech et al., 2013), and by modeling studies (Broccoli et al., 2006; Chiang et al. 2003; Chiang and Bitz, 2005; Kang et al., 2008; Frierson and Hwang, 2012; Donohoe et al., 2013; McGee et al., 2014). It was also summarized in literature reviews (e.g. Chiang and Friedman, 2012; Schneider et al., 2014). As a result, several locations in the Southern Hemisphere became wetter, e.g. during the Heinrich Stadial 1 and the Younger Dryas in southeast Africa (e.g. Schefuß et al., 2011) and during the Little Ice Age (LIA) in the tropical Pacific (e.g. Sachs et al., 2009). Multiple proxies from Stalagmite DP1 from northeastern Namibia suggested an abrupt transition from drier to wetter conditions at 1.8 ka, when climate in the Northern Hemisphere (NH) cooled, and another transition from drier to wetter conditions at the Medieval Warm Period and Little Ice Age transition, when cooling also prevailed in the NH (Sletten et al., 2013). The aim of this paper is to investigate in much detail if such cooling has persistently affected the hydroclimate in northeastern Namibia at shorter time interval, between ca. AD 1400 and 1950. In this regard, we study the upper portion of Stalagmite DP1 at very high resolution (ca. 1 to 2 years) to provide a more comprehensive paleoclimate data set from

northeastern Namibia, and to link information from such data to regional and global conditions.

Namibia is a critical location to study paleoclimate for the following reasons. High-resolution paleorecords from the past millennium prior to the advent of instrumental records, are presently scarce in the region (e.g. Neukom and Gergis, 2012), despite the increasing number of paleo-archives in continental Africa (e.g. Nicholson et al., 2013; Neukom et al., 2013; Neukom et al., 2014a). Thus, records from Namibia should fill gaps in paleoclimate reconstruction in the Southern Hemisphere (e.g. Neukom et al., 2013). Northeastern Namibia is also located in a climatically sensitive region, where rainfall is linked to the Inter-Tropical Convergence Zone (ITCZ), the Inter-Ocean Convergence Zone (IOCZ), and the Angola-Benguela Front (ABF) (Figure 2.1). Namibia is one of the driest countries in sub-Saharan Africa (Reid et al., 2007), and about one-third of all years can be described as drought- or flood-prone (Jury and Engert, 1999). Recent studies also suggest that the dune systems in the Kalahari basin that are used in pastoral and agricultural activities will be reactivated by 2099 (Thomas et al., 2005). In dry years Namibia becomes a desert and failures of small farming operations are very likely (Jury and Engert, 1999). Thus, Namibia is among regions in Africa where sensitivity to climate changes is substantial (Devereux and Næraa, 1996; Dirkx et al., 2008; Niang et al., 2014; Thomas et al., 2005).

The interval studied here, AD 1400-1950, is particularly important because it is characterized by regional to global-scale variations in temperature and insolation. It is characterized by the LIA (Bradley and Jones, 1993; Chambers, 2015; Mann, 2002; Mann et al., 2009) and by the warming of the last century (e.g. Bradley, 2000; Crowley, 2000;

Folland et al, 1990) of more than 0.5°C over most parts of Africa (Niang et al., 2014 and ref. therein). The LIA is recognized in the NH as a time of exceptionally cold temperature, whereas in the SH it seems to be a time distinguished by change in precipitation and winds (e.g., Chambers et al., 2014; Moy et al., 2008). This interval is also characterized by three events of low solar activity (Spörer, Maunder, and Dalton minima), which may have contributed to the LIA's coldest phases (cf. Hathaway, 2010; Mauquoy et al., 2002; Muscheler et al., 2007; Usoskin et al., 2003; 2007; Figure 2.5a, b, c). These conditions in turn could have amplified the temperature gradient between the two hemispheres (cf. Neukom et al., 2014b), and could have affected the dynamics of the ITCZ (e.g. Chiang and Bitz, 2005; Yan et al., 2015).

Stalagmites were investigated because they can be accurately dated (e.g. Dorale et al., 2004; Edwards et al., 1987). They have a potential in storing valuable climatic information in several proxies (e.g. Fairchild and Baker, 2012); stable isotopes, petrography, and mineralogy are the main proxies used. Stalagmite multiple proxy analyses have been shown to provide comprehensive paleoclimate information from regions (e.g. Brook et al., 2009, 2015; Railsback et al., 2014; Sletten et al., 2013) where cave monitoring and/or sample replication are often impossible due to the high cost and/or other environmental regulations (e.g. Sletten et al., 2013).

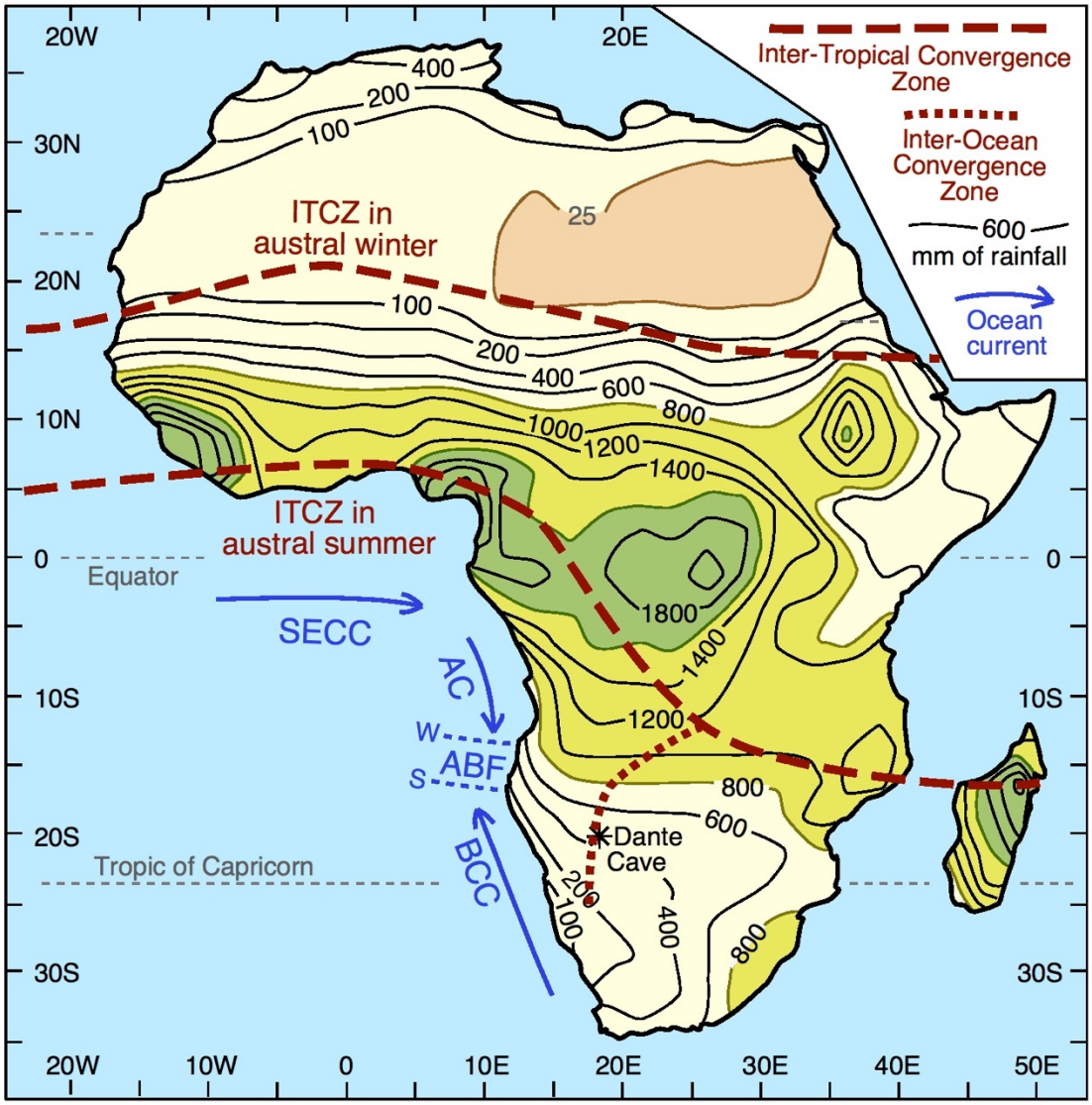
20W
20E
30N
20N
10N
0
Equator
10S
20S
Tropic of Capricorn
30S
20W
10W
0
10E
20E
30E
40E
50E
Inter-Tropical Convergence Zone
Inter-Ocean Convergence Zone
600
mm of rainfall
Ocean current
ITCZ in austral winter
ITCZ in austral summer
SECC
AC
W
S
ABF
BCC
Dante Cave
25
100
200
400
600
800
1000
1200
1400
1800

Figure 2.1. Map of Africa with thick red lines showing position of the Inter-Tropical Convergence Zone (ITCZ) in austral winter and austral summer, and with a thinner red line showing the position of the Congo Air Boundary (CAB), Zaire Air Boundary (ZAB), or Inter-Oceanic Convergence Zone (IOCZ) in austral summer. Contours and colored fields show geographic variation of mean annual atmospheric precipitation for 1979 to 2011 from the Global Precipitation Climatology Project (GPCP) of the U.S. National Aeronautics and Space Administration (NASA). Currents in the southeastern Atlantic are Southern Equatorial Counter Current (SECC), Angola Current (AC), and Benguela Coastal Current (BCC). ABF is the Angola-Benguela Front in austral winter (W) and austral summer (S). The currents and position of ABF are from Benthien et al. (2002), Veitch (2006), and Dupont et al. (2008). The lines for the ITCZ are compromises between the lines shown by Dupont et al. (2008), Nicholson (2009), Wang (2009), and Ziegler et al. (2013). The line for the IOCZ is a compromise between the lines shown by van Heerden and Taljaard (1998), Dupont et al. (2008), and Schefuß et al. (2011). Note that, east of about 15°E, land is distributed symmetrically with respect to the Equator, and the winter and summer positions of the ITCZ are likewise positioned symmetrically with respect to the Equator. By contrast, west of about 15°E, African land is dominantly in the NH, and the ITCZ is restricted to the NH. The location of Dante Cave is shown with a large asterisk.

## 2.2. Setting

### 2.2.1. Physical setting of Dante Cave

Stalagmite DP1 was collected from the Purgatory Chamber of Dante Cave (19° 24′ S; 17° 53′ E). It was accidentally toppled, during surveying of the chamber in 1988 (Figure 2.2). The sample was collected in 2007, and the absence of sediment or staining indicated that the stalagmite had not been submerged after it was toppled. Dante Cave is one of the longest (828 m) and deepest (65 m) caves in the Namibia's Karstveld (Sletten et al., 2013, and references therein). Purgatory Chamber is the cave's lowest room, with hot and humid conditions that give it its name. The chamber is located at about 100 m from the cave's entrance shaft and about 60 m below the entrance. It is one of the most difficult chambers of Dante Cave to access. The cave itself is accessible through a single vertical entrance in the roof of the southernmost chamber, which is 9 m above a cone of debris of collapsed rocks.

Dante Cave is located in the Kalahari basin (Figure 1 of Thomas et al., 2005), on the northeastern margin of the Otavi Mountainland, also referred to as Namibia's Karstveld (Irish et al., 2001), in the Otjozondjupa region of northeastern Namibia. The region is characterized by poorly developed underground karst in the carbonate succession of the Otavi Group. It developed in dolomites of the upper Tsumeb Subgroup, one of the two carbonate sequences deposited between 730 and 700 Ma in the Damara Supergroup Complex (Miller, 1983).

Dante Cave is in a semi-arid region, with a mean rainfall of ca. 500 mm/yr (Figure 1 of Sletten et al., 2013; Figure 2 of Rohde and Hoffman, 2012). Vegetation in the Otavi Mountainland is dominated by deciduous woodland savanna with a relatively high diversity of scattered tall trees (Mendelsohn et al., 2002; Rohde and Hoffman, 2012; Sletten et al., 2013). Rohde and Hoffman (2012) showed that, within the region, vegetation cover in areas with rainfall around 500 mm/yr is strongly dependent on changes in rainfall, a relationship further supported by the positive correlation between $\delta^{13}C$ and $\delta^{18}O$ in stalagmite DP1 (Sletten et al., 2013).

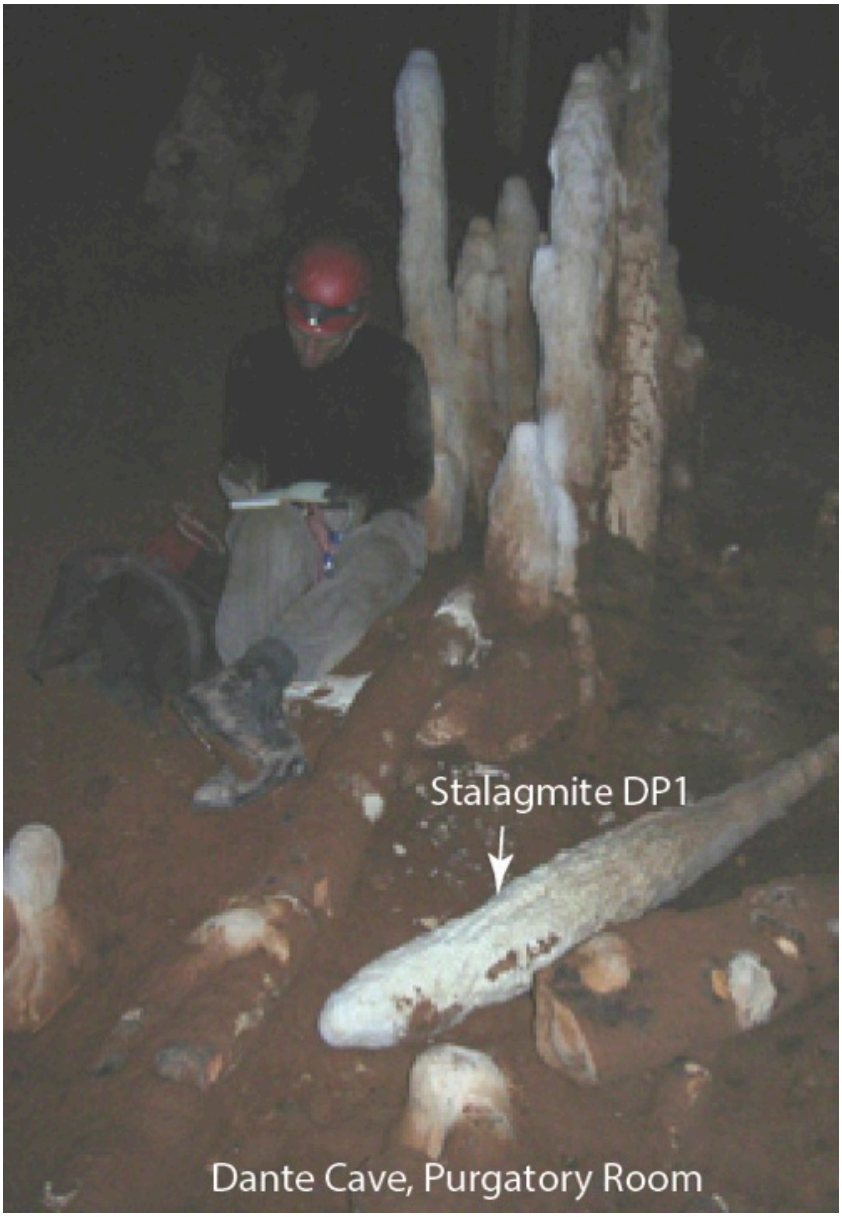
Stalagmite DP1
Dante Cave, Purgatory Room

Figure 2.2. Photograph of Stalagmite DP1 lying in the Purgatory Room of Dante Cave, with Ben Hardt for scale (Photograph by Eugene Marais).

### 2.2.2. Climate of northern Namibia

Northern Namibia, including Dante Cave is in the austral summer rainfall zone of southern Africa and receives most of its monsoonal rainfall from October to May (Burrough et al., 2007; see also Figure 1 of Brook et al., 2015). Rainfall is linked to the annual migration of the ITCZ and the associated Inter-Ocean Convergence Zone (IOCZ), or Congo or Zaire Air Boundary (van Heerden and Taljaard, 1998), a branch of the ITCZ where the Atlantic and Indian Ocean air-streams converge (Figure 2.1). Rainfall in northern Namibia is also affected by the location of the Angola-Benguela Front (ABF), the boundary between the south-flowing warm Angola ocean current and the north-flowing cold Benguela current in the tropical SE Atlantic. For example, Nicholson and Entekhabi (1987) found that an anomalously warm SE tropical Atlantic current (with a SST > 28°C off northern Angola) leads to an increase in rainfall amount (above average) along the Angolan (6-17.5°S) and along the Namibian (17.5-29°S) coasts. This is also observed inland (Nicholson and Entekhabi, 1987), and it happens in late austral summer, from February to April (Rouault et al., 2003). A more southerly position of the ABF thus increase evaporation and the level of moisture associated with the IOCZ, bringing more rainfall to Angola and Namibia (Florenchie et al., 2003; Jury and Engert, 1999; Rouault et al., 2003; Rouault, 2012). This latitudinal migration of the ABF is expected to follow the latitudinal migration of the ITCZ, but this aspect has not been fully investigated.

## 2.3. Methods

This paper reports on the upper 261 mm of Stalagmite DP1, providing a record of much higher resolution than that of Sletten et al. (2013). Within that interval, Sletten et al. (2013) reported 3 U-Th ages and 66 stable isotope analysis. In contrast, this paper reports 18 U-Th ages and 264 stable isotope analyses.

### 2.3.1. Radiometric dating

Eighteen samples (including 2 replicates) of 100-150 mg each were drilled for U-Th radiometric analyses to determine the depositional age of the stalagmite (Table 2.1). Analyses were performed using an inductively-coupled plasma mass spectrometry (ICP-MS) on a Finnigan-MAT Element at the University of Minnesota. Uranium and thorium were separated following the chemical procedures described in Shen et al. (2002). Decay constants used for $^{230}$Th, $^{234}$U, and $^{238}$U are similar to those reported in Cheng et al. (2000), which are 9.1577 x $10^{-6}$ years$^{-1}$, 2.8263 x $10^{-6}$ years$^{-1}$, and 1.55125 x $10^{-10}$ years$^{-1}$ respectively. Corrected $^{230}$Th assumes the initial $^{230}$Th/$^{232}$Th ratio of 4.4±2.2 x $10^{-6}$ as explained in Table 1. Dates are reported as “Years BP” where BP means “Before Present” and “Present” is AD 1950.

**Table 2.1.** $^{230}$Th dating results. The error is 2σ.

| Distance from top (mm) | Sample Number | $^{238}$U (ppb) | | $^{232}$Th (ppt) | | $^{230}$Th / $^{232}$Th (atomic x10$^{-6}$) | | $\delta^{234}$U* (measured) | | $^{230}$Th / $^{238}$U (activity) | | $^{230}$Th Age (yr) (uncorrected) | | $^{230}$Th Age (yr) (corrected) | | $\delta^{234}U_{initial}$** (corrected) | | $^{230}$Th Age (yr BP)*** (corrected ) | |
|---|---|---|---|---|---|---|---|---|---|---|---|---|---|---|---|---|---|---|---|
| 1.9 | DP1-T | 2073 | ±5.7 | 209 | ±1 | 142 | ±40 | 300.1 | ±1.9 | 0.0009 | ±0.0002 | 73 | ±21 | 71 | ±21 | 300.2 | ±1.9 | 14 | ±21 |
| 6 | [a]DP1-U1 | 2651.7 | ±5.4 | 685 | ±19 | 150 | ±20 | 287.6 | ±2.2 | 0.0023 | ±0.0003 | 199 | ±27 | 193 | ±27 | 288 | ±2 | 131 | ±27 |
| 21.5 | DP1-U2 | 2325.3 | ±3.7 | 242 | ±14 | 188 | ±55 | 287.1 | ±1.9 | 0.0012 | ±0.0003 | 101 | ±29 | 98 | ±29 | 287 | ±2 | 36 | ±29 |
| 44 | DP1-U3 | 3673.5 | ±7.0 | 533 | ±28 | 170 | ±50 | 282.6 | ±2.0 | 0.0015 | ±0.0004 | 127 | ±36 | 124 | ±37 | 283 | ±2 | 62 | ±37 |
| 44 | [b]DP1-U3B | 3529.8 | ±5.6 | 538 | ±13 | 169 | ±15 | 283.5 | ±1.8 | 0.0016 | ±0.0001 | 133 | ±11 | 130 | ±12 | 284 | ±2 | 68 | ±12 |
| 57.5 | UP1-U4 | 5522.8 | ±12.2 | 954 | ±24 | 167 | ±16 | 283.1 | ±2.0 | 0.0017 | ±0.0002 | 148 | ±13 | 144 | ±14 | 283 | ±2 | 82 | ±14 |
| 77 | DP1-U5 | 3886.8 | ±7.3 | 386 | ±15 | 309 | ±34 | 284.7 | ±1.9 | 0.0019 | ±0.0002 | 158 | ±17 | 156 | ±17 | 285 | ±2 | 94 | ±17 |
| 103 | DP1-103 | 4840 | ±9.6 | 37 | ±1 | 5108 | ±134 | 284.5 | ±1.6 | 0.0023 | ±0.0001 | 200 | ±4 | 200 | ±4 | 284.7 | ±1.6 | 143 | ±4 |
| 112 | DP1-U6 | 3834.5 | ±7.4 | 869 | ±19 | 199 | ±11 | 281.9 | ±2.1 | 0.0027 | ±0.0001 | 233 | ±12 | 228 | ±12 | 282 | ±2 | 166 | ±12 |
| 155 | DP1-U7 | 2931.6 | ±5.5 | 514 | ±13 | 299 | ±17 | 289.5 | ±1.9 | 0.0032 | ±0.0002 | 269 | ±14 | 265 | ±14 | 290 | ±2 | 203 | ±14 |
| 193.5 | DP1-U8 | 1515.2 | ±2.3 | 114 | ±9 | 794 | ±100 | 290.4 | ±2.2 | 0.0036 | ±0.0004 | 306 | ±30 | 304 | ±30 | 291 | ±2 | 242 | ±30 |
| 234 | DP1-U9 | 5774.0 | ±11.4 | 579 | ±13 | 624 | ±17 | 287.2 | ±2.0 | 0.0038 | ±0.0001 | 322 | ±5 | 320 | ±5 | 287 | ±2 | 258 | ±5 |
| 238 | DP1-U11A | 3071.4 | ±4.4 | 326 | ±13 | 677 | ±42 | 291.6 | ±1.7 | 0.0044 | ±0.0002 | 369 | ±18 | 366 | ±18 | 292 | ±2 | 304 | ±18 |
| 245 | DP1-U11C | 1819.9 | ±2.2 | 100 | ±6 | 1413 | ±106 | 289.4 | ±1.7 | 0.0047 | ±0.0002 | 400 | ±17 | 398 | ±17 | 290 | ±2 | 336 | ±17 |
| 250 | DP1-U11B | 962.6 | ±1.0 | 134 | ±4 | 591 | ±28 | 292.6 | ±2.0 | 0.0050 | ±0.0002 | 422 | ±16 | 419 | ±16 | 293 | ±2 | 357 | ±16 |
| 252 | DP1-250 | 1091.7 | ±2.7 | 34 | ±1 | 2768 | ±109 | 299.6 | ±2.8 | 0.0052 | ±0.0002 | 440 | ±16 | 439 | ±16 | 300 | ±2.8 | 382 | ±16 |
| 261 | DP1-U10 | 1056.8 | ±1.6 | 267 | ±18 | 445 | ±70 | 287.8 | ±2.0 | 0.0068 | ±0.0010 | 579 | ±83 | 573 | ±83 | 288 | ±2 | 511 | ±83 |
| 261 | [b]DP1-U10 | 1183.9 | ±1.2 | 252 | ±5 | 529 | ±13 | 290.3 | ±1.8 | 0.0068 | ±0.0001 | 577 | ±8 | 572 | ±9 | 291 | ±2 | 510 | ±9 |

[a] Sample not used in the age model because it has more $^{232}$Th relative to DP1-T, a sample collected from the same layer of aragonite of the top of the stalagmite.
[b] Replicate samples, which have lower uncertainty in the value of $^{230}$Th (corrected age) relative to the former analyzed sample, and are used to reconstruct the age model (see Figure 2.3).

*$\delta^{234}U = ([^{234}U/^{238}U]_{activity} - 1) \times 1000$. ** $\delta^{234}U_{initial}$ was calculated based on $^{230}$Th age (T), i.e., $\delta^{234}U_{initial} = \delta^{234}U_{measured} \times e^{\lambda_{234} \times T}$.

Corrected $^{230}$Th ages assume the initial $^{230}Th/^{232}Th$ atomic ratio of 4.4 ±2.2 x10$^{-6}$. Those are the values or a material at secular

equilibrium, with the bulk earth $^{232}Th/^{238}U$ value of 3.8. The errors are arbitrarily assumed to be 50%.

***B.P. stands for "Before Present" where the "Present" is defined as the year 1950 A.D.

### 2.3.2. Stable isotopes

A total of 264 samples of 50 to 100 micrograms were drilled along the growth axis of the top 261 mm of DP1 using a Micro-Cut dental drill with SSW HP1/4 (ref14820) drill bits in the Sedimentary Geochemistry Laboratory, Department of Geology, at UGA. The samples were transferred to round-bottomed 4.5 ml borosilicate vials (Labco Limited, Lampeter, UK) and were analyzed using the GasBench II technique in continuous flow IRMS. Analytical methods were similar to those described in Paul and Skrzypek (2007): (1) the vials were flushed with high purity He to replace air contained in the vials, (2) about 0.06 ml of 100% ortho-phosphoric acid was injected into the vials to produce sample $CO_2$ gases into the exetainer headspace, (3) the samples were allowed to react with the acid for a minimum of 2 hours before the headspace was measured, (4) the headspace $CO_2$ was then analyzed for $\delta^{13}C$ and $\delta^{18}O$ (also see Skrzypek and Paul, 2006 for the procedures). Measurements were done on a Delta V Plus at 50°C, with NBS-19 interspersed among the samples (every six samples) to allow calibration relative to the Vienna Pee Dee Belemnite (VPDB) standard. All the analyses were performed at the Alabama Stable Isotope Laboratory of the University of Alabama. Isotope ratios were reported in per mil (‰) relative to VPDB, and isotope error was about ± 0.1‰ for both $^{13}C$ or $^{18}O$. As per convention, the $^{13}C/^{12}C$ and $^{18}O/^{16}O$ ratios (R) are expressed in the delta notation as follows: $\delta x = [(R_{sample}-R_{standard})/R_{standard}] * 10^3$ (where x represents $^{13}C$ or $^{18}O$ and R is the ratio). For comparison with calcite values, $\delta^{18}O$ and $\delta^{13}C$ values from aragonite layers were adjusted by subtracting 1.7 ‰ (Romanek et al., 1992) and 0.8‰ (Kim et al., 2007), respectively, to account for the increased fractionation of heavier isotopes in aragonite.

### 2.3.3. Mineralogy and petrography

Microscopic examination of thin sections using the Leitz Laborlux 12 Pol of the Sedimentary Geochemistry Lab at UGA was done to characterize boundaries between adjacent spelean layers. These boundaries are classified in three categories (Figure 2.4b; also see Railsback et al., 2013): (1) conformal, when minerals grow without truncation; (2) erosional or Type E surfaces (Railsback et al., 2013) when truncation of the underlying and thus earlier mineral or layer is observed, and (3) Type L surfaces or boundary of lesser deposition (Railsback et al., 2013), which are easily identifiable as a thinning toward the margin of the stalagmites. Type L surfaces can also be identified in hand sample.

Each identified layer-bounding surface was marked on a scanned copy of the thin section (our log image), imported to Adobe Illustrator as a new layer overlain on top of the scanned image of stalagmite DP1, digitized, and saved electronically (Figure 2.3b). The distance from the top of the stalagmite to where these surfaces were identified was then converted to age with respect to the age model.

Scanning Electron Microscopy (SEM) and X-ray diffraction (Figure 2.4) were performed to analyze a very unusual layer located between 237 and 250 mm from the top of stalagmite DP1. For the SEM, a chip of the sample was carbon coated and then copper-taped and imaged at high vacuum using the Zeiss 1450EP (Carl Zeiss, Inc., Thornwood, NY) at Georgia Electron Microscopy, a facility at UGA. The Zeiss 1450EP is equipped with an Oxford SDD-EDX system (Oxford Inc, Scotts Valley, CA). For X-ray diffraction, powdered samples of 3 g were extracted and scanned from 20 to 65° 2θ with CoKα radiation using a Bruker D8 X-ray Diffractometer in the Department of Geology of the University of Georgia.

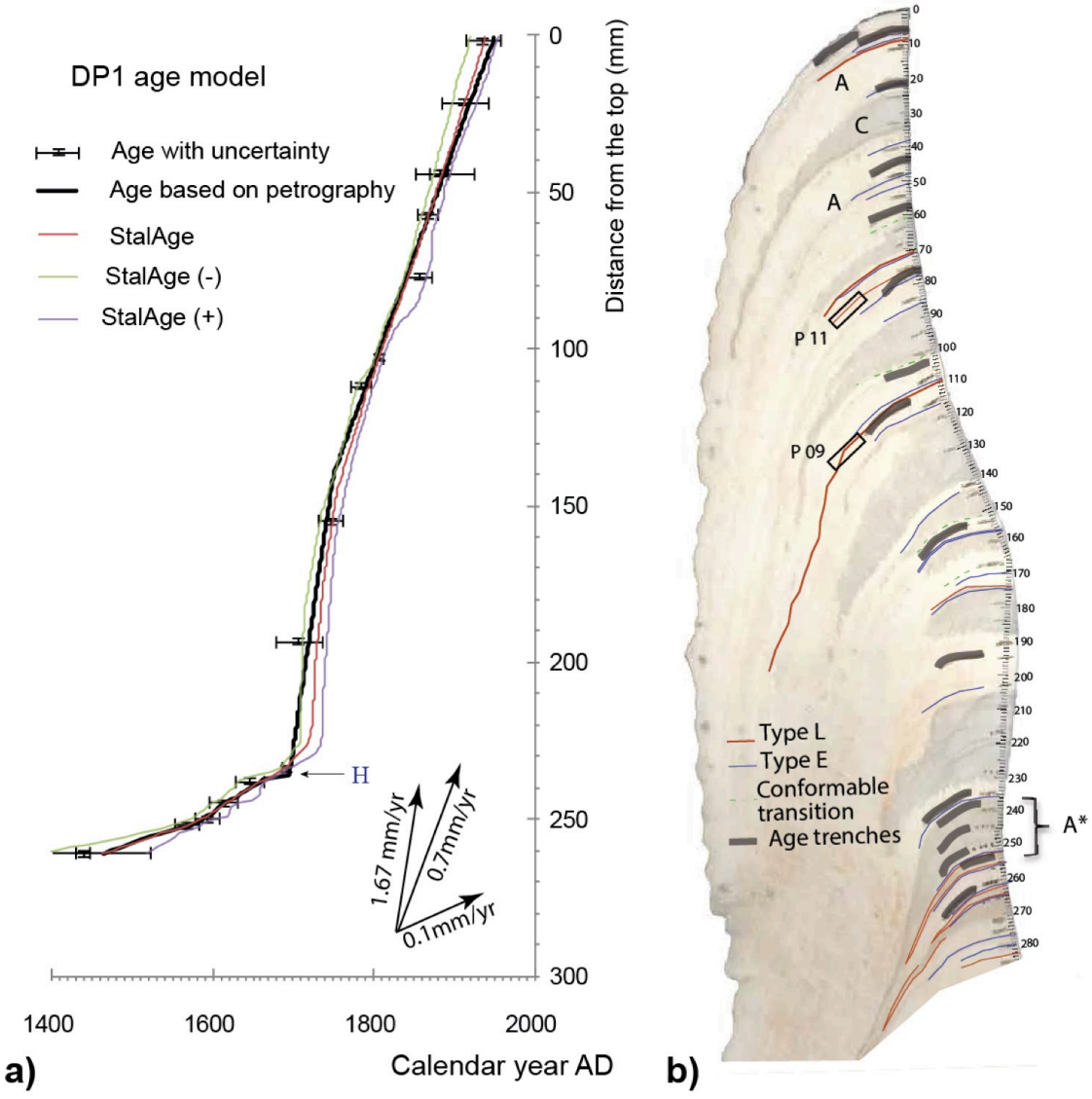
DP1 age model
Age with uncertainty
Age based on petrography
StalAge
StalAge (-)
StalAge (+)
H
1.67 mm/yr
0.7mm/yr
0.1mm/yr
Distance from the top (mm)
0
50
100
150
200
250
300
1400
1600
1800
2000
Calendar year AD
a)
A
C
A
P 11
P 09
Type L
Type E
Conformable transition
Age trenches
A*
b)

Figure 2.3. a) Age model of Stalagmite DP1 based on stalAge (Sholz and Hoffman, 2011) and based on petrography (Railsback et al., 2013). "H" indicates the hiatal Type E surface discussed in the text. b) Scanned image of the uppermost 285 mm of stalagmite DP1 showing the location of the age trenches (grey lines) and the identified layer-bounding surfaces (see Railsback et al., 2013 for details on these Type E and type L surfaces). A and C denote layers composed of aragonite and calcite. A* denotes the layer of coarse aragonite that has been analyzed under X-ray diffraction and SEM (see Figures S3b and S3d). P09 and P11 represent locations of series of microphotographs (see Figure S3c) used to illustrate the two main types of layer-bounding surfaces (E and L) identified in stalagmite DP1.

## 2.4. Results

### 2.4.1. Radiometric results and age model

Results from the 18 radiometric analyses for U-Th dating show that stalagmite DP1 has high $^{238}U$ concentrations that range from 962.6 ±1.0 to 5774.0±11.4 ppb and generally low $^{232}Th$ concentrations that range from 34±1 to 954 ± 24 ppb (Table 2.1). Three results were rejected. The first sample, DP1-U1, was rejected because of its large $^{232}Th$ concentration (685 ppt), and it was not in stratigraphic order. It was then replaced by Sample DP1-T from a slightly higher horizon with a smaller $^{232}Th$ concentration (209 ppt). The two other samples, DP1-U3 and DP1-U10, were rejected because of the large uncertainties. These samples were replicated and replaced by samples with more precise ages from the same horizons (Table 2.1). The remaining 15 ages were all in stratigraphic order, i.e. becoming younger steadily towards the top of the stalagmite (Table 2.1).

The age model for Stalagmite DP1 was constructed using both the StalAge1.0 algorithm of Scholz and Hoffman (2011) and recognition of likely hiatal surfaces as proposed by Railsback et al. (2013; see their Figure 9). The former generates a best estimate of a sample's age at that sample's specific depth in an uninterrupted sequence, but it is not well-suited to identification or location of hiatuses, whereas the latter specifically identifies hiatal surfaces and thus localizes offsets in age models. Thus, the kink in the StalAge model for Stalagmite DP1 was replaced with a hiatal offset, at a Type E surface (Figure 2.3).

The U-Th ages indicate that the interval of Stalagmite DP1 studied for this project was deposited from ca. AD 1450 to 1950 (Figure 2.3a). The modeling of U-Th ages using

StalAge and petrographic evidence combine to suggest a hiatus of about 30 years at about 235 mm from the top of the stalagmite. The hiatal Type E surface is supported by an abrupt shift of ca. 4‰ in $\delta^{18}O$ values, from –7.8 to –11.7‰ relative to VPDB, and by a major change in growth rate from 0.1mm/year to 1.67 mm/ year (Figure 2.3a). The age of this hiatus is best estimated at ca. AD 1660-1690.

### 2.4.2. Stable isotopes

After the transformation of the isotopic values from aragonite discussed in the method section, values of $\delta^{18}O$ in Stalagmite DP1 range from –7.3 to –11.9‰ relative to the VPDB and values of $\delta^{13}C$ range from –6.8 to –10.8‰, relative to the VPDB. The Pearson correlation test described in the supplementary document shows that $\delta^{18}O$ and $\delta^{13}C$ are correlated with great statistical significance (t=14.02, n=263, $r^2$=0.43, p<2.2e-16) and a positive linear relationship (Figure A1).

Values of both $\delta^{18}O$ and $\delta^{13}C$ are significantly greater (between ca. –9 to –7 ‰, vs. VPDB) in the time interval from AD 1450 to 1660 (Figure 2.5). An abrupt decrease in $\delta^{18}O$ from –7.8 to –11.7‰ vs. VPDB and in $\delta^{13}C$ from –7.1 to –10.1‰ vs. VPDB is observed around ca. 1680-1700. Following this change, $\delta^{18}O$ shows a general trend toward greater values from ca. AD 1715 to ca. AD 1950 (Figure 2.5), when growth of Stalagmite DP1 ceased and did not resume prior to the stalagmite's fall in 1988. Values of $\delta^{18}O$ and $\delta^{13}C$ are lowest in layers of calcite and highest in layers of aragonite. In addition, low values coincide with Type E surfaces and high values with Type L surfaces (Figure 2.5c).

### 2.4.3. Mineralogy and petrography

Mineralogy is distinct below and above the hiatus at 235 mm. Below the hiatus the interval of Stalagmite DP1 studied consists solely of aragonite with different fabrics: (1) the common white, soft, opaque, and fibrous crystals of aragonite (Railsback, 2000) and (2) the uncommon pale-yellow, compact, translucent, and prismatic crystals of aragonite (Figure 2.3b). The uncommon crystals of aragonite, at 237 to 250 mm from the top of stalagmite DP1, are much wider than the aragonite in the rest of the stalagmite (Figures A3a and A3b). This aragonite is very similar to the "ray aragonite" described by Frisia et al. (2002) and to the elongated columnar aragonite described by Duan et al. (2012). It has consistently high values of $\delta^{18}O$ and $\delta^{13}C$ (Figure 2.5). Above that hiatal surface, the interval of Stalagmite DP1 studied consists of alternating thick layers of calcite (8) and aragonite (8) with a mean thickness of ca. 15 mm (Figures 2.3b and 2.5). We did not find any evidence of post-depositional alteration of aragonite to calcite in Stalagmite DP1 (c.f. Green et al., 2015).

For petrography, 26 Type E surfaces and 8 Type L surfaces were identified. Type E surfaces are surfaces below which layers are truncated, particularly toward the crest of the stalagmite, in wetter conditions. Type L surfaces are surfaces below which layers thin toward the flank and thus indicate reduced deposition rate in response to lesser dripwater in drier conditions (Railsback et al., 2013; 2014).

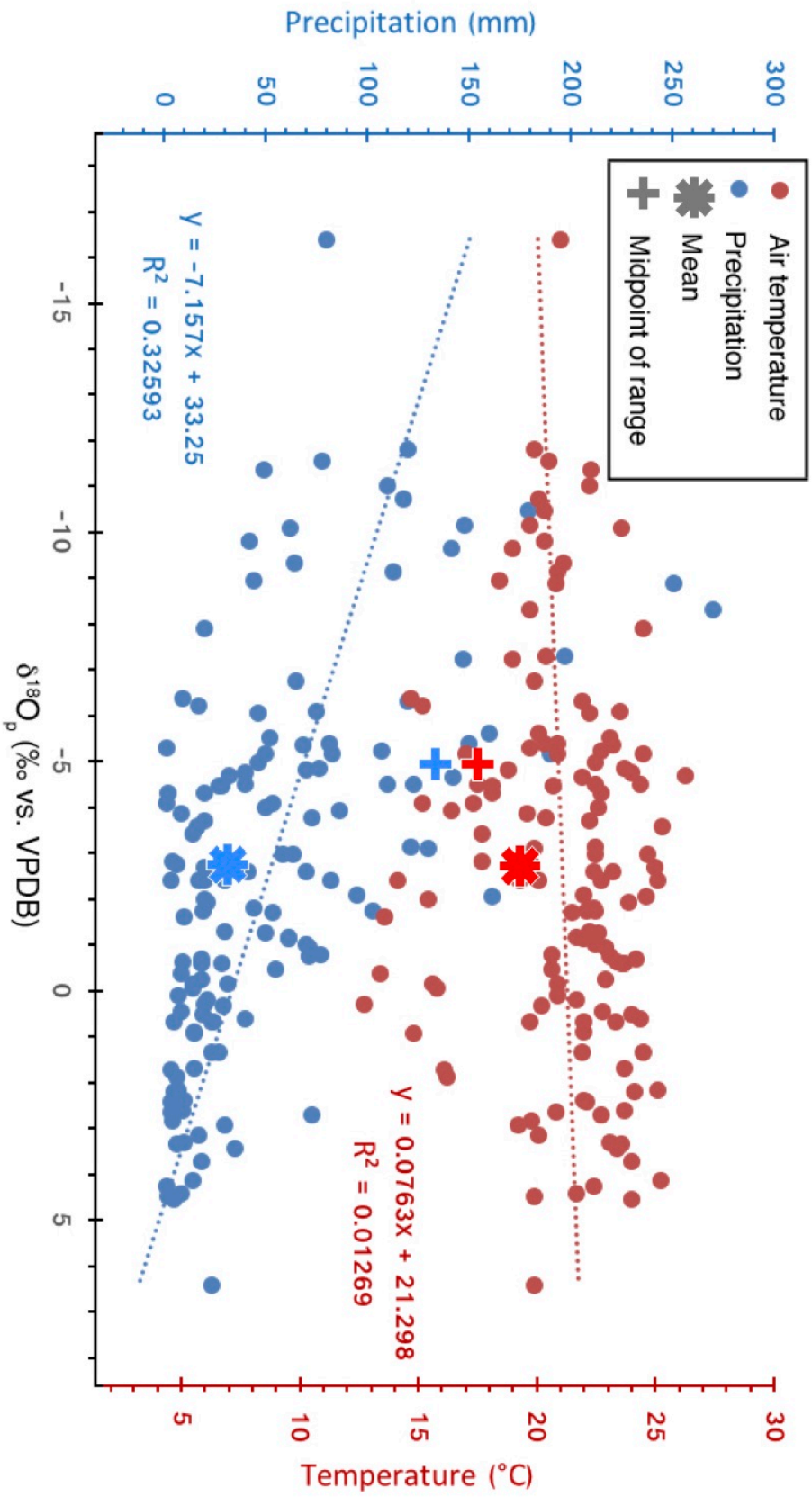
Precipitation (mm)
300
250
200
150
100
50
0
Air temperature
Precipitation
Mean
Midpoint of range
y = -7.157x + 33.25
R² = 0.32593
y = 0.0763x + 21.298
R² = 0.01269
δ18Op (‰ vs. VPDB)
-15
-10
-5
0
5
Temperature (°C)
5
10
15
20
25
30

**Figure 2.4**. Plot of $\delta^{18}O$ of rainfall at Windhoek, Namibia (horizontal axis) plotted against amount of rainfall (left vertical axis) and atmospheric temperature (right vertical axis). Note that winter months have commonly no rainfall (Namibia Weather, 2016; IAEA/WMO, 2014), thus the $\delta^{18}O$ values presented here are values for summer precipitation. Each filled circle represents one month between 1961 and 1987, with additional monthly data from 1999-2000. Additional symbols show means and midpoints for two arrays of data (precipitation-$\delta^{18}O$ and temperature-$\delta^{18}O$). In blue, an amount effect (smaller $\delta^{18}O$ with greater rainfall) seems evident from the value of $r^2$ and from the position of the mean relative to the midpoint (see text for discussion). In red, a less pronounced temperature effect (greater $\delta^{18}O$ with higher temperature) is suggested by the position of the mean of data in the direction of higher temperature and greater $\delta^{18}O$ relative to the midpoint of the ranges of those parameters. Data are from IAEA/WMO (2014).

## 2.5. Discussion

### 2.5.1. Interpretation of Stalagmite DP1's multiple proxies

*Oxygen isotopes.* The $\delta^{18}O$ of stalagmite $CaCO_3$ reflects the $\delta^{18}O$ of the dripwater and the temperature in the cave (Hoefs, 1997). Temperature inside a cave usually represents the mean annual atmospheric temperature (McDermott, 2004). Thus its effect is minor on speleothem $\delta^{18}O$ compared to the effect of water. However, long term changes in atmospheric temperature could be expected to leave signals in speleothem $\delta^{18}O$ (see for example the trend in Figure 2.5).

In contrast, dripwater $\delta^{18}O$ is determined by $\delta^{18}O$ of atmospheric precipitation and its subsequent evaporation, both during precipitation events (Lee et al., 2012) and thereafter (Cuthbert et al., 2014). The $\delta^{18}O$ of atmospheric precipitation is in turn controlled by the $\delta^{18}O$ of the vapor source, the distance of transport from the source (the "continent effect" resulting from Rayleigh distillation), the amount of precipitation (the "amount effect"), and the atmospheric temperature during precipitation (the "temperature effect") (McDermott, 2004; Lachniet, 2009; Dansgaard, 1964, Rozanski et al., 1993, Kurita et al., 2009).

In Namibia, precipitation occurs almost exclusively in summer (Namibia Weather, 2016), and $\delta^{18}O$ is influenced by changes in amount of summer rainfall, with more negative values in wetter months and more positive values in drier months (Figure 2.4). This relationship between $\delta^{18}O$ and monthly rainfall in Namibia appears very similar to the amount effect defined by Dansgaard (1964, p. 445). However, Dansgaard (1964, p. 445) attributed the amount effect to differing degrees of cooling in the atmosphere, to differing

amounts of falling water in the atmosphere, and to evaporation from falling raindrops (as was documented by Lee et al., 2012). Namibia's semi-arid climate suggests that evaporation from falling raindrops may indeed be important in determining $\delta^{18}O_w$ of rainfall. However, the rainfall-$\delta^{18}O_w$ relationship in Namibia may be additionally and perhaps better ascribed to varying latitudinal migration of the ITCZ during austral summers. That is because monsoonal air is moister, lessening evaporation from falling raindrops during each rain event while allowing more rain events and thus more rainfall in months when the ITCZ is present.

In addition to evaporation from falling raindrops (Lee et al., 2012), evaporation outside or within the cave additionally leads to higher $\delta^{18}O_w$ values of soil water and dripwater and thus ultimately to higher $\delta^{18}O_c$ values of spelean $CaCO_3$ (e.g. Fleitmann et al., 2007; Cuthbert et al., 2014; Deininger et al., 2012).

*Carbon isotopes.* The $\delta^{13}C$ of stalagmite carbonate is determined by the $\delta^{13}C$ of the total dissolved inorganic carbon of the dripwater. This variable is in turn controlled by a number of factors (e.g. Quade, 2004; Brook et al., 2006; Wong and Breecker, 2015). First is the $\delta^{13}C$ of atmospheric $CO_2$. It is known to have changed because of the Suess effect (Suess, 1955; Verburg, 2007) wherein burning of fossil fuels has added $^{13}C$-poor $CO_2$ to the atmosphere. For some comparisons, we have used the equation of Verburg (2007) to correct our $\delta^{13}C$ data from Stalagmite DP1 for the Suess effect, but the change is small compared to the variability of $\delta^{13}C$ in the stalagmite (Figure A2). Second is the biological input through roots and/or decay of plant matter in soil. High input of soil $CO_2$ could

decrease the speleothem $\delta^{13}C$ values during wetter and warmer seasons (e.g., Hesterberg and Siegenthaler, 1991; Lauritzen and Lundberg, 1999; Baldini et al., 2005). Third is the flow conditions above the cave that could decrease (open system) or increase (closed system) the $\delta^{13}C$ values (e.g., Clark and Fritz, 1997; Fairchild and Baker, 2012). An open system reflects a longer residence time of the percolating water, allowing it to exchange $CO_2$ with the soil. A closed system reflects a shorter residence time of the percolating water before reaching the cave, and this is often the case with less vegetation cover and/or with less soil bioproductivity (e.g. Brook et al., 2006; 2015). Fourth is degassing. After passage of water through the soil and bedrock, degassing to the cave atmosphere occurs because of the difference in $pCO_2$ between the cave dripwater and the $pCO_2$ of the cave atmosphere, and the result is an increase in $\delta^{13}C$ (Dreybrodt and Scholz, 2011). Degassing depends on the soil biological activity (e.g. Dreybrodt and Scholz, 2011), but it can also depend on cave ventilation (e.g. James et al., 2015). The fifth and last factor is "prior calcite precipitation" or more broadly "prior carbonate precipitation" (PCP). It can result in an increase in speleothem $\delta^{13}C$ in response to Rayleigh-type enrichment in $^{13}C$ with progressive degassing (e.g. Mickler et al., 2004; Oster et al., 2010) prior to calcite deposition on the speleothem. The effect of PCP is also more likely during drier times when saturation states are higher and cave $PCO_2$ may be lower (e.g. Johnson et al., 2006; Cross et al., 2015).

The dependence of soil biological activity, extent of degassing, and PCP on wetness and thus rainfall combine to suggest that greater $\delta^{13}C$ of stalagmite carbonate is typically an indicator of drier conditions (e.g. Johnson et al., 2006; Cross et al., 2015). The linkage

of $\delta^{13}C$ of Stalagmite DP1 to rainfall is further supported by the historical relationship between vegetation distribution and spatial distribution of rainfall in inland Namibia (Rohde and Hoffman, 2012).

*Mineralogy and petrography.* The deposition of spelean aragonite rather than calcite is largely affected by temperature (Moore, 1956; Railsback et al., 1994) and trace or minor element composition of the dripwater (Fischbeck, 1976; González and Lohmann, 1988; Railsback et al., 1994; Caddeo et al., 2011; Riechelman et al., 2014), which can in turn be a function of bedrock lithology and PCP (Riechelman et al., 2014). However, because drier conditions lead to higher saturation states and (concomitantly) more extensive PCP, deposition of aragonite is most commonly linked to drier conditions (Murray, 1954; Pobeguin, 1965; Siegel, 1965; Thrailkill, 1971; Cabrol and Coudray, 1982; Railsback et al. 1994; Frisia et al., 2002. In these regards, the overall higher $\delta^{18}O$ and $\delta^{13}C$ values of aragonite layers of Stalagmite DP1 suggests dryness, and the overall lower $\delta^{18}O$ and $\delta^{13}C$ values of calcite layers suggests wetness.

For petrography, Type E and Type L surfaces in Stalagmite DP1 are characterized by low and high $\delta^{18}O$, respectively (Figure 2.5). This agrees with the findings of Railsback et al. (2013), suggesting that Type E surfaces are indicative of exceptionally wet conditions, and Type L surfaces are indicative of exceptionally dry conditions.

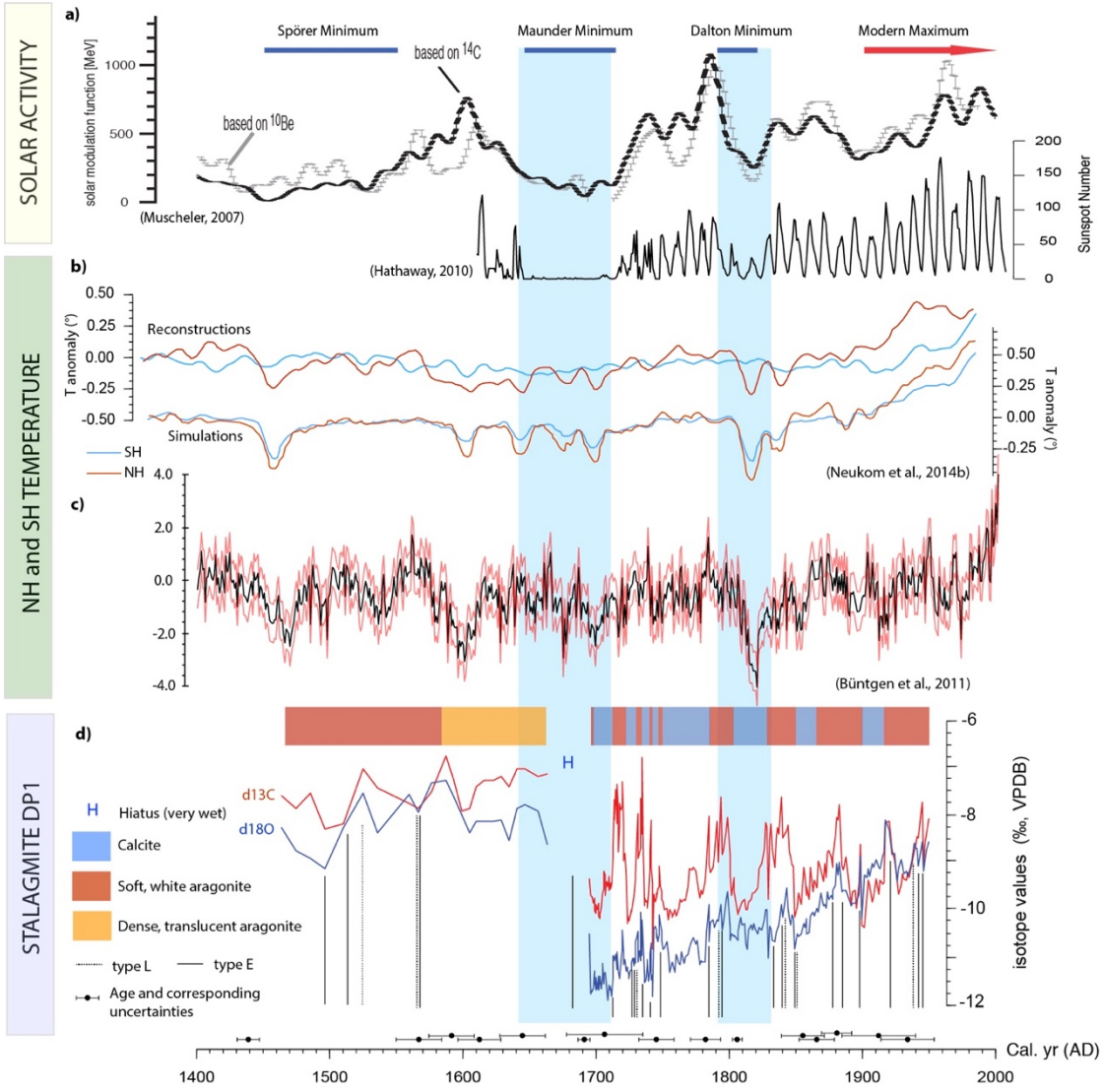
SOLAR ACTIVITY
NH and SH TEMPERATURE
STALAGMITE DP1
a)
Spörer Minimum
Maunder Minimum
Dalton Minimum
Modern Maximum
based on 14C
based on 10Be
solar modulation function [MeV]
1000
500
0
(Muscheler, 2007)
(Hathaway, 2010)
200
150
100
50
0
Sunspot Number
b)
T anomaly (°)
0.50
0.25
0.00
-0.25
-0.50
Reconstructions
Simulations
SH
NH
(Neukom et al., 2014b)
c)
4.0
2.0
0.0
-2.0
-4.0
(Büntgen et al., 2011)
d)
H
Hiatus (very wet)
Calcite
Soft, white aragonite
Dense, translucent aragonite
type L
type E
Age and corresponding uncertainties
d13C
d18O
-6
-8
-10
-12
isotope values (‰, VPDB)
1400
1500
1600
1700
1800
1900
2000
Cal. yr (AD)

Figure 2.5. Time series comparison. a) Time series of solar activity (Muscheler, 2007; Hathaway, 2010). b) Paleotemperature reconstructions and simulations from several records of the two hemispheres (Neukom et al., 2014b). c) The reconstruction of NH temperature from Büntgen et al. (2011). The black line is the best estimate, and uncertainty is shown in red. d) Mineralogical, stable isotope, and petrographic data from Stalagmite DP1. Vertical blue rectangles highlight significant wetting during solar minima (here the Maunder and the Dalton minimum) and intervals of colder NH temperatures relative to the Southern Hemisphere. These intervals coincide with wetter conditions in Dante Cave. The layer-bounding surfaces identified in Figure 3b are plotted as vertical lines.

***Summary.*** The four paleoenvironmental proxies reported from Stalagmite DP1 studied here agree with the generalization of Fairchild and McMillan (2007) that speleothems are indicators of wet and dry periods. Lower $\delta^{18}O$ and $\delta^{13}C$ values, calcite, and Type E surfaces combine to suggest wetter conditions. Higher $\delta^{18}O$ and $\delta^{13}C$ values, aragonite, and Type L surfaces combine to suggest drier conditions (Figure 2.5).

### 2.5.2. Paleoclimate significance inferred from Stalagmite DP1

The hiatus of ca. 1660-1690. One of the most striking features of the DP1 record is the hiatus of about thirty years in the late 1600s (Figure 2.3). That hiatus is required by an abrupt change in U-Th ages of 46 years in the interval from 238 to 234 mm from the top of the stalagmite, which is by far the most abrupt change of age in the series of U-Th ages from DP1. It coincides with a Type E surface that resulted from dissolutional corrosion, suggestive of exceptional wet conditions (Railsback et al., 2013), and it coincides with an abrupt shift of both $\delta^{18}O$ and $\delta^{13}C$ to more negative values, likewise suggestive of a transition to wetter conditions, as discussed above. We therefore conclude that the most parsimonious interpretation of the hiatus ca.1660-1690 is one of dissolution and non-deposition during an exceptionally wet period.

Wetter conditions in northeastern Namibia during low solar activity and cold intervals in Northern Hemisphere. The records from Stalagmite DP1 suggest that wet intervals in northeastern Namibia are linked to low solar activity and cold intervals in Northern Hemisphere (Figure 2.5). At ca. AD 1660-1710, the decrease in both $\delta^{18}O$ and $\delta^{13}C$, the presence of Type E surface at ca. 237 mm from the top of Stalagmite DP1, and

the abrupt change in growth rate (from 0.1 to 1.67 mm/yr) combine to suggest wetter conditions. This interval coincides with the Maunder minimum (Figure 2.5a) and a decreased temperature (specifically, colder NH relative to SH) in the global reconstructions (Neukom et al., 2014b; Figure 2.5b-c). At ca. AD 1790-1830, the decrease in $\delta^{18}O$ and $\delta^{13}C$, and the presence of a calcite layer bounded by Type E surfaces suggest another wetter period in northeastern Namibia. This younger interval coincides with the Dalton solar minimum and with the coldest period in the NH temperature reconstructions by Büntgen et al. (2011) and Neukom et al. (2014b) (Figure 2.5).

Long-term trends in $\delta^{18}O$ in DP1 from AD 1750 to 1950. Values of $\delta^{18}O$ in Stalagmite DP1 show an increasing trend from ca. AD 1750 to 1950 ($r^2$ = 0.82). The increase starts from ca. –11.8 to –8.5‰ (Figure 2.5). In contrast, there is no significant trend in $\delta^{13}C$ ($r^2$ = 0.02), even if those $\delta^{13}C$ data were transformed to account for the Suess effect using the equation of Verburg (2007) (Figure A2).

The $\delta^{18}O$ trend could be ascribed to a more northward migration of the ITCZ, when the NH is warmer (Figure 2.5; Neukom et al., 2014b), so that Namibia went from being on the fringes of the Tropics in the 18$^{th}$ century to being more arid and subtropical. This new climatic conditions in turn leads to reduced precipitation and drier austral summers, combining to increase the raindrop re-evaporation effect (Lee et al., 2012) and the extent of evaporation from the land surface. The coeval increase in global temperature and increase in stalagmite DP1 $\delta^{18}O$ after ca. 1715 (Figure 2.5) suggest that, although instrumental data show a weak relationship between $\delta^{18}O$ and temperature (Figure 4)

(IAEA/WMO, 2014), northeastern Namibia not only became drier but also could have become warmer.

### 2.5.3. Regional comparison

The wet interval observed between ca. AD 1660 and AD 1710 in northeastern Namibia is not a local event. Similar climatic response is observed in Cold Air Cave, South Africa (Holmgren et al. 1999; Sundqvist et al., 2013) (Figure 2.6). Although these authors mainly use $\delta^{18}O$ as a proxy for temperature reconstruction, their stable isotope records from two stalagmites, T5 and T7, from Cold Air Cave around AD 1650-1750 (Figure 4 of Holmgren et al., 1999, also see Sundqvist et al., 2013) could also suggest wetter conditions. These wet intervals commonly coincide with the Maunder solar minimum and with periods of globally cold climate, with colder NH relative to the SH (Figures 2.5 and 2.6). They collectively fall in the period of coldest temperatures in several locations around the world from AD 1570 to 1730 (Bradley and Jones, 1993). Wetter conditions in northeastern Namibia and in South Africa also coincide with the most extreme minimum in the time-averaged record of English instrumental records of temperature (AD 1690-1699) (Manley, 1974), with AD 1684, the coldest winter in English instrumental records of temperature (Manley, 2011).

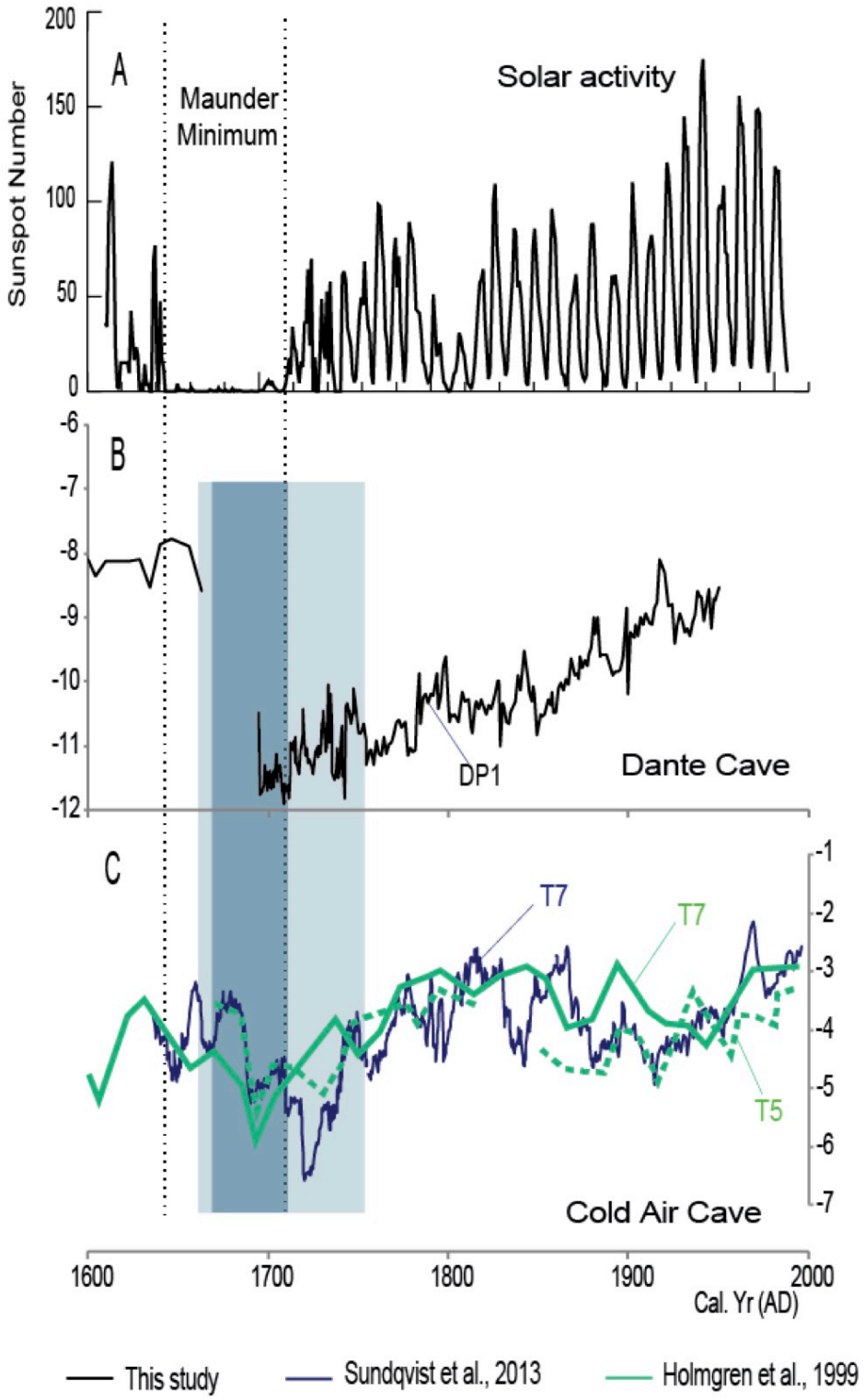
A
Maunder Minimum
Solar activity
Sunspot Number
200
150
100
50
0
B
-6
-7
-8
-9
-10
-11
-12
DP1
Dante Cave
C
T7
T7
T5
-1
-2
-3
-4
-5
-6
-7
Cold Air Cave
1600
1700
1800
1900
2000
Cal. Yr (AD)
This study
Sundqvist et al., 2013
Holmgren et al., 1999

Figure 2.6. Time series, regional comparison. A) Plot of solar activity (Hathaway, 2010). B) Stable isotopes of oxygen profile of Stalagmite DP1 from Dante Cave (this study). C) Stable isotopes of oxygen profile of Stalagmites T5 and T7 from Cold Air Cave (Sundqvist et al., 2013; Holmgren et al., 1999). The two dashed vertical lines represent the lower and upper limit of the Maunder minimum. The shaded area represents the estimated wetter interval in Dante and Cold Air Cave, with darker shade highlighting very wet interval within the Maunder sunspot minimum according to Stalagmite DP1, T5 and T7 records. Note that $\delta^{18}O$ in Dante Cave is more depleted than $\delta^{18}O$ in Cold Air Cave.

### 2.5.4. Global implications

Latitudinal migration of the ITCZ linked to solar activity and global conditions. Hydroclimate response in southern Africa to the latitudinal migration of the ITCZ is revealed in the paleorecords between AD 1400 and 1950. The wet intervals inferred from Stalagmite DP1 ca. AD 1660-1690 and ca.AD 1790-1830 in northeastern Namibia and the wet interval inferred from Stalagmite T5 and T7 from South Africa around AD 1700 coincides with solar minima and globally colder conditions, specifically a much cooler NH (Figure 2.5). This "solar activity-global temperature- rainfall" relationship is very similar to the findings of Sachs et al. (2009) in the Pacific Ocean between AD 1400 and 1850 during the LIA. Sachs et al. (2009) concluded that lesser solar irradiance, which could have caused the colder conditions in the NH (e.g. Mauquoy et al., 2002; Shindell et al., 2003), may have driven the ITCZ south. Thus, the wet interval in Namibia could be the result of a southward migration of the ITCZ (Peterson et al., 2000; Haug et al., 2001; Chiang et al., 2003; Koutavas and Lynch-Stieglitz, 2004; Chiang and Bitz, 2005; Broccoli et al., 2006; Sachs et al., 2009; Sinha et al., 2011; Schefuß et al., 2011; Chiang and Friedman, 2012; Arbuszewski et al, 2013; Donohoe et al., 2013).

In contrast, the drying trend since ca. AD 1750 inferred from Stalagmite DP1 in northeastern Namibia coincides with an overall higher solar activity and globally warmer conditions, when NH is warmer (Figure 2.5). This condition favors a northward migration of the ITCZ toward Earth's warmer hemisphere (Kang et al., 2008; McGee et al., 2014; Frierson and Hwang, 2012; Sachs et al., 2009).

The DP1 record suggests that specific sunspot minima (i.e. Maunder and Dalton) associated with a significant temperature gradient between the two hemispheres (i.e. cooler NH than SH) could have intensified rainy seasons in northeastern Namibia, parallel with a southward migration of the ITCZ. This southward migration of the ITCZ could have also affected the IOCZ. As a result, summer seasons in northeastern Namibia must have been wetter and could have lasted longer than they are today. In contrast, warming of the NH since the end of the LIA (Figure 2.5b) has driven the ITCZ northward, leading to shorter wet summer seasons and longer dry winter seasons in northeastern Namibia.

Estimates of the latitudinal shift of the ITCZ with NH cooling vary considerably, but they could be used to estimate the change in rainfall in northeastern Namibia during those extended wet periods. McGee et al. (2014) suggested a shift of at most 1° of latitude during the Last Glacial Maximum, whereas Sachs et al. (2009) inferred a shift during the LIA of as much as 500 km, or about 4.4° of latitude. In northern Namibia and southern Angola, rainfall increases northward at a rate of about 100 mm/yr per degree of latitude. In reference to this latitudinal variability of rainfall in Namibia, the estimates of McGee et al. (2014) and Sachs et al. (2009) would suggest increases of 100 to 440 mm/yr of rainfall respectively, which would be significant compared to the present rainfall of about 500 mm/yr at Dante Cave.

Possible movement of the Angola-Benguela Front accounting for wetter conditions in northern Namibia. The widely accepted notion of southward shifts of the ITCZ with cooling of the NH (Arbuszewski et al., 2013; Broccoli et al., 2006; Chiang and Bitz, 2005; Chiang and Friedman, 2012; Chiang et al., 2003; Haug et al., 2001; Donohoe et al., 2013;

Koutavas and Lynch-Stieglitz, 2004; Peterson et al., 2000; Sachs et al., 2009; Sinha et al., 2011; Schefuß et al., 2011) is understood as an atmospheric phenomenon: a southward shift of the convergence of the easterly trade winds. However, because of the significance of those easterly winds to low-latitude ocean circulation (e.g., Knauss, 1963), it seems likely that a southward shift of the ITCZ could lead to some southward shift of low-latitude currents. For example, with regard to the eastern tropical Atlantic, Li and Philander (1997) concluded that sea-surface temperature there varies seasonally as a "passive response of the ocean to the changes in the winds" and thus to seasonal change of the ITCZ. If that thought extends to the Angola Current, the coastal down-current expression of the Atlantic's Southern Equatorial Countercurrent (Figure 2.1), it suggests that the southern limit of the Angola Current at the Angola-Benguela Front may have shifted southward during southward shifts of the ITCZ (as it does seasonally). The southern limit of the Angola Current is relevant to rainfall in northern Namibia because southward advances of that warm current promote offshore evaporation that leads to more rainfall inland (Rouault et al., 2003), and the position of the Angola-Benguela front has been shown to vary interannually as well as seasonally (Colberg and Reason, 2007). Thus, the linkage between wet intervals in northeastern Namibia and the southward movement of the ITCZ inferred above, combined with the possible linkage of the southern limit of the Angola Current to the position of the ITCZ, suggests that rainfall in northeastern Namibia may have been

linked to changes in ocean currents resulting in an SST anomaly that favored rainfall on the continent.

*The isotopic shift at ca. 1680: change in cave hydrology*. The significant change in growth rate (from 0.1 to 1.67 mm/yr), the difference in isotopic values before and after ca. 1680, and the significant decrease in stable isotope values (of ca. 4‰ and 3‰ for $\delta^{18}O$ and $\delta^{13}C$, respectively) around ca. 1680, could represent a significant change in the cave hydrology linked to ITCZ and the ABF in northeastern Namibia. Climate in northeastern Namibia was drier prior to ca. AD 1680 as suggested by the stable isotope values and mineralogy (Figure 2.5), and it became wetter during the Maunder minimum. After the wet Maunder minimum, rainfall has receded. In this scenario, the alternating long-term and pronounced wet and dry periods agrees well with the north-south migration of the ITCZ.

*A different point of view*: possible changes in moisture flux before and after ca. 1680. The difference in isotopic signals in Stalagmite DP1 before and after ca. 1680 could also be linked to changes in moisture flux from the primary western Indian Ocean source and the secondary tropical SE Atlantic source that converge over northern Angola and southern Congo (Rouault et al., 2003). Moisture fluxes examination by Rouault et al. (2003) suggests that the size of rainfall anomalies in western Angola/Namibia is influenced by the local circulation anomaly imposed on the mean easterly from the western Indian Ocean. This local circulation anomaly seems to originate in tropical SE Atlantic (Rouault et al.,

2003). Although the $\delta^{18}O$ of the Indian Ocean and the Atlantic water only differs by ca. 2-3‰, the greater speleothem $\delta^{18}O$ values prior to ca. 1680 could suggest a dominance of moisture flux from a relatively near marine source, presumably the nearby Atlantic Ocean, which is today the source of $^{18}O$-rich rainfall ($\delta^{18}O_p$ = ~ –2 to –3‰; Bowen, 2013) to the Namib Desert along Namibia's Atlantic Coast, west of the IOCZ. This condition could be similar to the 1995 event, when SST anomaly in tropical SE Atlantic was largest but the inflow into Angola/Namibia from the Indian Ocean was weaker (Rouault et al., 2003). According to Jury and Engert (1999) this climatic condition is similar to an Atlantic El Niño, when summer rainfall over northern Namibia was 50% below normal. In contrast to a southward push of the ABF, climatic conditions in northeastern Namibia prior to ca. 1680 could have been linked to a northward push of the ABF by the cold Benguela current, resulting in much drier conditions over the region.

This condition immediately shifted at ca. 1660 with a southward push of the ITCZ and the ABF, as discussed above. At the same time, easterly flux from the Indian Ocean could have been enhanced. This new condition is similar to the 1984 and 1986 events discussed in Rouault et al. (2013). Thus the much lower $\delta^{18}O_c$ values after ca. 1680 may have resulted from transport from a more distant source, presumably the Indian Ocean, which is today the dominant source for more $^{18}O$-depleted ($\delta^{18}O_p$ = ~ –4 to –5‰; Bowen; 2013) rainfall to eastern Namibia, east of the IOCZ (Figure 2.1). This dominance of moisture flux from the Indian Ocean is supported by the more enriched values of speleothem $\delta^{18}O$

in Cold Air Cave, in South Africa (Holmgren et al. 1999; Sundqvist et al., 2013) and the more depleted speleothem $\delta^{18}O$ in Dante Cave, Namibia (Figure 6).

If this point of view on moisture flux is correct, it implies that hydrology over northeastern Namibia around the Maunder minimum was controlled by not only a southward shift in ITCZ and ABF, but also a strengthening of the easterly flux from the Indian Ocean.

## 2.6. Conclusions

Examination of the uppermost 261 mm of Stalagmite DP1 suggests that climate in northeastern Namibia responded to changes in solar activity and changes in global temperature. The record shows that not only the LIA in general, but specific sunspot minima, i.e. Maunder and Dalton, associated with a significant temperature gradient between the two hemispheres (i.e. cooler NH than SH) have driven the ITCZ and the IOCZ southwestward, and also have driven the ABF southward. As a result, wet summer seasons in northeastern Namibia could have lasted longer than they are today. In contrast, warming of the NH since the end of the LIA, estimated around AD 1715 in northeastern Namibia, has driven the ITCZ northeastward, leading to shorter wet summer seasons in favor of dry winter seasons in northeastern Namibia.

The practical significance of these conclusions lies in their implications for future changes in rainfall in northeastern Namibia and more generally in the summer rainfall zone of southern Africa (e.g. Niang et al., 2014; Thomas et al., 2005). Warming of climate in the coming century is predicted for Earth in general and especially for high-latitude regions of

the Northern Hemisphere (IPCC, 2013, Figure SPM.8). The correlation of past dry periods in northeastern Namibia with warmer conditions in the NH (both reported in this paper and in Sletten et al., 2013), and the inferred northward shift of the ITCZ toward a warmed NH, suggests that warming will lead to less rainfall in the future in a region with a presently semi-arid climate and will cause dune reactivation by 2099 (Thomas et al., 2005).

## REFERENCES


Arbuszewski JA, Demenocal PB, Cleroux C, et al. (2013) Meridional shifts of the Atlantic intertropical convergence zone since the Last Glacial Maximum. Nature Geoscience 6: 959-962.

Baldini JUL, McDermott F, Baker A, et al. (2005) Biomass effects on stalagmite growth and isotope ratios: A 20th century analogue from Wiltshire, England. Earth and Planetary Science Letters 240: 486-494.

Benthien A, Andersen N, Schulte S, et al. (2002) Carbon isotopic composition of the C37:2 alkenone in core top sediments of the: South Atlantic Ocean: Effects of $CO_2$ and nutrient concentrations. Global Biogeochemical Cycles 16(1): 1012. doi:10.1029/2001GB001433.

Bowen GJ, (2013) WaterIsotopes.org. Available at: http://wateriso.utah.edu/waterisotopes/index.html

Bradley R. (2000) 1000 years of climate change. Science 288: 1353-1355. Doi:10.1126/science.288.5470.1353.

Bradley RS and Jones PD (1993) “Little Ice Age” summer temperature variations: their nature and relevance to recent global warming trends. The Holocene 3,4: 367-376.

Broccoli AJ, Dahl KA and Stouffer RJ. (2006) Response of the ITCZ to Northern Hemisphere cooling. Geophysical Research Letters 33.

Brook GA, Ellwood BB, Railsback LB, et al. (2006) A 164 ka record of environmental change in the American Southwest from a Carlsbad Cavern speleothem. Palaeogeography Palaeoclimatology Palaeoecology 237: 483-507.

Brook GA, Scott L, Railsback LB, et al. (2009) A 35 ka pollen and isotope record of environmental change along the southern margin of the Kalahari from a stalagmite and animal dung deposits in Wonderwerk Cave, South Africa. Journal of Arid Environments 74: 870-884.

Brook, G.A., Railsback, L. B., Scott, L., et al. (2015) Late Holocene Stalagmite and Tufa Climate Records for Wonderwerk Cave: Relationships Between Archaeology and Climate in Southern Africa: African Archaeological Review 32(4), p. 1-32.

Brown ET and Johnson TC. (2005) Coherence between tropical East African and South American records of the Little Ice Age. Geochemistry Geophysics Geosystems 6.

Büntgen U, Tegel W, Nicolussi K, et al. (2011) 2500 Years of European Climate Variability and Human Susceptibility. Science 331: 578-582.

Burrough SL, Thomas DSG, Shaw PA, et al. (2007) Multiphase quaternary highstands at lake Ngami, Kalahari, northern Botswana. Palaeogeography Palaeoclimatology Palaeoecology 253: 280-299.

Cabrol P and Coudray J (1982) Climatic fluctuations influence the genesis and diagenesis of carbonate speleothems in southwestern France. National Speleological Society Bulletin 44, 112–117.

Caddeo GA, De Waele J, Frau F, et al. (2011) Trace element and stable isotope data from a flowstone in a natural cave of the mining district of SW Sardinia (Italy): evidence for $Zn^{2+}$-induced aragonite precipitation in comparatively wet climatic conditions. International Journal of Speleology 40: 181-190.

Chambers FM. (2015) The ‘Little Ice Age’: the first virtual issue of the Holocene. The Holocene, 1-3. DOI: 10.1177/0959683615593688

Chambers FM, Brain SA, Mauquoy D, et al. (2014) The 'Little Ice Age' in the Southern Hemisphere in the context of the last 3000 years: Peat-based proxy-climate data from Tierra del Fuego. The Holocene 24: 1649-1656.

Cheng H, Edwards RL, Hoff J, et al. (2000) The half-lives of uranium-234 and thorium-230. Chemical Geology 169, 17–33.

Chiang JCH and Bitz CM. (2005) Influence of high latitude ice cover on the marine Intertropical Convergence Zone. Climate Dynamics 25: 477-496.

Chiang JCH, Biasutti M and Battisti DS. (2003) Sensitivity of the Atlantic Intertropical Convergence Zone to Last Glacial Maximum boundary conditions. Paleoceanography 18.

Chiang JCH and Friedman AR. (2012) Extratropical Cooling, Interhemispheric Thermal Gradients, and Tropical Climate Change. Annual Review of Earth and Planetary Sciences 40: 383-412.

Clark ID and Fritz P. (1997) Environmental isotopes in hydrogeology: Lewis Publishers.

Colberg F and Reason CJC (2007) A model investigation of internal variability in the Angola Benguela Frontal Zone. Journal of Geophysical Research-Oceans 112, C7.

Cross M, McGee D, Broecker, WS, et al. (2015) Great Basin hydrology, paleoclimate, and connections with the North Atlantic: A speleothem stable isotope and trace element record from Lehman Caves, NV. Quaternary Science Reviews 127, 186–198.

Crowley TJ. (2000) Causes of climate change over the past 1000 years. Science 289: 270-277.

Cuthbert MO, Baker A, Jex CN., et al. (2014) Drip water isotopes in semi-arid karst: implications for speleothem paleoclimatology. Earth and Planetary Science Letters 395, 194-204.

Dansgaard W. (1964) Stable isotopes in precipitation. Tellus 16, 436–468.

Deininger M, Fohlmeister J, Scholz D, et al. (2012) Isotope disequilibrium effects: The influence of evaporation and ventilation effects on the carbon and oxygen isotope composition of speleothems - A model approach. Geochimica Et Cosmochimica Acta 96: 57-79.

Donohoe A, Marshall J, Ferreira D., et al. (2013) The relationship between ITCZ location and cross-equatorial atmospheric heat transport: from the seasonal cycle to the last glacial maximum. Journal of Climate 26: 3597–3618.

Dorale JA, Edwards RL, Alexander JrEC, et al. (2004) Uranium-series disequilibrium dating of speleothems: Current techniques, limits, and applications. In Mylroie J and Sasowsky ID (eds) Studies of Cave Sediments: Physical and Chemical Records of Paleoclimate: New York, Kluwer Academic/ Plenum Publishers, 177–197.

Dreybrodt W and Scholz D (2011) Climatic dependence of stable carbon and oxygen isotope signals recorded in speleothems: from soil water to speleothem calcite. Geochimica Et Cosmochimica Acta 75, 734–752.

Duan WH, Cai BG, Tan M, et al. (2012) The growth mechanism of the aragonitic stalagmite laminae from Yunnan Xianren Cave, SW China revealed by cave monitoring. Boreas 41: 113-123.

Dupont L, Behling H and Kim JH (2008) Thirty thousand years of vegetation development and climate change in Angola (Ocean Drilling Program Site 1078), Climate of Past Discussion 4: 111–147. doi:10.5194/cpd- 4-111-2008.

Edwards RL, Chen JH and Wasserburg GJ. (1987) U-238 U-234-Th-230-Th-232 Systematics and the Precise Measurement of Time over the Past 500000 Years. Earth and Planetary Science Letters 81: 175-192.

Fairchild IJ and Baker A. (2012) Speleothem Science: From Processes to Past Environments: Wiley-Blackwell.

Fairchild IJ and McMillan EA. (2007) Speleothems as indicators of wet and dry periods. International Journal of Speleology 36: 69-74.

Fischbeck, R. (1976): Mineralogie und Geochemie carbonatischer Ablagerungen in europäischen Höhlen - ein Beitrag zur Bildung und Diagenese von Speleothemen. Neues Jahrbuch für Mineralogie, Abhandlungen 126: 269-291

Fleitmann D, Burns SJ, Mangini A, et al. (2007) Holocene ITCZ and Indian monsoon dynamics recorded in stalagmites from Oman and Yemen (Socotra). Quaternary Science Reviews 26: 170-188.

Florenchie P, Lutjeharms JRE, Reason CJC, et al. (2003) The source of Benguela Ninos in the South Atlantic Ocean. Geophysical Research Letters 30.

Folland CK, Karl TR and Vinnikov KY (1990) Observed climate variations and change. The IPCC Scientific Assessment. Cambridge University Press, Cambridge: 194-238.

Frierson DMW and Hwang YT. (2012) Extratropical Influence on ITCZ Shifts in Slab Ocean Simulations of Global Warming. Journal of Climate 25: 720-733.

Frisia S, Borsato A, Fairchild IJ, et al. (2002) Aragonite–calcite relationships in speleothems (Grotte de Clamouse, France): environment, fabrics, and carbonate geochemistry. Journal of Sedimentary Research 772: 687-699.

González LA and Lohmann KC (1988) Controls on mineralogy and composition of spelean carbonates: Carlsbad Caverns, New Mexico. In: James NP and Choquette PW (eds.), Paleokarst. Springer-Verlag, New York: 81–101.

Hathaway DH. (2010) The Solar Cycle. Living Reviews in Solar Physics 7.

Haug GH, Hughen KA, Sigman DM, et al. (2001) Southward migration of the intertropical convergence zone through the Holocene. Science 293: 1304-1308.

Hesterberg R and Siegenthaler U. (1991) Production and Stable Isotopic Composition of Co2 in a Soil near Bern, Switzerland. Tellus Series B-Chemical and Physical Meteorology 43: 197-205.

Hoefs, J. (1997) Stable Isotope Geochemistry (fourth edition). Berlin, Springer, 201 p.

Holmgren K, Karlen W, Lauritzen SE, et al. (1999) A 3000-year high-resolution stalagmite-based record of palaeoclimate for northeastern South Africa. The Holocene 9: 295-309.

IAEA/WMO (2014) Global Network of Isotopes in Precipitation. The GNIP Database.

IPCC (2013) Summary for Policymakers. In: Stocker TF, Qin D, Plattner GK, et al. (eds.) Climate Change 2013: The Physical Science Basis. Contribution of Working Group I to the Fifth Assessment Report of the Intergovernmental Panel on Climate Change: Cambridge University Press, Cambridge, United Kingdom and New York, NY, USA.

Irish J, Marais E, Juberthie C, et al. (2001) Namibia. Encyclopedia Biospeologica: 1639–1650.

James E W, Banner JL and Hardt B (2015), A global model for cave ventilation and seasonal bias in speleothem paleoclimate records, Geochemistry, Geophysics, Geosystem 16: 1044– 1051, doi:10.1002/2014GC005658.

Johnson KR, Hu C, Belshaw NS, et al. (2006) Seasonal trace-element and stable-isotope variations in a Chinese speleothem: The potential for high-resolution paleomonsoon reconstruction. Earth and Planetary Science Letters 244: 394–407.

Jury MR and Engert S. (1999) Teleconnections modulating inter-annual climate variability over northern Namibia. International Journal of Climatology 19: 1459-1475.

Kang SM, Held IM, Frierson DMW, et al. (2008) The response of the ITCZ to extratropical thermal forcing: Idealized slab-ocean experiments with a GCM. Journal of Climate 21: 3521-3532.

Kim ST, O'Neil JR, Hillaire-Marcel C, et al. (2007) Oxygen isotope fractionation between synthetic aragonite and water: Influence of temperature and Mg2+ concentration. Geochimica Et Cosmochimica Acta 71: 4704-4715.

Knauss JA (1963) Equatorial current systems. In: Hill MN (eds) The Sea: Interscience, New York, 235-252.

Koutavas A and Lynch-Stieglitz J. (2004) Variability of the marine ITCZ over the eastern Pacific during the past 30,000 years - Regional perspective and global context. Hadley Circulation: Present, Past and Future 21: 347-369.

Kurita N, Ichiyanagi K, Matsumoto J, et al. (2009) The relationship between the isotopic content of precipitation and the precipitation amount in tropical regions. Journal of Geochemical Exploration 102: 113-122.

Lachniet MS. (2009) Climatic and environmental controls on speleothem oxygen-isotope values. Quaternary Science Reviews 28: 412-432.

Lauritzen SE and Lundberg J. (1999) Speleothems and climate: a special issue of The Holocene. The Holocene 9: 643-647.

Lee JE, Risi C, Fung I, et al. (2012) Asian monsoon hydrometeorology from TES and SCIAMACHY water vapor isotope measurements and LMDZ simulations: Implications for speleothem climate record interpretation. Journal of Geophysical Research-Atmospheres 117.

Leech PJ, Lynch-Stieglitz J and Zhang R. (2013) Western Pacific thermocline structure and the Pacific marine Intertropical Convergence Zone during the Last Glacial Maximum. Earth and Planetary Science Letters 363: 133-143.

Li T and Philander SGH (1997) On the Seasonal Cycle of the Equatorial Atlantic Ocean. Journal of Climate 10: 813-817.

McDermott F. (2004) Palaeo-climate reconstruction from stable isotope variations in speleothems: a review. Quaternary Science Reviews 23: 901-918.

McGee D, Donohoe A, Marshall J, et al. (2014) Changes in ITCZ location and cross-equatorial heat transport at the Last Glacial Maximum, Heinrich Stadial 1, and the mid-Holocene. Earth and Planetary Science Letters 390: 69-79.

Manley G (1974) Central England temperatures: monthly means 1659 to 1973. Quarterly Journal of the Royal Meteorological Society 100, 389–405.

Manley G (2011) 1684: The coldest winter in the english instrumental record. Weather 30: 382–388.

Mann ME. (2002) Little Ice Age. In: MacCracken MC and Perry JS (eds) The Earth system: physical and chemical dimensions of global environmental change. John Wiley & Sons, Ltd, 504-509.

Mann ME, Zhang ZH, Rutherford S, et al. (2009) Global Signatures and Dynamical Origins of the Little Ice Age and Medieval Climate Anomaly. Science 326: 1256-1260.

Mauquoy D, Van Geel B, Blaauw M et al. (2002) Evidence from North-West European bogs shows 'Little Ice Age' climatic changes driven by variations in solar activity. The Holocene 12: 1–6.

Mendelsohn J, Jarvis A, Roberts C, et al. (2002) The Atlas of Namibia: a Portrait of the Land and Its People. David Phillip Publishers, Cape Town.

Mickler PJ, Banner JL, Stern L, et al. (2004) Stable isotope variations in modern tropical speleothems: Evaluating equilibrium vs. kinetic isotope effects. Geochimica Et Cosmochimica Acta 68: 4381-4393.

Miller RMCG (1983) The Pan-African Damara Orogen of Namibia. In: Miller RMCG (ed.), Evolution of the Damara Orogen of South West Africa/Namibia: Special Publication of the Geological Society of South Africa 11: 431–515.

Moore GW (1956) Aragonite speleothem as indicators of paleotemperature: American Journal of Science 254: 746-753.

Moy CM, Dunbar RB, Moreno PI, et al. (2008) Isotopic evidence for hydrologic change related to the westerlies in SW Patagonia, Chile, during the last millennium. Quaternary Science Reviews 27: 1335-1349.

Murray JW (1954) The deposition of calcite and aragonite in caves. Journal of Geology 62, 481–492.

Muscheler R, Joos F, Beer J, et al. (2007) Solar activity during the last 1000 yr inferred from radionuclide records. Quaternary Science Reviews 26: 82-97.

Namibia Weather (2016) Rain history for Windhoek between 1891 and 2011: Monthly Precipitation Totals (mm) for Windhoek. Available at http://weather.namsearch.com/Windhoekrainhistory.php (Accessed 6 June 2016)

Nash DJ and Endfield GH. (2008) 'Splendid rains have fallen': links between El Nino and rainfall variability in the Kalahari, 1840-1900. Climatic Change 86: 257-290.

Neukom R and Gergis J. (2012) Southern Hemisphere high-resolution palaeoclimate records of the last 2000 years. Holocene 22: 501-524.

Neukom R, Nash DJ, Endfield GH, et al. (2014a) Multi-proxy summer and winter precipitation reconstruction for southern Africa over the last 200 years. Climate Dynamics 42: 2713-2726.

Neukom R, Gergis J, Karoly DJ, et al. (2014b) Inter-hemispheric temperature variability over the past millennium. Nature Climate Change 4: 362-367.

Neukom R, Nash DJ, Endfield GH, et al. (2013) Multi-proxy summer and winter precipitation reconstruction for southern Africa over the last 200 years. Climate Dynamic. doi: 10.1007/ s00382-013-1886-6.

Niang I, Ruppel OC, Abdrabo MA, et al. (2014). Africa. In: Barros VR, Field CB, Dokken DJ, et al. (eds.) Climate Change 2014: Impacts, Adaptation, and Vulnerability. Part B: Regional Aspects. Contribution of Working Group II to the Fifth Assessment Report of the Intergovernmental Panel on Climate Change. Cambridge University Press, Cambridge, United Kingdom and New York, NY, USA, pp. 1199-1265.

Nicholson SE. (2009) A revised picture of the structure of the "monsoon" and land ITCZ over West Africa. Climate Dynamics 32: 1155-1171.

Nicholson, S. E., and D. Entekhabi, The nature of rainfall variability in equatorial and southern Africa: Relationships with SST along the south- western coast of Africa, J. Clim. Applied Meteorol., 26, 561–578, 1987.

Nicholson SE, Nash DJ, Chase BM, et al. (2013) Temperature variability over Africa during the last 2000 years. The Holocene 23: 1085-1094.

Oster JL, Montanez IP, Guilderson TP, et al. (2010) Modeling speleothem delta C-13 variability in a central Sierra Nevada cave using C-14 and Sr-87/Sr-86. Geochimica Et Cosmochimica Acta 74: 5228-5242.

Paul D and Skrzypek G (2007) Assessment of carbonate-phosphoric acid analytical technique performed using GasBench II in continuous flow isotope ratio mass spectrometry. International Journal of Mass Spectrometry 262: 180-186.

Peterson L, Haug G, Hughen K, et al. (2000) Rapid changes in the hydrologic cycle of the tropical Atlantic during the last glacial. Science 290: 1947–1951.

Pobeguin T (1965) Sur les concretions calcaires Observées dans la Grotte de Moulis (Ariège). Société Géologique de la France, Compte Rendu 241: 1791–1793.

Quade J (2004) Isotopic records from ground-water and cave speleothem calcite in North America. In: Gillespie, A., Porter, S. C., Atwater, B.F. (eds.), Developments in Quaternary Science 1. Elsevier Science, New York: 205–219.

Railsback, L.B. (2000) Atlas of Speleothem Microfabrics. Available at: www.gly.uga.edu/railsback/speleoatlas/SAindex1.html. (Accessed 15 January 2016)

Railsback LB, Akers PD, Wang LX, et al. (2013) Layer-bounding surfaces in stalagmites as keys to better paleoclimatological histories and chronologies. International Journal of Speleology 42: 167-180.

Railsback LB, Brook GA, Chen J, et al. (1994) Environmental Controls on the Petrology of a Late Holocene Speleothem from Botswana with Annual Layers of Aragonite and Calcite. Journal of Sedimentary Research Section a-Sedimentary Petrology and Processes 64: 147-155.

Railsback LB, Xiao HL, Liang FY, et al. (2014) A stalagmite record of abrupt climate change and possible Westerlies-derived atmospheric precipitation during the Penultimate Glacial Maximum in northern China. Palaeogeography Palaeoclimatology Palaeoecology 393: 30-44.

Riechelmann S, Schröder-Rtizrau A, Wassenburg JA, et al. (2014) Physicochemical characteristics of drip waters: Influence on mineralogy and crystal morphology of recent cave carbonate precipitates. Geochimica et Cosmochimica Acta 145: 13–29.

Rohde RF and Hoffman MT. (2012) The historical ecology of Namibian rangelands: Vegetation change since 1876 in response to local and global drivers. Science of the Total Environment 416: 276-288.

Romanek CS, Grossman EL and Morse JW. (1992) Carbon Isotopic Fractionation in Synthetic Aragonite and Calcite - Effects of Temperature and Precipitation Rate. Geochimica Et Cosmochimica Acta 56: 419-430.

Rouault M, Florenchie P, Fauchereau N, et al. (2003) South east tropical Atlantic warm events and southern African rainfall. Geophysical Research Letters 30: 8009. doi:10.1029/2002GL014840.

Rouault M (2012) Bi-annual intrusion of tropical water in the northern Benguela upwelling. Geophysical Research Letters 39: L12606. doi:10.1029/2012GL052099

Rozanski K, Araguas-Araguas L and Gonfiantini R (1993) Isotopic patterns in modern global precipitation. In: Swart PK et al. (eds.), Climate Change in Continental Isotopic Record: American Geophysical Union Monograph 78: 1–36.

Russell JM and Johnson TC. (2005) Late Holocene climate change in the North Atlantic and equatorial Africa: Millennial-scale ITCZ migration. Geophysical Research Letters 32.

Sachs JP, Sachse D, Smittenberg RH, et al. (2009) Southward movement of the Pacific intertropical convergence zone AD 1400-1850. Nature Geoscience 2: 519-525.

Schefuß E, Kuhlmann H, Mollenhauer G, et al. (2011) Forcing of wet phases in southeast Africa over the past 17,000 years. Nature 480: 509-512.

Schneider T, Bischoff T and Haug GH. (2014) Migrations and dynamics of the intertropical convergence zone. Nature 513: 45-53.

Scholz D and Hoffmann D (2011) StalAge – an algorithm designed for construction of speleothem age models. Quaternary Geochronology 6: 369–382.

Shen CC, Edwards RL, Cheng H, et al. (2002) Uranium and thorium isotopic and concentration measurements by magnetic sector inductively coupled plasma mass spectrometry. Chemical Geology 185: 165–178.

Shindell DT, Schmidt GA, Miller RL, et al. (2003) Volcanic and solar forcing of climate change during the preindustrial era. Journal of Climate 16: 4094-4107.

Siegel FR (1965) Aspects of calcium carbonate deposition in Great Onyx Cave, Kentucky. Sedimentology 4: 285–299.

Sinha A, Stott L, Berkelhammer M, et al. (2011) A global context for megadroughts in monsoon Asia during the past millennium. Quaternary Science Reviews 30: 47-62.

Skrzypek G and Paul D (2006) $\delta^{13}C$ analyses of calcium carbonate: comparison between the GasBench and elemental analyzer techniques. Rapid Communication Mass Spectrometry 20: 2915-2920, doi: 10.1002/rcm.2688.

Sletten HR, Railsback LB, Liang F, et al. (2013) A petrographic and geochemical record of climate change over the last 4600 years from a northern Namibia stalagmite, with evidence of abruptly wetter climate at the beginning of southern Africa's Iron Age. Palaeogeography Palaeoclimatology Palaeoecology 376: 149-162.

Suess HE (1955) Radiocarbon concentration in modern wood. Science 122:415–417

Sundqvist HS, Holmgren K, Fohlmeister J, et al. (2013) Evidence of a large cooling between 1690 and 1740 AD in southern Africa. Scientific Reports 3.

Thomas D, Knight M and Wiggs G (2005) Remobilization of southern African desert dune systems by twenty-first century global warming. Nature 435: 1218-1221.

Thrailkill J (1971) Carbonate deposition in Carlsbad Caverns. Journal of Geology 79: 683–695.

Usoskin IG, Solanki SK, Schussler M, et al. (2003) Millennium-scale sunspot number reconstruction: Evidence for an unusually active Sun since the 1940s. Physical Review Letters 91.

Usoskin I.G., Solanki S.K., Kovaltsov G. A. (2007) Grand minima and maxima of solar activity: new observational constraints. Astron. Astrophys. 471:301–309, doi:10.1051/0004-6361:20077704.

Van Heerden J and Taljaard JJ (1998) Africa and surrounding waters. In: Koroly DJ and Vincent DG (eds.), Meteorology of the Southern Hemisphere: Meteorological Monographs of the American Meteorological Society 27:141–174.

Veitch, J, Florenchie P and Shillington F (2006) Seasonal and interannual fluctuations of the Angola-Benguela frontal zone (ABFZ) using 4.5 km resolution satellite imagery from

1982 to 1999, International Journal of Remote Sensing 27: 987–998. doi:10.1080/01431160500127914.

Verburg P (2007) The need to correct for the Suess effect in the application of d13C in sediment in autotrophic Lake Tanganyika, as a productivity proxy in the anthropocene. Journal of Paleolimnololgy 37: 591–602.

Wong CI and Breecker DO (2015) Advancements in the use of speleothems as climate archives. Quaternary Science Reviews 127: 1–18.

Yan H, Wei W, Soon W, et al. (2015) Dynamics of the intertropical convergence zone over the western Pacific during the Little Ice Age. Nature Geoscience 8: 315-320.

# CHAPTER 3

## MULTIPLE PROXY ANALYSES OF A U/TH-DATED STALAGMITE TO RECONSTRUCT PALEOENVIRONMENTAL CHANGES IN NORTHWESTERN MADAGASCAR BETWEEN 370 CE AND 1300 CE[3]

[3] Voarintsoa, N.R. G., Wang, L., Railsback, L.B., Brook, G.A., Liang, F., Cheng, H., Edwards, R.L. Palaeogeography, Palaeoclimatology, Palaeoecology, 2017, v. 469, 138-155. http://dx.doi.org/10.1016/j.palaeo.2017.01.003

Reprinted here with permission of the publisher [Elsevier, 2017]

## ABSTRACT

The timing and causes of paleoenvironmental changes in Madagascar have been debated, specifically in respect to human activity following the settlement in the late Holocene. Here we present $\delta^{18}O$, $\delta^{13}C$, layer-bounding surfaces, layer-specific width, mineralogy, and distribution of macroholes from Stalagmite MA3 from Anjohibe Cave to provide a detailed understanding of the paleoenvironmental changes in northwestern Madagascar between AD 370 and AD 1300. The stable isotope records of Stalagmite MA3 are compared with stable isotope records of Stalagmites ANJ94-5 and MA2.

Detailed examination of the proxies suggests three distinct intervals of changes. (1) Prior to AD 795, changes in vegetation seem to have responded to changes in monsoonal rainfall linked to the relative position of the ITCZ. The period between ca. AD 755 and 795 was the driest, and the Stalagmite MA3 record is consistent with sediment records (pollen and lithology) from Lake Mitsinjo, northwestern Madagascar, and with sediment records (fossil pollen and charcoal) from Sainte Luce, southeastern Madagascar. (2) Between AD 795 and 870, the environmental conditions became more favorable, when vegetation recovered from the driest interval. The new conditions must have been suitable for community development in the region as suggested by archaeological evidence around Lake Mitsinjo and the Boeny region, and the establishment of the stone town of Mahilaka. (3) After AD 870, a gradational change in plant communities from $C_3$ to $C_4$ marks the record until around AD 1130, after which vegetation was dominated by $C_4$ plants. This change cannot be explained by climate alone, as there is no clear relationship in the climate-

sensitive proxies. Instead, it could have been caused by “Tavy”, a variety of “swidden” agriculture practiced in the region.

## 3.1. Introduction

The late Holocene paleoenvironmental history of Madagascar, an island located ca. 400-500 kilometers east of Africa, has become an interesting subject of scientific investigation because its ecosystem is very dynamic and paleo-records are still scarce (e.g. Burney et al., 2004; Virah-Sawmy et al., 2010; Dewar and Richards, 2012; Douglass and Zinke, 2015). Records from Madagascar help us better understand its own paleoenvironmental change and will potentially complete gaps in paleoclimate reconstruction in the Southern Hemisphere, such as understanding the dynamics of the Inter-Tropical Convergence Zone (ITCZ). Madagascar is particularly interesting because the timing of a major loss from its ecosystem, e.g. its large animals, seems to coincide with the timing of human arrival (e.g. see Table 1 of Virah-Sawmy et al., 2010; MacPhee and Burney, 1991; Burney et al., 1997c; Crowley, 2010; Crowley et al., 2010). Evidence suggests that human settlement of Madagascar could have started in the mid-Holocene, around 4-5 ka B.P. (Dewar, 2014), but paleo-records indicating island-wide human presence are dated around 2000 B.C (e.g. Dewar et al., 2013; Burney et al., 2004), and large-scale African and Asian (mostly Indonesian) seafarers did not occur until ca. AD 200–500 (Cox et al., 2012; Thompson et al., 2011; Tyson, 2013). Those maritime traders introduced new crops (e.g. Beaujard, 2011; Crowther et al., 2016). Although the timing for this human settlement poses some ambiguity, (e.g. Burney et al., 1987a; MacPhee and Burney, 1991; Godfrey and

Jungers, 2003; Virah-Sawmy et al., 2010; Gommery et al., 2011; Cox et al., 2012; Dewar et al., 2013), several authors have concluded that various human impacts and natural factors, such as desiccation, could have interacted synergistically to produce the megafaunal collapse (e.g. Burney and MacPhee, 1988; MacPhee and Burney, 1991; Burney, 1993a, b; Godfrey and Jungers, 2003; Burns et al., 2016; Crowley et al., 2016). Similarly, more than 70% of Madagascar's surface is covered by $C_4$ savannah and grasslands (e.g. Thompson et al., 2011; MEF, 2014), the cause of which has been a subject of debate. Earlier authors argued for an anthropogenic origin (e.g. Humbert, 1927; Lavauden, 1931; Perrier de la Bâthie, 1921); whereas recent researchers argued for non-anthropogenic origins (e.g. Burney, 1987a; 1987b; Willis et al., 2008; Bond et al., 2008).

Although the causal factors of Madagascar's ecosystem changes and the first timing of human settlement on the island are still a subject for debate, much remains to be learned about how the processes and changes of climate and environment are recorded in Madagascar's paleoclimate archives. Understanding such processes using proxies is key to making better inferences about the likely changes of Madagascar's environment in the past. Here we investigate stalagmites. Stalagmites provide a unique opportunity to study paleoclimate in greater detail because they can be accurately dated (e.g. Edwards et al., 1987; Dorale et al., 2004), they contain several proxies that have been shown to be very useful indicators of continental change in climate (e.g. Fairchild and Baker, 2012, p. 9–10), and their isotopic records are replicable (e.g. Burns et al., 2016).

In this study, we combine six proxies from Stalagmite MA3, from Anjohibe Cave, to reconstruct both paleoclimate and paleovegetation in northwestern Madagascar between

AD 370 and AD 1300. We use $\delta^{18}O$, $\delta^{13}C$, layer-bounding surfaces, layer-specific width, mineralogy, and distribution of macroholes (large cavities). Stalagmite MA3 is compared with two other stalagmites, MA2 and ANJ94-5 (see Section 3.2.1). The goal is to provide robust and comprehensive paleoenvironmental records for northwestern Madagascar, and to a larger extent the Southern Hemisphere.

## 3.2. Setting

### 3.2.1. Geography and geology

Stalagmites MA3, MA2, and ANJ94-5 were collected in 1994 from Anjohibe Cave (15.53°S, 46.88°E). The cave is located about 73 km northeast of Madagascar's second largest city, Majunga, about 125 km northeast from Lake Mitsinjo, and approximately 500 km drive southwest of the Swahili stone town and archaeological urban center of Mahilaka (Figs.3.1, B1). It was originally known as the "Grotte d'Andranoboka" (Gunn, 2004) and was often called "Anjohiandranoboka" (Middleton and Middleton, 2002). Anjohibe is located ca. 15 km south of the village of Mitsinjo. The cave is reached by following the main dirt track coming from Majunga, which crosses the Mariarano River (Fig. 3.1). "Anjohibe" means "big cave" and is the biggest cave in the region of Majunga (Brook et al., 1999; Decary and Kiener, 1970), with a length of over 5.3 km (Gunn, 2004). It forms a complex of passages through the base of a single hill, with more than thirteen entrances and about 5330 m of mapped passages (Fig. 3.1b) (Middleton and Middleton, 2002).

Most of the limestone caves in Madagascar are in the karst areas that are hardly accessible to humans (e.g. Middleton and Middleton, 2002). That inaccessibility created

oases of exceptional and commonly endemic fauna and flora surrounded by typical savannah landscapes (Middleton and Middleton, 2002). Anjohibe Cave is nonetheless fairly accessible (Middleton and Middleton, 2002), and it was partly developed as a commercialized show cave with electric lighting during the colonial period, around the 1940s (Gunn, 2004; Middleton and Middleton, 2002). It is no longer lit but still appears to be popular with adventure-tour operators (Middleton and Middleton, 2002 and reference therein).

Anjohibe Cave lies within the Narinda Karst region (Fig. 3.1a), specifically called Narinda South (Middleton and Middleton, 2002). The Narinda Karst is part of gently dipping (3-5° W) layers of Eocene limestone. The area is 50 m to 200 m above sea level, where it forms cone karst topography with rounded hills rising 20 to 40 m above a palm savannah. The base of the area is very pure limestone, and the tops of the hills are often completely dolomite (Gunn, 2004).

Stalagmites MA2 and MA3 were active at the time of collection in 1994, and Stalagmite ANJ94-5 was a two-meter fallen stalagmite. Stalagmite ANJ94-5 has been investigated by Wang (2016; see also Wang and Brook, 2013). The stalagmites were collected approximately 200 m from the main entrance, which is about 50 m east of the large dolline (Fig. 3.1b). The sector where these stalagmites were collected was well-ventilated at the time of sample collection, as the chamber was located near the collapsed roof, but ventilation could have been different in the past. Cave dripwaters, collected in 1994, were relatively dilute, with total dissolved solids estimated at 130 to 220 ppm (see Table 1 of Brook et al., 1999). The temperature of the cave varies between 24.5° and 26°C,

the relative humidity ranges between 72 and 87%, and the cave $PCO_2$ ranges between 400 and 500 ppm . These temperature, relative humidity, and cave $PCO_2$ measurements were obtained during Voarintsoa and co-workers' recent field expedition in May 2014.

### 3.2.2. Vegetation

Local vegetation around Anjohibe Cave is characterized by savanna grasses with sparse endemic satra palms (*Medemia nobilis*) and other trees adapted to the long dry season and periodic fires (Brook et al., 1999; von Cabanis et al., 1969; Wright et al., 1996; also see Fig. 1b of Crowley and Samonds, 2013). Dry mesic woodlands and forest patches are only found in areas of higher soil moisture. In fact, more than 80 % of the surface of western Madagascar is now covered with secondary grassland or wooded grassland, and this is burned each year with the practice of "tavy" (IUCN/UNEP/WWF, 1987; Thompson et al., 2011), a Malagasy form of "swidden agriculture" (e.g. Conklin, 1954; Dove, 1993) by local subsistence farmers.

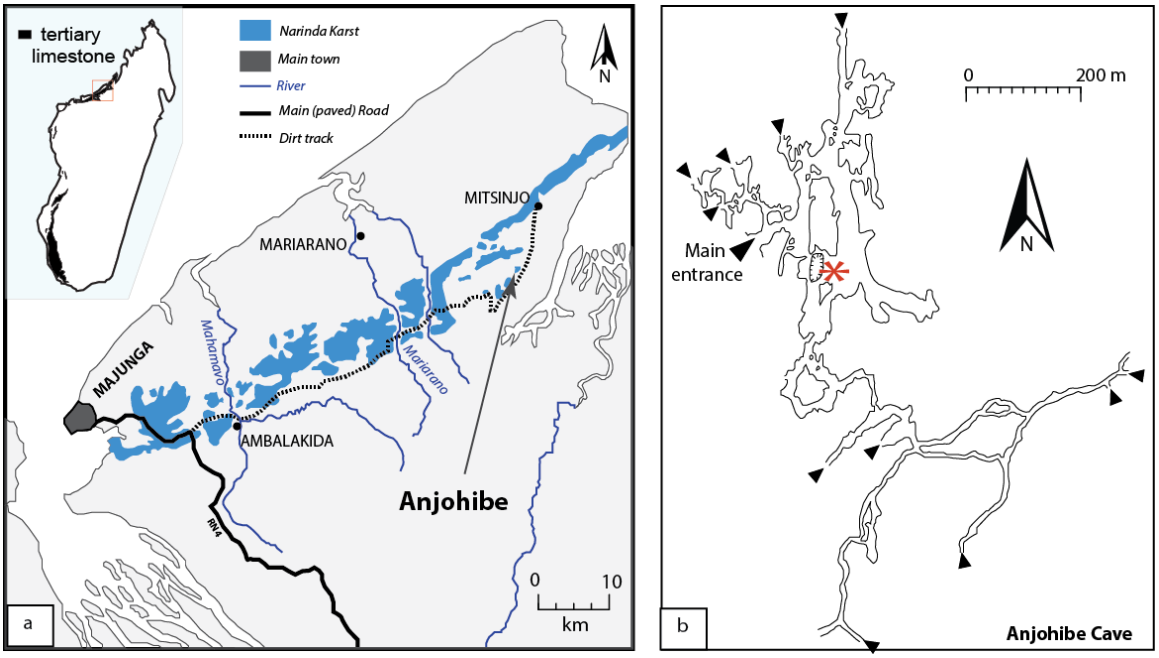
tertiary limestone
Narinda Karst
Main town
River
Main (paved) Road
Dirt track
N
MITSINJO
MARIARANO
MAJUNGA
Mahamavo
Maritarano
AMBALAKIDA
Anjohibe
RN4
0
10
km
a
0
200 m
N
Main entrance
b
Anjohibe Cave

Figure 3.1: Geological and geographical setting of Anjohibe Cave. a) Map showing the southwest part of the Narinda karst and location of Anjohibe Cave. The inset figure is a map of Madagascar showing the extent of tertiary limestone cover b) Sketch of Anjohibe cave (after Saint-Ours, 1959). Stalagmite MA3 was collected at location marked with a star. Detailed map showing the other locations (Lake Mitsinjo, Boeny, Mahilaka, Lake Amparihibe) mentioned in this study can be found in Fig. B1.

At the larger perspective, vegetation in northwestern Madagascar is less dense than the moister forests in the region's northeastern and eastern counterparts (Fig. B2a, also see modern Google Earth image). This difference in vegetation distribution is mainly controlled by the orographic effect created by the north-south mountain belt along the eastern escarpment of the island. Geology has also been used to refine the vegetation zones in Madagascar (e.g. duPuy and Moat, 1996, 2003). Trees in the west are not more than 12 m tall, which distinguishes secondary grasslands in the west from secondary grasslands in the east. Additionally, there are fewer lianas (French "lianes") and evergreen species on the calcareous plateau of western Madagascar than in the eastern counterpart. Besides savanna, dry deciduous forest and thickets also characterize the region, with numerous succulents and plants with swollen stems (IUCN/UNEP/WWF, 1987). Vegetation in Anjohibe and its surroundings is presently dominated by plants utilizing the $C_4$ photosynthetic pathway.

### 3.2.3. Climate

As an island located between the tropics of Cancer and Capricorn, Madagascar has a unique climate because of its mountainous nature, its position in the Indian Ocean, the seasonal migration of the Inter-Tropical Convergence Zone (ITCZ), and the changes in monsoon strength. Details about Madagascar's dominant climate mechanisms are reviewed in Douglass and Zinke (2015, p. 281–299). Rainfall is influenced alternately by dry easterly trade-winds in austral winter (May-October) and monsoon-driven northwesterly tropical storms in austral summer (November-April) (Fig. B3). This alternation of wind

direction between winter and summer defines the island's seasonality (DGM, 2008; Jury, 2003; Tadross et al., 2008). At inter-annual scale, Madagascar's rainfall has been linked to the Indian Ocean Dipole (Zinke et al., 2004), an air-sea interaction in the Indian Ocean (Saji et al., 1999), which is also teleconnected with El Niño Southern Oscillation or ENSO (Schott et al., 2009; Brook et al., 1999; Dunham et al., 2011). At much longer time scale, little is known, but Madagascar's hydroclimate could be influenced by the latitudinal migration of the ITCZ in response to changing global conditions (e.g. Chiang and Bitz, 2005), such as has been the case in southern and eastern Africa (e.g. Schefuß et al., 2011; Russell and Johnson, 2005).

Regionally distinct rainfall gradients from east to west and from north to south are evident across the entirety of Madagascar (Figs. B2b and B4; see also Fig. 1 of Dewar and Richard, 2007), with the southern region being the driest (DGM, 2008; Jury, 2003). The east-west gradient is controlled by orographic uplift (Williams, 1990), responsible for the six- to seven-month long dry and cold winter in the western region. This orographic effect ensures regular rainfall and a dense cover of tropical rainforest in the eastern regions (Madagascar National Adaptation Plan for Action, 2007; Jury, 2003). Thus, eastern Madagascar is always humid all year long, whereas western Madagascar has distinct warm and wet summers and cold and dry winters. Additionally, the mountain chain (~1200-1500 m high from north to south) constituting the backbone of Madagascar acts to split the shallow trade winds from the Indian Ocean approaching the eastern and northeastern coast of Madagascar during both seasons.

In contrast to the east-west gradient, the north-south gradient is entirely dependent on the convective activity and thunderstorms linked to the southward migration of the ITCZ during the austral summer from November to April (Fig. B3b). The ITCZ brings north or northwesterly monsoon winds to the island, in a pattern that the Service Météorologique of Madagascar calls the "Malagasy monsoon". The Malagasy monsoon belongs to the South African Monsoon, but it is also influenced by the Indian Monsoon (see Wang, 2009; Wang and Ding, 2008). The central uplands and drier western regions receive their summer rainfall through the convective activity linked to the ITCZ, which lies across the northern parts of the island during this time of the year (Tadross et al., 2008). In the same regions, rainfall is reduced or absent during the winter, usually between April and October, because the Indian Ocean anticyclone is intensified.

Located on the western coast of Madagascar (Figs. 3.1 and B2), Anjohibe is a good candidate for this paleoclimate and paleoenvironmental study because it is highly sensitive to the seasonality of rainfall in Madagascar and to the dynamics of the ITCZ. The mean annual rainfall is around 1160 mm. The mean maximum temperature in November, the hottest month in the summer, is about 32°C. The mean minimum temperature in July, the coldest month of the dry winter, is about 18°C.

### 3.2.4. Temporal and spatial variability of rainfall $\delta^{18}O$

Rainfall $\delta^{18}O$ values change distinctly between the two seasons in Madagascar, with greater $\delta^{18}O$ during cold and dry winter and smaller $\delta^{18}O$ during warm and wet summer (Figs. 3.2 and B4). This relationship suggests a seasonal effect on $\delta^{18}O$. The negative

relationship between rainfall and $\delta^{18}O$ and between temperature and $\delta^{18}O$ could also suggest an amount effect over $\delta^{18}O$, which is the observed decrease in rainfall $\delta^{18}O$ values with increased rainfall amount (Dansgaard, 1964; Rozanski et al., 1993; Bony et al., 2008; Risi et al. 2008; McDermott, 2004; Kurita et al., 2009; Lachniet, 2009). The amount effect is not only observed in Madagascar but also in other climatically sensitive and/or tropical regions where deep vertical convection is common (e.g. Kurita et al., 2009).

Although temperature and $\delta^{18}O$ are statistically correlated ($r^2$= 0.35; Fig. 3.2), the absence of rainfall during cold seasons (i.e. winter) precludes evaluation of the temperature effect on $\delta^{18}O$. However, because summers in Madagascar are always warm and wet, temperature has less influence on $\delta^{18}O$ than seasonality and rainfall amount (Fig. 3.2). The high $\delta^{18}O$ values before and after summer seasons could reflect an evaporation effect, specifically a raindrop re-evaporation effect (e.g. Lee et al., 2012), when temperature gets warmer and precipitation is low.

Beyond the temporal scale, the relationship between rainfall amount and $\delta^{18}O$ is also reflected by the latitudinal and longitudinal variability of rainfall across all of Madagascar (Fig. B4). Isotopic modelling indicates that the rainiest region in Madagascar, i.e. the eastern part, has the most negative $\delta^{18}O$ (Bowen, 2013). In contrast, $\delta^{18}O$ is greatest in the southern/southwestern part of the country, the region that receives the least rainfall.

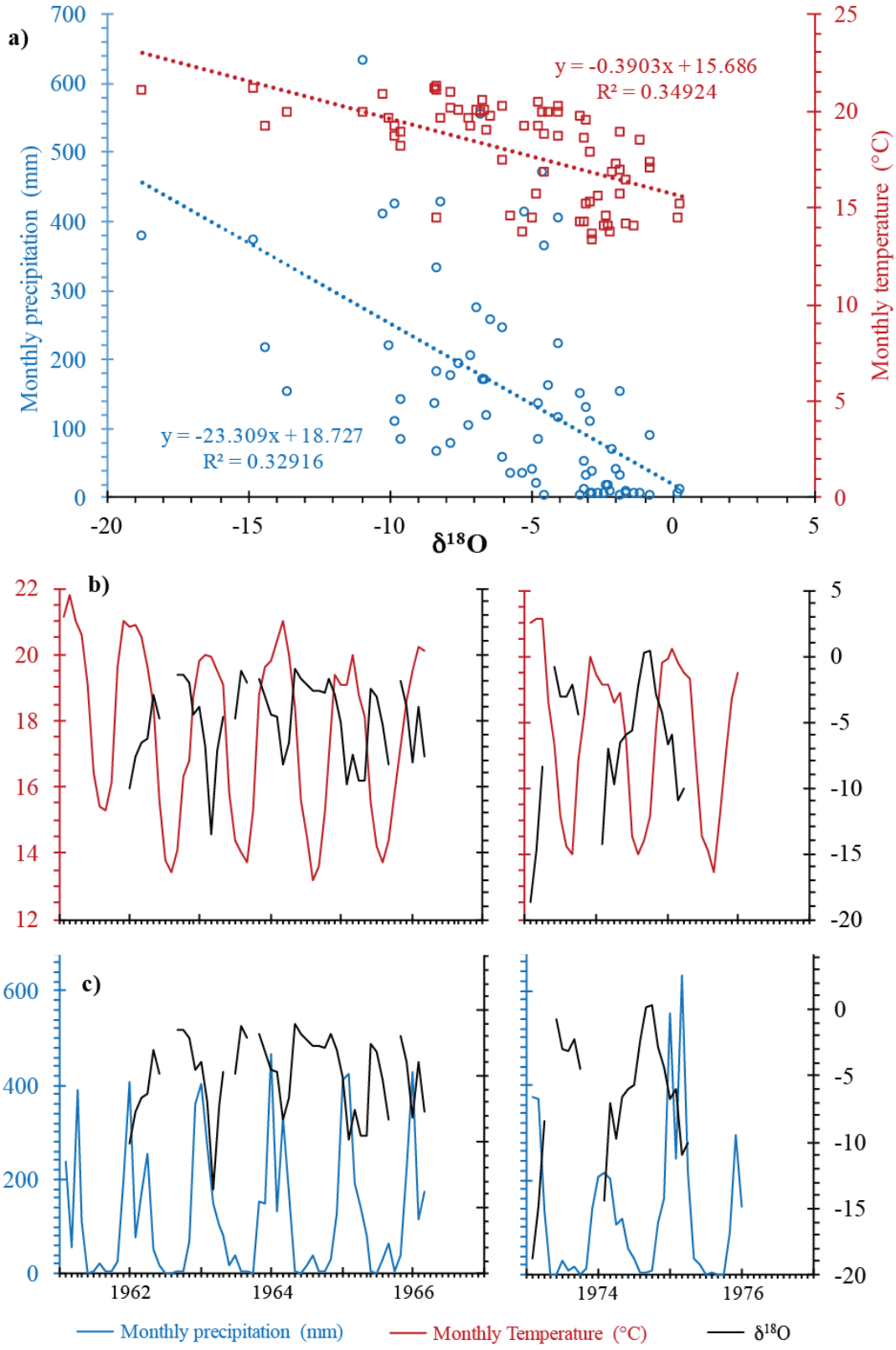
a)
y = -0.3903x + 15.686
R² = 0.34924
y = -23.309x + 18.727
R² = 0.32916
Monthly precipitation (mm)
Monthly temperature (°C)
δ18O
b)
c)
1962
1964
1966
1974
1976
Monthly precipitation (mm)
Monthly Temperature (°C)
δ18O

Figure 3.2: Modern rainfall-temperature-$\delta^{18}O$ in Antananarivo, Madagascar. (a) Plot of precipitation and temperature as a function of $\delta^{18}O$ in Antananarivo, Madagascar. (Lat. 18°54'00''; Long. 047°31'48''; Alt. 1300 m). Time series of (b) temperature-$\delta^{18}O$ and (c) rainfall-$\delta^{18}O$ from the same location showing relationship between changes in $\delta^{18}O$ and seasons. On the x-axis of (b) and (c), the minor ticks represent the twelve months of the year, starting from January to December. In both figures, $\delta^{18}O$ is greater in winters (with none or little rainfall) and smaller in summers. Data are from IAEA, WMO (2014).

## 3.3. Methods

Three stalagmites, MA3 (in its entirety), MA2 (its upper 116 mm), and ANJ94-5 (its upper 50 mm), were investigated. Six proxies were studied from Stalagmite MA3 to provide a comprehensive paleoclimate reconstruction in Anjohibe. These are $\delta^{18}O$, $\delta^{13}C$, layer-bounding surfaces, layer-specific width, mineralogy, and macrohole distribution. Stalagmites MA2 and ANJ94-5 were used to understand the stable isotope records from Stalagmite MA3. This approach was performed because it could provide robust evidence that the isotope data can be interpreted directly in terms of external forcing factors (e.g. Fairchild and Baker, 2012, p.272). Procedures for sample preparation (e.g. halving samples, extracting powders, thin section) and laboratory analyses (radiometric dating, stable isotopes) were identical for three stalagmites. Below we provide detailed description of different methods on Stalagmite MA3, the sample on which several proxies have been investigated.

### 3.3.1. Materials and sample preparation

Stalagmite MA3 was photographed, halved, and polished. The polished surface was scanned and saved as a.tiff image (see Section 3.3.3), which in turn was imported to Adobe Illustrator for indexing. This indexing step is essential for keeping consistent records of the depth and labeling of radiometric, isotopic, and other necessary sampling procedures or additional measurements, such as measuring the layer-specific width (Sletten et al., 2013; Railsback et al., 2014) and determining the mineralogy at specific distance from the top of the sample.

### 3.3.2. Radiometric analysis

For radiometric analyses, 21 samples from Stalagmite MA3, 11 samples from Stalagmite MA2, and 6 samples from Stalagmite ANJ94-5 were obtained by drilling (Tables B1, B2, B3). Drilling was done using a hand-held dental drill, allowing us to trace a specific trench for each selected spelean layer. We used carbide dental burrs that range in size from 0.5 to 1.2 mm (SSW-HP4), producing a trench approximately 1-2 mm wide. The milled powders were gently scraped from the polished surface of the speleothem onto a pre-weighed weighing paper and were then transferred to a flat bottom cylindrical glass vial. Each sample's weight varied between 100 and 250 mg, depending on its expected uranium concentration.

The age was determined using advanced techniques for measuring $^{234}U$ and $^{230}Th$ on Faraday cups with precision of 1-3 epsilon units (Cheng et al., 2013) on a multi-collector inductively coupled plasma mass spectrometer (MC-ICPMS), Thermo-Scientific Neptune of the Minnesota Isotope Laboratory at the University of Minnesota. These new techniques minimize the errors calculated for the half-life values of $^{234}U$ and $^{230}Th$, to 245,620 ±70 and 75,584±30 (within 2$\sigma$ uncertainty) respectively, and the 2$\sigma$ uncertainties in the age of the sample being analyzed (Cheng et al., 2013). The chemical procedure used to separate U and Th and the methods used in U/Th analysis were similar to that described in Shen et al. (2002) and Cheng et al. (2013). Corrected $^{230}Th$ ages assume the initial $^{230}Th/^{232}Th$ atomic ratio of $4.4 \pm 2.2 \times 10^{-6}$. This is a ratio for a "bulk earth" or crustal material at secular equilibrium, with a $^{232}Th/^{238}U$ value of 3.8. The error of this "bulk earth" value is assumed to be ± 50%. The error in the final "corrected age" incorporates this uncertainty. The

radiometric data are reported as year B.P., where B.P. means Before Present and "present" represents the year AD 1950.

### 3.3.3. Stable isotope analysis

For stable isotope analysis, 367 samples from Stalagmite MA3, 164 samples from Stalagmite MA2, and 120 samples from Stalagmite ANJ94-5 were individually hand-drilled using a conventional dental drill. Drilling was done along the growth axis of the stalagmite at an interval of 1 mm on average for Stalagmite MA3 and MA2, and at an interval of 0.5 mm for Stalagmite ANJ94-5. Stalagmite ANJ94-5 was sampled at smaller intervals because of its slower growth rate, as it grew during the dry interval described in Section 3.5.1.2 (see also Section 3.4.1). About 50 to 100 micrograms of powdered $CaCO_3$ were weighed for each sample. Weighing was done using the Cubis® Sartorius precision balance at the Sedimentary Geochemistry Lab of the Geology Department at UGA. The weighed samples were transferred into special Labco exetainer ® vials compatible with the GasBench-IRMS machine of the Alabama Stable Isotope Laboratory. Analytical methods and procedures are identical to those described in Paul and Skrzypek (2007) and Skrzypek and Paul (2006).

All the isotope ratios from these three stalagmites are reported in ‰ relative to Vienna Pee Dee Belemnite standard (VPDB). As per convention, those ratios ($^{13}C/^{12}C$ and $^{18}O/^{16}O$) are expressed in the delta notation as follows: $\delta_x=[(R_{sample}-R_{standard})/R_{standard}] * 10^3$ (where x represents $^{13}C$ or $^{18}O$ and R is the ratio). Isotope error was about +/- 0.1 ‰ for both $\delta^{13}C$ and $\delta^{18}O$. The $\delta^{18}O$ and $\delta^{13}C$ of the spelean aragonite were transformed, by a subtraction of 1.7 ‰ (Romanek et al., 1992) and 0.8‰ (Kim et al., 2007) respectively.

These transformations were done to compensate for the aragonite's inherent fractionation of heavier isotopes. With these transformations, the corrected isotopic values remove the mineralogical bias in isotopic interpretation between calcite and aragonite.

### 3.3.4. Mineralogy and petrographic analysis

The three stalagmites were macroscopically investigated to compare their petrography and internal texture between each other. Stable isotope profiles were also used to evaluate the relationship between petrography and stable isotopes.

Detailed macroscopic examination of Stalagmite MA3 consisted of a physical description of the sample both externally and internally, and measuring the layer-specific width. The outer surface was described based on its overall structure and texture (smooth vs. rough surface) and the shape of the stalagmite. The stalagmite's internal surface was investigated based on the overall distribution of cavities and pores, the nature of the spelean carbonate, and the overall distribution of the spelean minerals throughout the sample. The layer-specific width is the horizontal distance between two points on the flanks, i.e. points at maximum convexity, at which the spelean layer changes dip direction to ca. 10° in Stalagmite MA3. The width was measured perpendicular to the stalagmite's growth axis following the method described in Section 3.3.2 and Figure 3.2 of Sletten et al. (2013). This measurement was done at macroscopically traceable layers and plotted as a function of depth (Fig. 3.3e).

Twenty-five regular (1x2 in) to oversized (2x3 in) thin sections of MA3 were examined using a Leitz Laborlux 12 PolS microscope to identify the mineralogy and to specify the nature of the layer-bounding surfaces, known as Type E and Type L surfaces (Railsback et al., 2013) from the top to the bottom of the stalagmite. Type E surfaces are surfaces below which layers are truncated, particularly toward the crest of the stalagmite, as the result of dissolution in extremely wet conditions. Type L surfaces are surfaces below which layers thin toward the flank and thus indicate reduced deposition rate in response to lesser dripwater in drier conditions (Railsback et al., 2013). These boundaries are interpreted to indicate extreme wet (Type E) or dry conditions (Type L) (Railsback et al., 2011; 2013), and thus they complement the information obtained from stable isotopes. Each of the identified layer-bounding surfaces was traced on a set of transparent papers overlain on top of the polished surface of the stalagmite. These transparent papers were then scanned, saved as a ".tiff" image (at 600 dpi), and imported into Adobe Illustrator file with the scanned image of the stalagmite. The final electronic version of the traces was vectorized (Fig. 3.3c) using the Pen Tool of Adobe Illustrator and was permanently saved.

Finely powdered samples of ca. 3 grams were analyzed by X-ray diffraction to identify the spelean mineralogy. We specifically analyzed the layer between 240 and 250 mm from the top of the stalagmite for three reasons: (1) the textural appearance is different (yellow pale color, greasy luster, and the mineral is translucent to opaque), (2) the layer-specific width is narrow (2.8 cm), and (3) we identified a Type L surface. The X-ray diffraction consists of scanning the powdered sample on a Bruker D8 X-ray

Diffractometer in the Department of Geology at the University of Georgia. The diffraction angle 2$\theta$ was set between 20 and 60° and the radiation used was CoK$\alpha$.

## 3.4. Results

### 3.4.1. Mineralogy and petrography

Stalagmite MA3 is 38 cm tall and has a rounded white top. Its external upper 20 cm are smooth, whereas the bottom 18 cm are covered with popcorn-like coralloids (e.g. Caddeo et al., 2015). The upper ~20 cm of the inner polished surface of Stalagmite MA3 are also characterized by a significant number of macroholes (cavities of one to two millimeters wide and five to fifteen millimeters long), whereas its bottom part has very low porosity and cavities are smaller and are located near the flanks (Fig. 3.3). Laminations (<1 mm thick spelean layers) are also evident in the bottom part of Stalagmite MA3.

Comparison of the overall texture of the polished half of MA3 with the models of stalagmite shape and growth rate in Figs. 7.5 and 7.9 of Fairchild and Baker (2012) suggest that MA3 approximates the shape of a candlestick (similar to example 3b of their Fig. 7.9), with some irregularities at the flanks. Stalagmite MA3 is fairly wide (ca. 8 to 10 cm in diameter). The measured layer-specific width is greater near the top (average 6.8 cm for the upper 18 cm) and smaller near the bottom (ca. 5.0 cm in average) with notably much narrower width at 190 mm (ca. 3.5 cm) and at 240 mm (ca. 2.8 cm) from the top (Fig. 3.3e).

The stalagmite's growth axis has also shifted at least four times. The largest shift is observable at 20 cm from the stalagmite's top. This position marks a boundary between the cavity-poor bottom part and the cavity-rich upper part of Stalagmite MA3. Sampling

for stable isotopes analysis thus shifts laterally to follow the direction of the stalagmite's growth axis (Fig. 3.3a).

With regard to mineralogy, Stalagmite MA3 is almost entirely composed of calcite. Layers of aragonite are very thin and rare. These are only observed at 240 to 250 mm, 259 to 262 mm, 281 mm, 286 to 287 mm, 306 mm, and 354 mm from the top of MA3 (Fig. 3.3). Regarding the other two samples, the upper portion of Stalagmite MA2 is composed of calcite and the upper portion of Stalagmite ANJ94-5 consists of aragonite. The $\delta^{18}O$ and $\delta^{13}C$ values of these aragonite layers were transformed to compensate for the aragonite's inherent fractionation of heavier isotopes (see Section 3.3.2).

The distribution of layer-bounding surfaces throughout Stalagmite MA3 varies significantly. They are abundant and much more pronounced in the bottom 15 cm of the stalagmite, with more Type Ls than Type Es. In contrast, the upper part of Stalagmite MA3 has fewer layer-bounding surfaces, with more Type E surfaces than L. Darker brown layers less than 1 mm thick at intervals of 1 to 2 cm are also observable throughout much of MA3. These layers are rich in detrital material (mostly clay-rich, as identified under microscope), but most importantly they coincide with Type E surfaces. Type L surfaces are macroscopically observable as a pinching-out of the layers toward the flanks (Fig. 3.3c). Overall, at least 19 Type L surfaces and 70 Type E surfaces were identified, and these are mapped in Figure 3.3c.

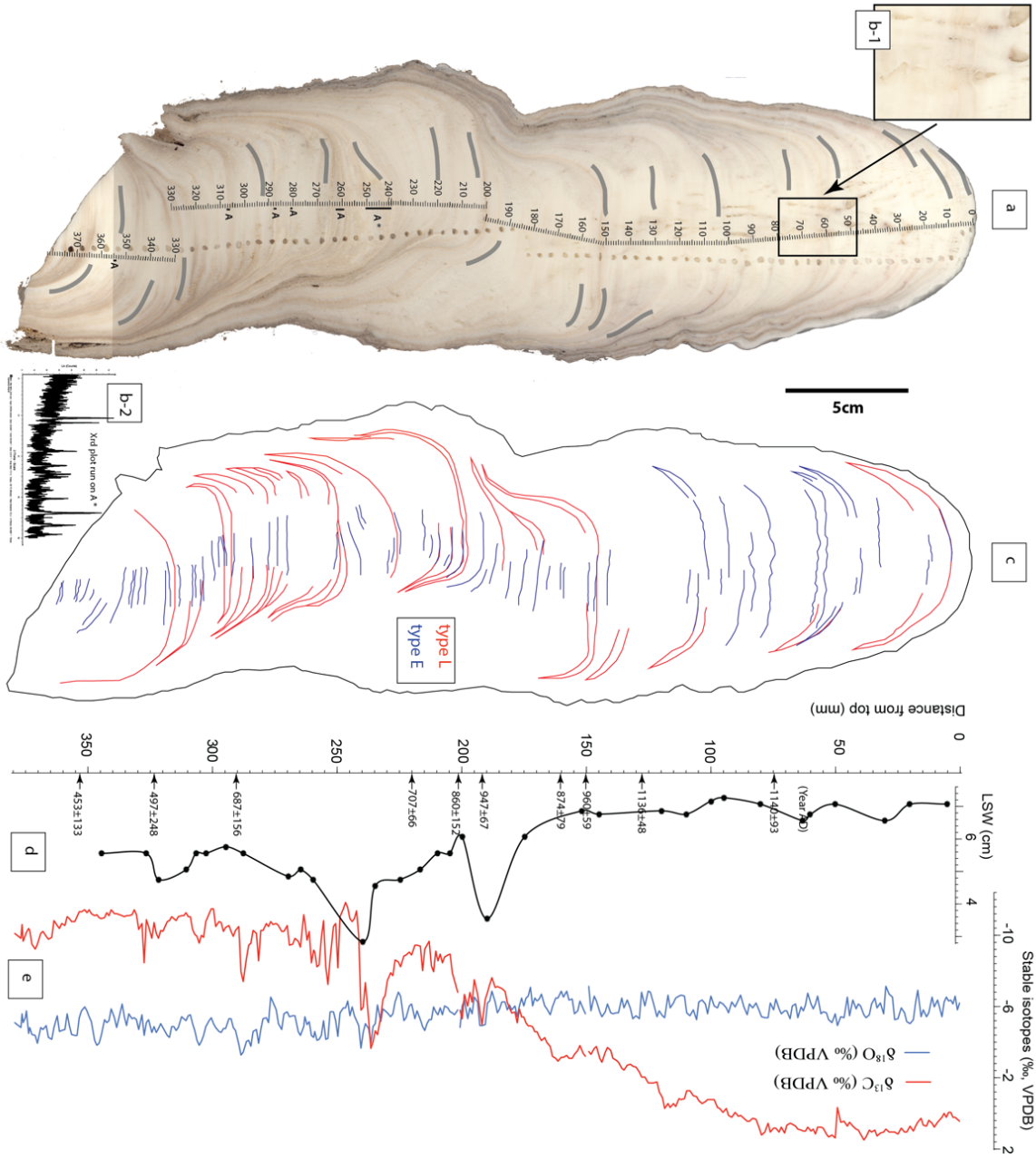
a
b-1
b-2
5cm
Xrd plot run on A *
c
type L
type E
Distance from top (mm)
d
LSW (cm)
(Year AD)
453±133
497±248
687±156
707±66
860±152
947±67
874±79
960±59
1136±48
1147±93
e
δ13C (‰ VPDB)
δ18O (‰ VPDB)
Stable isotopes (‰, VPDB)

Figure 3.3: Scanned image of Stalagmite MA-3 and multi-proxy records data. a) Scanned image of the inner polished half of stalagmite MA3 showing the traces of trenches for radiometric analysis. “A” denotes aragonite and their respective position in the sample as discussed in Section 3.4.1. b-1) Close-up of the axial holes as discussed in Section 3.4.1. b-2) X-ray Diffraction plot of sample A* at 240-250 mm. c) Sketch tracing the layer-bounding surfaces (Type L and Type E). d) Depth series of the specific width of the spelean layers (LSW= layer-specific width, measured in cm). e) Depth series of $\delta^{18}O$ and $\delta^{13}C$ of Stalagmite MA3.

### 3.4.2. Radiometric age data and age model

Concentrations of $^{238}U$ and $^{232}Th$ in Stalagmite MA3 are highly variable, and we acknowledge that for such a young sample, the chronology is poorly constrained (Table B1). The uranium content is generally low, detrital contents are rather high, and age uncertainties are large. Consequently, eleven U/Th results were rejected before constructing the age model based on the following criteria (Table B1, Fig. 3.4). First, some samples have very low $^{238}U$ concentration (< 100 ppb; e.g. MA3-U008 and MA3-U2). Second, other samples have high $^{232}Th$ concentration (> 1500 ppt; e.g. MA3-U1, MA3-U2, MA3-U3, MA3-U10, MA3-U336, and MA3-U13). Third, relative to the neighboring samples, some have higher $^{232}Th$ (i.e. higher detrital materials) and were also rejected. This is the case for samples MA3-U5 and MA3-U6 that were discarded. Fourth, one age is not in stratigraphic order (e.g. MA3-U4, which also fulfills criteria #3). Finally, petrographic observations show evidence of dissolution (Type E surfaces) and recrystallization (e.g. MA3-U9).

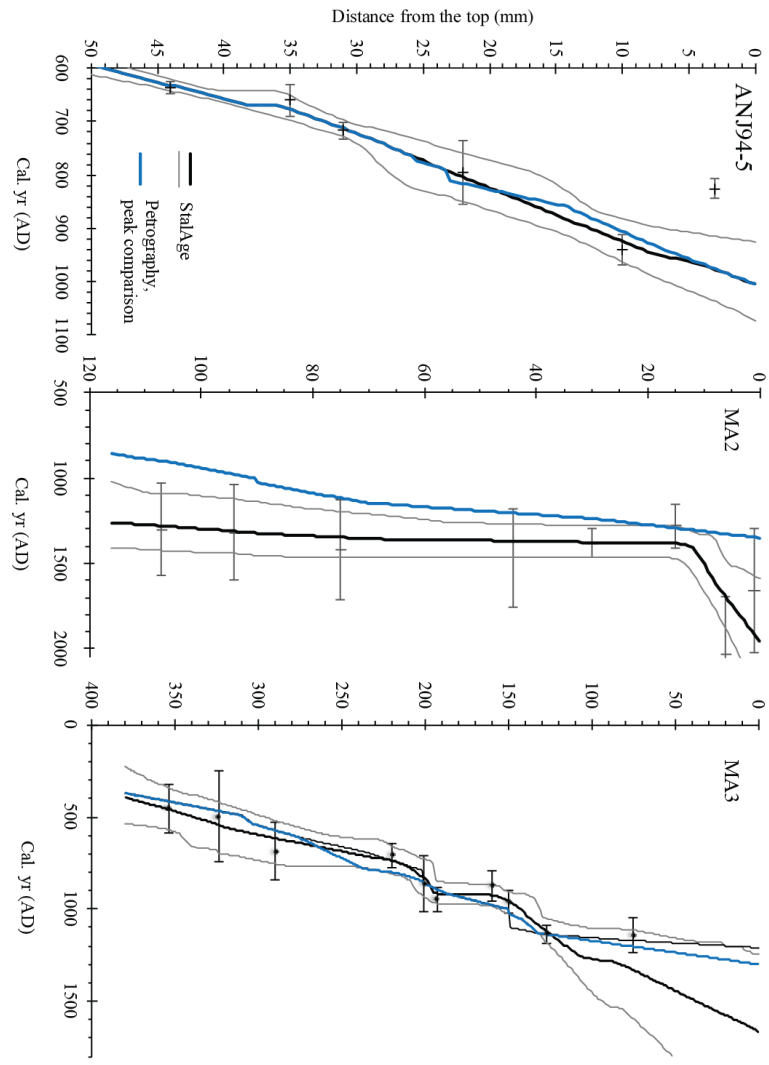
Distance from the top (mm)
ANJ94-5
MA2
MA3
StalAge
Petrography, peak comparison
Cal. yr (AD)

Figure 3.4: Age models for Stalagmite ANJ94-5, MA2, and MA3 (see Section 3.4.2 and Fig. 3.5 for details)

Because our age data are relatively weak, the chronology has undergone two steps of adjustment. We used the StalAge1.0 algorithm of Scholz and Hoffman (2011) to obtain an age estimate, including the uncertainty, for each isotope sample of each stalagmite. For Stalagmite MA3, the age model was constructed using the remaining acceptable age data (i.e. $^{238}U<100ppb$ and $^{232}Th>1500ppt$). No significant long-term hiatal surfaces were identified in the stalagmites. The pronounced brown layers at 150 and 200 mm in Stalagmite MA3, at 39, 71, 89, and 104 mm in Stalagmite MA2, and at 29mm in Stalagmite ANJ94-5 are seemingly layers of detritals deposited during very wet seasons. We finally tuned the chronology model by matching peaks and troughs of the stable isotope profiles. To do this, we used the depth series profile of $\delta^{13}C$ of all three stalagmites (Figs. 3.5 and 3.6). We started wiggle-matching Stalagmite MA3 and Stalagmite ANJ94-5, two of the stalagmites that are better constrained, for the interval between AD 600 and 1100. Then, we wiggle matched Stalagmite MA3 and Stalagmite MA2 for the interval between AD 850 and AD 1350. To validate our age model reconstruction, we compared the reconstructed stable isotope profile with previously published stable isotope profiles from the same cave (Fig. 3.7).

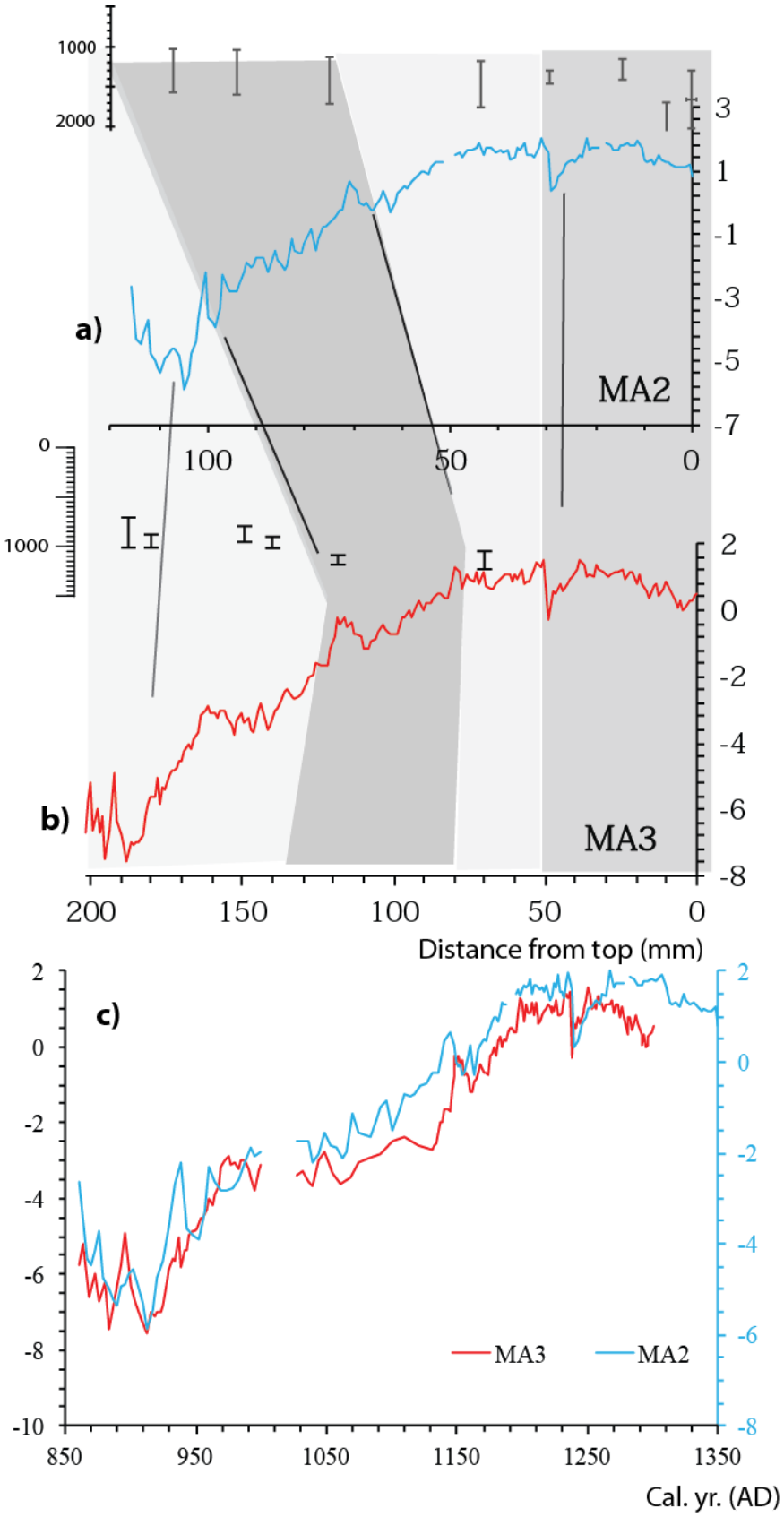
1000
2000
a)
MA2
3
1
-1
-3
-5
-7
100
50
0
0
1000
b)
MA3
2
0
-2
-4
-6
-8
200
150
100
50
0
Distance from top (mm)
c)
2
0
-2
-4
-6
-8
-10
MA3
MA2
850
950
1050
1150
1250
1350
Cal. yr. (AD)

**Figure 3.5**: Steps in peak comparison (wiggle-matching) between $\delta^{13}C$ of (a) Stalagmite MA2 and (b) Stalagmite MA3 (note that $\delta^{13}C$ is chosen for comparison because its profile for both stalagmites is very similar, making comparison easier). The different shaded areas represent similar profiles in Stalagmites MA2 and MA3. The small vertical bars above each depth series are radiometric data for each respective sample and their respective uncertainty. The resulting time series is shown at the bottom figure (c), and Fig. 3.6. The reconstructed stable isotope profile of Stalagmite MA3 is further compared with already published records (Fig. 3.7).

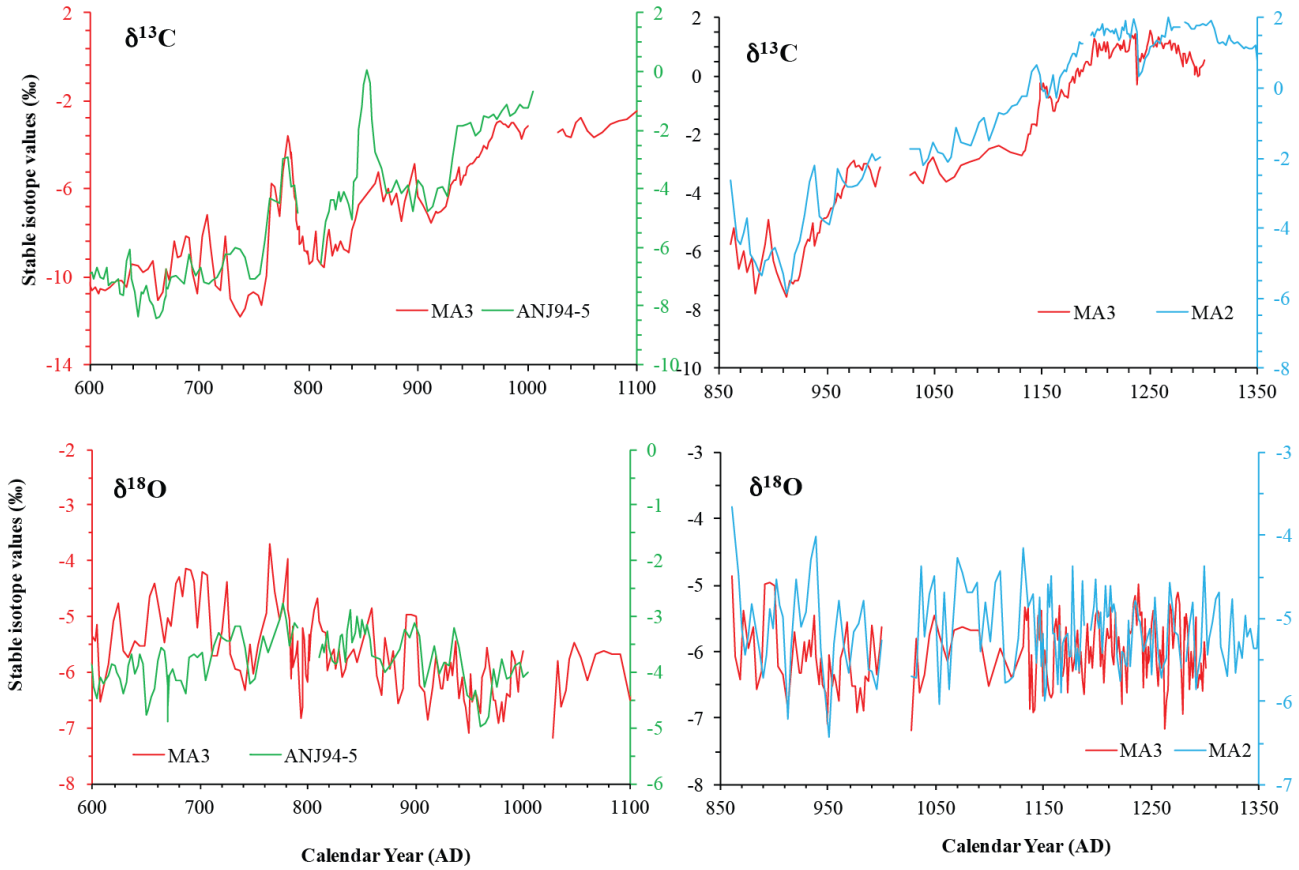
δ13C
Stable isotope values (‰)
MA3
ANJ94-5
δ13C
MA3
MA2
δ18O
MA3
ANJ94-5
δ18O
MA3
MA2
Calendar Year (AD)
Calendar Year (AD)

Figure 3.6: Time series of oxygen and carbon stable isotope ratios (‰, vs. VPDB) for Stalagmite MA3 (red), ANJ94-5 (green), and MA2 (blue). The series of figures indicate that stable isotope records from Stalagmite MA3 are comparable with Stalagmite MA2 (between AD 850 and AD 1350) and Stalagmite ANJ94-5 (between AD 600 and AD 1100).

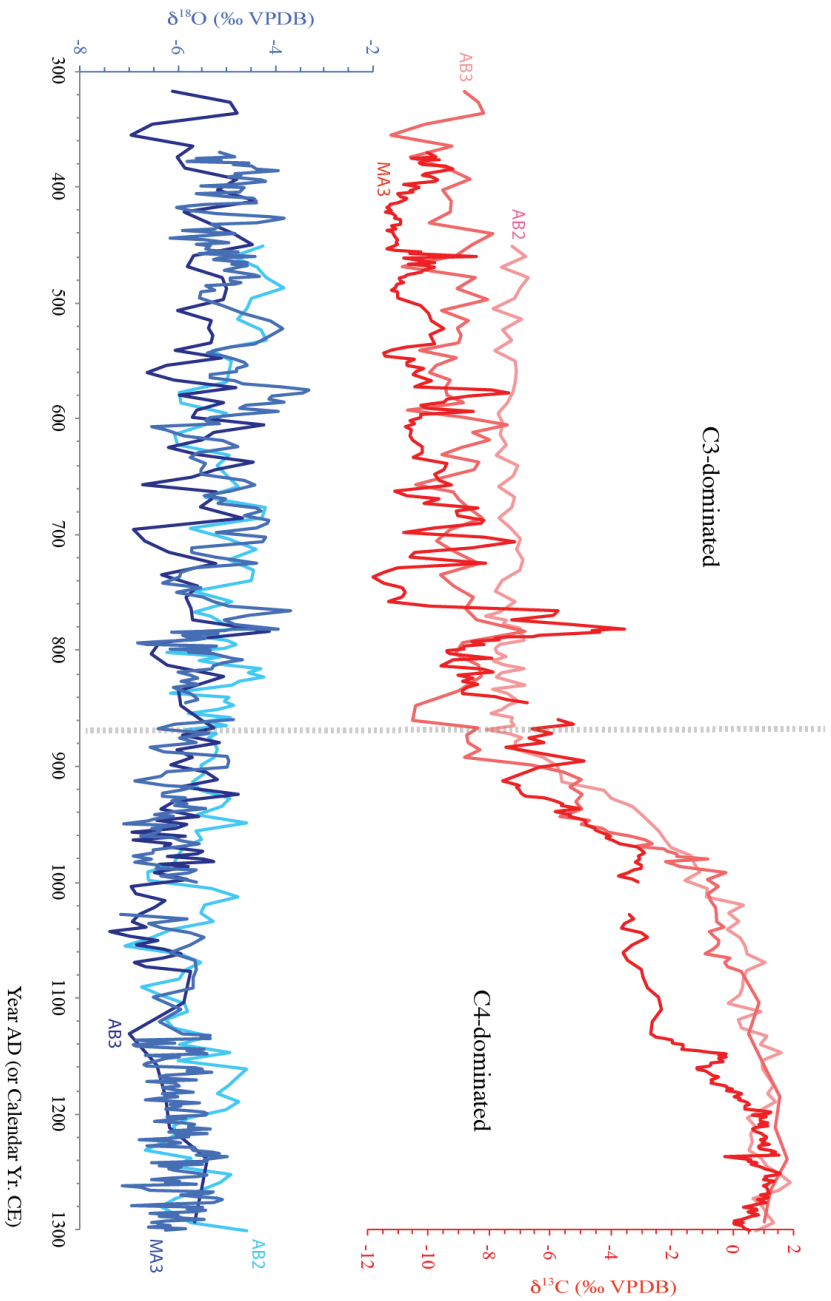
δ18O (‰ VPDB)
-8
-6
-4
-2
300
400
500
600
700
800
900
1000
1100
1200
1300
Year AD (or Calendar Yr. CE)
AB3
MA3
AB2
C3-dominated
C4-dominated
AB3
MA3
AB2
-12
-10
-8
-6
-4
-2
0
2
δ13C (‰ VPDB)

Figure 3.7: Comparison of stable isotope profile of $\delta^{18}O$ and $\delta^{13}C$ of Stalagmite MA3 (this study) and two other stalagmites (AB2 and AB3; Burns et al., 2016) of the late Holocene in Madagascar from Anjohibe Cave's stalagmites showing that although the chronology of our stalagmites is not very robust, the best estimate age model using StalAge and peak comparison provide oxygen and carbon stable isotope profile that is comparable to previously published research (Burns et al., 2016).

### 3.4.3. Stable isotopes

The stable isotopic time series of Stalagmite MA3 is characterized by relatively constant $\delta^{18}O$, ranging from –7.2 to –2.9 ‰, vs. VPDB, while the values of $\delta^{13}C$ show an overall increasing trend from –11.5 to +1.5 ‰, vs. VPDB (Figs. 3.3d, 3.6, 3.8), with a significant increase starting ca. AD 870. One striking aspect of the records is the covariance of $\delta^{18}O$ and $\delta^{13}C$ before ca. AD 795 and the lack of correlation after ca. AD 870, with the marked increasing $\delta^{13}C$ trend (Figs. 3.3d, 3.8b).

## 3.5. Discussion

### 3.5.1. Multiple proxies as indicators of past hydroclimate

Six proxies from Stalagmite MA3 combine to provide a record of variation between wetter and drier conditions in northwestern Madagascar. These proxies are summarized in Table 3.1, and their relevance to understanding paleoclimate in northwestern Madagascar is discussed further below.

**Table 3.1**: Summary of the six proxies with a list of possible controlling factors and their climatic significance, when known or available. Indicated with an asterisk (*) are the immediate controls for $\delta^{18}O$ and $\delta^{13}C$ for Stalagmite MA3.

| PROXIES | DEFINITION/CONTROLLING FACTORS | REFERENCES |
|---|---|---|
| $\delta^{18}O$ | $\delta^{18}O=[(^{18}O/^{16}O)_{sample}-(^{18}O/^{16}O)_{standard})]/ (^{18}O/^{16}O)_{standard}$<br>• Variations in $\delta^{18}O$ of moisture source supplying drip water to the cave. This is mainly significant to decipher glacial (greater $\delta^{18}O$) and interglacial intervals (smaller $\delta^{18}O$).<br>• Variations in atmospheric temperature: although $\delta^{18}O$ values are typically lower in the winter and higher in the summer in several regions, the opposite has been observed in Madagascar (greater $\delta^{18}O$ during winter, smaller $\delta^{18}O$ during summers)<br>• Distance of transport from the vapor source (continental effect): typically water $\delta^{18}O$ values decrease with distance from the ocean, but it could be influenced by high $\delta^{18}O$ recycled continental moisture back to the atmosphere from evaporation of soil water, lakes, and rivers.<br>• Altitude effect: smaller $\delta^{18}O$ with increasing elevation.<br>• * Variations in the $\delta^{18}O_w$ of the dripwater which reflect the $\delta^{18}O$ of atmospheric precipitation (amount effect). It varies depending on seasonality of rainfall (e.g in tropical warm summers, $\delta^{18}O$ is smaller with increased rainfall amount; whereas in mid-latitude colder regions, mean winter rainfall is often more depleted in $^{18}O$)<br>• Variations in cave temperature: greater $\delta^{18}O$ with colder temperature, and smaller $\delta^{18}O$ with warmer temperature<br>• Magnitude of kinetic fractionation of dripwater or water films precipitating carbonate<br>• Evaporation inside and outside the cave: greater $\delta^{18}O$ with increased evaporation. | Burns et al., 2002<br>Clark and Fritz, 1997<br>Cuthbert et al., 2014<br>Dansgaard, 1964<br>Deininger et al., 2012<br>Fairchild and Treble, 2009<br>Hoefs, 2009<br>Koster et al., 1993<br>Lachniet, 2009;<br>McDermott, 2004<br>Quade, 2004<br>Railsback, 2010<br>Rozanski et al., 1993<br>Wong and Breeker, 2015 |
| $\delta^{13}C$ | $\delta^{13}C =[(^{13}C/^{12}C)_{sample}-(^{13}C/^{12}C)_{standard})]/ (^{13}C/^{12}C)_{standard}$<br>• Variations of $\delta^{13}C$ of $CO_2$ in the atmosphere<br>  o Smaller $\delta^{13}C$ due to the Suess effect<br>  o Smaller $\delta^{13}C$ during glacial and greater $\delta^{13}C$ during interglacial<br>• * Photosynthetic pathway: smaller $\delta^{13}C$ for $C_3$ plants and greater $\delta^{13}C$ for $C_4$ plants.<br>• * Extent of vegetation, soil biomass productivity (as a function of meteoric precipitation): smaller $\delta^{13}C$ with more vegetation cover<br>• * Rate of passage of water through soil to limestone<br>  o Closed system: greater $\delta^{13}C$ with faster passage if water and thus lesser input of soil $CO_2$<br>  o Open system: lesser $\delta^{13}C$ with slower passage of water and thus greater input of soil $CO_2$<br>• $\delta^{13}C$ of limestone<br>• * Extent of degassing of $CO_2$ and Prior Calcite Precipitation (or more generally Prior Carbonate Precipitation). The relationship between degassing and prior calcite precipitation results in systematic rises in $\delta^{13}C$.<br>• Cave ventilation which could accelerate the rate of degassing and PCP, leading to an increase in $\delta^{13}C$. | Baldini et al., 2005<br>Brook et al., 1999, 20010<br>Brook et al., 2006<br>Burns et al., 2016<br>Cross et al., 2015<br>Cruz et al., 2006<br>Denniston et al., 2013<br>Dreybrodt and Scholz, 2011<br>Fairchild and McMillan, 2007<br>Frisia et al., 2011<br>Genty et al., 2001; 2003; 2006<br>Hesterberg and Siegenthaler, 1991<br>Johnson et al., 2006<br>Lauritzen and Lundberg, 1999<br>Meyer et al., 2014<br>Mickler et al., 2004, 2006;<br>Moreno et al., 2010<br>Quade, 2004<br>Railsback, 2010<br>Suess, 1955<br>Verburg, 2007<br>Wong and Breecker, 2015 |
| Layer bounding surfaces | Surfaces between two spelean layers that delimit series of layers and represent periods of non-deposition<br>Type E: surfaces below which spelean layers are truncated, microscopic examination shows signs of dissolution<br>• Type E surfaces represent exceptionally wet conditions and faster drip rate.<br>Type L: surfaces below which layers thin upward and/or have lesser lateral extent upward (the layer-specific width decreases)<br>• Type L surfaces represent exceptionally dry conditions and slower drip rate. | Railsback et al. 2011, 2013<br>Sletten et al., 2013<br>Voarintsoa et al., 2016 |

| | | |
|---|---|---|
| Layer-specific width | The width across the stalagmite between the points at which the layer is tangent to a line inclined at specific angle (here it is 10°) relative to the growth axis of the stalagmite<br>• Smaller values represent drier conditions and reduced drip rate.<br>• Greater values represent wetter conditions and increased drip rate. | Dreydbrodt (1999)<br>Railsback et al 2014<br>Sletten et al 2013<br>Yadava et al., 2004 |
| Macroholes | Axial holes: Syngenetic holes aligned along the stalagmite axis and maintain open contact with the cave atmosphere during stalagmite formation<br>• Local variation in the rate of calcite precipitation: increased deposition rate as drip water loses $CO_2$ to the cave atmosphere (this degassing process start where the falling drop first meets the stalagmite surface): could indicate wetter conditions, particularly when layers dip toward the growth axis of the stalagmite<br>Off axis holes: elongated, ellipsoidal, post-depositional holes parallel to the growth axis of the spelean layers. They often crosscut growth layers after an internal erosion of the previously formed stalagmite<br>• no known significant climatic meaning, but could suggest wetter conditions | Shtober-Zisu et al., 2012<br>Shtober-Zisu et al., 2014 |
| Mineralogy | There are several spelean minerals but the most common ones are calcite and aragonite. Factors directly favoring the formation of aragonite, rather than calcite, under cave conditions are:<br>• high temperature,<br>• drip water composition in trace elements (high concentration of Mg, Sr, Pb), which could reflect the composition of the bedrock<br>• drier conditions<br>• extensive evaporation<br>• seasonal dryness<br>• prior carbonate precipitation | Bischoff and Fyfe, 1968<br>Bischoff, 1968<br>Cabrol and Coudray, 1982<br>Caddeo et al., 2011<br>Fischbeck, 1976<br>Frisia et al., 2002<br>González and Lohmann, 1988<br>Hill and Forti, 1997<br>McMillan, 2005<br>Moore, 1956<br>Murray, 1954<br>Pobeguin, 1965<br>Railsback et al. 1994<br>Riechelman et al., 2014<br>Siegel, 1965<br>Sletten et al., 2013<br>Thrailkill, 1971 |

#### *3.5.1.1. Co-variance of $\delta^{18}O$ and petrographic indicators of hydroclimatic history*

Values of $\delta^{18}O$ (and/or $\delta^{13}C$), the nature of the stalagmite's layer-bounding surfaces, known as Type E and Type L surfaces, the variations in layer-specific width, and the distribution of macroholes throughout Stalagmite MA3 combine to provide a meaningful record of variation between wetter and drier conditions in Anjohibe and its surroundings. Greater $\delta^{18}O$ is associated with abundant Type L surfaces, reduced layer-specific width, and fewer macroholes. All of this suggests that an overall increase in $\delta^{18}O$ in Stalagmite MA3 reflects drier conditions (Table 3.1). On the other hand, smaller $\delta^{18}O$ is associated with abundant Type E surfaces, greater layer-specific width, and axial holes, suggesting wetter conditions (Table 3.1). In this respect, Stalagmite MA3 follows the generalization of Fairchild and McMillan (2007) that stalagmites are indicators of wetter and drier conditions.

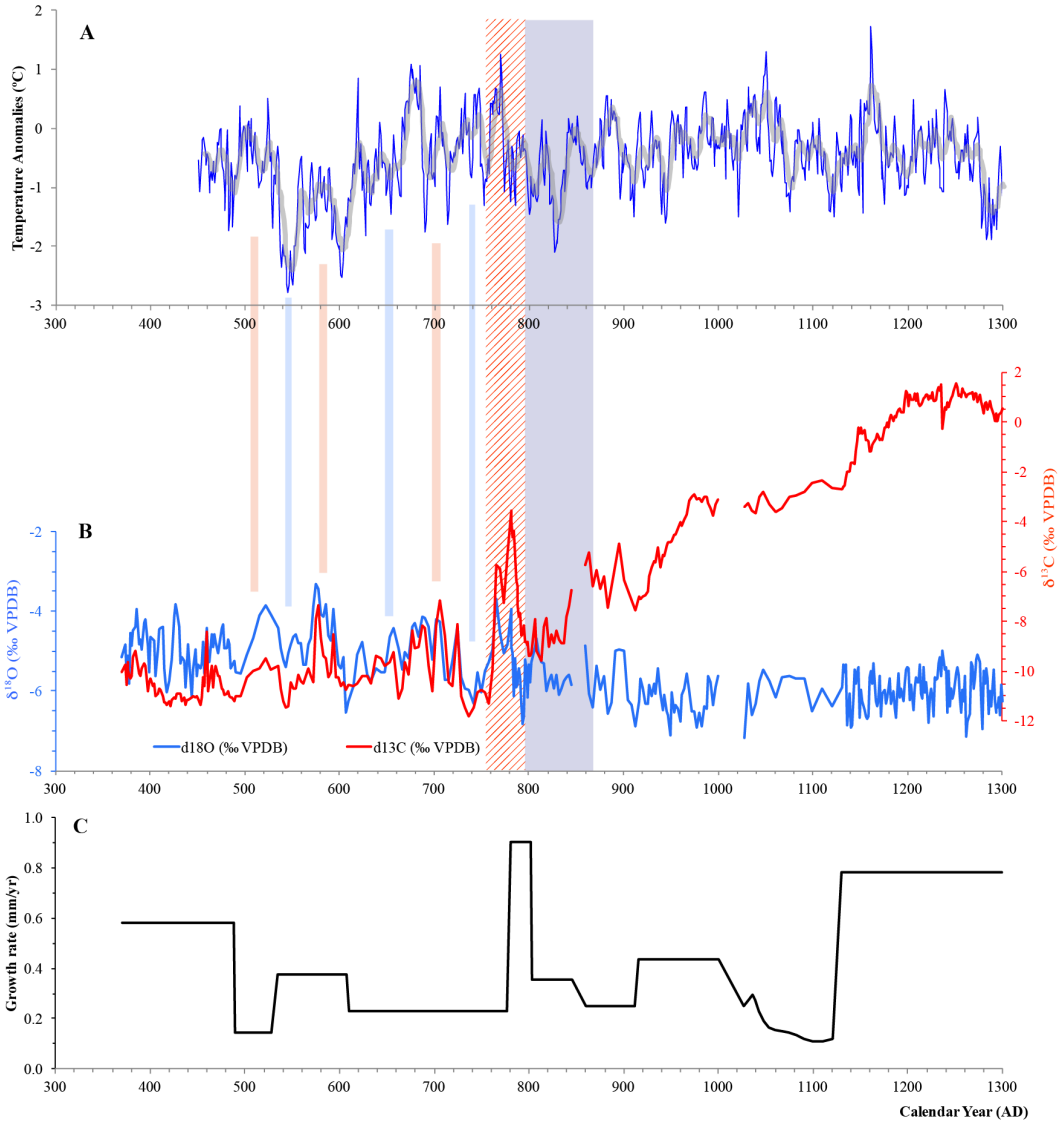
A
Temperature Anomalies (°C)
2
1
0
-1
-2
-3
300
400
500
600
700
800
900
1000
1100
1200
1300
B
δ18O (‰ VPDB)
δ13C (‰ VPDB)
d18O (‰ VPDB)
d13C (‰ VPDB)
C
Growth rate (mm/yr)
1.0
0.8
0.6
0.4
0.2
0.0
Calendar Year (AD)

Figure 3.8: Comparison of the paleoclimate record of Stalagmite MA3 with temperature anomaly records from Europe (see Section 3.5.1.2, 3.5.1.3, and 3.5.2.3 for discussion). A. Temperature anomaly from Europe (Büntgen et al., 2011) (the focus on European records is discussed in Supplementary Text 2). The gray line is a 20 pt. running average. B. Stable isotope of oxygen and carbon ($\delta^{18}O$ and $\delta^{13}C$) profile of Stalagmite MA3. C. Growth rate of Stalagmite MA3. The vertical light orange and blue bars represent period of drier and wetter conditions, respectively, in northwestern Madagascar coinciding with positive/negative temperature anomaly in the European records. The hachured vertical bar is the driest interval in the record. The blue-gray vertical bar is the transition period (see Section 3.5.1.2). Intervals of human settlement in northwestern/northern Madagascar are summarized in Fig. 3.9)

*3.5.1.2. Hydroclimatic history*

Multiple proxy records from Stalagmite MA3 suggest three intervals of changing hydroclimate, presented here in chronological order (Fig. 3.8):

a) Prior to ca. AD. 795, the greater mean values of $\delta^{18}O$ (–4.8‰, vs. VPDB) relative to the sample's mean $\delta^{18}O$ value (–5.6 ‰, vs. VPDB), the abundance of Type L surfaces in the lowest 200 mm of Stalagmite MA3, and the smaller values of the layer-specific width (avg. 50 mm) relative to the sample's layer-specific in the upper portion of the stalagmite (avg. 67.8 mm) combine to suggest an overall drier condition in northwestern Madagascar. This climatic inference is further supported by a widely ranging $\delta^{18}O$ values and a strong linear correlation between $\delta^{18}O$ and $\delta^{13}C$ ($r^2$= 0.44), indicative of kinetic fractionation (Hendy, 1971; Linge et al., 2001). This overall dryness prior to AD. 795 could have increased the evaporation rate, degassing rate (and prior carbonate precipitation, PCP), and cave ventilation, allowing kinetic fractionation to dominate the partitioning of isotopes between the degassed dripwater and the precipitated calcium carbonate minerals (Hendy, 1971; Linge et al., 2001).

In Sainte Luce, southeastern Madagascar, fossil pollen and charcoal in sediment sequences also suggest a pronounced climatic desiccation between ca. 1200 and 700 cal. yr. BP (ca. AD 750-1250) (Virah-Sawmy et al., 2010), a time interval that could coincide with the drier interval in northwestern Madagascar, if uncertainty in both chronologies is considered.

The driest interval within the whole Stalagmite MA3 record occurred between ca. AD 755 and ca. AD 795, at ca. 240–250 mm from its top (Fig. 3.9). In addition to greater

$\delta^{18}O$ (–3.7‰, vs. VPDB) and to the presence of a Type L surface, values of $\delta^{13}C$ also show a large increase from –11.3‰ to –3.9‰ (vs. VPDB), and the layer-specific width is narrow (28 mm, Fig. 3.3). Furthermore, X-ray diffraction of this specific layer demonstrates that the mineralogy is aragonite (Fig. 3.3. b-2). Aragonite is the polymorph of $CaCO_3$ that forms under drier conditions (see references in Table 3.1), and this dry event is consistent with the drying of Lake Mitsinjo, at around AD 750 (Matsumoto and Burney, 1994).

b) Between ca. AD 795 and 870, following the driest period at AD 755-795, the decrease in $\delta^{18}O$ values from –3.0 to –6.0‰ (vs. VPDB), the decrease in $\delta^{13}C$ value from –4 to –10 ‰ (vs. VPDB), the increase in growth rate (from 0.1 to 0.9 mm/yr), the decrease in abundance of Type L surfaces, and the increase of layer-specific width all combine to suggest a change in hydrology from drier to slightly wetter conditions (Table 1). We classify this interval as a transition period for three reasons. First, the mean value of $\delta^{18}O$ (–5.7‰, vs. VPDB) is intermediate between the mean $\delta^{18}O$ value of the interval prior to AD 795 (–4.8‰, vs. VPDB) and the mean $\delta^{18}O$ value of the interval after AD 870 (–6.0‰, vs. VPDB). Second, the gradual decrease in $\delta^{13}C$ could suggest a recovery in vegetation cover above the cave that required sufficient moisture to increase the soil biomass productivity (details regarding $\delta^{13}C$ and vegetation are discussed in Section 3.5.2.2). Third, if one considers the uncertainties of radiometric ages of our stalagmites, the roughly contemporaneous development of an urban center and trading port in the large Swahili stone town of Mahilaka between ca. AD 900–1300 (Radimilahy, 1998; Crowther et al., 2016), northeast

of Anjohibe (Fig. B1) could suggest that climate was favorable to accommodate population migration then.

c) After AD 870, the overall lower $\delta^{18}O$ value (avg. –6.0‰, vs. VPDB) relative to the sample's mean $\delta^{18}O$ (–5.6 ‰, VPDB), the greater layer-specific width (ca. 67.8 mm), and the abundance of Type E surfaces in the upper ca. 150 mm of Stalagmite MA3 (Fig. 3.3c, d) combine to suggest much wetter conditions in northwestern Madagascar. These Type E surfaces could reflect faster groundwater recharge from heavier rainfall (Railsback et al., 2013) during summers. Thus, one could speculate that northwestern Madagascar received more summer rainfall after AD 870 than before then. That increase could reflect either an increase in the amount of monthly rainfall received during the summer or an increase in the number of rainy months in summer.

One striking feature of the upper portion of Stalagmite MA3 is the presence of millimeter-to-centimeter internal cavities elongated along the growth axis of the stalagmite (Fig. 3.3a, b-1). Cavities like these are named "macroholes" or "axial holes" (Shtober-Zisu et al., 2012, 2014). They develop as the newly precipitated layers are sufficiently unconsolidated to allow the falling droplet of water to carve into the precipitated spelean layers as it degases to create cavities (Shtober-Zisu et al., 2014). At these axial holes, the layers are curved toward the center of the stalagmite (Fig. 3.3b-1). In this scenario, these axial holes could be related to an increased depositional rate (here from 0.1 to 0.8 mm/year) of the spelean carbonates as the drip water progressively loses $CO_2$ to the cave atmosphere and stagnates at the top of the stalagmite (Shtober-Zisu et al.,

2012, 2014), as suggested by the FLOW-model of Romanov et al. (2008). In that case, macroholes would reflect wetter conditions.

#### *3.5.1.3. Rainfall in northwestern Madagascar and the influence of the ITCZ/Monsoon*

A broad screening of the $\delta^{18}O$ profile of Stalagmite MA3 from AD 370 to AD 1300 suggests a relatively stable hydroclimate in Northwestern Madagascar, which could reflect the seasonal visit of the ITCZ to the island every summer. However, closer examination of the $\delta^{18}O$ records reveals a semi-centennial (average 50 years) variability prior to AD 870 as opposed to the period after then (Fig. 3.8). This semi-centennial variability could be ascribed to the length of visit of the ITCZ over northwestern Madagascar. During longer visits, northwestern Madagascar receives more rainfall and the cold/dry winter seasons are shorter (reflected in the smaller $\delta^{18}O$). During briefer visits of the ITCZ, northwestern Madagascar receives less rainfall and the cold/dry seasons become longer (reflected in the greater $\delta^{18}O$).

At longer time scales, the variation of the length of visits of the ITCZ in northwestern Madagascar could be linked to global conditions, specifically to the extent of global ice cover and to the difference in temperature between the Northern and Southern Hemisphere (e.g. Broccoli et al., 2006; Chiang and Bitz, 2005; Chiang and Friedman, 2012; Schneider et al., 2014). During colder intervals, the ITCZ is pushed southward (Broccoli et al., 2006; Chiang and Bitz, 2005), and as a result, several regions in the low to mid-latitudes in the Southern Hemisphere receive more rainfall (e.g. Brown and Johnson, 2005; Russell and Johnson, 2007; Schefuß et al, 2011; Voarintsoa et al., 2016). This is relevant because

wetter and drier periods in northwestern Madagascar as suggested by the proxy records in Stalagmite MA3 correlate with temperature anomalies reconstructed from tree rings in Europe (Büntgen et al., 2011) (the focus on European records is discussed in Supplementary Text 2). Lower $\delta^{18}O$ values in MA3 coincide with negative temperature anomalies in the European records, suggesting that an increase in precipitation (or possibly longer wet seasons) over northwestern Madagascar coincided with longer southward visits of the ITCZ when the NH was cooler. On the other hand, greater $\delta^{18}O$ values in MA3 coincide with positive temperature anomalies in the European records and could suggest a decrease in precipitation (or shorter wet seasons, but longer cold/dry winters) in response to shorter visits of the ITCZ. This could correspond to a more northward migration of the ITCZ.

### 3.5.2. Speleothem $\delta^{13}C$ as an indicator of past vegetation and human impact

#### *3.5.2.1. Perspectives on the nature of changing vegetation in northwestern Madagascar*

The nationwide distribution of $C_4$ grassland in Madagascar has been a major subject of debate (e.g. Virah-Sawmy et al., 2010; Willis et al., 2008; also see the review on page 2353 of Irwin et al., 2010). On one hand, it was interpreted to result from human activities following the first settlement. Humbert (1927), for example, adopted the hypothesis that Madagascar was covered by continuous, dense, and climax forest prior to human arrival, a hypothesis that was later supported by Lavauden (1931, p. 821). On the other hand, the nationwide distribution of $C_4$ grassland was argued to be natural (Willis et al., 2008) as a response to the worldwide expansion of $C_4$ grassy biomes after the late Miocene (Bond et

al., 2008), in response to cold and dry climates (Bonnefille, 1985; Burney, 1997a) linked to a decrease in $CO_2$ (Bouchenak-Khelladi et al., 2009).

A natural origin of $C_4$ grasslands in western Madagascar seems to be supported by the region's climatic regime: the region only receives rainfall during summer months. Additionally, it experiences the orographic effect during winter, when the warm vapor from the Indian Ocean is blocked by the chain of mountains that stretches North-South along the eastern escarpment of Madagascar (Section 3.2.3). Drier conditions lead to a sparser vegetation cover with fewer temperature-tolerant trees but with more $C_4$ grasses, typical of western Madagascar as opposed to eastern Madagascar.

Paleoenvironmental study using pollen stratigraphy at Lake Mitsinjo, located southwest of Anjohibe Cave, suggests a mosaic of dry forest and grassland that dominated the area from ca. 3500 BP until the lake dried up, around 1200 BP (Matsumoto and Burney, 1994). That landscape then changed to savanna from ca. 1000 to 500 BP, a period of human disturbance recorded by archaeological evidence (Fig.9; Matsumoto and Burney, 1994). According to Matsumoto and Burney (1994), the last 500 years were characterized by a highly disturbed landscape of grassland with fire-adapted trees and ruderal herbs, the cause of which was linked to human disturbance.

At present, swidden agriculture, known as "tavy", is a very typical mode of cultivation in Madagascar, at least since the French colonization. These activities could have started long before Austronesian migration to the island. "Tavy" can be explained as follow: former vegetation is burned and is replaced with various crops, mostly with dry-land rice or "vary an-tanety", which are planted for a few years until the soils are

impoverished, and then abandoned (see also Conklin, 1954; Dove, 1993; Raharimalala et al., 2010). The degraded lands are then succeeded by secondary grasslands and other fire-prone open vegetation ecosystems, named "savoka" (Irwin et al., 2010) or "monka" (Raharimalala et al. 2010), including woodland, bushland, and shrubland as briefly reviewed on page 56 of Ingram and Dawson (2005). This could significantly alter the $\delta^{13}C$ signals in speleothems by influencing the rate of passage of water through the soil and limestone (e.g. Bar-Matthews et al., 1996; Baldini et al., 2005), as discussed in the following Section 3.5.2.2.

### *3.5.2.2. Possible controls on speleothem $\delta^{13}C$*

Changes in speleothem $\delta^{13}C$ largely depend on the changes in $\delta^{13}C$ of three reservoirs: the atmosphere, the soil, and the limestone bedrock. Table 3.1 provides a summary of the possible controlling factors for speleothem $\delta^{13}C$ and supplementary materials provide details on the roles these factors play in influencing the speleothem $\delta^{13}C$. Among the reservoir sources, atmospheric $CO_2$ has little influence on speleothem $\delta^{13}C$ because the concentration of carbon dioxide ($CO_2$) in the atmosphere stayed constant between AD 370 and AD 1300, during which Stalagmite MA3 grew. Here, $\delta^{13}C$ of the soil is fundamental, and it varies depending on the nature of vegetation and the rate of biological activity (e.g. Cerling et al., 1991; Talma and Vogel, 1992; Brook et al., 1999, 2015). The $\delta^{13}C$ of speleothems can be linked to climate-driven vegetation changes (e.g. Dorale and Liu, 2009; Dorale et al., 1998; Hellstrom et al., 1998; Baldini et al., 2005; Sletten et al., 2013; Baker et al., 1997; Fairchild et al. 2000). For example, more biological activity

favors greater input of low-$\delta^{13}C$ $CO_2$ to soil gas via root respiration and/or decay of organic matter (e.g. Hesterberg and Siegenthaler; 1991; Baldini et al., 2005; Amundson et al., 1998; Genty et al., 2003; Drysdale et al., 2004). When the percolating water is en route to the cave system, its $\delta^{13}C$ can still be altered by several factors, such as the residence time of the water above the cave (e.g. Clark and Fritz, 1997; Baldini et al., 2005). Inside the cave, additional changes can occur. Those changes could be linked to evaporation (Hendy, 1971; Linge et al., 2001), the dripwater rate (e.g. Yadava and Ramesh, 2006), the degassing rate and prior carbonate precipitation, PCP (Dreybrodt and Scholz, 2011; Baker et al., 1997; Fairchild et al., 2000; Johnson et al., 2006; Cruz et al., 2007; Fairchild and McMillan, 2007; Fairchild and Treble, 2009; Oster et al., 2009; 2010), the $CaCO_3$ precipitation rate (Hendy, 1971; Wigley et al 1978; Bar-Matthews et al 1996; Hellstrom et al., 1998) and cave ventilation (e.g. James et al., 2015; Spötl et al., 2005; Banner et al., 2007; Kowalczk and Froelich, 2010; Mattey et al., 2010; Boch et al., 2011; Frisia et al., 2011; Lambert and Aharon, 2011; Tremaine et al., 2011; Wong et al., 2011). All these factors could enhance kinetic isotope fractionation in speleothems.

#### *3.5.2.3. Changing vegetation in northwestern Madagascar: evidence from speleothem $\delta^{13}C$*

Changes in $\delta^{13}C$ of Stalagmite MA3, replicated by Stalagmites ANJ94-5 and MA2, suggest three distinct intervals of vegetation change between AD 370 and AD 1300 in northwestern Madagascar (Fig. 3.8).

(1) Prior to AD 795 the $\delta^{13}C$ records, with an average of –9.8‰ (vs. VPDB) within that interval, suggest that vegetation was dominated by $C_3$ plants, and the covariance between $\delta^{13}C$ and $\delta^{18}O$ suggest that changes in vegetation were primarily driven by climate (Dorale and Liu, 2009; Dorale et al., 1998; Hellstrom et al., 1998; Baldini et al., 2005; Sletten et al., 2013). We ascribe this climatic control to the latitudinal migration of the ITCZ (Section 3.5.1.3). The significant shift in $\delta^{13}C$ between AD 755 and 795 could suggest a significant decrease in biological activity above the cave in response to dry conditions (Section 3.5.1.2), enhancing kinetic fractionation in Anjohibe cave (Section 3.5.2.2) or in response to natural fires (e.g. Burney, 1997b; Nagra et al., 2016).

(2) Between AD 795 and AD 870, the record suggests a vegetation recovery following the driest interval described earlier (see Section 3.5.1.2). The gradual decrease in $\delta^{13}C$ in Stalagmite MA3 probably reflects an increase in vegetation cover and biomass activity above the cave when climate was relatively wetter (Section 3.5.1.2). This in turn could be associated with an increased moisture and humidity favoring bio-productivity in the soil epikarst. In addition, the percolating water could have longer residence times to exchange carbon with the soil epikarst (i.e., in an open system). Thus, speleothem $\delta^{13}C$ became depleted (Baldini et al., 2005; Bar-Matthews et al., 1996). Changes in speleothem $\delta^{13}C$ at that time could have also been influenced by human activities, such as the practice of swidden agriculture (e.g. Conklin, 1954; Dove, 1993) and the introduction of crops by foreign settlers (e.g. Crowther et al. 2016), but as the timing of human colonization in the study area is not fully refined, our hypothesis in linking human activity and $\delta^{13}C$ during this interval requires further investigation.

(3) After AD 870, the gradational but very large shift in $\delta^{13}C$ from ca. –9.0‰ to ca. +1.5‰ (vs. VPDB) suggests that vegetation cover around Anjohibe Cave changed completely, if gradually, and became dominated by $C_4$ plants by ca. AD 1130. This change corresponds to a landscape transition to an open savanna (e.g. Crowley and Samonds, 2013). The absence of correlation between $\delta^{13}C$ and $\delta^{18}O$ in Stalagmite MA3 suggests that the change in vegetation was controlled by something other than climate. Extensive human land use could be the main factor leading to this change (Burns et al., 2016; Crowley and Samonds, 2013). The practice of "tavy" by burning former vegetation former vegetation in favor of various crops, mostly with dry-land rice or "vary an-tanety" must have been the factors responsible of this $\delta^{13}C$ shift. These crops are planted for a few years until the soils are impoverished, and then abandoned, leaving naked land that later transform to secondary grasslands (see Section 3.5.2.1, see also Conklin, 1954 and Dove, 1993). This perspective is similar to changes in vegetation around the Brown's Folly Mine, Wiltshire, in England (Baldini et al., 2005). In the Brown's Folly Mine's scenario, re-vegetation above the mine increased the input of isotopically light biogenic carbon to the total dissolved inorganic carbon (DIC), resulting in lower spelean $\delta^{13}C$ (Baldini et al., 2005). In Anjohibe Cave, however, land clearance followed by growth of new secondary $C_4$ vegetation resulted in higher speleothem $\delta^{13}C$. The Anjohibe scenario after AD 870 is an example of a closed system under $C_4$ vegetation cover, when seeping water has less residence time to exchange $CO_2$ with the soil.

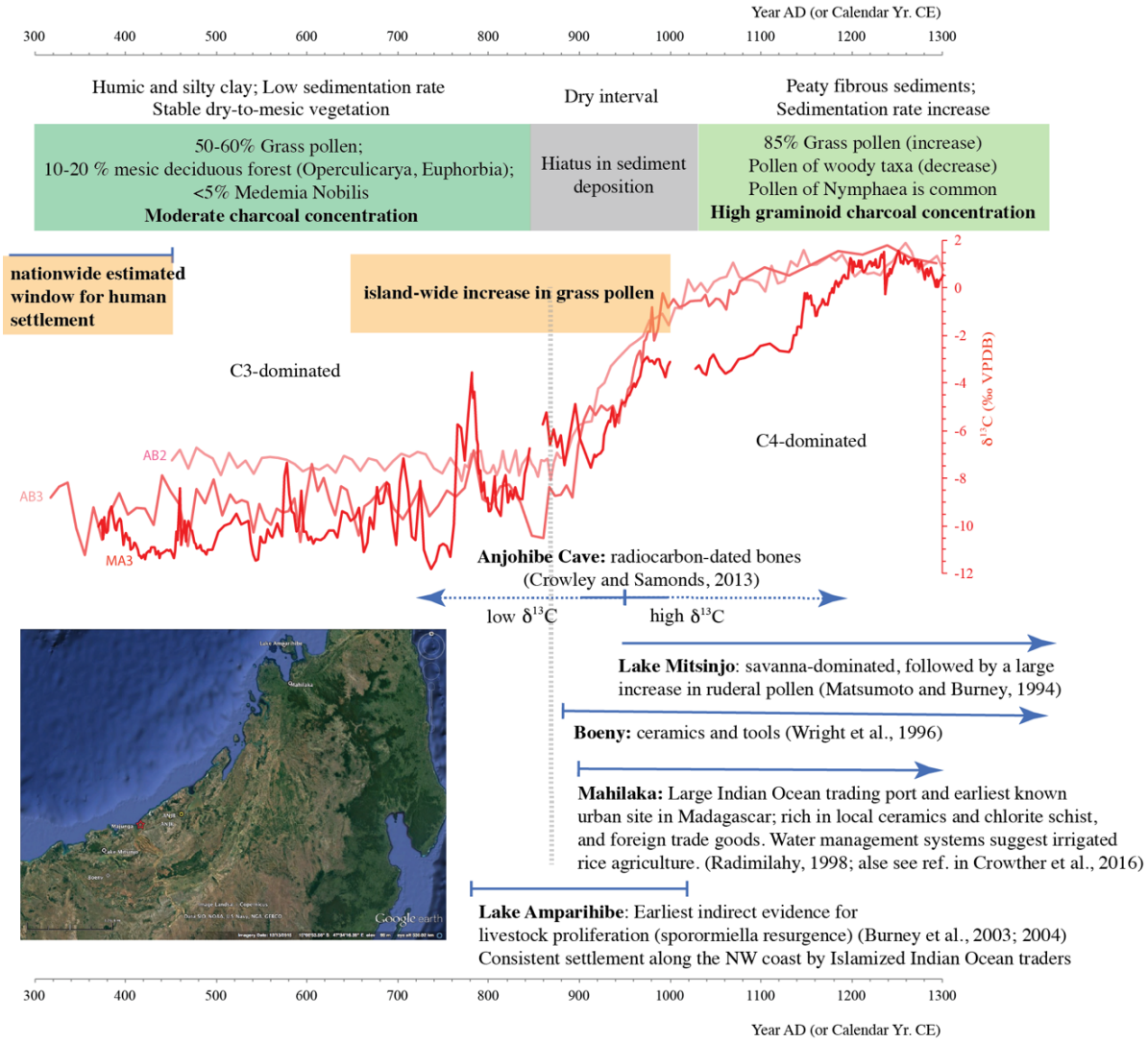
Year AD (or Calendar Yr. CE)
300 400 500 600 700 800 900 1000 1100 1200 1300
Humic and silty clay; Low sedimentation rate
Stable dry-to-mesic vegetation
Dry interval
Peaty fibrous sediments;
Sedimentation rate increase
50-60% Grass pollen;
10-20 % mesic deciduous forest (Operculicarya, Euphorbia);
<5% Medemia Nobilis
Moderate charcoal concentration
Hiatus in sediment deposition
85% Grass pollen (increase)
Pollen of woody taxa (decrease)
Pollen of Nymphaea is common
High graminoid charcoal concentration
nationwide estimated window for human settlement
island-wide increase in grass pollen
C3-dominated
C4-dominated
AB2
AB3
MA3
δ13C (‰ VPDB)
2 0 -2 -4 -6 -8 -10 -12
Anjohibe Cave: radiocarbon-dated bones
(Crowley and Samonds, 2013)
low δ13C
high δ13C
Lake Mitsinjo: savanna-dominated, followed by a large increase in ruderal pollen (Matsumoto and Burney, 1994)
Boeny: ceramics and tools (Wright et al., 1996)
Mahilaka: Large Indian Ocean trading port and earliest known urban site in Madagascar; rich in local ceramics and chlorite schist, and foreign trade goods. Water management systems suggest irrigated rice agriculture. (Radimilahy, 1998; alse see ref. in Crowther et al., 2016)
Lake Amparihibe: Earliest indirect evidence for livestock proliferation (sporormiella resurgence) (Burney et al., 2003; 2004)
Consistent settlement along the NW coast by Islamized Indian Ocean traders
300 400 500 600 700 800 900 1000 1100 1200 1300
Year AD (or Calendar Yr. CE)

Figure 3.9: Summary of human settlement evidence in northern/northwestern Madagascar, which is compared with the carbon stable isotope profile of Stalagmites MA3 (this study), AB2, and AB3 (Burns et al., 2016). Paleoenvironmental inferences are from Matsumoto and Burney (1994), Wright et al. (1996), Burney et al. (2003), Crowley and Samonds (2013), and Burns et al. (2016). Archaeological evidences are from Wright et al. (1996), Radimilahy (1998), Crowther et al. (2016), and Burney et al. (2003, 2004). The map shows the locations of the archaeological and paleoenvironmental sites listed in the summary (higher resolution of the map is available in Fig. B1).

### 3.5.3. Reconstructing population settlement and land use in northwestern Madagascar

Human settlement in northwestern Madagascar seems to have occurred between AD 795 and AD 870 (Fig. 3.8), an interval we assume of "favorable conditions". Favorable conditions mean potentially prosperous lands, as suggested by archaeological evidence (e.g. Wright et al., 1996) during wetter conditions, as suggested by Stalagmite MA3's stable isotopes (lower $\delta^{18}O$ and $\delta^{13}C$) and petrography (greater layer-specific width and more Type E surfaces) (Section 3.5.1.2). These conditions could have attracted foragers, who were thought to be the initial settlers of Madagascar (Wright et al., 1996; Beaujard, 2011; Dewar et al., 2013; Douglass and Zinke, 2015), followed by maritime traders, who brought new crops on the island (e.g. Cox et al., 2012; Crowther et al., 2016). Several lines of evidence (archaeological, linguistic, broad geographical screening) support this migration (e.g. Battistini et al., 1963; Vérin, 1975; Dewar, 1984; Dewar et al., 2013; Beaujard, 2011; Cox et al., 2012). Figure 3.9 provides a summary of this settlement in northwestern/northern Madagascar.

Cox et al. (2012) found that the island's initial settlement was around AD 830 (see their page 2766), based on their coalescent simulation. According to them, this date is consistent with evidence from linguistics, which links the colonization of Madagascar to the expansion of Indonesian trading networks during the Srivijaya Empire (Adelaar, 2009). Settlers are believed to have come from Indonesia and Africa (e.g. Matsumoto and Burney, 1994; Cox et al., 2012; Crowther et al., 2016). In the Boeny region, located 25 km north of Lake Mitsinjo, human settlement dates to AD 1100 or earlier, and herding and cultivation practices by those settlers could have affected the vegetation in the surrounding locations

(Matsumoto and Burney, 1994; Wright et al., 1996). In the region of Mahilaka, about 500 km drive north of Anjohibe, massive evidence indicates human settlement occurred ca. AD 900 (Radimilahy, 1998; Crowther et al., 2016).

Although the timing of settlement is not fully refined, and although the mode of settlement is not clear in Madagascar, either as a single colonization event or via repeated settlement waves from the same source of population, known as "ranto" (Adelaar, 2009; Ottino, 1974; Beaujard, 2003), it is likely that population in Madagascar had grown in numbers since ca. 50 BC-AD 950, and the need for more land increased. This population growth has led to extensive human activities in the region, specifically the practice of swidden agriculture, which could have shaped the landscape of the region. This argument seems to agree with the late-Holocene increases in charcoal, grass pollen, and grasslands documented at Anjohibe cave (Burney et al., 1997c; Crowley and Samonds, 2013) and around Lake Mitsinjo (Matsumoto and Burney, 1994). After land abandonment, secondary $C_4$ vegetation became dominant (Fig.3.7–3.9; Conklin, 1954; Dover, 1993; Raharimalala et al., 2010), as suggested by greater $\delta^{13}C$ values in Stalagmite MA3 (this study), carbon isotope values from radiocarbon-dated bones from Anjohibe Cave (Crowley and Samonds, 2013), and the dominance of Graminaea and Nymphaea pollen in the Mitsinjo area (Matsumoto and Burney, 1994).

Because some human modification of the landscape can lead to direct damage to the ecosystem, one might conclude that human activities were also the causes of past megafaunal loss in Madagascar, especially when one sees the island's forest cover that has diminished since the colonial period (e.g. Allnutt et al., 2008). However, the situation is

more complex for the following reasons. Madagascar experienced extreme but natural climate-related events such as droughts, fires, cyclones, and land loss due to erosion long before human arrival (e.g. Battistini, 1971; Mahé and Sourdat, 1972; MacPhee, 1986; Wells and Andriamihaja, 1993, 1997; Cox et al., 2009). In addition, the western part of Madagascar has never been fully forested, and it is not clear how much of the island was originally covered with forest. Furthermore, the considerable differences in climate from the eastern region to the western Madagascar (Section 3.2.3) could suggest an independent history of environmental changes, particularly with regard to human, plant, and animal interactions. Above all, since Madagascar's isolation from Africa and India ca. 165 Ma (e.g. Wells, 2003), many species of the Malagasy megafauna were endemic and were prone to extinction given the dry climatic conditions around 2-3 ka (e.g. Battistini, 1971; Mahé and Sourdat, 1972; MacPhee, 1986). In brief, even though there is a link between population growth and ecosystem alteration in Madagascar, land use alone need not be held responsible for the megafaunal loss in Madagascar (e.g., Jarosz, 1993), and linking megafaunal loss to any paleoclimate study should be done carefully.

## 3.6. Conclusion

Multiple proxy analyses from a U/Th-dated Stalagmite MA3 provide detailed information about paleoenvironmental changes in Madagascar. A comprehensive understanding of the processes controlling each of these proxies suggests that prior to AD 795 ecosystem and hydroclimate changes in northwestern Madagascar were linked to the latitudinal migration of the ITCZ. Specifically, wetter or drier climate was a response to a

cooler or warmer Northern Hemisphere, respectively, in accord with climate models (e.g. Chiang and Bitz, 2005). This interval ended with very dry conditions from ca. AD 755 to 795. It was followed by a transition period between AD 795 and 870 with evidence of human settlement in the region (Matsumoto and Burney, 1994). The following interval, i.e. after AD 870, was marked by a gradational change in plant community from $C_3$ to $C_4$-dominated vegetation and by a landscape transformation from more dense to less dense vegetation cover. This change could be linked to land use, such as the practice of "Tavy", or swidden agriculture, in the area. Although there is a link between land practice and ecosystem change in Madagascar after ca. AD 870, the megafaunal loss throughout the history of Madagascar should be interpreted very carefully.

## REFERENCES


Adelaar, A., 2009. Loanwords in Malagasy, in Haspelmath, M., Tadmor, U, (Eds.), Loanwords in the world's languages: a comparative handbook, Berlin, Germany, pp. 717 – 746.

Allnutt, T.F., Ferrier, S., Manion, G., Powell, G.V.N., Ricketts, T.H., Fisher, B.L., Harper, G.J., Irwin, M.E., Kremen, C., Labat, J.N., Lees, D.C., Pearce, T.A., Rakotondrainibe, F., 2008. A method for quantifying biodiversity loss and its application to a 50-year record of deforestation across Madagascar. Conservation Letters 1, 173-181.

Amundson, R., Stern, L., Baisden, T., Wang, Y., 1998. The isotopic composition of soil and soil-respired $CO_2$: Geoderma 82, 83-114.

Baker, A., Ito, E., Smart, P.L., McEwan, R.F., 1997. Elevated and variable values of C-13 in speleothems in a British cave system. Chem. Geol. 136, 263-270.

Baldini, J.U.L., McDermott, F., Baker, A., Baldini, L.M., Mattey, D.P., Railsback, L.B., 2005. Biomass effects on stalagmite growth and isotope ratios: A 20th century analogue from Wiltshire, England. Earth Planet. Sci. Let. 240, 486-494.

Banner, J.L., Guilfoyle, A., James, E.W., Stern, L.A., Musgrove, M., 2007. Seasonal variations in modern speleothem calcite growth in Central Texas, U.S.A. J Sediment Res 77, 615-622.

Bar-Matthews, M., Ayalon, A., Matthews, A., Sass, E., Halicz, L., 1996. Carbon and oxygen isotope study of the active water-carbonate system in a karstic Mediterranean cave: Implications for paleoclimate research in semiarid regions. Geochim. Cosmochim. Acta 60, 337-347.

Battistini, R., Vérin, P., Raison, R., 1963. La site archéologique de Talaky: Cadre géographique et géologique, premiers travaux de fouilles, notes ethnographiques sur le village actuel proche du site. Ann. Univ. Madagascar 1, 112-134.

Battistini, R., Petit, M., 1971. Géomorphologie. In: Le Bourdiec, F., Battistini, R., LeBourdiec, P. (Eds.), Atlas de Madagascar: Tananarive, Bureau pour le Development de la Production Agricole, pp. 14-16.

Beaujard, P., 2003. Les arrivées austronésiennes à Madagascar: vagues ou continuum?. Etud. Océan Ind. 35–36, 59–147.

Beaujard, P., 2011. The first migrants to Madagascar and their introduction of plants: linguistic and ethnological evidence. Azania 46, 169-189.

Bischoff, J.L., Fyfe, W.S., 1968. Catalysis, inhibition, and the calcite-aragonite problem. I. The Aragonite-Calcite transformation. Amer. J. Sci. 266, 65-79.

Bischoff, J.L., 1968. Catalysis, inhibition, and the calcite-aragonite problem. II. The Vaterite-Aragonite transformation. Amer. J. Sci. 266, 80-90.

Boch, R., Spötl, C., and Frisia, S., 2011. Origin and paleoenvironmental significance of lamination in stalagmites from Katerloch Cave, Austria. Sedimentology 58, 508-531.

Bond, W.J., Silander, J.A., Ranaivonasy, J., Ratsirarson, J., 2008. The antiquity of Madagascar's grasslands and the rise of C(4) grassy biomes. J. Biogeogr. 35, 1743-1758.

Bonnefille, R., 1985. Evolution of the Continental Vegetation - the Paleobotanical Record from East-Africa. S. Afr. J. Sci. 81, 267-270.

Bony, S., Risi, C., Vimeux, F., 2008. Influence of convective processes on the isotopic composition ($\delta^{18}O$ and $\delta D$) of precipitation and water vapor in the tropics: 1. Radiative-convective equilibrium and Tropical Ocean–Global Atmosphere–Coupled Ocean–Atmosphere Response Experiment (TOGA-COARE) simulations. J. Geophys. Res. Atmos. 113, D19305. http://dx.doi.org/10.1029/ 2008JD009942.

Bouchenak-Khelladi, Y., Verboom, G.A., Hodkinson, T.R., Salamin, N., Francois, O., Ni Chonghaile, G., and Savolainen, V., 2009. The origins and diversification of C-4 grasses and savanna-adapted ungulates. Global Change Biol. 15, 2397-2417.

Bowen, G., 2013. Gridded maps of the isotopic composition of meteoric waters: Africa/Madagascar. http://www.waterisotopes.org.

Broccoli, A.J., Dahl, K.A., Stouffer, R.J., 2006. Response of the ITCZ to Northern Hemisphere cooling. Geophys. Res. Lett. 33, L01702.

Brook, G.A., Ellwood, B.B., Railsback, L.B., Cowart, J.B., 2006. A 164 ka record of environmental change in the American Southwest from a Carlsbad Cavern speleothem. Palaeogeogr. Palaeoclimatol. Palaeoecol. 237, 483-507.

Brook, G.A., Rafter, M.A., Railsback, L.B., Sheen, S.W., Lundberg, J., 1999. A high-resolution proxy record of rainfall and ENSO since AD 1550 from layering in stalagmites from Anjohibe Cave, Madagascar. Holocene 9, 695-705.

Brook, G.A., Railsback, L.B., Scott, L., Voarintsoa, N.R.G., Liang, F., 2015. Late Holocene Stalagmite and Tufa Climate Records for Wonderwerk Cave: Relationships Between Archaeology and Climate in Southern Africa. Afr. Arch. Rev. 32, 1-32.

Brook, G.A., Scott, L., Railsback, L.B., Goddard, E.A., 2010. A 35 ka pollen and isotope record of environmental change along the southern margin of the Kalahari from a stalagmite and animal dung deposits in Wonderwerk Cave, South Africa. J Arid Environ 74, 870-884.

Brown, E.T., Johnson, T.C., 2005. Coherence between tropical East African and South American records of the Little Ice Age. Geochem. Geophys. Geosys. 6.

Büntgen, U., Tegel, W., Nicolussi, K., McCormick, M., Frank, D., Trouet, V., Kaplan, J.O., Herzig, F., Heussner, K.U., Wanner, H., Luterbacher, J., Esper, J., 2011. 2500 Years of European Climate Variability and Human Susceptibility. Science 331, 578-582.

Burney, D., 1997a, Theories and Facts regarding Holocene Environmental Change before and after Human Colonization. In Goodman, S.M., Patterson, B.D. (Eds.), Natural Change and Human Impact in Madagascar.

Burney, D.A., 1997b, Tropical islands as paleoecological laboratories: Gauging the consequences of human arrival. Human Ecol. 25, 437-457.

Burney, D. A., James, H. F., Grady, F. V., Rafamantanantsoa, J. G., Ramilisonina, Wright, H. T., and Cowart, J. B., 1997c, Environmental change, extinction and human activity: evidence from caves in NW Madagascar. J. Biogeogr. 24, 755–767.

Burney, D.A., 1987a, Late Quaternary stratigraphic charcoal records from Madagascar. Quaternary Research 28, 274-280.

Burney, D.A., 1987b, Late Holocene Vegetational Change in Central Madagascar: Quat. Res. 28, 130-143.

Burney, D.A., 1993a, Late Holocene Environmental-Changes in Arid Southwestern Madagascar. Quat. Res. 40, 98-106.

Burney, D.A., 1993b, Recent Animal Extinctions - Recipes for Disaster. American Scientist 81, 530-541.

Burney, D.A., 2003. Madagascar's prehistoric ecosystems. In Goodman, S.M., Benstead, J.P. (Eds.), The Natural History of Madagascar. University of Chicago Press, pp. 47-51.

Burney, D.A., Burney, L.P., Godfrey, L.G., Jungers, W.L., Goodman, S.M., Wright, H.T., Jull, A.J.T., 2004. A chronology for late prehistoric Madagascar. J. Human Evol., 47, 25–63.

Burney, D.A., MacPhee, R.D.E., 1988. Mysterious island: what killed Madagascar's large native animals? Natural History 97, 46-55.

Burns, S.J., Fleitmann, D., Mudelsee, M., Neff, U., Matter, A., and Mangini, A., 2002. A 780-year annually resolved record of Indian Ocean monsoon precipitation from a speleothem from south Oman. J. Geophys. Res. Atm. 107, D20.

Burns, S.J., Godfrey, L.R., Faina, P., McGee, D., Hardt, B., Ranivoharimanana, L., Randrianasy, J., 2016, Rapid human-induced landscape transformation in Madagascar at the end of the first millennium of the Common Era. Quat. Sci. Rev. 134, 92-99.

Cabrol, P., Coudray, J., 1982. Climatic fluctuations influence the genesis and diagenesis of carbonate speleothems in southwestern France. Natl. Spel. Soc. Bul. 44, 112–117.

Caddeo, G.A., De Waele, J., Frau, F., Railsback, L.B., 2011. Trace element and stable isotope data from a flowstone in a natural cave of the mining district of SW Sardinia (Italy): evidence for $Zn^{2+}$–induced aragonite precipitation in comparatively wet climatic conditions. Intl. J. Spel. 40, 181-190.

Caddeo, G.A., Railsback, L.B., De Waele, J., and Frau, F., 2015. Stable isotope data as constraints on models for the origin of coralloid and massive speleothems: The interplay of substrate, water supply, degassing, and evaporation. Sed. Geol. 318,130-141.

Cerling, T.E., Solomon, D.K., Quade, J., Bowman, J.R., 1991. On the isotopic composition of carbon in soil carbon dioxide. Geochem. Cosmochim. Acta 55, 3403-3405.

Cheng, H., Edwards, R.L., Shen, C.C., Polyak, V.J., Asmerom, Y., Woodhead, J., Hellstrom, J., Wang, Y.J., Kong, X.G., Spötl, C., Wang, X.F., Alexander, E.C., 2013. Improvements in Th-230 dating, Th-230 and U-234 half-life values, and U-Th isotopic measurements by multi-collector inductively coupled plasma mass spectrometry: Earth Planet. Sci. Lett. 371, 82-91.

Chiang, J.C.H., Bitz, C.M., 2005. Influence of high latitude ice cover on the marine Intertropical Convergence Zone. Clim. Dyn. 25, 477-496.

Chiang, J.C.H., Friedman, A.R., 2012. Extratropical Cooling, Interhemispheric Thermal Gradients, and Tropical Climate Change. Ann. Rev. Earth Planet. Sci. 40, 383-412.

Clark, I.D., Fritz, P., 1997. Environmental isotopes in hydrogeology. Lewis Publishers.

Conklin, H.C., 1954. An Ethnoecological Approach to Shifting Agriculture. T New York Acad Sci 17, 133-142.

Cox, R., Bierman, P., Jungers, M., Rakotondrazafy, A.F.M., 2009. Erosion rates and sediment sources in Madagascar inferred from $^{10}$Be analysis of lavaka, slope, and river sediment. J. Geol., 117, 363-376.

Cox, M.P., Nelson, M.G., Tumonggor, M.K., Ricaut, F.X., Sudoyo, H., 2012. A small cohort of Island Southeast Asian women founded Madagascar. Proc. R. Soc. B–Biol. Sci. 279, 2761-2768.

Cross, M., McGee, D., Broecker, W.S., Quade, J., Shakun, J.D., Cheng, H., Lu, Y., Edwards, R.L., 2015. Great Basin hydrology, paleoclimate, and connections with the North Atlantic: A speleothem stable isotope and trace element record from Lehman Caves, NV. Quat. Sci. Rev. 127, 186–198.

Crowley, B.E., 2010. A refined chronology of prehistoric Madagascar and the demise of the megafauna. Quaternary Sci Rev 29, 2591-2603.

Crowley, B.E., Godfrey, L.R., Bankoff, R.J., Perry, G.H., Culleton, B.J., Kennett, D.J., Sutherland, M.R., Samonds, K.E., Burney, D.A., 2016. Island-wide aridity did not trigger recent megafaunal extinctions in Madagascar. Ecography, (in press). doi:10.5061/dryad.s5s2n

Crowley, B.E., Godfrey, L.R., Burney, D.A., 2010. New support for a human hand in the collapse of Madagascar's megafaunal community: Using C-14 dates to track species persistence and population decline during the Holocene. Am J Phys Anthropol, 88-88.

Crowley, B.E., Samonds, K.E., 2013. Stable carbon isotope values confirm a recent increase in grasslands in northwestern Madagascar. The Holocene 23, 1066-1073.

Crowther, A., Lucas, L., Helm, R., Horton, M., Shipton, C., Wright, H.T., Walshaw, S., Pawlowicz, M., Radimilahy, C., Douka, K., Picornell-Gelabert, L., Fuller, D.Q., Boivin, N.L., 2016. Ancient crops provide first archaeological signature of the westward Austronesian expansion. P Natl Acad Sci USA 113, 6635-6640.

Cruz, F.W., Burns, S.J., Karmann, I., Sharp, W.D., Vuille, M., Ferrari, J.A., 2006. A stalagmite record of changes in atmospheric circulation and soil processes in the Brazilian subtropics during the Late Pleistocene. Quat. Sci. Rev. 25, 2749-2761.

Cruz, F., Burns, S., Jercinovic, M., Karmann, I., Sharp, W., Vuille, M., 2007. Evidence of rainfall variations in Southern Brazil from trace element ratios (Mg/Ca and Sr/Ca) in a Late Pleistocene stalagmite. Geochim. Cosmochim. Acta 71, 2250– 2263.

Cuthbert, M.O., Baker, A., Jex, C.N., Graham, P.W., Treble, P.C., Andersen, M.S., Acworth, R.I., 2014. Drip water isotopes in semi-arid karst: Implications for speleothem paleoclimatology. Earth Planet. Sci. Lett. 395, 194-204.

Dansgaard, W., 1964. Stable isotopes in precipitation. Tellus 16, 436–468.

Decary, R., Kiener, A., 1970. Les Cavités souterraines de Madagascar, Ann. Spéléologie 25, 409-440.

Deininger, M., Fohlmeister, J., Scholz, D., Mangini, M., 2012. Isotope disequilibrium effects: The influence of evaporation and ventilation effects on the carbon and oxygen isotope composition of speleothems - A model approach. Geochim. Cosmochim. Acta 96, 57-79.

Denniston, R.F., Asmerom, Y., Lachniet, M., Polyak, V.J., Hope, P., An, N., Rodzinyak, K., Humphreys, W.F., 2013. A last glacial maximum through middle Holocene stalagmite record of coastal Western Australia climate. Quat. Sci. Rev. 77, 101–112. http://dx.doi.org/10.1016/j.quascirev.2013.07.002.

Dewar, R.E., 1984. Extinctions in Madagascar. In Martin, P.G., Klein, R.G. (Eds.), Quaternary extinctions. Tucson: University of Arizona Press, pp. 574-599.

Dewar, R.E., 2014. Early human settlers and their impact on Madagascar's landscapes. Earth Conserv Dev, 44-64.

Dewar, R.E., Radimilahy, C., Wright, H.T., Jacobs, Z., Kelly, G.O., Berna, F., 2013. Stone tools and foraging in northern Madagascar challenge Holocene extinction models. Proceed. Nat. Acad. Sci. U.S.A. 110, 12583-12588.

Dewar, R.E., Richard, A.F., 2007. Evolution in the hypervariable environment of Madagascar. P Natl Acad Sci USA 104, 13723-13727.

Dewar, R.E., Richard, A.F., 2012. Madagascar: A History of Arrivals, What Happened, and Will Happen Next. Annu Rev Anthropol 41, 495-517.

DGM [Direction Générale de la Météorologie], 2008. Le changement climatique à Madagascar.

Dorale, J.A., Edwards, R.L., Alexander, Jr. E.C., Shen, C.-C., Richards, D.A., Cheng, H., 2004. Uranium-series disequilibrium dating of speleothems: Current techniques, limits, and applications. In Mylroie, J., Sasowsky, I.D. (Eds.), Studies of Cave Sediments: Physical and Chemical Records of Paleoclimate, New York, Kluwer Academic/ Plenum Publishers, pp. 177–197.

Dorale, J.A., Liu, Z.H., 2009. Limitations of Hendy Test Criteria in Judging the Paleoclimatic Suitability of Speleothems and the Need for Replication. J. Cave Karst Studies 71, 73-80.

Dorale, J.A., Edwards, R.L., Ito, E., Gonzalez, L.A., 1998. Climate and vegetation history of the midcontinent from 75 to 25 ka: A speleothem record from Crevice Cave, Missouri, USA. Science 282, 1871–1874.

Douglass, K., Zinke, J., 2015. Forging Ahead By Land and By Sea: Archaeology and Paleoclimate Reconstruction in Madagascar. Afr Archaeol Rev 32, 267-299.

Dove, M.R., 1993. Smallholder Rubber and Swidden Agriculture in Borneo - a Sustainable Adaptation to the Ecology and Economy of the Tropical Forest. Econ Bot 47, 136-147.

Dreybrodt, W., 1999. Chemical kinetics, speleothem growth and climate. Boreas 28, 347-356.

Dreybrodt, W., Scholz, D., 2011. Climatic dependence of stable carbon and oxygen isotope signals recorded in speleothems: from soil water to speleothem calcite. Geochim. Cosmochim. Acta 75, 734–752.

Drysdale, R.N., Zanchetta, G., Hellstrom, J.C., Fallick, A.E., Zhao, J.X., Isola, I., Bruschi, G., 2004. Palaeoclimatic implications of the growth history and stable isotope ($\delta^{18}O$ and $\delta^{13}C$) geochemistry of a Middle to Late Pleistocene stalagmite from central-western Italy. Earth Planet. Sci. Lett. 227, 215–229.

Dunham, A.E., Erhart, E.M., Wright, P.C., 2011. Global climate cycles and cyclones: consequences for rainfall patterns and lemur reproduction in southeastern Madagascar. Global Change Biol. 17, 219-227.

DuPuy, D.J., Moat, J., 1996. A refined classification of the primary vegetation of Madagascar based on the underlying geology: Using GIS to map its distribution and to assess its conservation status. Biogeography and Madagascar, 205-218.

DuPuy, D.J., Moat, J., 2003. Using Geological Substrate to Identify and Map Primary Vegetation Types in Madagascar and the implications for planning biodiversity conservation, in: Goodman, S.M., Benstead, J.P. (Eds.), The Natural History of Madagascar. University of Chicago Press, Chicago, pp. 51-74.

Edwards, R.L., Chen, J.H., Wasserburg, G.J., 1987. U-238 U-234-Th-230-Th-232 Systematics and the Precise Measurement of Time over the Past 500000 Years. Earth Planet. Sci. Lett. 81, 175-192.

Fairchild, I.J., Baker, A., 2012. Speleothem Science: From Processes to Past Environments, Wiley-Blackwell.

Fairchild, I.J., McMillan, E.A., 2007. Speleothems as indicators of wet and dry periods. Intl. J. Speleol. 36, 9-74.

Fairchild, I.J., Treble, P.C., 2009. Trace elements in speleothems as recorders of environmental change. Quat. Sci. Rev. 28, 449–468.

Fairchild, I.J., Borsato, A., Tooth, A.F., Frisia, S., Hawkesworth, C.J., Huang, Y.M., McDermott, F., Spiro, B., 2000. Controls on trace element (Sr-Mg) compositions of carbonate cave waters: implications for speleothem climatic records. Chem. Geol.

166, 255–269.

Frisia, S., Borsato, A., Fairchild, I.J., McDermott, F., Selmo, E.M., 2002. Aragonite–calcite relationships in speleothems (Grotte de Clamouse, France): environment, fabrics, and carbonate geochemistry. J. Sed. Res. 772, 687-699.

Frisia S., Fairchild I.J., Fohlmeister J., Miorandi R., Spötl C., Borsato A., 2011. Carbon mass-balance modelling and carbon isotope exchange processes in dynamic caves. Geochim. Cosmochim. Acta 75, 380–400.

Fischbeck, R., 1976. Mineralogie und Geochemie carbonatischer Ablagerungen in europäischen Höhlenein Beitrag zur Bildung und Diagenese von Speleothemen. Neues Jahrbuch für Mineralogie, Abhandlungen 126, 269-291.

Genty, D., Baker, A., Massault, M., Proctor, C., Gilmour, M., Pons-Branchu, E., Hamelin, B., 2001. Dead carbon in stalagmites: carbonate bedrock paleodissolution vs. ageing of soil organic matter: Implications for $^{13}C$ variations in speleothems. Geochim. Cosmochim. Acta 65, 3443–3457.

Genty, D., Blamart, D., Ouahdi, R., Gilmour, M., Baker, A., Jouzel, J., Van-Exter, S., 2003. Precise dating of Dansgaard-Oeschger climate oscillations in western Europe from stalagmite data. Nature 421, 833–837.

Genty, D., Blamart, D., Ghaleb, B., Plagnes, V., Causse, Ch., Bakalowicz, M., Zouari, K., Chkir, N., Hellstrom, J., Wainer, K., Bourges, F., 2006. Timing and dynamics of the last deglaciation from European and North African $\delta^{13}C$ stalagmite profiles — comparison with Chinese and South Hemisphere stalagmites. Quat. Sci. Rev. 25, 2118–2142.

Godfrey, L.R., Jungers, W.L., 2003. The extinct sloth lemurs of Madagascar. Evol. Anthropol. 12, 252-263.

Gommery, D., Ramanivosoa, B., Faure, M., Guerin, C., Kerloc'h, P., Senegas, F., Randrianantenaina, H., 2011. Oldest evidence of human activities in Madagascar on subfossil hippopotamus bones from Anjohibe (Mahajanga Province). Comptes Rendus Palevol 10, 271-278.

González, L.A., Lohmann, K.C., 1988. Controls on mineralogy and composition of spelean carbonates: Carlsbad Caverns, New Mexico. In: James, N.P., Choquette, P.W. (Eds.), Paleokarst. Springer-Verlag, New York, pp. 81–101.

Gunn, J., 2004. Encyclopedia of caves and karst science, New York: Fitzroy Dearborn.

Hellstrom, J., MCculloch, M., Stone, J., 1998. A detailed 31,000-year record of climate and vegetation change, from the isotope geochemistry of two New Zealand speleothems. Quat. Res. 50, 167–178.

Hendy, C.H., 1971. The isotopic geochemistry of speleothems I: the calculation of the effects of different modes of formation on the isotopic composition of speleothems and their applicability as palaeoclimatic indicators. Geochim. Cosmochim. Acta 35, 801–824.

Hesterberg, R., Siegenthaler, U., 1991. Production and Stable Isotopic Composition of $CO_2$ in a Soil near Bern, Switzerland. Tellus Series B-Chem. Phys. Met. 43, 197-205.

Hill, C., Forti, P., 1997. Cave Minerals of the World. National Speleological Society, Huntsville, AL, 463 p.

Hoefs, J., 2009. Stable Isotope Geochemistry, sixth ed. Springer, Berlin, 293 p.

Humbert, H., 1927. La destruction d'une flore insulaire par le feu. Principaux aspects de la végétation à Madagascar. Mem. Acad. Malgache 5, 1-78.

Ingram, J.C., Dawson, T.P., 2005. Climate change impacts and vegetation response on the island of Madagascar. Phil. Trans. R. Soc. A-Math. Phys. Engineer. Sci. 363, 55-59.

IAEA/WMO, 2014. Global Network of Isotopes in Precipitation. The GNIP Database. Available from: <http://isohis.iaea.org>.

Irwin, M.T., Wright, P.C., Birkinshaw, C., Fisher, B.L., Gardner, C.J., Glos, J., Goodman, S.M., Loiselle, P., Robeson, P., Raharison, J.L., Raherilalao, M.J., Rakotondravony, D., Raselimanana, A., Ratsimbazafy, J., Sparks, J.S., Wilme, L., and Ganzhorn, J.U., 2010. Patterns of species change in anthropogenically disturbed forests of Madagascar. Biol. Conserv. 143, 2351-2362.

IUCN/UNEP/WWF, 1987. Madagascar, an environmental profile. IUCN, Gland, Switzerland and Cambridge, U.K.

James, E.W., Banner, J.L., Hardt, B., 2015. A global model for cave ventilation and seasonal bias in speleothem paleoclimate records. Geochem. Geophys. Geosys. 16, 1044–1051. doi:10.1002/2014GC005658.

Jarosz, L., 1993. Defining and explaining tropical deforestation: shifting cultivation and population growth in colonial Madagascar (1896–1940). Econ Geogr 69, 366–379.

Johnson, K.R., Hu, C.Y., Belshaw, N.S., Henderson, G.M., 2006. Seasonal trace-element and stable-isotope variations in a Chinese speleothem: the potential for high-resolution paleomonsoon reconstruction. Earth Planet Sci. Lett. 244, 394–407.

Jury, M.R., 2003. The Climate of Madagascar. In Goodman, S.M., Benstead, J.P. (Eds.), The Natural History of Madagascar, University of Chicago, pp. 75-87.

Kim, S.T., O'Neil, J.R., Hillaire-Marcel, C., Mucci, A., 2007. Oxygen isotope fractionation between synthetic aragonite and water: Influence of temperature and Mg2+ concentration. Geochim Cosmochim Ac 71, 4704-4715.

Koster, R.D., Devalpine, D.P., Jouzel, J., 1993. Continental water recycling and $H_2O$ concentrations. Geophys. Res. Lett. 20, 2215–2218.

Kowalczk, A., Froelich, P., 2010. Cave air ventilation and $CO_2$ outgassing by radon-222 modeling: how fast do caves breathe? Earth Planet. Sci. Lett. 289, 209–219.

Kurita, N., Ichiyanagi, K., Matsumoto, J., Yamanaka, M.D., Ohata, T., 2009. The relationship between the isotopic content of precipitation and the precipitation amount in tropical regions. J. Geochem. Expl. 102, 113-122.

Lachniet, M.S., 2009. Climatic and environmental controls on speleothem oxygen-isotope values. Quat. Sci. Rev. 28, 412-432.

Lambert W.J., Aharon, P., 2011. Controls on dissolved inorganic carbon and $\delta^{13}C$ in cave waters from DeSoto Caverns: implications for speleothem $\delta^{13}C$ assessments. Geochim. Cosmochim. Acta 75, 753–768.

Lauritzen, S.E., Lundberg, J., 1999. Speleothems and climate: a special issue of The Holocene. The Holocene 9, 643-647.

Lavauden, L., 1931. Le déboisement et la végétation de Madagascar. Rev. Botanique Appl. Agr. Col. 122, 817-824.

Lee, J. E., Risi, C., Fung, I., Worden, J., Scheepmaker, R.A., Lintner, B., Frankenberg, C., 2012. Asian monsoon hydrometeorology from TES and SCIAMACHY water vapor isotope measurements and LMDZ simulations: Implications for speleothem climate record interpretation. J. Geophys. Res. Atm. 117, D15112. doi:10.1029/2011JD017133.

Linge, H., Lauritzen, S.E., Lundberg, J., Berstad, I.M., 2001. Stable isotope stratigraphy of Holocene speleothems: examples from a cave system in Rana, northern Norway. Palaeogeogr. Palaeoclimatol. Palaeoecol., v. 167, no. 3-4, p. 209-224.

McMillan, E. A., Fairchild, I. J., Frisia, S., Borsato, A., McDermott, F., 2005. Annual trace element cycles in calcite–aragonite speleothems: evidence of drought in the western Mediterranean 1200–1100 yr BP. J. Quaternary Sci. 20, 423–433.

MacPhee, R.D.E., 1986. Environment, extinction, and Holocene Vertebrate Localities in Southern Madagascar. Natl. Geogr. Res. 2, 441-455.

MacPhee RDE, Burney, D.A., 1991. Dating of Modified Femora of Extinct Dwarf Hippopotamus from Southern Madagascar - Implications for Constraining Human Colonization and Vertebrate Extinction Events. J. Archaeol. Sci. 18, 695-706.

Madagascar National Adaptation Plan for Action, 2007. Programme D'action National D'adaptation Au Changement Climatique.

Mahé, J., Sourdat, M., 1972. Sur l'extinction des vertébrés subfossiles et l'aridification du climat dans le Sud-Ouest de Madagascar. Bull. Société Géol. France 14, 295-309.

Matsumoto, K., Burney, D.A., 1994. Late Holocene environments at Lake Mitsinjo, northwestern Madagascar. The Holocene 4, 16-24.

Mattey, D.P., Fairchild, I.J., Atkinson, T.C., Latin, J.-P., Ainsworth, M., Durell, R., 2010. Seasonal microclimate control of calcite fabrics, stable isotopes and trace elements in modern speleothem from St Michaels Cave, Gibraltar. Geol. Soc. Lond. Spec. Publ. 336, 323–344.

McDermott, F., 2004, Palaeoclimate reconstruction from stable isotope variations in speleothems: a review: Quat. Sci. Rev., v. 23, no. 7-8, p. 901-918.

MEF (Ministry of Environment and Forests), 2014. Fifth national report to the convention on biological diversity – Madagascar. 221p.

Meyer, K.W., Feng, W., Breecker, D.O., Banner, J.L., Guilfoyle, A., 2014. Interpretation of speleothem calcite $\delta^{13}C$ variations: evidence from monitoring soil $CO_2$, drip water, and modern speleothem calcite in central Texas. Geochim. Cosmochim. Acta 142, 281–298. http://dx.doi.org/10.1016/j.gca.2014.07.027.

Middleton, J., Middleton, V., 2002. Karst and caves of Madagascar. Cave Karst Sci. 29, 13-20.

Mickler, P.J., Banner, J.L., Stern, L., Asmerom, Y., Edwards, R.L., Ito, E., 2004. Stable isotope variations in modern tropical speleothems: Evaluating equilibrium vs. kinetic isotope effects. Geochem. Cosmochim. Acta 68, 4381-4393.

Mickler, P.J., Stern, L.A., Banner, J.L., 2006. Large kinetic isotope effects in modern speleothems. Geol. Soc. Amer. Bull. 118, 65-81.

Moore, G.W., 1956. Aragonite speleothem as indicators of paleotemperature. Amer. J. Sci. 254, 746-753.

Moreno, A., Stoll, H., Jimenez-Sanchez, M., Cacho, I., Valero-Garces, B., Ito, E., Edwards, R.L., 2010. A speleothem record of glacial (25-11.6 kyr BP) rapid climatic changes from northern Iberian Peninsula. Glob. Planet. Change 71, 218–231. http://dx.doi.org/10.1016/j.gloplacha.2009.10.002.

Murray, J.W., 1954. The deposition of calcite and aragonite in caves. J. Geol. 62, 481–492.

Ottino, P., 1974. Le Moyen-Age de l'Océan Indien et le peuplement de Madagascar. Ann. Pays l'Océan Ind. 1, 197 – 221.

Nagra, G., Treble, P.C., Andersen, M.S., Fairchild, I.J., Coleborn, K., Baker, A., 2016. A post-wildfire response in cave dripwater chemistry. Hydrology & Earth System Sciences 20, 2745-2758.

Oster, J.L., Montanez, I.P., Sharp, W.D., Cooper, K.M., 2009. Late Pleistocene California droughts during deglaciation and Arctic warming. Earth Planet. Sci. Lett., v. 288, no. 3-4, p. 434-443.

Oster, J.L., Montanez, I.P., Guilderson, T.P., Sharp, W.D., Banner, J.L., 2010. Modeling speleothem delta C-13 variability in a central Sierra Nevada cave using C-14 and Sr-87/Sr-86. Geochem. Cosmochim. Acta 74, 5228-5242.

Paul, D., Skrzypek, G., 2007. Assessment of carbonate-phosphoric acid analytical technique performed using GasBench II in continuous flow isotope ratio mass spectrometry. Intl. J. Mass Spec. 262, 180-186.

Perrier de la Bâthie, H., 1921. La végétation Malgache. Ann. Mus. Colon. Marseille 9, 1–266.

Pobeguin, T., 1965. Sur les concretions calcaires observées dans la Grotte de Moulis (Ariège). Soc. Géol. France, Compte Rendu 241, 1791–1793.

Quade, J., 2004. Isotopic records from groundwater and cave speleothem calcite in North America. In Gillespie, A., Porter, S.C., Atwater, B.F. (Eds.), Developments in Quaternary Science Elsevier Science, New York, pp. 205– 219.

Radimilahy, C., 1998. Mahilaka: an archaeological investigation of an early town in northwestern Madagascar. Uppsala, Dept. of Archaeology and Ancient History.

Raharimalala, O., Buttler, A., Ramohavelo, C.D., Razanaka, S., Sorg, J.P., Gobat, J.M., 2010. Soil-vegetation patterns in secondary slash and burn successions in Central Menabe, Madagascar. Agr Ecosyst Environ 139, 150-158.

Railsback, L.B., 2010. Controls on the $\delta^{13}C$ of spelean CaCO3, in Railsback, L.B., Some Fundamentals of Mineralogy and Geochemistry. Available at: www.gly.uga.edu/railsback/Fundamentals/C&OIsotopesSpeleanCaCO3Controls.jpg.

Railsback, L.B., Akers, P.D., Wang, L., Holdridge, G.A., Voarintsoa, N.R.G., 2013. Layer-bounding surfaces in stalagmites as keys to better paleoclimatological histories and chronologies. Intl. J. Spel. 42, 167-180.

Railsback, L.B., Liang, F.Y., Romani, J.R.V., Grandal-d'Anglade, A., Rodriguez, M.V., Fidalgo, L.S., Mosquera, D.F., Cheng, H., Edwards, R.L., 2011. Petrographic and isotopic evidence for Holocene long-term climate change and shorter-term environmental shifts from a stalagmite from the Serra do Courel of northwestern Spain, and implications for climatic history across Europe and the Mediterranean. Palaeogeogr. Palaeoclimatol. Palaeoecol. 305, 172–184.

Railsback, L.B., Xiao, H.L., Liang, F.Y., Akers, P.D., Brook, G.A., Dennis, W.M., Lanier, T.E., Tan, M., Cheng, H., Edwards, R.L., 2014. A stalagmite record of abrupt climate change and possible Westerlies-derived atmospheric precipitation during the Penultimate Glacial Maximum in northern China. Palaeogeogr. Palaeoclimatol. Palaeoecol. 393, 30–44.

Railsback, L.B., Brook, G.A., Chen, J., Kalin, R., Fleisher, C.J., 1994. Environmental Controls on the Petrology of a Late Holocene Speleothem from Botswana with Annual Layers of Aragonite and Calcite. J. Sed. Res. Section A-Sed. Petrol. Process. 64, 147–155.

Railsback, L.B., 2000. Atlas of Speleothem Microfabrics. Available at: www.gly.uga.edu/railsback/speleoatlas/SAindex1.html. (Accessed 15 January 2016).

Romanek, C.S., Grossman, E.L., Morse, J.W., 1992. Carbon Isotopic Fractionation in Synthetic Aragonite and Calcite - Effects of Temperature and Precipitation Rate. Geochim Cosmochim Ac 56, 419-430.

Romanov, D., Kaufmann, G., Dreybrodt, W., 2008. Modeling stalagmite growth by first principles of chemistry and physics of calcite precipitation. Geochem. Cosmochim. Acta 72, 423–437.

Riechelmann, S., Schröder-Rtizrau, A., Wassenburg, J.A., et al. (2014) Physicochemical characteristics of drip waters: Influence on mineralogy and crystal morphology of recent cave carbonate precipitates. Geochem. Cosmochim. Acta 145, 13–29.

Risi, C., Bony, S., Vimeux, F., 2008. Influence of convective processes on the isotopic composition ($\delta^{18}O$ and $\delta D$) of precipitation and water vapor in the tropics: 2.

Physical interpretation of the amount effect. J. Geophys. Res. 113. doi:10.1029/2008JD009943.

Rozanski, K., Araguás-Araguás, L., Gonfiantini, R., 1993. Isotopic patterns in modern global precipitation. In: Swart, P.K., Lohmann, K.L., McKenzie, J., Savin, S. (Eds.), Climate Change in Continental Isotopic Records. Amer. Geophys. Union, 1–37.

Russell, J.M., Johnson, T.C., 2007. Little Ice Age drought in equatorial Africa: Intertropical Convergence Zone migrations and El Niño-Southern Oscillation variability. Geology 35, 21-24.

Russell, J.M., Johnson, T.C., 2005. Late Holocene climate change in the North Atlantic and equatorial Africa: Millennial-scale ITCZ migration. Geophys. Res. Lett. 32.

Saint-Ours, J.D., 1959. Les phénomènes karstiques à Madagascar. Ann. Spéléol. 14, 275-291.

Saji, N.H., Goswami, B.N., Vinayachandran, P.N., Yamagata, T., 1999. A dipole mode in the tropical Indian Ocean. Nature 401, 360-363.

Schefuß, E., Kuhlmann, H., Mollenhauer, G., Prange, M., Patzold, J., 2011. Forcing of wet phases in southeast Africa over the past 17,000 years. Nature 480, 509-512.

Schneider, T., Bischoff, T., Haug, G.H., 2014. Migrations and dynamics of the intertropical convergence zone. Nature 513, 45-53.

Scholz, D., Hoffmann, D.L., 2011. StalAge - An algorithm designed for construction of speleothem age models. Quat Geochronol 6, 369-382.

Schott, F.A., Xie, S.P., McCreary, J.P., 2009. Indian Ocean Circulation and Climate Variability. Rev. Geophys. 47.

Shen, C.C., Edwards, R.L., Cheng, H., Dorale, J.A., Thomas, R.B., Moran, S.B., Weinstein, S.E., Edmonds, H.N., 2002. Uranium and thorium isotopic and concentration measurements by magnetic sector inductively coupled plasma mass spectrometry. Chem. Geol. 185, 165–178.

Shtober-Zisu, N., Schwarcz, H.P., Chow, T., Omelon, C.R., Southam, G., 2014. Caves in caves: evolution of post-depositional macroholes in stalagmites. Intl. J. Spel. 43, 323-334.

Shtober-Zisu, N., Schwarcz, H.P., Konyer, N., Chow, T., Noseworthy, M.D., 2012. Macroholes in stalagmites and the search for lost water. J. Geophys. Res. Earth Surf. 117, F04009.

Siegel, F.R., 1965. Aspects of calcium carbonate deposition in Great Onyx Cave, Kentucky. Sedimentology 4, 285–299.

Skrzypek, G., Paul, D., 2006. Delta C-13 analyses of calcium carbonate: comparison between the GasBench and elemental analyzer techniques. Rapid Comm. Mass Spectr. 20, 2915-2920.

Sletten, H.R., Railsback, L.B., Liang, F.Y., Brook, G.A., Marais, E., Hardt, B.F., Cheng, H., Edwards, R.L., 2013. A petrographic and geochemical record of climate change over the last 4600 years from a northern Namibia stalagmite, with evidence of abruptly wetter climate at the beginning of southern Africa's Iron Age. Palaeogeogr. Palaeoclimatol. Palaeoecol. 376, 149-162.

Spötl, C., Fairchild, I. J., and Tooth, A. F., 2005, Cave air control on dripwater geochemistry, Obir Caves (Austria): Implications for speleothem deposition in dynamically ventilated caves: Geochem. Cosmochim. Acta, v. 69, no. 10, p. 2451-2468.

Suess, H.E., 1955. Radiocarbon concentration in modern wood. Science 122, 415–417.

Tadross, T., Randriamarolaza, L., Rabefitia, Z., Yip, Z.K., 2008. Climate Change in Madagascar: recent, past, and future.

Talma, A.S., Vogel, J.C., 1992. Late Quaternary palaeotemperatures derived from a speleothem from Cango Caves, Cape Province, South Africa. Quat. Res. 37, 203–213.

Thompson, C., van Bogaert, O., Hughes, R., Lippuner, M., Ramahaleo, T., and Rafiadanantsoa, S., 2011. Treasure Island: New biodiversity on Madagascar (1999-2010). WWF Report 2011.

Thrailkill, J., 1971. Carbonate deposition in Carlsbad Caverns. J. Geol. 79, 683–695.

Tremaine, D.M., Froelich, P.N., Wang, Y., 2011. Speleothem calcite farmed in situ: modern calibration of $\delta^{18}O$ and $\delta^{13}C$ paleoclimate proxies in a continuously- monitored natural cave system. Geochim. Cosmochim. Acta 75, 4929–4950. http://dx.doi.org/10.1016/j.gca.2011.06.005.

Tyson, P., 2013. The eighth continent: life, death, and discovery in the lost world of Madagascar. William Morrow, New York.

Verburg, P., 2007. The need to correct for the Suess effect in the application of $\delta^{13}C$ in sediment in autotrophic Lake Tanganyika, as a productivity proxy in the anthropocene. J. Paleolimnol. 37, 591–602.

Vérin, P., 1975. Les échelles anciennes du commerce sur les cotes nord de Madagascar. Lille: Service des Thèse.

Virah-Sawmy, M., Willis, K.J., Gillson, L., 2010. Evidence for drought and forest declines during the recent megafaunal extinctions in Madagascar. J. Biogeogr. 37, 506–519.

Voarintsoa, N.R.G., Brook, G.A., Liang, F., Marais, E., Hardt, B., Cheng, H., Edwards, R.L., Railsback, L.B., Stalagmite multi-proxy evidence of wet and dry intervals in northeastern Namibia: Linkage to latitudinal shifts of the Inter-Tropical Convergence Zone and changing solar activity from AD 1400 to 1950. The Holocene, In press, DOI: 10.1177/0959683616660170.

von Cabanis, Y., Chabouis, L., Chabouis, F., 1969. Végétaux et Groupements végétaux de Madagascar I. Tananarive: Bureau pour le Développement de la Production Agricole.

Wang, B., Ding, Q.H., 2008. Global monsoon: Dominant mode of annual variation in the tropics. Dyn. Atm. Oceans 44, 165–183.

Wang., L., 2016. Late Quaternary paleoenvironmental changes in Southern Africa and Madagascar: evidence from aeolian, fluvial, and cave deposits. Unpublished dissertation. University of Georgia. 312p.

Wang, L., Brook, G.A., 2013. Holocene climate changes in northwest Madagascar: evidence from a two-meter-long stalagmite from the Anjohibe Cave, Meeting Program of the Association of American Geographers, published online. Session 1512: Paleorecords of our Changing Earth I: Climate History and Human-Environment Interaction in the Old and New World Tropics, 2013.

Wang, P.X., 2009. Global monsoon in a geological perspective. Chinese Sci. Bull. 54, 1113–1136.

Wells, N.A., 2003. Some Hypotheses on the Mesozoic and Cenozoic Paleoenvironmental History of Madagascar. In Goodman, S.M., Benstead, J.P. (Eds.), The Natural History of Madagascar. Universtity of Chicago, pp. 16-34.

Wells, N.A., Andriamihaja, B., 1993. The initiation and growth of gullies in Madagascar: are humans to blame? Geomorphology 8, 1-46.

Wells, N.A., Andriamihaja, B., 1997. Extreme gully erosion in Madagascar and its natural and anthropogenic causes. In: Goodman, S.M., Patterson, B.D. (Eds.), Natural Change and Human Impact in Madagascar. Smithsonian Institution Press, Washington, pp. 44-74.

Wigley, T.M.L., Plummer, L.N., Parson, Jr., F.J., 1978. Mass transfer and carbon isotope evolution in natural water systems. Geochim. Cosmochim. Acta 42, 1117–l139.

Williams, J.B., 1990. Some temporal and regional variations of climate in Madagascar, Chatham Marina, Kent. Technical Report, Overseas Develop. Natl. Res. Inst., 147 p.

Willis, K.J., Gillson, L., Virah-Sawmy, M., 2008. Nature or nurture: the ambiguity of C-4 grasslands in Madagascar. J. Biogeogr. 35, 1741–1742.

Wong, C., Banner, J.L., Musgrove, M.L., 2011. Seasonal dripwater Mg/Ca and Sr/Ca variations driven by cave ventilation: implications for and modeling of speleothem paleoclimate records. Geochim. Cosmochim. Acta 75, 3514–3529. http://dx.doi.org/10.1016/j.gca.2011.03.025.

Wong, C.I., Breecker, D.O., 2015. Advancements in the use of speleothems as climate archives. Quat. Sci. Rev. 127, 1–18.

Wright, H.T., Vérin, P., Ramilisonina, Burney, D., Burney, L.P., Matsumoto, K., 1996. The Evolution of settlement systems in the Bay of Boeny and the Mahavavy River Valley, north-western Madagascar. Azania XXXI, 37-73.

Yadava, M.G., Ramesh, R., 2006. Stable oxygen and carbon isotope variations as monsoon proxies: A comparative study of speleothems from four different locations in India. J. Geol. Soc. India 68, 461-475.

Yadava, M.G., Ramesh, R., Pant, G.B., 2004. Past monsoon rainfall variations in Peninsular India recorded in a 331-year old speleothem. The Holocene, 14, 517–524.

Zinke, J., Dullo, W.C., Heiss, G.A., Eisenhauer, A., 2004. ENSO and Indian Ocean subtropical dipole variability is recorded in a coral record off southwest Madagascar for the period 1659 to 1995. Earth Planet. Sci. Lett. 228, 177–19.

# CHAPTER 4

# THREE DISTINCT HOLOCENE INTERVALS REVEALED IN NW MADAGASCAR: EVIDENCE IN TWO STALAGMITES FROM TWO CAVES, AND IMPLICATIONS FOR ITCZ DYNAMICS[4]

[4] Voarintsoa, NRG, LB Railsback, GA Brook, L Wang, G Kathayat, H Cheng, X Li, RL Edwards, AFM Rakotondrazafy, MO Madison Razanatseheno.

Submitted to Climate of the Past, Special Issue 2016 [26 December 2016], Accepted for publication as a Discussion paper at Climate of the Past Discussion [13 January 2017] doi:10.5194/cp-2016-137, 2017. Reprinted here with permission of the publisher [Copernicus Publications, 2017]

## ABSTRACT

Petrographic features, mineralogy, and stable isotopes from two stalagmites collected from Anjohibe and Anjokipoty Cave allow distinction of three intervals of the Holocene in northwestern Madagascar. The Malagasy early (between ca. 9.8 and 7.8 ka) and late (after ca. 1.6 ka) Holocene intervals (MEHI and MLHI, respectively) record evidence of stalagmite deposition. The Malagasy middle Holocene (MMHI, between ca. 7.8 ka and 1.6 ka) interval, however, is marked by a depositional hiatus lasting for ca. 6500 years.

The simplest interpretation of the MEHI, MMHI, and MLHI in NW Madagascar could be linked to changes in the cave's hydrologic system and changes in vegetation. These changes, in turn, could be linked to climate. Deposition of Stalagmites ANJB-2 and MAJ-5 from Anjohibe and Anjokipoty Caves, respectively, during the MEHI and the MLHI suggests that these intervals were relatively wetter; whereas the long-term depositional hiatus likely suggests that the MMHI was relatively drier. The alternating "wet/dry/wet" during each of these Holocene intervals could be linked to the long-term migration of the Inter-Tropical Convergence Zone (ITCZ). When the ITCZ's mean position is further south, NW Madagascar experienced wetter conditions, such as during the MEHI and MLHI, and when it moved north, NW Madagascar climate becomes drier, such as during the MMHI.

Stable isotope records also suggest that although the MEHI and MLHI were wetter, the stronger correlation between $\delta^{18}O$ and $\delta^{13}C$ suggest that the early Holocene vegetation closely responds to changes in climate. In contrast, the weaker correlation between $\delta^{18}O$ and $\delta^{13}C$ and the positive shift in $\delta^{13}C$ suggest that the late Holocene vegetation was

controlled by something other than climate, and the plausible explanation for such changes is the practice of swidden agriculture.

Beyond these three subdivisions, the evidence of the 8.2 ka event in the stalagmite records also suggests that climate in Madagascar was sensitive to abrupt climate changes, such as the abrupt influx of the Laurentide Ice Sheet meltwater to the North Atlantic. The freshwater influx into the N. Atlantic, known to have weakened the Atlantic Meridional Overturning Circulation (AMOC), also led to an enhanced temperature gradient between the two hemispheres, i.e. cold NH and warm SH, shifting the mean position of the ITCZ further south. This brought wet conditions in the SH monsoon regions, such as northwestern Madagascar, and dry conditions in the NH monsoon regions, including the Asian Monsoon and the East Asian Summer Monsoon.

## 4.1. Introduction

Although much is known about Holocene climate change worldwide (Mayewski et al., 2004; Wanner and Ritz, 2011; Wanner et al., 2011; 2015), high-resolution climate data for the Holocene period is still regionally limited in the Southern Hemisphere (SH) (e.g. Wanner et al. 2008; Marcott et al. 2013; Wanner et al., 2015). This uneven distribution of data hinders our understanding of the spatio-temporal characteristics of Holocene climate change, including our understanding of the most important climate forcings. For example, some of these forcings influence the Inter-Tropical Convergence Zone (ITCZ) behavior and the monsoonal response in low- to mid-latitude regions (e.g. Wanner et al., 2015; Talento and Barreiro, 2016). Madagascar is particularly a strategic location where such records are needed because it holds a key position in the Indian Ocean (Fig. 4.1a), and it is seasonally

visited by the ITCZ with a karst region crossing latitudinal belts (Fig. 4.1c). Thus, records from Madagascar could fill gaps in paleoclimate reconstruction in the SH. Records from Madagascar could also help refine paleoclimate simulations that could provide better understanding of the global circulation and the land-atmosphere-ocean interaction during the Holocene.

To fill the knowledge gap about Holocene climate change in the SH and particularly in Madagascar, and to better understand the paleohydrology of northwestern (NW) Madagascar during the Holocene, we present multiproxy records (stable isotopes, petrography, mineralogy, variability of layer-specific width) from stalagmites in two caves, Anjohibe and Anjokipoty Caves, in northwestern Madagascar. Stalagmites are used because of their potential to store significant climatic information (e.g. Fairchild and Baker, 2012, p. 9–10), and in Anjohibe Cave, recent studies have shown the replicability of paleoclimate records from stalagmites (e.g. Burns et al., 2016). The two stalagmites investigated here provide replication of paleoclimate records, which allows us to characterize Holocene climate change in northwestern Madagascar. First, we will develop a record of climate change using the stalagmite records. With a better understanding of Madagascar's paleoclimate, we will then investigate the possible climatic drivers of tropical climate changes to draw a more comprehensive conclusion on the major factors controlling the hydrological cycle in this region.

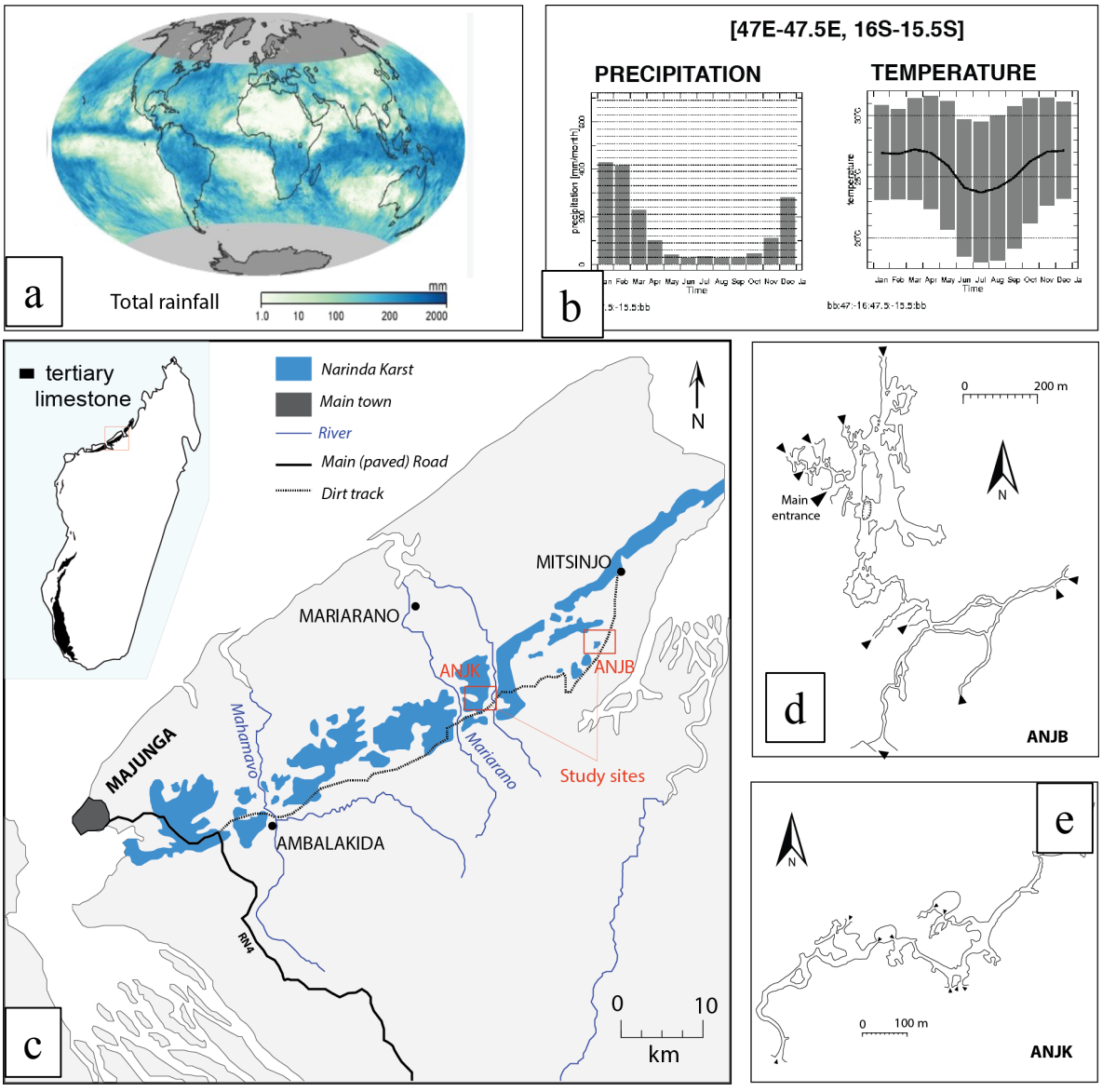
a
Total rainfall
mm
1.0
10
100
200
2000
b
[47E-47.5E, 16S-15.5S]
PRECIPITATION
TEMPERATURE
Time
Time
c
tertiary limestone
Narinda Karst
Main town
River
Main (paved) Road
Dirt track
N
MITSINJO
MARIARANO
ANJK
ANJB
Mahamavo
Mariarano
Study sites
MAJUNGA
AMBALAKIDA
RN4
0
10
km
d
0
200 m
N
Main entrance
ANJB
e
N
0
100 m
ANJK

Figure 4.1: Climatological and geographic setting of Madagascar and the study area. (a) Global rainfall maps recorded by NASA's Tropical Rainfall Measuring Mission (TRMM) satellite showing the total monthly rainfall in millimeters and the overall position of the ITCZ during November, 2006. Darker blue shades indicate regions of higher rainfall (source: NASA Earth Observatory, 2016; available at http://earthobservatory.nasa.gov/GlobalMaps/view.php?d1=MOD_LSTAD_M&d2=TRMM_3B43M). (b) Barplots of the monthly climatology of precipitation, and the monthly average of daily maximum, minimum, and mean temperature in northwestern Madagascar. The base period used for the climatology is 1971-2000. Source: http://iridl.ldeo.columbia.edu/ (accessed August 31, 2016). (c) Simplified map showing the southwest part of the Narinda karst and the location of the study areas. Inset figure is a map of Madagascar showing the extent of the Tertiary limestone cover that makes up the Narinda karst. (d-e) Maps of Anjohibe (ANJB) and Anjokipoty (ANJK) Caves (St-Ours, 1959; Middleton and Middleton, 2002). See Figs. C1–S3 for additional information about the study locations.

## 4.2. Setting

### 4.2.1. Regional environment

Two stalagmites, ANJB-2 and MAJ-5, were collected from Anjohibe and Anjokipoty Cave, respectively, in the Majunga region of northwestern Madagascar (Fig. 4.1). The two caves have provided many insights about the paleoenvironmental and archaeological history of northwestern Madagascar (e.g. Burney et al., 1997, 2004; Brook et al., 1999; Gommery et al., 2011; Jungers et al., 2008; Vasey et al., 2013; Burns et al., 2016).

Anjohibe (S15° 32' 33.3"; E046° 53' 07.4") and Anjokipoty (S15° 34' 42.2"; E046° 44' 03.7") are about 16.5 km apart (Fig. 4.1c). Their location in the zone visited by the ITCZ (e.g. Nassor and Jury, 1998) makes them ideal sites to test for the latitudinal migration of the ITCZ (e.g. Chiang and Bitz, 2005; Broccoli et a., 2006; Chiang and Friedman, 2012; Schneider et al., 2014). The ITCZ brings north or northwesterly monsoon winds to Madagascar during austral summers, in a pattern that the Service Météorologique of Madagascar calls the “Malagasy monsoon”. Majunga has a tropical savanna climate (Aw) according to the Köppen-Geiger climate classification, with a distinct wet summer (from October to April) and dry winter (May-September). The mean annual rainfall is around 1160 mm. The mean maximum temperature in November, the hottest month in the summer, is about 32°C. The mean minimum temperature in July, the coldest month of the dry winter, is about 18°C (Fig. 4.1b).

### 4.2.2. The Holocene in northwestern Madagascar

Little is known about Holocene climate change in NW Madagascar nor about the major drivers of long-term climatic changes there. Most paleoclimate information from NW Madagascar covers the last two millennia with more focus on the anthropogenic effects on the Malagasy ecosystems (e.g. Crowley and Samonds, 2013; Burns et al., 2016). This is because several studies revealed coincidence of Madagascar's megafaunal extinctions with human arrival around 2-3 ka BP (e.g. see Table 1 of Virah-Sawmy et al., 2010; MacPhee and Burney, 1991; Burney et al., 1997c; Crowley, 2010). Long-term paleoclimate records are very scarce and the only ones that cover a long time interval are sediment cores collected from Lake Mitsinjo (3,500 yr. BP; Matsumoto and Burney, 1994) and cave sediments from Anjohibe Cave (40,000 yr. BP; Burney et al. 1997). Both records provided useful information about paleoenvironmental changes in Madagascar, but linkages to global climatic changes, such as the linkages to the ITCZ, are not fully understood. Madagascar is however a key location in the SH and could provide meaningful paleoclimate information about the global atmospheric and oceanic circulation during the Holocene.

## 4.3. Methods

Stalagmites ANJB-2 and MAJ-5 were radiometrically dated using the multi-collector ICP-MS of the University of Minnesota, USA and of the Stable Isotopes Laboratory of Xi'an, in Jiaotong, China. Twenty-two powdered samples of approximately 50 to 200 mg were extracted from Stalagmite ANJB-2 and nine samples from Stalagmite MAJ-5 (Tables C1 and C2). Stalagmite chronologies were constructed using the StalAge1.0 algorithm of Scholz

and Hoffman (2011) and Scholz et al. (2012). The StalAge scripts were run on the statistics program R version 3.2.2 (2015-08-14). The age models were adjusted considering hiatal surfaces identified in the samples, using the approach of Railsback et al. (2013; see their Fig. 9).

Petrography and mineralogy of the two stalagmites were investigated by 1) examining polished surfaces and a scanned images of the sectioned stalagmites, with which we determined variations in layer-specific width, 2) observing eleven oversized thin sections (3 x2 in) under the Leitz Laborlux 12 Pol microscope in the Sedimentary Geochemistry Lab at UGA, and 3) analyzing about 3 g of powdered spelean layers on a Bruker D8 X-ray Diffractometer in the Department of Geology of the University of Georgia. For $CaCO_3$ identification between calcite and aragonite, we used CoK$\alpha$ radiation at a 2$\theta$ angle between 20° and 60°.

Oxygen and carbon isotope ratios were measured using the Finnigan MAT-253 mass spectrometer fitted with the Kiel IV Carbonate Device of the Xi'an Stable Isotope Laboratory in China (ANJB-2; n=654) and using the Delta V Plus at 50°C fitted with the GasBench-IRMS machine of the Alabama Stable Isotope Laboratory in USA (MAJ-5; n=286). Analytical procedures using the MAT 253 are identical to those described in Dykoski et al. (2005), with isotopic measurement errors of less than 0.1 ‰ for both $\delta^{13}C$ and $\delta^{18}O$. Analytical methods and procedures using the GasBench-IRMS machine are identical to those described in Skrzypek and Paul (2006), Paul and Skrzypek (2007), and Lambert and Aharon (2011), with ±0.1 ‰ errors for both $\delta^{13}C$ and $\delta^{18}O$. In both techniques, the results were reported relative to Vienna PeeDee Belemnite (VPDB) and with standardization

relative to NBS19. Inter-lab comparison of the isotopic results involved replicating every tenth sample of Stalagmite MAJ-5 on the MAT 253 mass spectrometer. The replicates suggest strong correlation (Fig. C4). Finally, the $\delta^{18}O$ and $\delta^{13}C$ of the spelean aragonite were transformed, by subtracting 1.7 ‰ (Romanek et al., 1992) and 0.8‰ (Kim et al., 2007) respectively. These transformations compensate for the different fractionation of heavier isotopes when aragonite is formed (see also Sletten et al., 2013; Voarintsoa et al., 2016, 2017). With these transformations, the corrected isotopic values remove the mineralogical bias in isotopic interpretation between calcite and aragonite.

## 4.4. Results

### 4.4.1. Radiometric data

Results from radiometric analyses of the two stalagmites are presented in Table C1 and Table C2. In Stalagmite ANJB-2 has a $^{234}U$ ranges from 64±0 to 9833±44 ppb and a $^{232}Th$ range from 180±8 to 39850±809 ppt. Corrected $^{230}Th$ ages suggests that it was deposited between ca. 8977±50 and 161±64 yr. BP. Stalagmite MAJ-5 has a $^{234}U$ range from 1224±4 to 12609±83 ppb and a $^{232}Th$ range from 3044±63 to 38990±842 ppt. Corrected $^{230}Th$ ages suggests that is was deposited between ca. 9796±64 and 150±24 yr. BP. These ages indicate stalagmite deposition at the beginning and the end of the Holocene. The StalAge model and petrography highlight three distinct intervals of the Holocene (Fig. 4.2): (1) evidence of $CaCO_3$ deposition between ca. 9.8 and 7.8 ka BP, (2) a noticeable long-term depositional hiatus between ca. 7.8 and 1.6 ka BP, and (3) resumption of $CaCO_3$ deposition after ca. 1.6 ka BP. In the rest of the paper, these intervals are referred

to as the Malagasy early Holocene interval (MEHI), Malagasy mid-Holocene interval (MMHI), and Malagasy late Holocene interval (MLHI) respectively.

### 4.4.2. Stable isotopes

Raw values of $\delta^{18}O$ and $\delta^{13}C$ for Stalagmite ANJB-2 range from –8.85 to –2.27‰, and from –11.00 to +5.15‰, respectively, relative to VPDB. The mean values are –4.97‰ and –4.18‰ respectively for $\delta^{18}O$ and $\delta^{13}C$. Raw values of $\delta^{18}O$ and $\delta^{13}C$ in Stalagmite MAJ-5 range from –8.80 to –0.85‰, and from –9.44 to +2.60‰, respectively, relative to VPDB. The mean values are –4.85‰ and –4.38‰ respectively for $\delta^{18}O$ and $\delta^{13}C$, but distinguishable between MEHI and the MLHI (Fig. 4.3). In both stalagmites, the amplitude of $\delta^{18}O$ fluctuations stayed constant throughout the Holocene; whereas the $\delta^{13}C$ profile shows a dramatic shift toward greater values (i.e. from -10.90‰ to +3.75‰, VPDB) at ca. 1.5 ka BP. Values of $\delta^{13}C$ only parallel those of $\delta^{18}O$ during the MEHI (Fig. 4.3).

The MEHI and the MLHI are isotopically distinct (Fig. 4.3a). The MEHI is characterized by statistically correlated $\delta^{18}O$ and $\delta^{13}C$ ($r^2$=0.65 and 0.53), and much depleted $\delta^{13}C$ values (ca. –11.0 to –4.0 ‰). The 8.2 ka event, a widespread event in the Northern Hemisphere (NH) (e.g. Alley et al., 1997), is also identified in the stalagmite records. Stalagmite $\delta^{18}O$ and $\delta^{13}C$ values both decreased to a minimum of –6.78 and –10.88‰, respectively at that interval (Figs. 3 and 7). In contrast to the MEHI, the $\delta^{18}O$ and $\delta^{13}C$ values during the MLHI are poorly correlated ($r^2$=0.25 and 0.17), and $\delta^{13}C$ values are more enriched (Fig. 4.3).

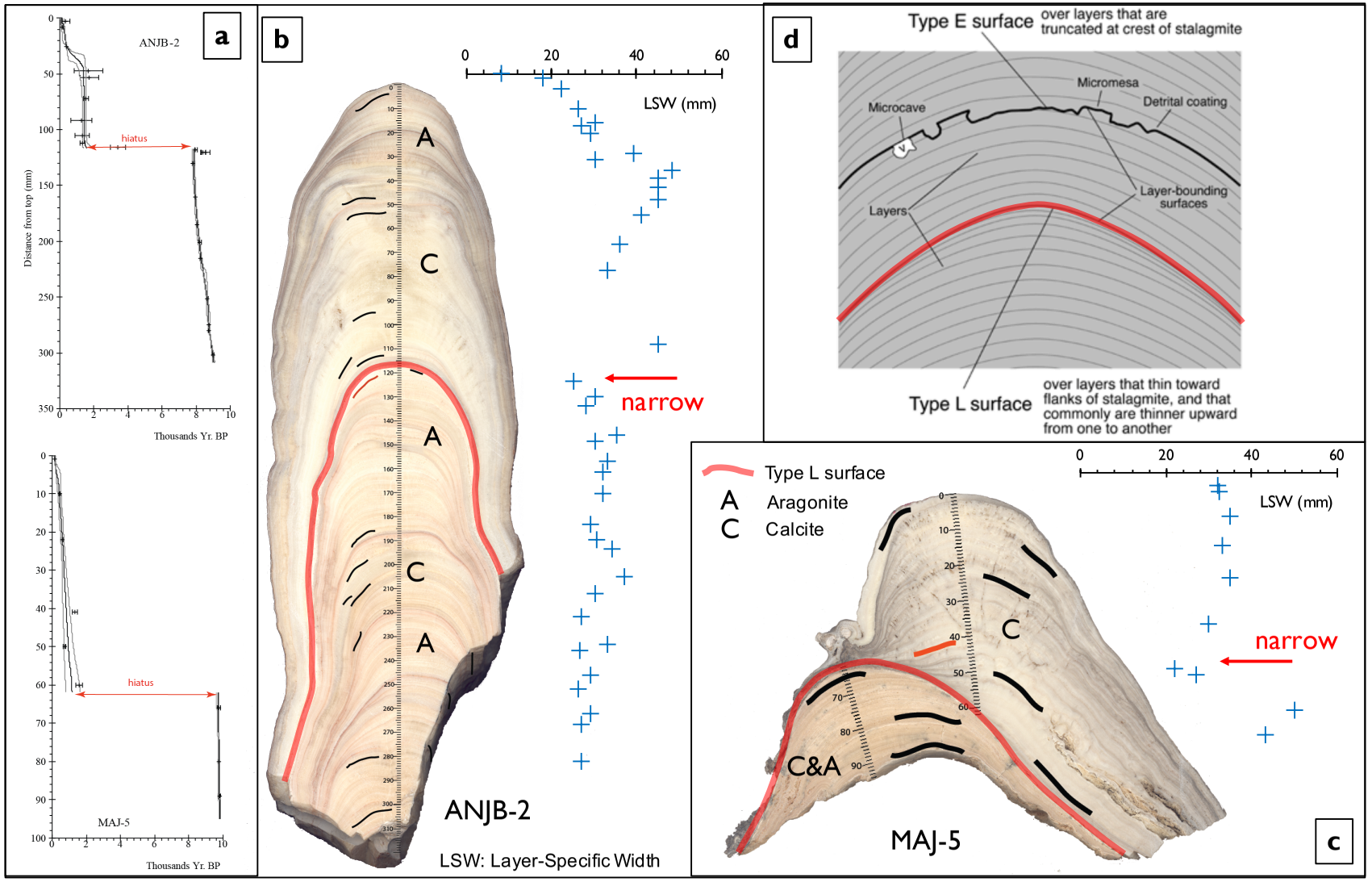
a
ANJB-2
hiatus
Distance from top (mm)
Thousands Yr. BP
MAJ-5
hiatus
Thousands Yr. BP
b
0
20
40
60
LSW (mm)
A
C
A
C
A
narrow
ANJB-2
LSW: Layer-Specific Width
d
Type E surface
over layers that are truncated at crest of stalagmite
Micromesa
Microcave
Detrital coating
Layer-bounding surfaces
Layers
Type L surface
over layers that thin toward flanks of stalagmite, and that commonly are thinner upward from one to another
Type L surface
A Aragonite
C Calcite
0
20
40
60
LSW (mm)
C
narrow
C&A
MAJ-5
c

Figure 4.2: Age model and petrography/mineralogy of Stalagmite ANJB-2 and MAJ-5. a) Age model constructed using the StalAge1.0 algorithm of Scholz and Hoffman (2011) and Scholz et al. (2012). b) Scanned image of Stalagmite ANJB-2 and the corresponding variations in layer-specific width (LSW). c) Scanned image of Stalagmite MAJ-5 and the corresponding layer-specific width (LSW). d) Sketches of typical layer-bounding surfaces (Type E and Type L) of Railsback et al. (2013). X-ray diffraction data are available in Fig. C5. Close-up of photographs of the hiatuses are shown in Fig C6.

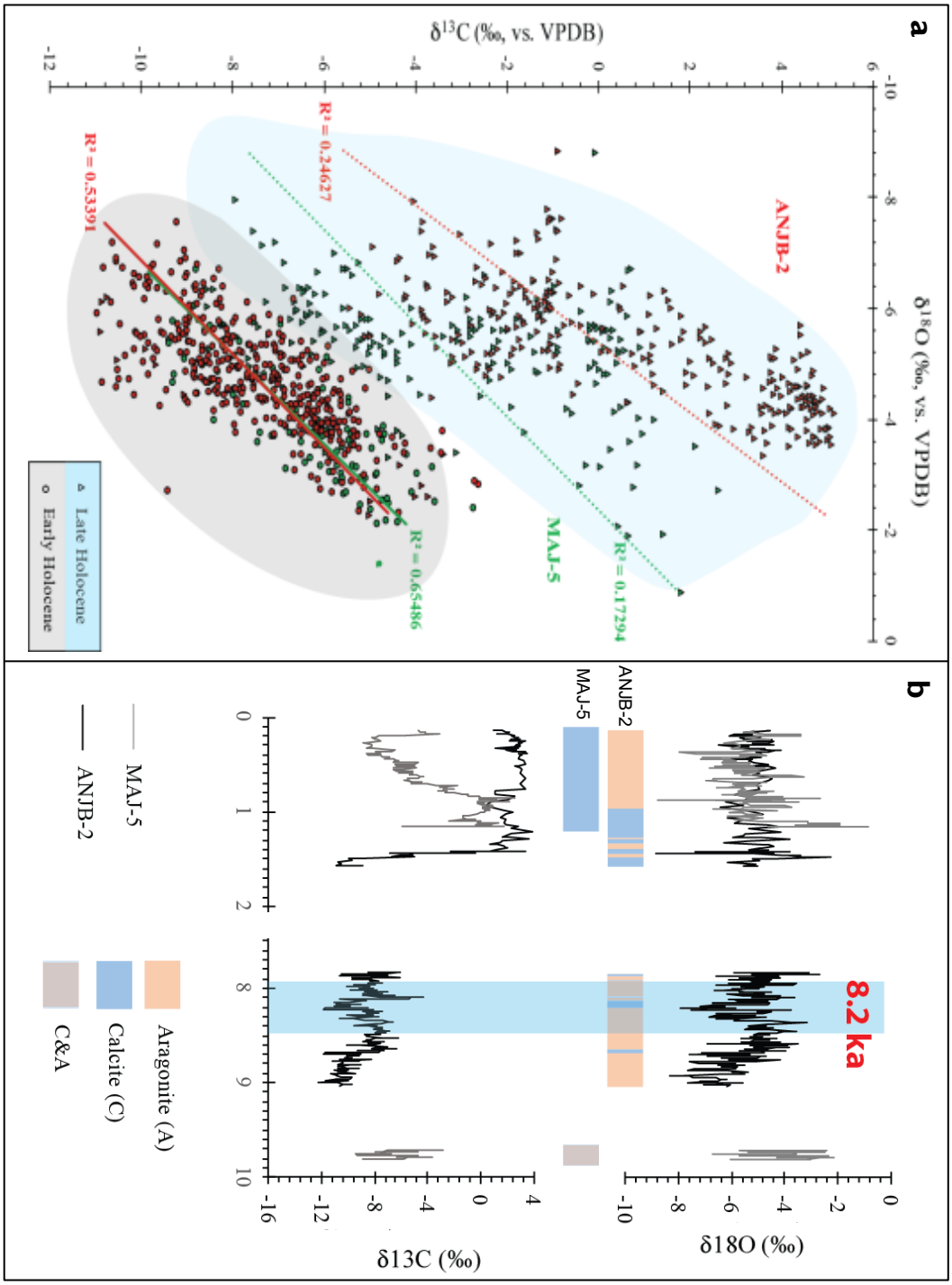
a
δ13C (‰, vs. VPDB)
δ18O (‰, vs. VPDB)
ANJB-2
MAJ-5
R² = 0.24627
R² = 0.17294
R² = 0.53391
R² = 0.65486
Late Holocene
Early Holocene
b
ANJB-2
MAJ-5
8.2 ka
δ18O (‰)
δ13C (‰)
MAJ-5
ANJB-2
Aragonite (A)
Calcite (C)
C&A

**Figure 4.3:** Stable isotope data. a) Scatterplots of $\delta^{13}C$ and $\delta^{18}O$ for Stalagmite MAJ-5 (green) and ANJB-2 (red) during the Malagasy early Holocene interval (circle) and the Malagasy late Holocene conditions (triangle). The plot shows distinctive early and late Holocene (roughly highlighted in gray and light blue shade, respectively). b) Variations in $\delta^{13}C$ and $\delta^{18}O$ and mineralogy in Stalagmite ANJB-2 and Stalagmite MAJ-5 with their corresponding mineralogy. More information about the late Holocene is presented in Fig. C7.

### 4.4.3. Mineralogy, petrography, and layer-specific width

In both stalagmites, the hiatus of deposition (see Sect. 4.4.1) is characterized by a well-developed Type L surface (Figs. 4.2b, C6). Petrography and mineralogy are distinct before and after this hiatus (Fig. 4.2). Below the hiatus, laminations are well preserved in both stalagmites. Above the hiatus, laminations are not well-preserved, although noted in some intervals.

In Stalagmite ANJB-2, the layer-specific width varies from 37 to 26.5 mm with a mean of 30 mm. It narrows to 28 mm at the hiatus (Fig. 4.2b). Below the hiatus, mineralogy is dominated by aragonite, although a few thick layers of calcite are also identified. A thin (~2-3 mm) but remarkable layer of white, very soft, and porous aragonite is identified just below the hiatus (Fig. C6). This layer is capped with a very thin layer of dirty material. Above the hiatus, mineralogy is also composed of calcite and aragonite, with dominance of calcite, and the calcite layers contain some macro-cavities that are mostly off-axis macroholes (Shtober-Zisu et al., 2012).

In Stalagmite MAJ-5, the layer specific width varies from 50 to 22 mm with a mean of 35.5 mm. It narrows to 22 mm at the hiatus (Fig. 4.2b). Below the hiatus, mineralogy is a mixture of calcite and aragonite. Above the hiatus, mineralogy is mainly calcite and macro-cavities are also distributed throughout that upper part of the stalagmite.

### 4.4.4. Summary of the results

The records from Stalagmites ANJB-2 and MAJ-5 suggest three distinct intervals of the Holocene. The MEHI (between ca. 9.8 and 7.8 ka BP), with evidence of stalagmite deposition, is characterized by statistically correlated $\delta^{18}O$ and $\delta^{13}C$ ($r^2$=0.65 and 0.53) and more negative $\delta^{13}C$ values (ca. –11.0 to –4.0 ‰). The MMHI (between ca. 7.8 to 1.6 ka BP) is marked by a long-term hiatus of deposition, which is preceded by a well-developed Type L surface in both Stalagmite ANJB-2 and MAJ-5 (Fig. 4.2; Fig. C6). The Type L surface is observed as an upward narrowing of the stalagmite's width and layer thickness. It is particularly well developed in Stalagmite MAJ-5 (Fig. C6). In the other Stalagmite ANJB-2, the hiatus at the Type L surface is preceded by approximately 3 mm-thick layer of highly porous, very soft, and fibrous white crystals of aragonite (the only aragonite with such properties). This aragonite is topped by a thin and well-defined layer of detrital materials (Fig. C6), further supporting the presence of a hiatus. Finally, the MLHI (after ca. 1.6 ka BP) is characterized by poorly correlated $\delta^{18}O$ and $\delta^{13}C$ ($r^2$=0.25–0.17). This interval is additionally marked by a shift in $\delta^{13}C$ toward higher values (Fig. 4.3).

## 4.5. Discussion

### 4.5.1. Paleoclimate significance of stalagmite growth and non-growth: implications for paleohydrology

Stalagmites are secondary cave deposits, which are $CaCO_3$ precipitates from cave dripwater. Calcium carbonate precipitation occurs by $CO_2$ degassing, which increases the pH of the dripwater and thus increases the concentration of $CO_3^{2-}$. In some cases,

evaporation, which increases the $Ca^{2+}$ and/or $CO_3^{2-}$ of the dripwater, may also be important. Degassing occurs because the high-$PCO_2$ water from the epikarst meets the low-$PCO_2$ cave air, while evaporation occurs when humidity inside the cave is relatively low. The fundamental equation for stalagmite deposition is shown in Eq. 4.1.

$$Ca^{2+}_{(aq)} + 2HCO^{-}_{3\,(aq)} \rightleftharpoons CaCO_{3\,(s)} + CO_{2\,(g)} + H_2O_{(l)} \text{ (Eq. 4.1)}$$

Growth and non-growth of stalagmites depends on several factors linked to water availability, which in turn is affected by climate (more water during warm/rainy seasons and less water during cold/dry seasons) and by the groundwater hydrology above the cave. Water is the main dissolution and transport agent for most chemicals in speleothems. Cave hydrology varies significantly over time in response to climate, and this variability influences the formation or dissolution of $CaCO_3$. In this regard, calcium carbonate does not form if the water feeding the cave is very little to absent, or if it is too much. Absence of groundwater recharge most typically occurs during extremely dry conditions, whereas excessive water input to the cave occurs during extremely wet conditions. In the latter scenario, water is undersaturated and flow rates are too fast to allow degassing. Often, water availability is reflected in the extent of vegetation above and around the cave, as this requires enough moisture from the soil or from the shallow groundwater. Surface biomass supplies most of the $CO_2$ to the soil epikarst, and this could contribute to the stalagmites' processes of formation. Growth and non-growth of stalagmites could be associated with cave dripwater fed by atmospheric precipitation, and this could be linked to climatic conditions at the time when stalagmites grew.

Major hiatuses in stalagmite deposition could be marked by variety of features, including the presence of erosional surfaces, chalkification, dirt bands/detrital layers, deviation of growth axis, and/or sometimes by color changes (e.g. Holmgren et al., 1995; Dutton et al., 2009; Railsback et al., 2013; Railsback et al., 2015; Voarintsoa et al., 2016). Railsback et al. (2013) were specifically able to identify significant features in stalagmites that allow distinction between non-deposition during extremely wet (Type E surfaces) and non-deposition during extremely dry conditions (Type L surfaces; Fig. 4.2b). Physical properties of stalagmites that support these extreme dry and wet events are summarized in Table 1 of Railsback et al. (2013) and the mechanism is explained in their Figure 5.

Type E surfaces are layer-bounding surfaces between two spelean layers when the underlying layers show evidence of truncation. The truncation results from dissolution or erosion (thus the name "E") of the previously-formed layers of stalagmite layers by abundant undersaturated water. Type E surfaces are commonly capped with a layer of calcite (Railsback et al., 2013). This mineralogical trend is not surprising in stalagmites as calcite commonly forms under wetter conditions (e.g. Murray, 1954; Pobeguin, 1965; Siegel, 1965; Thrailkill, 1971; Cabrol and Coudray, 1982; Railsback et al. 1994; Frisia et al., 2002). Additionally, non-carbonate detrital materials are commonly abundant with varying grain size (i.e. from silt- to sand-size; Railsback et al., 2013).

Type L surfaces, on the other hand, are layer-bounding surfaces where the layers became narrower upward and thinner toward the flank of the stalagmite. The decrease in thickness and width of the stalagmites upward is an indication of lessening in deposition (thus the name "L"; Railsback et al., 2013). Aragonite is a very common mineralogy below

the Type L surface, especially in warmer settings. Layers of aragonite commonly form under drier conditions (Murray, 1954; Pobeguin, 1965; Siegel, 1965; Thrailkill, 1971; Cabrol and Coudray, 1982; Railsback et al. 1994; Frisia et al., 2002). Non-carbonate detrital materials are scarce, and if they are present, they tend to form a very thin horizon of very fine dust material (Railsback et al., 2013), typical characteristics for a hiatus in deposition. Identification of Type L surfaces has been aided by measuring the layer-specific width, or LSW (e.g. Sletten et al., 2013; Railsback et al., 2014), an approach that is also performed in this study.

### 4.5.2. Holocene climate reconstruction in northwestern Madagascar

Although the specific boundaries between the early, mid, and late Holocene have been proposed for global application (Walker et al., 2012; Head and Gibbard, 2015), their use is still spatially limited (e.g. Wanner et al., 2015). The age models and the petrographic features of Stalagmites ANJB-2 and MAJ-5 suggest three distinct but different intervals (MEHI, MMHI, and MLHI; see Sect. 4.4.1) that could be used to characterize the Holocene in NW Madagascar. These intervals are illustrated in the three simplified sketches of Figure 4.4. In this paper, these Malagasy intervals are not intended to argue against the previously proposed intervals of the Holocene (Walker et al., 2012; Head and Gibbard, 2015). Instead, they are presented to aid discussion of the available records. For comparison, the intervals are shown in Fig. 4.4d.

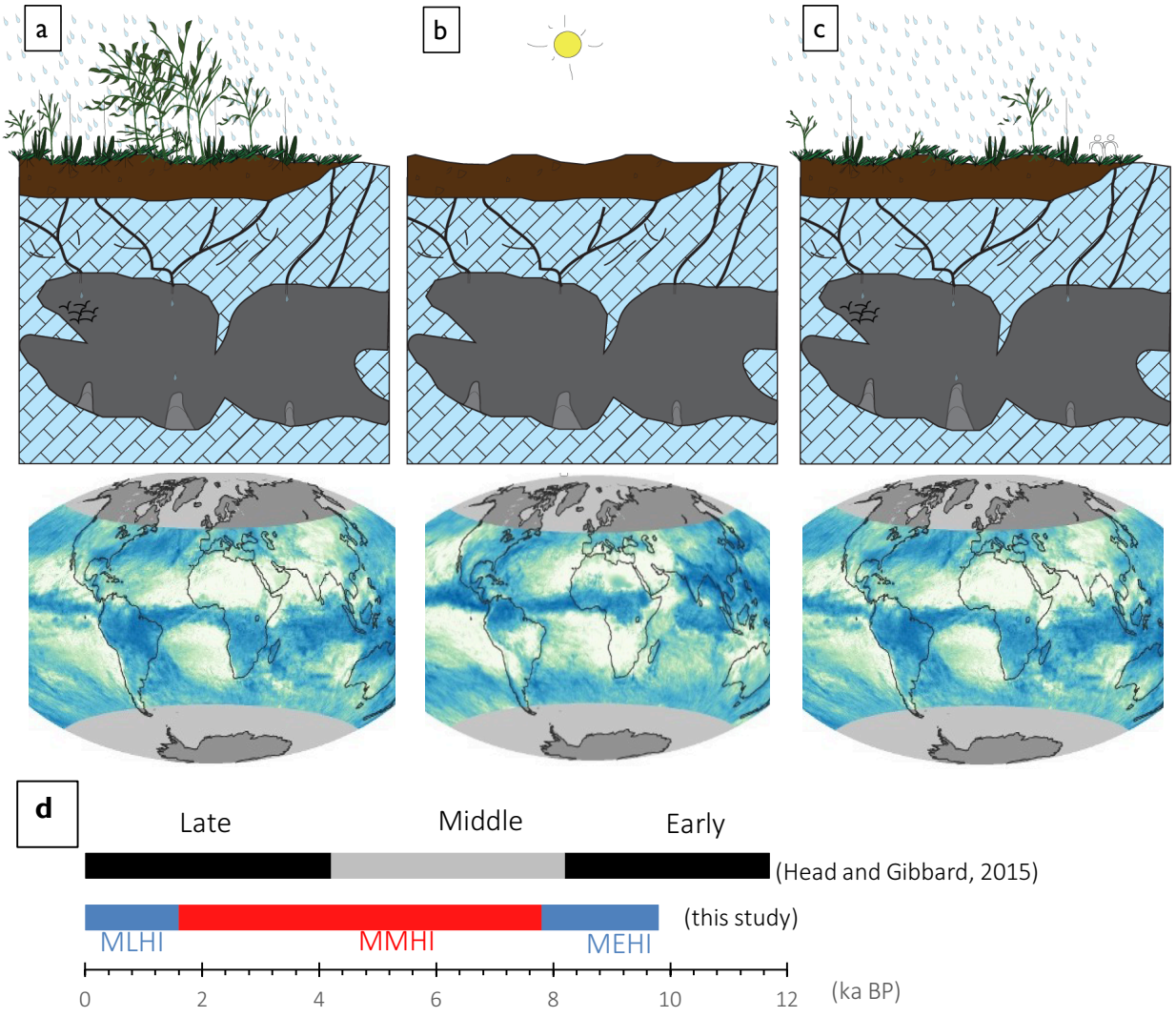
a
b
c
d
Late
Middle
Early
(Head and Gibbard, 2015)
(this study)
MLHI
MMHI
MEHI
0
2
4
6
8
10
12
(ka BP)

**Figure 4.4:** Simplified models portraying the Holocene climate change in northwestern Madagascar and the possible climatic conditions linked to the ITCZ. a) Wetter conditions during the early Holocene with ITCZ south (prior to ca. 7.8 ka), favorable for stalagmite deposition. b) Periodic dry conditions during the mid-Holocene (between ca. 7.8 and 1.6 ka) with ITCZ north that prevented stalagmite formation (refer to Sect. 4.5.2.2). c) Wetter conditions during the late Holocene (after ca. 1.6 ka) with ITCZ south, favorable for stalagmite deposition. For details about paleo-vegetation reconstruction, refer to Sect. 4.5.2 and Fig. C7. Drawings are not to scale. The bottom figures are from the same source as Fig. 1a, and they are only used here to give a perspective of the possible position of the ITCZ during the early, mid, and late Holocene. d) Comparison of the three Malagasy Holocene interval with the Head and Gibbard (2015) subdivision (see text for details, Sect. 4.5.2).

#### *4.5.2.1. Malagasy early Holocene interval (between ca. 9.8 to ca. 7.8 ka BP)*

Stalagmite deposition during the early Holocene suggests that Anjohibe and Anjokipoty cave chambers, where Stalagmites ANJB-2 and MAJ-5 were collected, were sufficiently supplied with water to allow $CaCO_3$ precipitation, in accord with Eq.1. This in turn implies relatively wet conditions that could reflect longer summer rainy seasons, or wet years in NW Madagascar (see Supplementary Text 1 and Fig. C9). The correlative $\delta^{13}C$ and $\delta^{18}O$ values further suggest that vegetation consistently responded to changes in moisture availability, which in turn was dependent on climate.

One striking aspect of the Stalagmite ANJB-2 $\delta^{18}O$ and $\delta^{13}C$ records is that they parallel the $\delta^{18}O$ of the Greenland ice core records at ca. 8.2 ka BP (Figs 4.3 and 4.7). X-ray diffraction data for this period, at 195–202 mm from the top of the stalagmite, suggest that the mineralogy at that age is 100% calcite (Fig. C8). The presence of fine laminations in the layer of calcite itself and petrographic comparison with known examples of primary and secondary calcite (e.g. Railsback, 2000; Perrin et al., 2014) suggest that the calcite is not diagenetic. The decrease $\delta^{18}O$ and $\delta^{13}C$ values and the presence of calcite at the same interval combine to suggest a wet 8.2 ka event in NW Madagascar. The 8.2 ka event is a prominent cold event in North Atlantic records and many NH terrestrial records. It may have been triggered by a release of freshwater from the melting Laurentide Ice Sheet into the North Atlantic basin (e.g. Alley et al., 1997; Barber et al., 1999). Freshwater influx to the Atlantic could have altered the Atlantic Meridional Overturning Circulation (AMOC, e.g. Clark et al., 2001), and could eventually have influenced the climate of Madagascar (Sect. 5.5.3.3). The $\delta^{18}O$ and $\delta^{13}C$ records from Stalagmite ANJB-2 show similar features to the

$\delta^{18}O$ of the Greenland ice core records (GRIP and NGRIP, Fig. 4.7), and suggest that the cold 8.2 ka event in the NH records coincides with a wet period in NW Madagascar. This is the first event in our records that reveals a strong link between paleoenvironmental changes in Madagascar and abrupt climatic events in the NH records, suggesting that Madagascar's climate was also very sensitive to such abrupt climate events.

The Malagasy early Holocene interval terminated with a trend toward drier conditions as suggested by increasing $\delta^{18}O$ and $\delta^{13}C$ values in Stalagmite ANJB-2 and a decrease in the LSW of the two stalagmites. This drier condition could have ended with a significant drought in the region, as suggested by a major Type L surface in both stalagmites and by the presence of a white thin (ca. 3 mm) porous aragonite in Stalagmite ANJB-2, very similar to the white porous fabric described in Niggemann et al. (2003). Aragonite is a $CaCO_3$ polymorph known to indicate intervals of drier conditions (Murray, 1954; Pobeguin, 1965; Siegel, 1965; Thrailkill, 1971; Cabrol and Coudray, 1982; Railsback et al. 1994; Frisia et al., 2002), and this specific layer is capped with a very thin layer of non-carbonate brownish materials, which could have accumulated on the surface by aerosol activity in the absence of dripwater (e.g. Railsback et al., 2013). A shift to drier conditions is also supported by isotopic data from Stalagmite ANJ94-5 from Anjohibe Cave (Wang and Brook, 2013) in which relatively low $\delta^{13}C$ and $\delta^{18}O$ values prior to 7600 BP give way to episodically greater values thereafter.

#### *4.5.2.2. Malagasy mid-Holocene interval (ca. 7.8 to 1.6 ka BP)*

It is unfortunate that stable isotope records are missing in the two stalagmites being studied to fully assess the climate conditions during the MMHI. However, we can speculate on the factors and the climatic conditions that may have been responsible for the long-term depositional hiatuses during the MMHI.

The documented severe dry conditions at the end of the MEHI (see Sect. 4.5.2.1) could have had a significant influence (1) on the cave hydrological system (e.g. Fig. 5 of Asrat et al., 2007; Bosák, 2011), such as the water conduits (primary or secondary porosity) to the chambers, and (2) on the vegetation cover above the caves, particularly above the chambers where Stalagmites ANJB-2 and MAJ-5 were collected. On one hand, it is possible that the dry conditions late in the MEHI could not only bring lesser water recharge to the cave, but also lowered the hydraulic head, and increased the rate of evapo-transpiration in the vadose zone. This condition possibly allowed more air to penetrate the aquifer, perhaps enhancing prior carbonate precipitation (PCP) in pores and conduits above the caves (e.g. Fairchild and McMillan, 2007; Fairchild et al., 2000; Johnson et al., 2006; Karmann et al., 2007; McDonald et al., 2007). This process must have blocked water moving towards Stalagmites ANJB-2 and MAJ-5. On the other hand, the late MEHI drying trend could have challenged vegetation to grow, and it is possible that some areas above Anjohibe and Anjokipoty Caves were devoid of vegetation. Consequently, biomass activities could have been reduced. Because vegetation contributes $CO_2$ to the carbonic acid dissolving $CaCO_3$, its absence in certain areas above the cave could decrease the pH of the percolating water, and perhaps dissolution did not occur.

In either of these two scenarios, the long term-depositional hiatus in Stalagmite ANJB-2 and MAJ-5 could suggest Anjohibe and Anjokipoty Caves experienced some disturbances. The disturbances could be inherited from the very dry conditions at the end of the MEHI, and/or due to the lack of water supply, perhaps associated with an increase in epikarst ventilation, and/or by the absence of vegetation. Water and vegetation are two components of the karst system that play an important role in $CaCO_3$ dissolution and precipitation (see Eq. 1). This is the simplest explanation of the hiatuses in Stalagmites ANJB-2 and MAJ-5 from ca. 7.8 to 1.6 ka, assuming that the trend to drier conditions late in the MEHI, inferred from the white porous aragonite in Stalagmite ANJB-2 and the major Type L surfaces in both stalagmites, persisted with relatively dry conditions through the MMHI compared to conditions of the MEHI.

Other evidence supports the idea of at least episodic dryness during the MMHI. A work in progress on a 2-meter long stalagmite (ANJ94-5) from Anjohibe Cave suggests episodic dryness during the MMHI and a depositional hiatus around the time when Stalagmite ANJB-2 and MAJ-5 stopped growing (Wang and Brook, 2013; Wang, 2016). Some dry spells were also felt in other regions, Central and Southeastern, of Madagascar (e.g. Gasse and Van Campo, 1998; Virah-Sawmy et al., 2009).

In summary, several lines of evidence suggest relatively drier climate during the MMHI compared to the MEHI in NW Madagascar. Drier intervals generally imply drier summer seasons with less rainfall (see Supplementary Text 1 and Fig. C9), perhaps reflecting shorter visits of the ITCZ. In this regard, even though the region received rainfall,

the necessary conditions could not have been attained to activate the growth of Stalagmites ANJB-2 and MAJ-5, thus the hiatuses.

#### *4.5.2.3. Malagasy late Holocene interval (ca. 1.6 ka to present)*

The resumption of stalagmite deposition after ca. 1.6 ka BP suggests that the cave's hydraulic system in the epikarst zone must have been reactivated, when climate in northwestern Madagascar returned to relatively wet conditions, at least similar to the early Holocene climate conditions. This reactivation could be associated with changes in vegetation cover above the cave. The $\delta^{13}C$ profiles display a shift from depleted to enriched values at ca. 1.5 ka BP (Fig. 4.3; Fig. C7), as have been observed in previous stable isotope profiles in Anjohibe (e.g. Burns et al., 2016; Voarintsoa et al., 2017), suggesting that the late Holocene vegetation was different from that of the early Holocene. This shift has been linked to a change from a $C_3$-dominated plant cover to a $C_4$-dominated plant cover, the cause of which has been linked to human activities (e.g. Crowley and Samonds, 2013; Burns et al., 2016; Crowther et al., 2016).

Although the last ca. 1.6 ka BP interval records overall wetter conditions, it was also interrupted by occasional dryness, as suggested by several positive peaks in the Stalagmite $\delta^{18}O$ records. Drier intervals during the late Holocene are observed in the Anjohibe data between ca. AD 755 and 795 (i.e. 1195–1155 yr. BP; Voarintsoa et al., 2017), and in previous paleoenvironmental studies, in which a peak drought around 1300–950 cal BP was reported (Burney, 1987a, b; Burney, 1993; Matsumoto and Burney, 1994; Virah-Sawmy et al., 2009).

### 4.5.3. Holocene climate in northwestern Madagascar: implications for the ITCZ dynamics

Deposition of the Stalagmites ANJB-2 and MAJ-5 in Anjohibe and Anjokipoty Caves, respectively, during the MEHI and the MLHI suggests that these intervals were relatively wetter than the MMHI. The absence of an increasing trend in the $\delta^{18}O$ values, with a consistent amplitude of fluctuations, during the MEHI and the MLHI suggests that NW Madagascar has been consistently visited by the ITCZ. However, the alternating "wet/dry/wet" intervals during the early, mid, and late Holocene suggest that, in addition to the seasonal migration of the ITCZ, these long-term climate changes could be associated with the duration of the ITCZ visit in the SH, leading to wetter or drier years in Madagascar (also see Supplementary Text 1 and Fig. C9).

The length of visit of the ITCZ in the NH or SH has been linked to the latitudinal shift or latitudinal migration of the ITCZ. When the ITCZ's mean position is south (often referred to as southward migration of the ITCZ), many regions in the SH become wetter because summer rainy seasons may get longer (e.g. Voarintsoa et al., 2016), and monsoonal rainfall during summer seasons may have been more intense. When the ITCZ's mean position is north (i.e. referred to as northward migration of the ITCZ), many regions in the SH become drier as summer rainy seasons become shorter, when monsoonal rainfall during summer seasons weakened.

In NW Madagascar, stalagmite deposition during the MEHI and the MLHI could suggests sufficient dripwater supply that could reflect wetter conditions. This could have been linked to a more southerly mean position of the ITCZ. The depositional hiatuses during the MMHI could suggest a northward migration of the ITCZ. Factors that could

influence the mean position of the ITCZ include change in insolation, difference in temperature between the two hemispheres, glaciers advances that indicate global cold conditions, and the alteration of the thermohaline circulation. These factors are discussed in detail further below.

#### *4.5.3.1. ITCZ and insolation*

The ITCZ migrates southward in austral summer and northward in boreal summer in response to seasonal insolation. This migration has also been observed at decadal, centennial, and millennial scale (e.g. Haug et al., 2001; Voarintsoa et al., 2016). If we assume that insolation is the sole driver of the ITCZ's latitudinal migration, comparison of the insolation curves of Berger and Loutre (1991) and the stable isotope profiles and the timing of deposition of stalagmites ANJB-2 and MAJ-5 (Fig. 4.5a) suggests that high winter insolation in the southern hemisphere could have been responsible for the southward migration of the ITCZ during the early Holocene. This could have increased the number of summer months in northwestern Madagascar, without necessarily intensifying the monsoon strength. On the other hand, the southward migration of the ITCZ during the late Holocene could be linked to high summer insolation (Fig. 4.5). In such conditions, it could be possible that monsoonal rainfall in northwestern Madagascar intensified (see Supplementary Text 1 and Fig. C9).

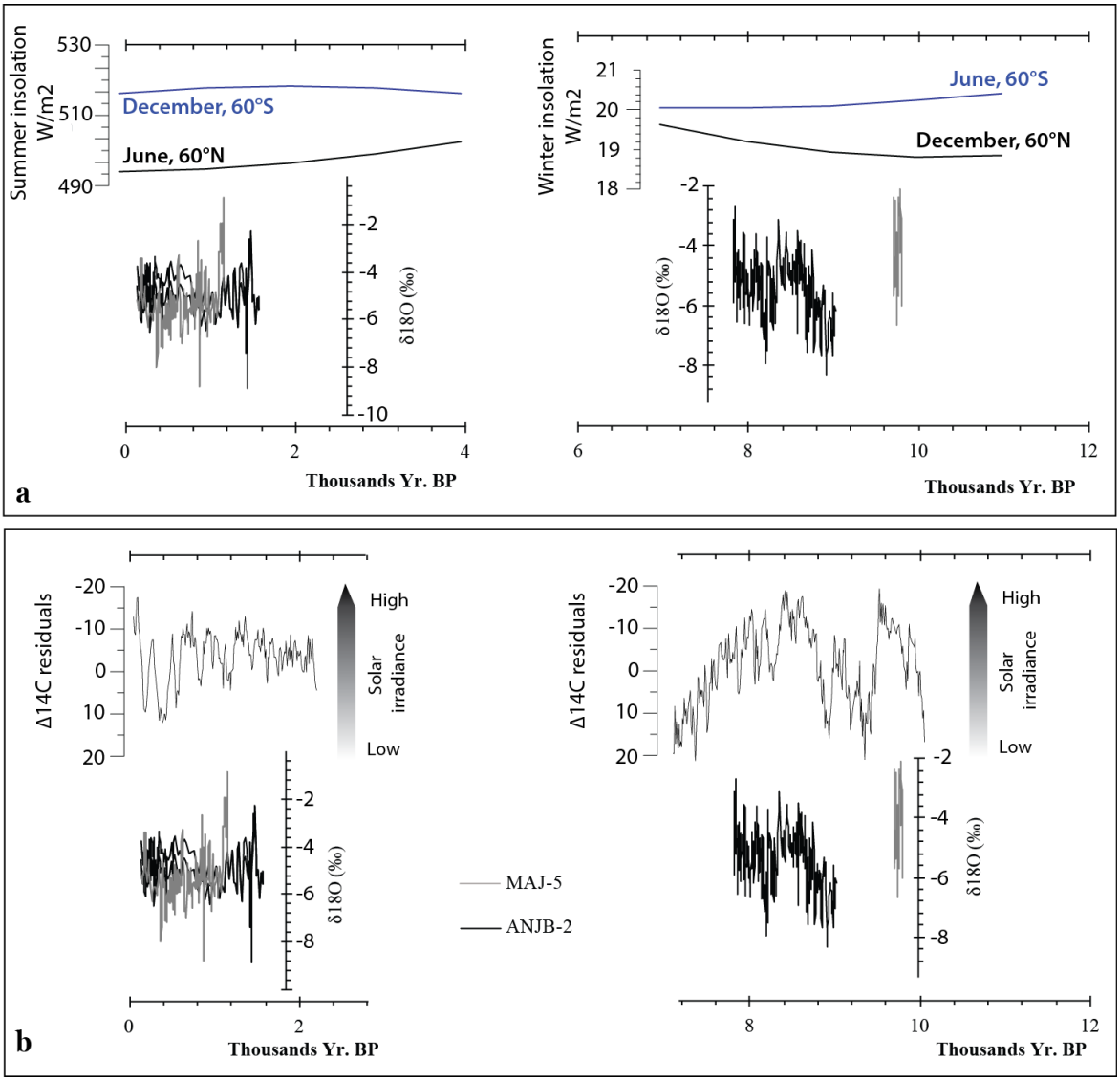
Summer insolation W/m2
530
510
490
December, 60°S
June, 60°N
-2
-4
-6
-8
-10
δ18O (‰)
0
2
4
Thousands Yr. BP
a
Winter insolation W/m2
21
20
19
18
June, 60°S
December, 60°N
-2
-4
-6
-8
δ18O (‰)
6
8
10
12
Thousands Yr. BP
Δ14C residuals
-20
-10
0
10
20
High
Solar irradiance
Low
-2
-4
-6
-8
δ18O (‰)
MAJ-5
ANJB-2
0
2
Thousands Yr. BP
b
8
10
12
Thousands Yr. BP

**Figure 4.5:** Paleoclimate of northwestern Madagascar compared with insolation. (a) Comparison between insolation curves (Berger and Loutre, 1991) and stalagmite $\delta^{18}O$. Timing of stalagmite deposition is coeval with high SH winter insolation during the early Holocene and high SH summer insolation during the late Holocene. (b) Reconstructed solar irradiance from $\Delta^{14}C$ residuals (Stuiver et al., 1998) compared with Stalagmite $\delta^{18}O$. Stalagmite $\delta^{18}O$ relates well to the reconstructed solar irradiance ($\Delta^{14}C$), particularly during the early Holocene.

Recognizing that application of the insolation curve of Berger and Loutre (1991) to paleohydrology in northwestern Madagascar might seem subjective, we also compared our records with the solar radiation reconstruction from $^{14}C$ residual records of Stuiver et al. (1998). The stalagmite $\delta^{18}O$ records relate well to the reconstructed solar irradiance fluctuations during the MEHI. Negative $\delta^{18}O$ values, indicative of wetter conditions in northwestern Madagascar, correspond to high $\Delta^{14}C$ residuals values, indicative of low solar irradiance (Fig. 4.5). A similar but opposite relationship has been observed during the Holocene Asian Monsoon in Dongge Cave, southern China, a region visited by the ITCZ during boreal summers (Wang et al., 2005). Figure 2 of Wang et al. (2005) suggests that higher solar irradiance (smaller $\Delta^{14}C$) corresponds to a stronger Asian Monsoon. This antiphase relationship between northwestern Madagascar's and southern China's monsoonal response, for example, could suggest that the distribution of energy related to solar irradiance leads to shifts of the ITCZ, and this is felt in both hemispheres.

Comparing the stalagmite $\delta^{18}O$ records with the same $^{14}C$ residual records of Stuiver et al. (1998), the MLHI paleohydrology linkage to insolation is not as obvious as the early Holocene. This could be explained by the complexity of the climate drivers during the late Holocene. Studies report that the late Holocene climate has changed in response to several overlapping effects of the orbitally driven insolation, volcanic eruptions, changes in solar irradiance (e.g. Wanner et al., 2008), and changes in regional to global-scale variations in temperature (e.g. Neukom et al., 2014; Chambers, 2015).

For the mid-Holocene, our inference of a relatively drier climate seems to agree with the paleoclimate simulation of Braconnot et al. (2007), suggesting that the NH

insolation increased. This insolation hypothesis was briefly reviewed in Chiang (2009; see his Fig. 6). Per Chiang's review, the predominant climate forcing of the mid-Holocene (centered at ~6 ka) was a pronounced change to the insolation, which was primarily due to precessional changes in the Earth's orbit. Chiang added that the Earth was nearer to the Sun in boreal summer than boreal winter, and NH summers were more intense than today. Quantification of the mean ITCZ position using a set of coupled ocean-atmosphere(-vegetation) simulations during the mid-Holocene (ca. ~6 ka) in the second phase of the Paleoclimate Modeling Intercomparison Project (PMIP2) suggests a northward displacement of the ITCZ at ~6 ka (Braconnot et al., 2007) in response to increased summer insolation (Braconnot et al., 2000). This northward migration increased the mean simulated precipitation over the northern edge of the ITCZ (Braconnot et al., 2007), but could have decreased the mean precipitation simulated over its southern edge, as in northwestern Madagascar (this study).

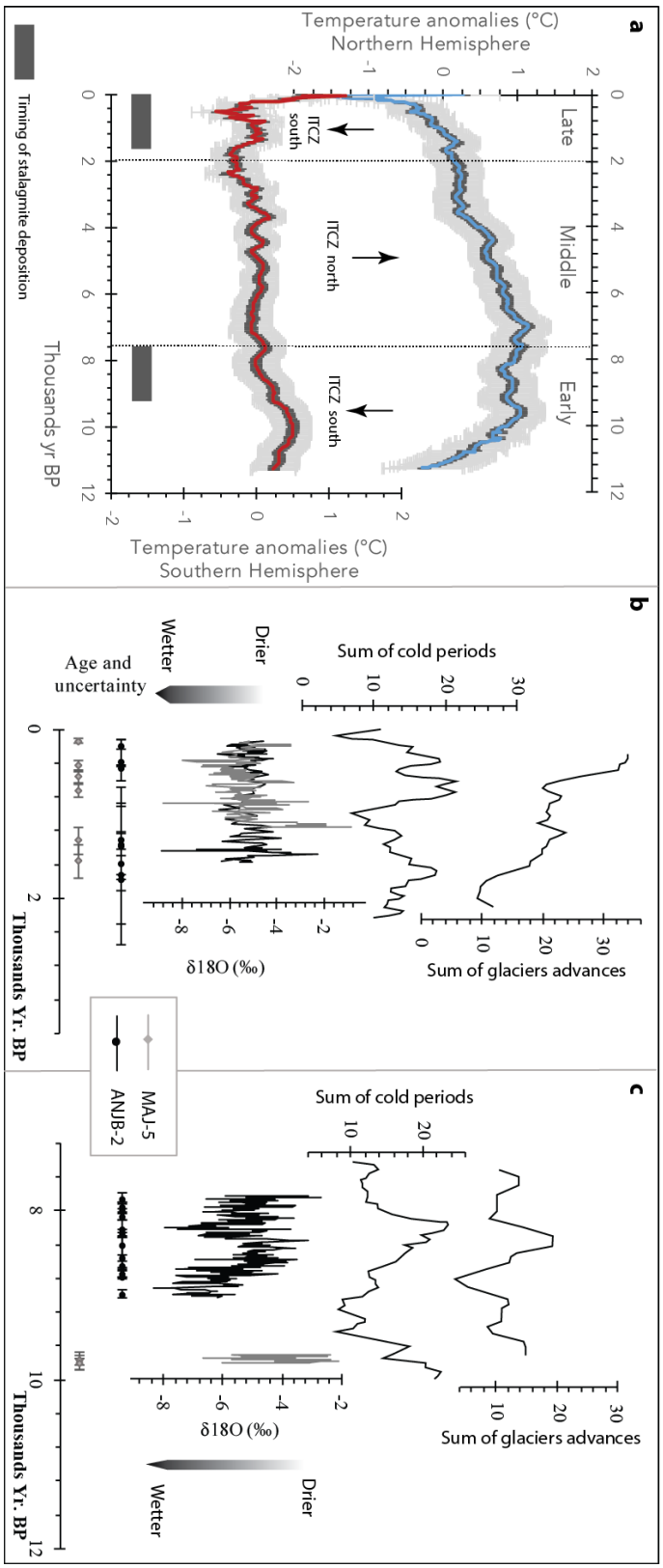
a
Temperature anomalies (°C)
Northern Hemisphere
Late
Middle
Early
ITCZ south
ITCZ north
ITCZ south
Thousands yr BP
Timing of stalagmite deposition
Temperature anomalies (°C)
Southern Hemisphere
b
Age and uncertainty
Wetter
Drier
Sum of cold periods
δ18O (‰)
Sum of glaciers advances
Thousands Yr. BP
MAJ-5
ANJB-2
c
Sum of cold periods
δ18O (‰)
Sum of glaciers advances
Wetter
Drier
Thousands Yr. BP

Figure 4.6: Climate of NW Madagascar compared with global temperature conditions. A) Average Holocene temperatures in the Northern Hemisphere 90°–30°N (blue) and the Southern Hemisphere 90°–30°S (red), referenced to the 1961–1990 mean temperature (Marcott et al., 2013), with 1σ uncertainty (gray). B–c) Curves representing the sum of glaciers advances from a set of global Holocene time series compiled from natural paleoclimate archives (Wanner et al., 2011) and curves representing the sum of cold periods from a set of global Holocene time series compiled from natural paleoclimate archives (Wanner et al., 2011) compared with the $\delta^{18}O$ profile of Stalagmite ANJB-2 (black) and MAJ-5 (gray) and their corresponding radiometric age data with the 2$\sigma$ error.

#### *4.5.3.2. Linkages to ocean-atmosphere dynamics: ITCZ and global cooling/warming conditions*

Besides insolation, the ITCZ's length of visit in either hemisphere also depends on global cooling/warming conditions (e.g. Chiang and Bitz, 2005; Broccoli et al., 2006). Global cooling and/or warming conditions are often reflected in the extent of glacial advances (e.g. Fig. 3 of Wanner et al., 2011). Model simulations using an AGCM– slab ocean model (Chiang and Bitz, 2005) suggest a southward shift in the ITCZ over all tropical ocean basins when extratropical cooling and enhanced sea-ice cover in the NH were imposed. Similar simulations revealed a northward shift in the ITCZ when a southern extratropical cooling was imposed, enhancing cooling in the SH (Broccoli et al., 2006). It has therefore been reported and widely agreed that the ITCZ's latitudinal migration is driven by the temperature gradient between the two hemispheres (Chiang and Bitz, 2005; Broccoli et al., 2006; Chiang and Friedman, 2012). The ITCZ moves from a cold hemisphere towards a warmer one (e.g. Kang et al., 2008; McGee et al., 2014; Talento and Barreiro, 2016), and this latitudinal migration has been the main driver of rainfall availability in tropical and semi-arid regions visited by the ITCZ at decadal to millennial scales (e.g. Haug et al., 2001; Voarintsoa et al., 2016).

Figure 6a suggests that deposition of Stalagmite ANJB-2 and MAJ-5 during the MEHI and the MLHI, i.e. the wetter intervals, coincided with the timing of southward migrations of the ITCZ, when the NH was cooler than the SH (Marcott et al., 2013). This timing of southward migration of the ITCZ coincided with intervals of global cooler conditions with a high number of glacial advances (Figs. 4.6b–c; Wanner et al., 2011). This scenario agrees

well with the model of Chiang and Bitz (2005), and the climatic responses are very similar to those observed in northeastern Namibia (e.g. Voarintsoa et al., 2016). In contrast, the hiatus in deposition during the mid-Holocene was coeval with a warmer NH and cooler SH, suggesting a northward migration of the ITCZ. This scenario agrees with the model simulation of Broccoli et al. (2006).

#### *4.5.3.3. ITCZ and AMOC: southward migration of the ITCZ during the 8.2 ka event*

Understanding the Atlantic Meridional Overturning Circulation (AMOC)'s influence on Madagascar's hydroclimate could fill gaps in our understanding the global atmospheric and oceanic circulation, particularly in the SH. The AMOC, a component of the Thermohaline Circulation (THC) or the Global Ocean Conveyor (Stommel, 1958; Gordon, 1986; Broecker, 1992, 1992; Delworth et al., 2008), is an important component of the Earth's climate system (Broecker 1991, 1992; Weaver et al. 1999; Delworth et al., 2008). It plays an essential role in maintaining global climate by transporting a large amount of heat from northern high latitude regions, starting for example at the North Atlantic Deep Water (NADW), to several regions worldwide (e.g., Broecker 1992; Weaver et al. 1999). It connects localized high latitude sinking cold water in the North Atlantic with tropical climate changes (e.g., Dong and Sutton 2002; Zhang and Delworth 2005). The AMOC was used to interpret the non-orbital periodicity (i.e. at millennial scale) of isotopic records, identified in ice cores, because of an abrupt influx of meltwater from the Laurentide ice sheet into the North Atlantic Ocean (e.g. Alley et al., 1997; Barber et al., 1999).

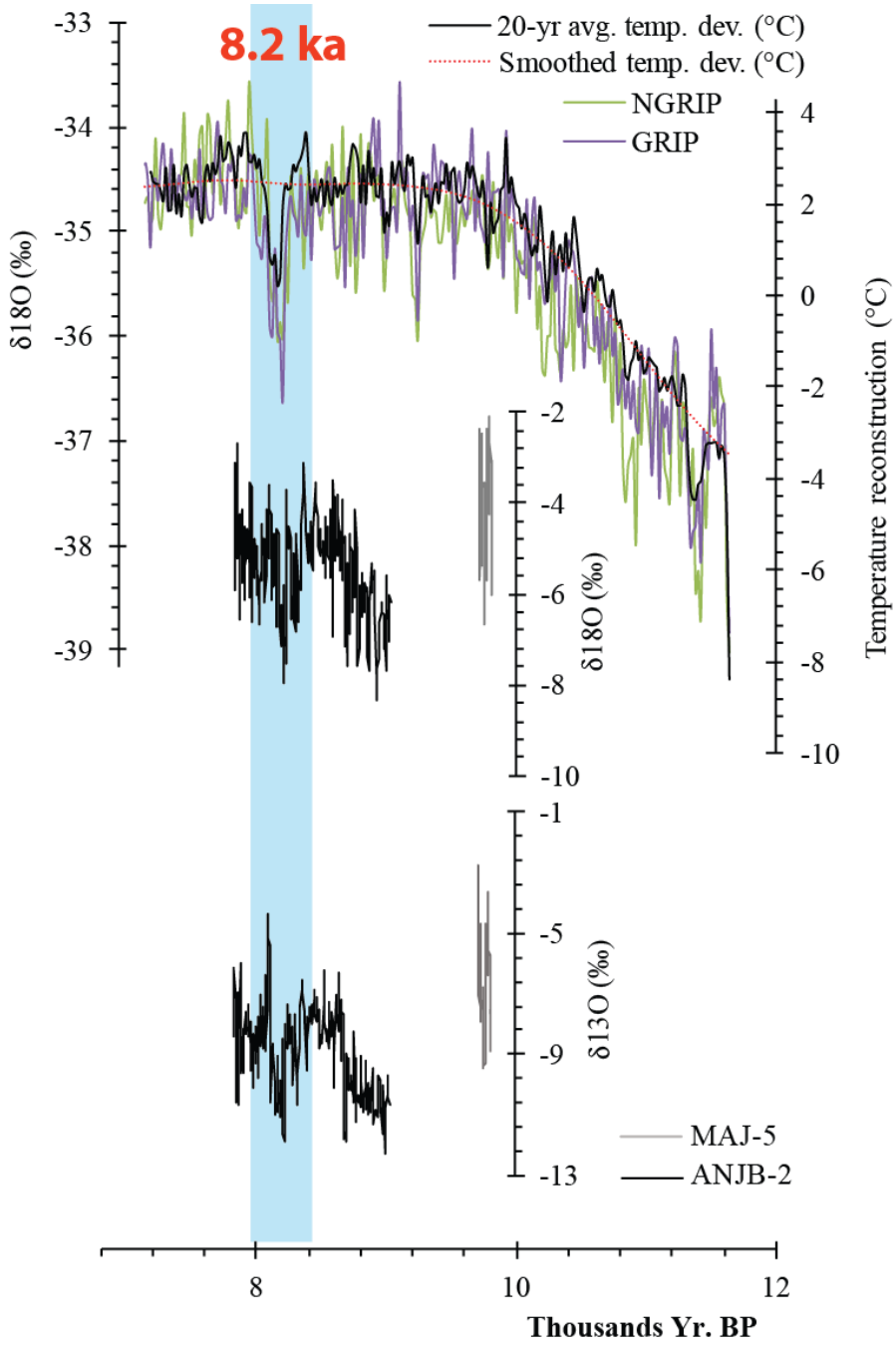
8.2 ka
20-yr avg. temp. dev. (°C)
Smoothed temp. dev. (°C)
NGRIP
GRIP
δ18O (‰)
Temperature reconstruction (°C)
δ18O (‰)
δ13O (‰)
MAJ-5
ANJB-2
Thousands Yr. BP

**Figure 4.7:** The 8.2 ka event in Madagascar. Oxygen isotope record from Greenland (GRIP and NGRIP) ice cores (Vinther et al., 2009) compared with Stalagmite ANJB-2 $\delta^{18}O$ and $\delta^{13}C$. Fig. C8 provides additional supporting evidence of the wet 8.2 ka event.

A more fundamental impact of the changes in the AMOC is the alteration of the temperature gradient between the two hemispheres, known to have been responsible for the latitudinal shift of the ITCZ in the tropical Atlantic (e.g. Dong and Sutton, 2007; Delworth et al., 2008, p. 309). The 8.2 ka event, a significant short-lived cooling of the early Holocene (Alley et al., 1997), revealed in northwestern Madagascar records as a wet interval (Figs. 4.3 and 4.7), is an ideal timeframe to investigate such "ocean-land-atmosphere" relationships during the early Holocene. The 8.2 ka event is a known interval of abrupt freshwater influx from the melting Laurentide Ice Sheet into the North Atlantic (Alley et al., 1997; Barber et al., 1999; Kleiven et al., 2008; Carlson et al., 2008; Renssen et al, 2010; Wiersma et al., 2011; Wanner et al., 2015). It is equivalent to the sharp peak of the Bond cycle number 5 (Bond et al. 1997, 2001). This influx of meltwater altered the density and salinity of the NADW. Thornalley et al. (2009) reported a decrease in the NADW salinity to approximately 34 p.s.u. during the early Holocene. This perturbation of the North Atlantic could partially or completely weaken the AMOC (e.g., Vellinga and Wood 2002; Dong and Sutton 2002, 2007; Dahl et al. 2005; Zhang and Delworth 2005). Weakening of the AMOC would result in a deepening of the thermocline level (Timmermann et al, 2005), which could eventually lead to an anomalous warming of the southern oceans.

In parallel to this, the weakening of the AMOC would result in a positive cooling feedback to NH regions because the Gulf Stream was shut down. This weakening of the AMOC would therefore cause a significant temperature gradient between the two hemispheres, with a cooler NH and warmer SH, suggesting a southward migration of the

ITCZ during the 8.2 ka event. Thus, northwestern Madagascar became wet, as suggested by the more negative stalagmite $\delta^{18}O$ and $\delta^{13}C$ values around the 8.2 ka event. This wetting could correspond to a stronger Malagasy monsoon during austral summers, a phenomenon identical to the South American Summer Monsoon, identified in Brazil (e.g. Cheng et al., 2009). In contrast, regions in the NH monsoon regions became dry as the Asian Monsoon and the East Asian Monsoon became weaker (e.g. Wang et al., 2005; Dykoski et al., 2005; Cheng et al., 2009; Liu et al., 2013).

## 4.6. Conclusion

Petrography, mineralogy, and stable isotope records from Stalagmite ANJB-2, from Anjohibe Cave, and Stalagmite MAJ-5, from Anjokipoty Cave, all combine to suggest three distinct intervals of climatic change in Madagascar during the Holocene: relatively wet conditions during MEHI, relatively drier conditions, possibly due to episodic dryness, during the MMHI, and relatively wet conditions during the MLHI. The timing of stalagmite deposition during the MEHI and the MLHI in NW Madagascar could be attributed to a more southward migration and/or an expanded ITCZ, increasing the duration of the summer rainy seasons, perhaps linked to a stronger Malagasy monsoon. This could have been tied to insolation, the temperature gradient between the two hemispheres, and weakening of the AMOC. In contrast, the ~6500 year-long depositional hiatus during the MMHI could reflect a northward migration of the ITCZ, leading to relatively drier conditions in NW Madagascar. The evidence of the 8.2 ka event in the Malagasy records further suggests a strong link between paleoenvironmental changes in Madagascar and abrupt climatic

events in the Northern Hemisphere records, suggesting that Madagascar climate was also very sensitive to such abrupt climate events.

## REFERENCES


Alley, R. B., Mayewski, P. A., Sowers, T., Stuiver, M., Taylor, K. C., and Clark, P. U.: Holocene climatic instability: A prominent, widespread event 8200 yr ago, Geology, 25, 483-486, 1997.

Asrat, A., Baker, A., Mohammed, M. U., Leng, M. J., Van Calsteren, P., and Smith, C.: A high-resolution multi-proxy stalagmite record from Mechara, Southeastern Ethiopia: palaeohydrological implications for speleothem palaeoclimate reconstruction, J Quaternary Sci, 22, 53-63, Doi 10.1002/Jqs.1013, 2007.

Barber, D. C., Dyke, A., Hillaire-Marcel, C., Jennings, A. E., Andrews, J. T., Kerwin, M. W., Bilodeau, G., McNeely, R., Southon, J., Morehead, M. D., and Gagnon, J. M.: Forcing of the cold event of 8,200 years ago by catastrophic drainage of Laurentide lakes, Nature, 400, 344-348, Doi 10.1038/22504, 1999.

Berger, A., and Loutre, M. F.: Insolation Values for the Climate of the Last 10 million years, Quaternary Sci Rev, 10, 297-317, Doi 10.1016/0277-3791(91)90033-Q, 1991.

Bond, G., Kromer, B., Beer, J., Muscheler, R., Evans, M. N., Showers, W., Hoffmann, S., Lotti-Bond, R., Hajdas, I., and Bonani, G.: Persistent solar influence on north Atlantic climate during the Holocene, Science, 294, 2130-2136, Doi 10.1126/Science.1065680, 2001.

Bond, G., Showers, W., Cheseby, M., Lotti, R., Almasi, P., deMenocal, P., Priore, P., Cullen, H., Hajdas, I., and Bonani, G.: A pervasive millennial-scale cycle in North Atlantic Holocene and glacial climates, Science, 278, 1257-1266, DOI 10.1126/science.278.5341.1257, 1997.

Bosák, P.: Dating of processes in karst and caves: implication for show caves presentation, 6th ISCA Congress Proceedings, Slovakia, 2011, 34-41, 2011.

Braconnot, P., Marti, O., Joussaume, S., and Leclainche, Y.: Ocean feedback in response to 6 kyr BP insolation, J Climate, 13, 1537-1553, 2000.

Braconnot, P., Otto-Bliesner, B., Harrison, S., Joussaume, S., Peterchmitt, J. Y., Abe-Ouchi, A., Crucifix, M., Driesschaert, E., Fichefet, T., Hewitt, C. D., Kageyama, M., Kitoh, A., Laine, A., Loutre, M. F., Marti, O., Merkel, U., Ramstein, G., Valdes, P., Weber, S. L., Yu, Y., and Zhao, Y.: Results of PMIP2 coupled simulations of the Mid-Holocene and Last Glacial Maximum - Part 1: experiments and large-scale features, Clim Past, 3, 261-277, 2007.

Broccoli, A. J., Dahl, K. A., and Stouffer, R. J.: Response of the ITCZ to Northern Hemisphere cooling, Geophys Res Lett, 33, 10.1029/2005gl024546, 2006.

Broecker, W. S.: The Great Ocean Conveyor, Oceanography, 4, 79-89, 1991.

Broecker, W. S.: The Great Ocean Conveyor, Global Warming: Physics and Facts, 247, 129-161, 1992.

Brook, G. A., Rafter, M. A., Railsback, L. B., Sheen, S. W., and Lundberg, J.: A high-resolution proxy record of rainfall and ENSO since AD 1550 from layering in stalagmites from Anjohibe Cave, Madagascar, Holocene, 9, 695-705, Doi 10.1191/095968399677907790, 1999.

Burney, D. A., Burney, L. P., Godfrey, L. R., Jungers, W. L., Goodman, S. M., Wright, H. T., and Jull, A. J. T.: A chronology for late prehistoric Madagascar, Journal of Human Evolution, 47, 25-63, Doi 10.1016/J.Jhevol.2004.05.005, 2004.

Burney, D. A., James, H. F., Grady, F. V., Rafamantanantsoa, J. G., Ramilisonina, Wright, H. T., and Cowart, J. B.: Environmental change, extinction and human activity: evidence from caves in NW Madagascar, Journal of Biogeography, 24, 755-767, 10.1046/J.1365-2699.1997.00146.X, 1997.

Burney, D. A.: Late Quaternary Stratigraphic Charcoal Records from Madagascar, Quaternary Res, 28, 274-280, Doi 10.1016/0033-5894(87)90065-2, 1987a.

Burney, D. A.: Late Holocene Vegetational Change in Central Madagascar, Quaternary Res, 28, 130-143, Doi 10.1016/0033-5894(87)90038-X, 1987.

Burns, S. J., Godfrey, L. R., Faina, P., McGee, D., Hardt, B., Ranivoharimanana, L., and Randrianasy, J.: Rapid human-induced landscape transformation in Madagascar at the end of the first millennium of the Common Era, Quaternary Sci Rev, 134, 92-99, 10.1016/j.quascirev.2016.01.007, 2016.

Cabrol, P., and Coudray, J.: Climatic fluctuations influence the genesis and diagenesis of carbonate speleothems in southwestern France, National Speleological Society Bulletin 44, 112-117, 1982.

Carlson, A. E., Legrande, A. N., Oppo, D. W., Came, R. E., Schmidt, G. A., Anslow, F. S., Licciardi, J. M., and Obbink, E. A.: Rapid early Holocene deglaciation of the Laurentide ice sheet, Nat Geosci, 1, 620-624, 10.1038/ngeo285, 2008.

Chambers, F. M.: The 'Little Ice Age': The first virtual issue of the Holocene, The Holocene, Epub ahead of print 29 June, DOI: 10.1177/0959683615593688, 2015.

Cheng, H., Fleitmann, D., Edwards, R. L., Wang, X. F., Cruz, F. W., Auler, A. S., Mangini, A., Wang, Y. J., Kong, X. G., Burns, S. J., and Matter, A.: Timing and structure of the 8.2

kyr BP event inferred from delta O-18 records of stalagmites from China, Oman, and Brazil, Geology, 37, 1007-1010, 10.1130/G30126a.1, 2009.

Chiang, J. C. H.: The Tropics in Paleoclimate, Annual Review of Earth and Planetary Sciences, 37, 263-297, 10.1146/annurev.earth.031208.100217, 2009.

Chiang, J. C. H., and Bitz, C. M.: Influence of high latitude ice cover on the marine Intertropical Convergence Zone, Clim Dynam, 25, 477-496, 10.1007/s00382-005-0040-5, 2005.

Chiang, J. C. H., and Friedman, A. R.: Extratropical Cooling, Interhemispheric Thermal Gradients, and Tropical Climate Change, Annual Review of Earth and Planetary Sciences, 40, 383-412, 10.1146/Annurev-Earth-042711-105545, 2012.

Crowley, B. E.: A refined chronology of prehistoric Madagascar and the demise of the megafauna, Quaternary Sci Rev, 29, 2591-2603, Doi 10.1016/J.Quascirev.2010.06.030, 2010.

Crowley, B. E., and Samonds, K. E.: Stable carbon isotope values confirm a recent increase in grasslands in northwestern Madagascar, The Holocene, 23, 1066-1073, Doi 10.1177/0959683613484675, 2013.

Crowther, A., Lucas, L., Helm, R., Horton, M., Shipton, C., Wright, H. T., Walshaw, S., Pawlowicz, M., Radimilahy, C., Douka, K., Picornell-Gelabert, L., Fuller, D. Q., and Boivin, N. L.: Ancient crops provide first archaeological signature of the westward Austronesian expansion, P Natl Acad Sci USA, 113, 6635-6640, 10.1073/pnas.1522714113, 2016.

Dahl, K., Broccoli, A., and Stouffer, R.: Assessing the role of North Atlantic freshwater forcing in millennial scale climate variability: a tropical Atlantic perspective, Clim Dynam, 24, 325-346, 10.1007/s00382-004-0499-5, 2005.

Delworth, T. L., Clark, P. U., Holland, M., Johns, W. E., Kuhlbrodt, T., Lynch-Stieglitz, J., Morrill, C., Seager, R., Weaver, A. J., and Zhang, R.: The potential for abrupt change in the Atlantic Meridional Overturning Circulation, in: Abrupt Climate Change. A report by the U.S. Climate Change Science Program and the Subcommittee on Global Change Research. U.S. Geological Survey Reston, VA, 117–162, 2008.

Dong, B. W., and Sutton, R. T.: Adjustment of the coupled ocean-atmosphere system to a sudden change in the Thermohaline Circulation, Geophys Res Lett, 29, 2002.

Dong, B., and Sutton, R. T.: Enhancement of ENSO variability by a weakened Atlantic thermohaline circulation in a coupled GCM, J Climate, 20, 4920-4939, 10.1175/Jcli4284.1, 2007.

Dutton, A., Bard, E., Antonioli, F., Esat, T. M., Lambeck, K., and McCulloch, M. T.: Phasing and amplitude of sea-level and climate change during the penultimate interglacial, Nat Geosci, 2, 355-359, 10.1038/Ngeo470, 2009.

Dykoski, C. A., Edwards, R. L., Cheng, H., Yuan, D. X., Cai, Y. J., Zhang, M. L., Lin, Y. S., Qing, J. M., An, Z. S., and Revenaugh, J.: A high-resolution, absolute-dated Holocene and deglacial Asian monsoon record from Dongge Cave, China, Earth Planet Sc Lett, 233, 71-86, 10.1016/j.epsl.2005.01.036, 2005.

Fairchild, I. J., and Baker, A.: Speleothem Science: From Processes to Past Environments, edited by: Bradley, R., Wiley-Blackwell, 2012.

Frisia, S., Borsato, A., Fairchild, I. J., McDermott, F., and Selmo, E. M.: Aragonite–calcite relationships in speleothems (Grotte de Clamouse, France): environment, fabrics, and carbonate geochemistry., J Sediment Res, 772, 687-699, 2002.

Gasse, F., and Van Campo, E.: A 40,000-yr pollen and diatom record from Lake Tritrivakely, Madagascar, in the southern tropics, Quaternary Res, 49, 299-311, Doi 10.1006/Qres.1998.1967, 1998.

Gommery, D., Ramanivosoa, B., Faure, M., Guerin, C., Kerloc'h, P., Senegas, F., and Randrianantenaina, H.: Oldest evidence of human activities in Madagascar on subfossil hippopotamus bones from Anjohibe (Mahajanga Province), Cr Palevol, 10, 271-278, 10.1016/j.crpv.2011.01.006, 2011.

Gordon, A. L.: Inter-Ocean Exchange of Thermocline Water, J Geophys Res-Oceans, 91, 5037-5046, DOI 10.1029/JC091iC04p05037, 1986.

Haug, G. H., Hughen, K. A., Sigman, D. M., Peterson, L. C., and Rohl, U.: Southward migration of the intertropical convergence zone through the Holocene, Science, 293, 1304-1308, Doi 10.1126/Science.1059725, 2001.

Head, M. J., and Gibbard, P. L.: Formal subdivision of the Quaternary System/Period: Past, present, and future, Quatern Int, 383, 4-35, 10.1016/j.quaint.2015.06.039, 2015.

Holmgren, K., Karlen, W., and Shaw, P. A.: Paleoclimatic Significance of the Stable Isotopic Composition and Petrology of a Late Pleistocene Stalagmite from Botswana, Quaternary Res, 43, 320-328, DOI 10.1006/qres.1995.1038, 1995.

Jungers, W. L., Demes, B., and Godfrey, L. R.: How big were the "Giant" extinct lemurs of Madagascar?, in: Elwyn Simons: A search for origins, edited by: Fleagle, J. G., and Gilbert, C. G., Springer, New York, 343-360, 2008.

Kang, S. M., Held, I. M., Frierson, D. M. W., and Zhao, M.: The response of the ITCZ to extratropical thermal forcing: Idealized slab-ocean experiments with a GCM, J Climate, 21, 3521-3532, 10.1175/2007jcli2146.1, 2008.

Kim, S. T., O'Neil, J. R., Hillaire-Marcel, C., and Mucci, A.: Oxygen isotope fractionation between synthetic aragonite and water: Influence of temperature and Mg2+ concentration, Geochim Cosmochim Ac, 71, 4704-4715, 10.1016/J.Gca.2007.04.019, 2007.

Kleiven, H. F., Kissel, C., Laj, C., Ninnemann, U. S., Richter, T. O., and Cortijo, E.: Reduced North Atlantic Deep Water coeval with the glacial Lake Agassiz freshwater outburst, Science, 319, 60-64, 10.1126/science.1148924, 2008.

Lambert, W. J., and Aharon, P.: Controls on dissolved inorganic carbon and delta C-13 in cave waters from DeSoto Caverns: Implications for speleothem delta C-13 assessments, Geochim Cosmochim Ac, 75, 753-768, 10.1016/j.gca.2010.11.006, 2011.

Liu, Y. H., Henderson, G. M., Hu, C. Y., Mason, A. J., Charnley, N., Johnson, K. R., and Xie, S. C.: Links between the East Asian monsoon and North Atlantic climate during the 8,200 year event, Nat Geosci, 6, 117-120, 10.1038/Ngeo1708, 2013.

Ljungqvist, F. C.: The Spatio-Temporal Pattern of the Mid-Holocene Thermal Maximum, Geografie-Prague, 116, 91-110, 2011.

MacPhee, R. D. E., and Burney, D. A.: Dating of Modified Femora of Extinct Dwarf Hippopotamus from Southern Madagascar - Implications for Constraining Human Colonization and Vertebrate Extinction Events, J Archaeol Sci, 18, 695-706, Doi 10.1016/0305-4403(91)90030-S, 1991.

Marcott, S. A., Shakun, J. D., Clark, P. U., and Mix, A. C.: A Reconstruction of Regional and Global Temperature for the Past 11,300 Years, Science, 339, 1198-1201, 10.1126/science.1228026, 2013.

Matsumoto, K., and Burney, D. A.: Late Holocene environments at Lake Mitsinjo, northwestern Madagascar, The Holocene, 4, 16-24, 1994.

Mayewski, P. A., Rohling, E. E., Stager, J. C., Karlen, W., Maasch, K. A., Meeker, L. D., Meyerson, E. A., Gasse, F., van Kreveld, S., Holmgren, K., Lee-Thorp, J., Rosqvist, G., Rack, F., Staubwasser, M., Schneider, R. R., and Steig, E. J.: Holocene climate variability, Quaternary Res, 62, 243-255, Doi 10.1016/J.Yqres.2004.07.001, 2004.

McGee, D., Donohoe, A., Marshall, J., and Ferreira, D.: Changes in ITCZ location and cross-equatorial heat transport at the Last Glacial Maximum, Heinrich Stadial 1, and the mid-Holocene, Earth Planet Sc Lett, 390, 69-79, 10.1016/J.Epsl.2013.12.043, 2014.

Middleton, J., and Middleton, V.: Karst and caves of Madagascar, Cave and Karst Science, 29, 13-20, 2002.

Murray, J. W.: The deposition of calcite and aragonite in caves., J Geol, 62, 481-492, 1954.

Global Maps: Land Surface Temperature Anomaly.: http://earthobservatory.nasa.gov/GlobalMaps/view.php?d1=MOD_LSTAD_M&d2=TRMM_3B43M, access: August 26th, 2016.

Nassor, A., and Jury, M. R.: Intra-seasonal climate variability of Madagascar. Part 1: Mean summer conditions, Meteorol Atmos Phys, 65, 31-41, Doi 10.1007/Bf01030267, 1998.

Neukom, R., Gergis, J., Karoly, D. J., Wanner, H., Curran, M., Elbert, J., Gonzalez-Rouco, F., Linsley, B. K., Moy, A. D., Mundo, I., Raible, C. C., Steig, E. J., van Ommen, T., Vance, T., Villalba, R., Zinke, J., and Frank, D.: Inter-hemispheric temperature variability over the past millennium, Nat Clim Change, 4, 362-367, 10.1038/Nclimate2174, 2014.

Niggemann, S., Mangini, A., Mudelsee, M., Richter, D. K., and Wurth, G.: Sub-Milankovitch climatic cycles in Holocene stalagmites from Sauerland, Germany, Earth Planet Sc Lett, 216, 539-547, Doi 10.1016/S0012-821x(03)00513-2, 2003.

Ottino, P.: Le Moyen-Age de l'Océan Indien et le peuplement de Madagascar, Ann. Pays l'Océan Ind., 1, 197-221, 1974.

Paul, D., and Skrzypek, G.: Assessment of carbonate-phosphoric acid analytical technique performed using GasBench II in continuous flow isotope ratio mass spectrometry, Int J Mass Spectrom, 262, 180-186, 10.1016/j.ijms.2006.11.006, 2007.

Perrin, C., Prestimonaco, L., Servelle, G., Tilhac, R., Maury, M., and Cabrol, P.: Aragonite–calcite speleothems: identifying original and diagenetic features, J Sediment Res, 84, 245-269, 2014.

Pobeguin, T.: Sur les concrétions calcaires observés dans la Grotte de Moulis (Ariège), Société Géologique de la France, Compte Rendus, 241, 1791-1793, 1965.

Railsback, L.B., 2000. Atlas of speleothem microfabrics. Available at: www.gly.uga.edu/

railsback/speleoatlas/SAindex1.html (Accessed 15 January 2016).

Railsback, L. B., Akers, P. D., Wang, L. X., Holdridge, G. A., and Voarintsoa, N. R.: Layer-bounding surfaces in stalagmites as keys to better paleoclimatological histories and chronologies, International Journal of Speleology, 42, 167-180, 10.5038/1827-806x.42.3.1, 2013.

Railsback, L. B., Brook, G. A., Ellwood, B. B., Liang, F., Cheng, H., and Edwards, R. L.: A record of wet glacial stages and dry interglacial stages over the last 560 kyr from a standing massive stalagmite in Carlsbad Cavern, New Mexico, USA, Palaeogeography, Palaeoclimatology, Palaeoecology, 438, 256-266, 10.1016/j.palaeo.2015.08.010, 2015.

Railsback, L. B., Brook, G. A., Chen, J., Kalin, R., and Fleisher, C. J.: Environmental Controls on the Petrology of a Late Holocene Speleothem from Botswana with annual layers of aragonite and calcite, J Sediment Res A, 64, 147-155, 1994.

Railsback, L. B., Xiao, H. L., Liang, F. Y., Akers, P. D., Brook, G. A., Dennis, W. M., Lanier, T. E., Tan, M., Cheng, H., and Edwards, R. L.: A stalagmite record of abrupt climate change and possible Westerlies-derived atmospheric precipitation during the Penultimate Glacial Maximum in northern China, Palaeogeogr Palaeocl, 393, 30-44, Doi 10.1016/J.Palaeo.2013.10.013, 2014.

Renssen, H., Goosse, H., Crosta, X., and Roche, D. M.: Early Holocene Laurentide Ice Sheet deglaciation causes cooling in the high-latitude Southern Hemisphere through oceanic teleconnection, Paleoceanography, 25, PA3204, doi10.1029/2009pa001854, 2010.

Romanek, C. S., Grossman, E. L., and Morse, J. W.: Carbon Isotopic Fractionation in Synthetic Aragonite and Calcite - Effects of Temperature and Precipitation Rate, Geochim Cosmochim Ac, 56, 419-430, Doi 10.1016/0016-7037(92)90142-6, 1992.

Saint-Ours, J. D.: Les phénomènes karstiques à Madagascar, Annales de Spéléologie, 14, 275-291, 1959.

Schneider, T., Bischoff, T., and Haug, G. H.: Migrations and dynamics of the intertropical convergence zone, Nature, 513, 45-53, 10.1038/Nature13636, 2014.

Scholz, D., and Hoffmann, D. L.: StalAge - An algorithm designed for construction of speleothem age models, Quat Geochronol, 6, 369-382, 10.1016/j.quageo.2011.02.002, 2011.

Scholz, D., Hoffmann, D. L., Hellstrom, J., and Ramsey, C. B.: A comparison of different methods for speleothem age modelling, Quat Geochronol, 14, 94-104, 10.1016/j.quageo.2012.03.015, 2012.

Shtober-Zisu, N., Schwarcz, H. P., Konyer, N., Chow, T., and Noseworthy, M. D.: Macroholes in stalagmites and the search for lost water, J Geophys Res-Earth, 117, F03020, Doi 10.1029/2011jf002288, 2012.

Siegel, F. R.: Aspects of calcium carbonate deposition in Great Onyx Cave, Kentucky, Sedimentology, 4, 285–299, 1965.

Siegel, F. R.: Calcite aragonite speleothems from a hand dug cave in northeast Kansas, International Journal of Speleology 2, 165-169, 1966.

Skrzypek, G., and Paul, D.: Delta C-13 analyses of calcium carbonate: comparison between the GasBench and elemental analyzer techniques, Rapid Commun Mass Sp, 20, 2915-2920, 10.1002/rcm.2688, 2006.

Sletten, H. R., Railsback, L. B., Liang, F. Y., Brook, G. A., Marais, E., Hardt, B. F., Cheng, H., and Edwards, R. L.: A petrographic and geochemical record of climate change over the last 4600 years from a northern Namibia stalagmite, with evidence of abruptly wetter climate at the beginning of southern Africa's Iron Age, Palaeogeogr Palaeocl, 376, 149-162, Doi 10.1016/J.Palaeo.2013.02.030, 2013.

Stommel, H.: The Abyssal Circulation, Deep-Sea Res, 5, 80-82, Doi 10.1016/S0146-6291(58)80014-4, 1958.

Stuiver, M., Reimer, P. J., Bard, E., Beck, J. W., Burr, G. S., Hughen, K. A., Kromer, B., McCormac, G., Van der Plicht, J., and Spurk, M.: INTCAL98 radiocarbon age calibration, 24,000-0 cal BP, Radiocarbon, 40, 1041-1083, 1998.

Talento, S., and Barreiro, M.: Simulated sensitivity of the tropical climate to extratropical thermal forcing: tropical SSTs and African land surface, Clim Dynam, 47, 1091-1110, 10.1007/s00382-015-2890-9, 2016.

Thornalley, D. J. R., Elderfield, H., and McCave, I. N.: Holocene oscillations in temperature and salinity of the surface subpolar North Atlantic, Nature, 457, 711-714, 10.1038/nature07717, 2009.

Thrailkill, J.: Carbonate Deposition in Carlsbad Caverns, J Geol, 79, 683-695, 1971.

Timmermann, A., An, S. I., Krebs, U., and Goosse, H.: ENSO suppression due to weakening of the North Atlantic thermohaline circulationLE, J Climate, 18, 3122-3139, Doi 10.1175/Jcli3495.1, 2005.

Vasey, N., Burney, D. A., and Godfrey, L.: Coprolites associated with Archaeolemur remains in North-western Madagascar suggest dietary diversity and cave use in a subfossil prosimian, in: Leaping Ahead: Advances in Prosimian Biology, edited by: Masters, J., Gamba, M., and Génin, F., Springer, New York, NY, 149–156, 2013.

Vellinga, M., and Wood, R. A.: Global climatic impacts of a collapse of the Atlantic thermohaline circulation, Climatic Change, 54, 251-267, Doi 10.1023/A:1016168827653, 2002.

Vinther, B. M., Buchardt, S. L., Clausen, H. B., Dahl-Jensen, D., Johnsen, S. J., Fisher, D. A., Koerner, R. M., Raynaud, D., Lipenkov, V., Andersen, K. K., Blunier, T., Rasmussen, S. O., Steffensen, J. P., and Svensson, A. M.: Holocene thinning of the Greenland ice sheet, Nature, 461, 385-388, 10.1038/nature08355, 2009.

Virah-Sawmy, M., Willis, K. J., and Gillson, L.: Evidence for drought and forest declines during the recent megafaunal extinctions in Madagascar, Journal of Biogeography, 37, 506-519, Doi 10.1111/J.1365-2699.2009.02203.X, 2010.

Virah-Sawmy, M., Willis, K. J., and Gillson, L.: Threshold response of Madagascar's littoral forest to sea-level rise, Global Ecol Biogeogr, 18, 98-110, 10.1111/j.1466-8238.2008.00429.x, 2009.

Voarintsoa, N. R. G., Brook, G. A., Liang, F., Marais, E., Hardt, B., Cheng, H., Edwards, R. L., and Railsback, L. B.: Stalagmite multi-proxy evidence of wet and dry intervals in

northeastern Namibia: linkage to latitudinal shifts of the Inter-Tropical Convergence Zone and changing solar activity from AD 1400 to 1950, The Holocene, In press, 1-13, doi:10.1177/0959683616660170, 2016.

Voarintsoa, N. R. G., Wang, L., Bruce Railsback, L., Brook, G. A., Liang, F., Cheng, H., and Lawrence Edwards, R.: Multiple proxy analyses of a U/Th-dated stalagmite to reconstruct paleoenvironmental changes in northwestern Madagascar between 370 CE and 1300 CE, Palaeogeography, Palaeoclimatology, Palaeoecology, 469, 138-155, http://dx.doi.org/10.1016/j.palaeo.2017.01.003, 2017.

Walker, M. J. C., Berkelhammer, M., Bjorck, S., Cwynar, L. C., Fisher, D. A., Long, A. J., Lowe, J. J., Newnham, R. M., Rasmussen, S. O., and Weiss, H.: Formal subdivision of the Holocene Series/Epoch: a Discussion Paper by a Working Group of INTIMATE (Integration of ice-core, marine and terrestrial records) and the Subcommission on Quaternary Stratigraphy (International Commission on Stratigraphy), J Quaternary Sci, 27, 649-659, 10.1002/jqs.2565, 2012.

Wang, L., 2016. Late Quaternary paleoenvironmental changes in Southern Africa and Madagascar: evidence from aeolian, fluvial, and cave deposits. Unpublished dissertation. University of Georgia. 312p.

Wang, L. and Brook, G. A. 2013. Holocene climate changes in northwest Madagascar: evidence from a two-meter-long stalagmite from the Anjohibe Cave, Meeting Program of the Association of American Geographers, published online. Session 1512: Paleorecords of our Changing Earth I: Climate History and Human-Environment Interaction in the Old and New World Tropics, 2013.

Wang, Y. J., Cheng, H., Edwards, R. L., He, Y. Q., Kong, X. G., An, Z. S., Wu, J. Y., Kelly, M. J., Dykoski, C. A., and Li, X. D.: The Holocene Asian monsoon: Links to solar changes and North Atlantic climate, Science, 308, 854-857, 10.1126/science.1106296, 2005.

Wanner, H., and Ritz, S. P.: A web-based Holocene Climate Atlas (HOCLAT): http://www.oeschger.unibe.ch/research/projects/holocene_atlas/, 2011.

Wanner, H., Beer, J., Butikofer, J., Crowley, T. J., Cubasch, U., Fluckiger, J., Goosse, H., Grosjean, M., Joos, F., Kaplan, J. O., Kuttel, M., Muller, S. A., Prentice, I. C., Solomina, O., Stocker, T. F., Tarasov, P., Wagner, M., and Widmann, M.: Mid- to Late Holocene climate change: an overview, Quaternary Sci Rev, 27, 1791-1828, 10.1016/j.quascirev.2008.06.013, 2008.

Wanner, H., Mercolli, L., Grosjean, M., and Ritz, S. P.: Holocene climate variability and change; a data-based review, J Geol Soc London, 172, 254-263, 10.1144/jgs2013-101, 2015.

Wanner, H., Solomina, O., Grosjean, M., Ritz, S. P., and Jetel, M.: Structure and origin of Holocene cold events, Quaternary Sci Rev, 30, 3109-3123, 10.1016/j.quascirev.2011.07.010, 2011.

Weaver, A. J., Bitz, C. M., Fanning, A. F., and Holland, M. M.: Thermohaline circulation: High-latitude phenomena and the difference between the Pacific and Atlantic, Annual Review of Earth and Planetary Sciences, 27, 231-285, DOI 10.1146/annurev.earth.27.1.231, 1999.

Wiersma, A. P., Roche, D. M., and Renssen, H.: Fingerprinting the 8.2 ka event climate response in a coupled climate model, J Quaternary Sci, 26, 118-127, 10.1002/jqs.1439, 2011.

Zhang, R., and Delworth, T. L.: Simulated tropical response to a substantial weakening of the Atlantic thermohaline circulation, J Climate, 18, 1853-1860, Doi 10.1175/Jcli3460.1, 2005.

# CHAPTER 5

# CONCLUSION

## 5.1. Importance of using the stalagmite multiple proxy approach

The research compiled in this dissertation thesis has been an investigation of past climate and vegetation changes in northeastern Namibia and northwestern Madagascar using multiple proxies ($\delta^{18}O$, $\delta^{13}C$, mineralogy, petrography, layer-specific width, macro-cavities distributions) from stalagmites. Stalagmites form when cave dripwater is supersaturated with $Ca^{2+}$ and $CO_3^{2-}$ and degasses $CO_2$ to precipitate $CaCO_3$. The precipitated carbonate preserves various signatures that reflect environmental conditions at the time of stalagmite deposition. These conditions can be seasonal, decadal, or they can represent long-term changes in climate (centennial, millennial). This multiple proxy approach has allowed us to check our interpretations across a range of chemical and physical systems to better understand the climatic regimes in the study area. Cave deposits could bring new insights on the possible changes of climate in the recent past, enabling better predictions of climate changes in the near future.

## 5.2. Implications for climate reconstruction

Although it has been known from paleoclimatological analyses (Koutavas and Lynch-Stieglitz, 2004; Russell and Johnson, 2007; Brown and Johnson, 2005; Sinha et al., 2011; Leech et al., 2013) and modeling studies (Broccoli et al., 2006; Chiang et al. 2003; Chiang and Bitz, 2005; Kang et al., 2008; Frierson and Hwang, 2012; Donohoe et al., 2013; McGee et al., 2014) that the latitudinal migration of the ITCZ could significantly influence the rainfall regimes in the tropics, additional data are needed to refine the spatial resolution. This research has allowed us to bring additional paleoclimate information to assess and refine our understanding of the dynamics of the ITCZ through time in the Southern Hemisphere. From our paleoclimatological reconstruction, the data suggest wet/dry conditions in northeastern Namibia (Chapter 2; Voarintsoa et al., 2016) and northwestern Madagascar (Chapter 3; Voarintsoa et al., accepted; Chapter 4; Voarintsoa et al., submitted), when the ITCZ is at its southward/northward position. This latitudinal migration is mainly driven by insolation and high temperature gradient between the two hemispheres. A southward migration of the ITCZ was also identified during the prominent 8.2 ka cold event. During this interval, the Atlantic Meridional Overturning Circulation (AMOC) weakened, and consequently, this intensified the temperature gradient between the NH (cold) and the SH (warm), pushing the ITCZ southward. This led to wet conditions in Madagascar, as suggested by the stalagmite multiple proxies.

Multiple proxy records from northwestern Madagascar have also improved our understanding in deciphering the difference between anthropogenic influence and climatic influence on landscape transformation (mainly discussed in Chapter 3; Voarintsoa

et al., accepted). Evidence has mainly been captured in stalagmites as a shift in $\delta^{13}C$. A more comprehensive paleoenvironmental reconstruction of the region has been helped by other proxies, such as $\delta^{18}O$, mineralogy, and petrographic features, and a thorough literature review of the region's archaeological evidence.

## 5.3. Research highlights

In Chapter 2, a multi-proxy approach using U-Th dating, $\delta^{18}O$, $\delta^{13}C$, mineralogy, and petrography from Stalagmite DP1 in Dante Cave, Namibia, revealed linkages to climate. These records suggest that wet and dry intervals in northeastern Namibia were linked to latitudinal shifts of the Inter-Tropical Convergence Zone (ITCZ) and changing solar activity from AD 1400 to 1950 (Voarintsoa et al., 2016, *The Holocene*).

In Chapter 3, stable isotopes of oxygen, variation in mineralogy, changes in the sample's layer-specific width, and macroholes (large cavities) distribution in Stalagmite MA3 from Anjohibe Cave also have helped understand in much detail the paleo-hydrology in northwestern Madagascar during the late-Holocene (Voarintsoa et al., 2017). Stable isotopes of carbon further suggest a linkage to landscape changes in the same study area. A significant shift in the stalagmite $\delta^{13}C$ since ca. AD 800 and a weak correlation between $\delta^{13}C$ and $\delta^{18}O$ ($r^2$= 0.05) were identified; whereas prior to that time, $\delta^{13}C$ does not change in trend and it shows better correlation with $\delta^{18}O$ ($r^2$=0.44). This multi-proxy analysis of stalagmites from Anjohibe Cave indicates a climatically-induced vegetation change prior to ca. AD 800 and a non-climatically-induced vegetation change thereafter. The timing of this $\delta^{13}C$ shift seems to coincide with increased land use, mainly the practice of "Tavy", a variety

of swidden agricultures, in Madagascar. This could be an additional evidence of human presence besides geological, archeological, and anthropological archives.

In Chapter 4, mineralogy, petrography, and stable isotopes have revealed three distinct intervals of the Holocene climate in northwestern Madagascar. They are named the Malagasy Early Holocene Interval (MEHI), the Malagasy Middle Holocene Interval (MMHI), and the Malagasy Late Holocene Interval (MLHI). The proxies suggest that the MMHI was relatively drier compared to the MEHI and MLHI. The 8.2 ka cold event is also identified in the records as an interval of wet conditions. This climate variability throughout the Holocene suggests a linkage between climate in northwestern Madagascar and the latitudinal migration of the ITCZ, which itself has moved in response to changes in solar insolation, interhemispheric difference in temperature, and changes in the Atlantic Meridional Ocean Circulation (AMOC).

## 5.4. Envisioning future work

The main motivation in undertaking studies on paleoclimate reconstruction is to be able to better understand the global climate system at different scales over time, and use such information as keys to predict the likely changes in the future. The 8.2 ka event is, for example, an ideal interval to test for climate models, and information from such test could be used for future climate prediction (e.g. Alley and Ágústsdóttir, 2005; Wiersma and Renssen, 2006; Tindall and Valdes, 2011; Holmes et al., 2016; Daley et al., 2011). Climate simulations, predictions, and reconstructions are better with higher resolution data. In the paleoclimatological standpoint, higher resolution data rely on the spatial distribution of

samples and on the temporal resolution of the samples being analyzed. The completed research for this dissertation presents an opportunity to continue research on paleoclimatology. The spatial distribution of paleoclimate records, particularly long-term records, is still limited, and some of the records themselves are still low in resolution.

## REFERENCES


Alley, R.B., Ágústsdóttir, A.M., 2005. The 8 k event: cause and consequences of a major Holocene abrupt climate change. Quaternary Science Reviews 24 (10–11), 1123–1149.

Broccoli, A. J., Dahl, K. A., and Stouffer, R. J., 2006, Response of the ITCZ to Northern Hemisphere cooling: Geophysical Research Letters, v. 33, no. 1.

Brown, E. T., and Johnson, T. C., 2005, Coherence between tropical East African and South American records of the Little Ice Age: Geochemistry Geophysics Geosystems, v. 6.

Chiang, J. C. H., and Bitz, C. M., 2005, Influence of high latitude ice cover on the marine Intertropical Convergence Zone: Climate Dynamics, v. 25, no. 5, p. 477-496.

Chiang, J. C. H., Biasutti, M., and Battisti, D. S., 2003, Sensitivity of the Atlantic Intertropical Convergence Zone to Last Glacial Maximum boundary conditions: Paleoceanography, v. 18, no. 4.

Daley, T.J., Thomas, E.R., Holmes, J.A., Street-Perrott, F.A., Chapman, M.R., Tindall, J.C., Valdes, P.J., Loader, N.J., Marshall, J.D., Wolff, E.W., Hopley, P.J., Atkinson, T., Barber, K.E., Fisher, E.H., Robertson, I., Hughes, P.D.M., Roberts, C.N., 2011. The 8200 yr BP cold event in stable isotope records from the north Atlantic region. Glob. Planet. Change 79, 288–302.

Donohoe, A., Marshall, J., Ferreira, D., McGee, D., 2013. The relationship between ITCZ location and cross equatorial atmospheric heat transport; from the sea- sonal cycle to the last glacial maximum. J. Climate 26, 3597–3618.

Frierson, D.M.W., Hwang, Y.T., 2012. Extratropical influence on ITCZ shifts in slab ocean simulations of global warming. J. Climate 25, 720–733.

Holmes, J. A., Tindall, J., Roberts, N., Marshall, W., Marshall, J. D., Bingham, A., Feeser, I., O'Connell, M., Atkinson, T., Jourdan, A.-L., March, A., and Fisher, E. H., 2016, Lake isotope records of the 8200-year cooling event in western Ireland: Comparison with model simulations: Quaternary Science Reviews, v. 131, Part B, p. 341-349.

Kang, S. M., Held, I. M., Frierson, D. M. W., and Zhao, M., 2008, The response of the ITCZ to extratropical thermal forcing: Idealized slab-ocean experiments with a GCM: Journal of Climate, v. 21, no. 14, p. 3521-3532.

Koutavas, A., and Lynch-Stieglitz, J., 2004, Variability of the marine ITCZ over the eastern Pacific during the past 30,000 years - Regional perspective and global context: Hadley Circulation: Present, Past and Future, v. 21, p. 347-369.

Leech, P. J., Lynch-Stieglitz, J., and Zhang, R., 2013, Western Pacific thermocline structure and the Pacific marine Intertropical Convergence Zone during the Last Glacial Maximum: Earth and Planetary Science Letters, v. 363, p. 133-143.

McGee, D., Donohoe, A., Marshall, J., and Ferreira, D., 2014, Changes in ITCZ location and cross-equatorial heat transport at the Last Glacial Maximum, Heinrich Stadial 1, and the mid-Holocene: Earth and Planetary Science Letters, v. 390, p. 69-79.

Russell, J. M., and Johnson, T. C., 2007, Little Ice Age drought in equatorial Africa: Intertropical Convergence Zone migrations and El Nino-Southern Oscillation variability: Geology, v. 35, no. 1, p. 21-24.

Sinha, A., Stott, L., Berkelhammer, M., Cheng, H., Edwards, R. L., Buckley, B., Aldenderfer, M., and Mudelsee, M., 2011, A global context for megadroughts in monsoon Asia during the past millennium: Quaternary Science Reviews, v. 30, no. 1-2, p. 47-62.

Tindall, J.C., Valdes, P.J., 2011. Modeling the 8.2 ka event using a coupled atmosphere-ocean GCM. Glob. Planet. Change 79, 312–321.

Voarintsoa, N. R. G., Brook, G. A., Liang, F., Marais, E., Hardt, B., Cheng, H., Edwards, R. L., and Railsback, L. B., 2016, Stalagmite multi-proxy evidence of wet and dry intervals in northeastern Namibia: linkage to latitudinal shifts of the Inter-Tropical Convergence Zone and changing solar activity from AD 1400 to 1950: The Holocene, v. In press, p. 1-13.

Voarintsoa, N.R. G., Wang, L., Railsback, L.B., Brook, G.A., Liang, F., Cheng, H., Edwards, R.L., (accepted), Multiple proxy analyses of a U/Th-dated stalagmite to reconstruct paleoenvironmental changes in northwestern Madagascar between AD 370 and AD 1300 Palaeogeography, Palaeoclimatology, Palaeoecology. Doi: 10.1016/j.palaeo.2017.01.003.

Wiersma, A.P., Renssen, H., 2006. Model-data comparison for the 8.2 ka BP event: confirmation of a forcing mechanism by catastrophic drainage of Laurentide Lakes. Quaternary Science Reviews 25 (1–2), 63–88.

# APPENDIX A

# SUPPLEMENTARY MATERIALS FOR CHAPTER 2

# "STALAGMITE MULTI-PROXY EVIDENCE OF WET AND DRY INTERVALS IN NORTHEASTERN NAMIBIA: LINKAGE TO LATITUDINAL SHIFTS OF THE INTER-TROPICAL CONVERGENCE ZONE AND CHANGING SOLAR ACTIVITY FROM AD 1400 TO 1950"

## Statistical testing

A test of the strength of the relationship between $\delta^{13}C$ and $\delta^{18}O$ values from Stalagmite DP1 using the parametric Pearson correlation coefficient was performed to evaluate the relationship between vegetation/soil biomass activity and precipitation in Dante Cave. The mathematical form of the correlation was expressed using the Major Axis (MA) of the Model II Regression. Analysis using MA produces unbiased slope estimates and accurate confidence intervals (Jolicoeur, 1990) and it assumes a bivariate normal distribution of the data. The DP1 data were log-transformed because they are right-skewed. These data are also random walks, so a data differencing for all variables were performed. This Model II Regression computes a parametric 95% confidence interval for the slope and intercept parameters; and statistical significance of the slopes and correlation coefficient is determined by a permutation test (Legendre, in mod2user of the lmodel2 package in R).

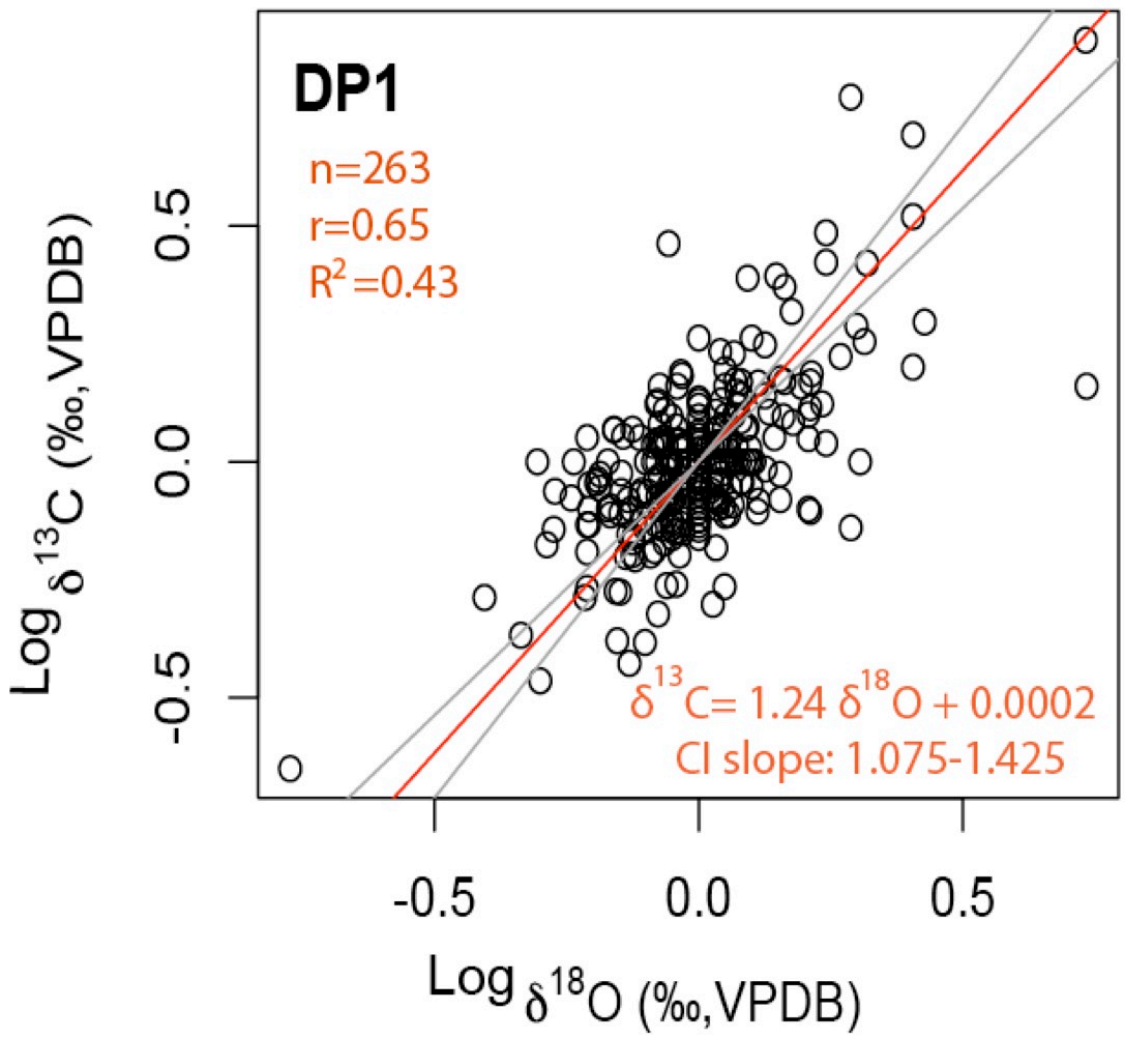


Figure A1. Major axis regression plot run on $\delta^{13}C$ and $\delta^{18}O$ of stalagmite DP1.

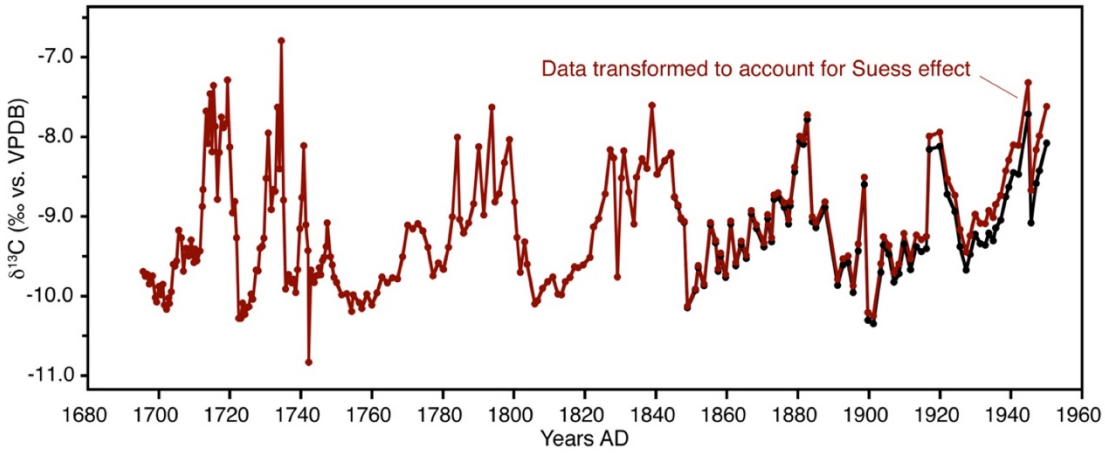


**Figure A2**. Variation in $\delta^{13}C$ in the DP1 record from 1695 to 1950. Black symbols show data transformed to account for aragonite's greater fractionation of $^{13}C$ relative to calcite; red symbols show the data additionally transformed to account for the Suess effect using the equation of Verburg (2007). $r^2 = 0.02$ for the untransformed data, and $r^2 = 0.05$ for data transformed to correct for the Suess effect.

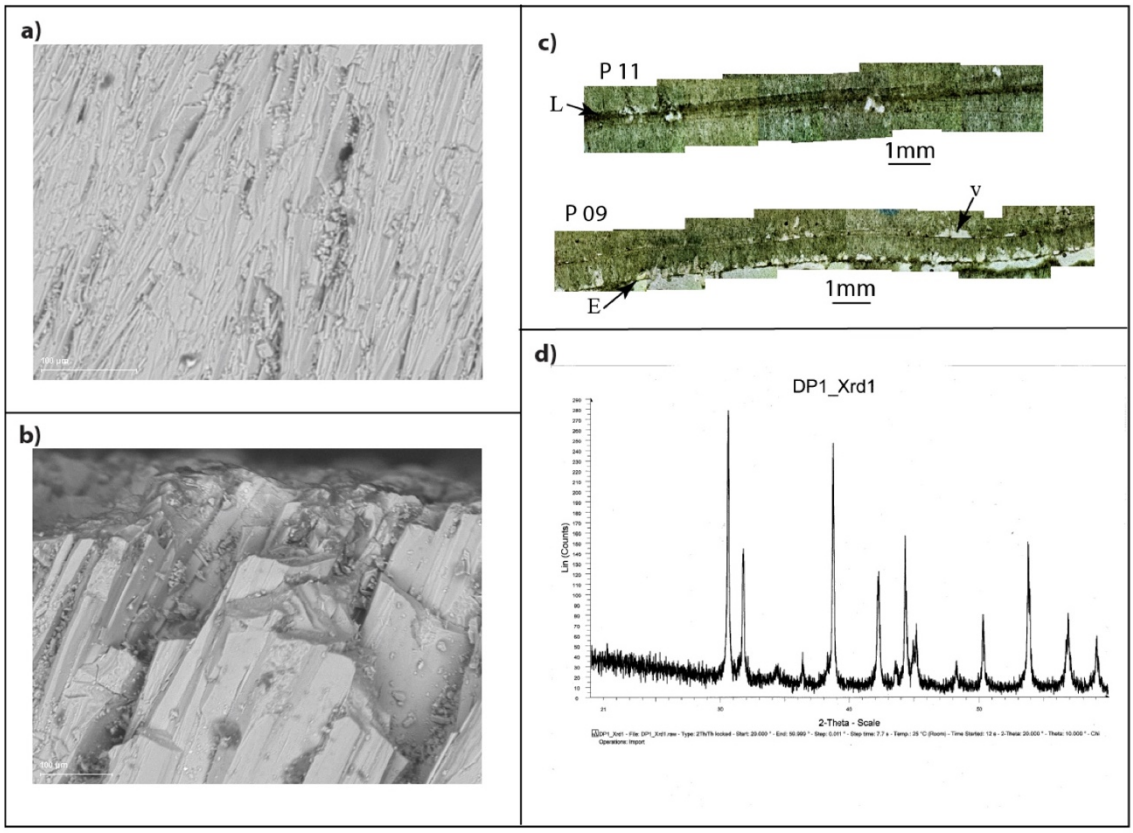


Figure A3. a) SEM image of typical aragonite at c. 255 mm from the top of Stalagmite DP1. b) SEM image of the unusual aragonite found 237 to 250 mm from the top of Stalagmite DP1, marked with "A*" in Figure 3b. c) Two microphotographs of selected major layer-bounding surfaces observed in stalagmite DP1 (refer to Figure 3b). L and E denote Type L (less deposition) and Type E (erosional) surfaces respectively in accord with the description of Railsback et al. (2013); v denotes voids, which are typical features associated with Type E surfaces. d) X-ray diffraction plot of the unusual layer of aragonite denoted A*in Figure 3b.

## REFERENCES

Jolicoeur P. (1990) Bivariate Allometry - Interval Estimation of the Slopes of the Ordinary and Standardized Normal Major Axes and Structural Relationship. Journal of Theoretical Biology 144: 275-285.

Verburg P (2007) The need to correct for the Suess effect in the application of d13C in sediment in autotrophic Lake Tanganyika, as a productivity proxy in the Anthropocene. Journal of Paleolimnology 37: 591–602.

Railsback LB, Akers PD, Wang L., et al. (2013) Layer-bounding surfaces in stalagmites as keys to better paleoclimatological histories and chronologies. International Journal of Speleology 42: 167-180.

# APPENDIX B

## SUPPLEMENTARY MATERIALS FOR CHAPTER 3

## "MULTIPLE PROXY ANALYSES OF A U/TH-DATED STALAGMITE TO RECONSTRUCT PALEOENVIRONMENTAL CHANGES IN NORTHWESTERN MADAGASCAR BETWEEN 370 CE AND 1300 CE"


**Figure B1**: Google Earth image showing the relevant archaeological and paleoenvironmental described in this study.

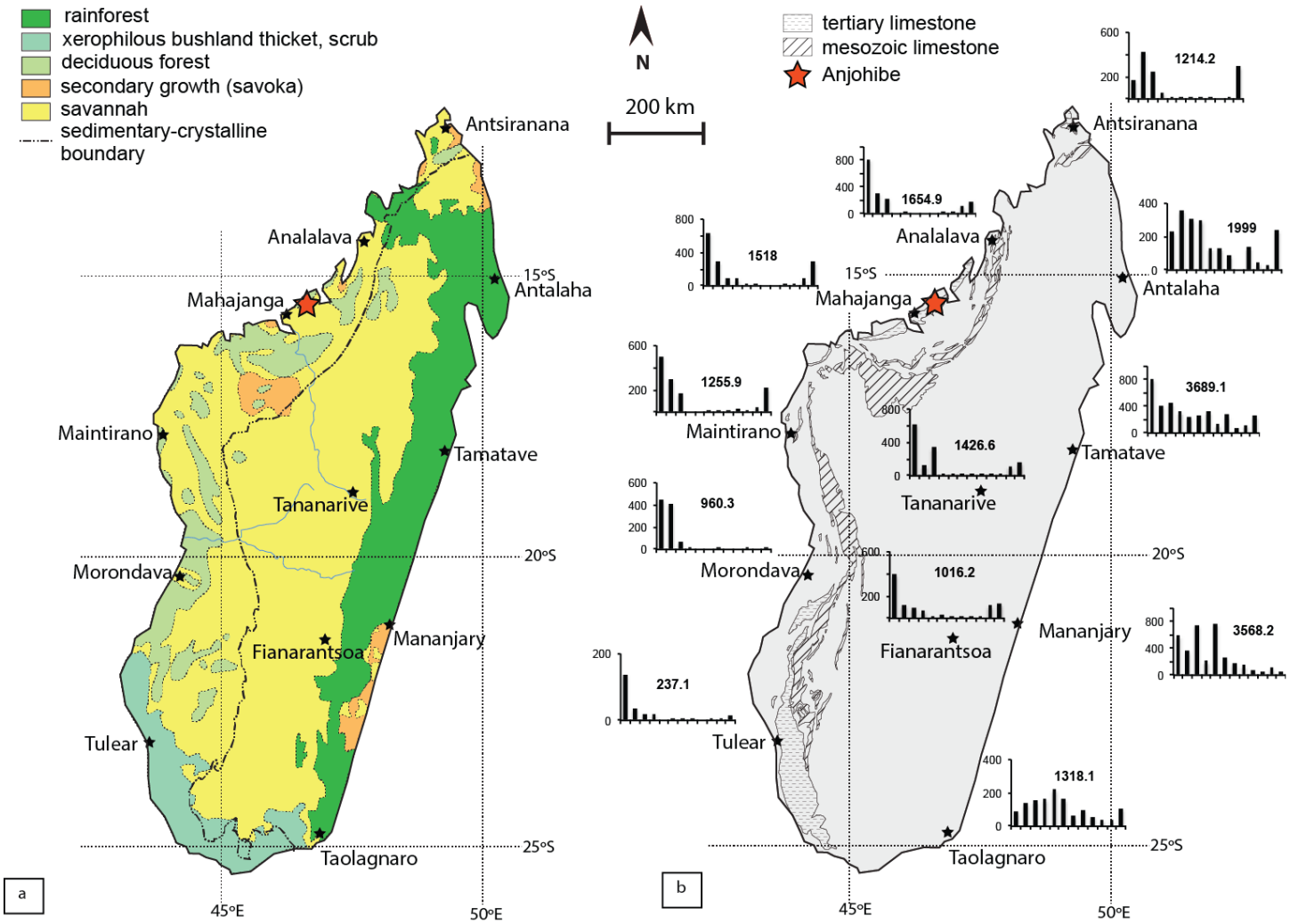
rainforest
xerophilous bushland thicket, scrub
deciduous forest
secondary growth (savoka)
savannah
sedimentary-crystalline boundary
Antsiranana
Analalava
Mahajanga
Antalaha
Maintirano
Tamatave
Tananarive
Morondava
Fianarantsoa
Mananjary
Tulear
Taolagnaro
15°S
20°S
25°S
45°E
50°E
a
N
200 km
tertiary limestone
mesozoic limestone
Anjohibe
1214.2
1654.9
1518
1999
1255.9
3689.1
1426.6
960.3
1016.2
3568.2
237.1
1318.1
b

Figure B2: General map showing (a) vegetation distribution (modified from MacPhee, 1986) and (b) limestone (Collins and Windley, 2002) and regional rainfall distribution (source: Direction Générale de la Météorologie, Madagascar) in Madagascar. Rainfall values are given in millimeter, the histograms represent monthly rainfall from January (left) to December (right), and the number above the bars represent the total annual rainfall (in mm) received in 2003 per region. For more up-to-date and detailed vegetation map, see DuPuy and Moat (1996, 2003) and the modern Landsat image of NASA using Google Earth.

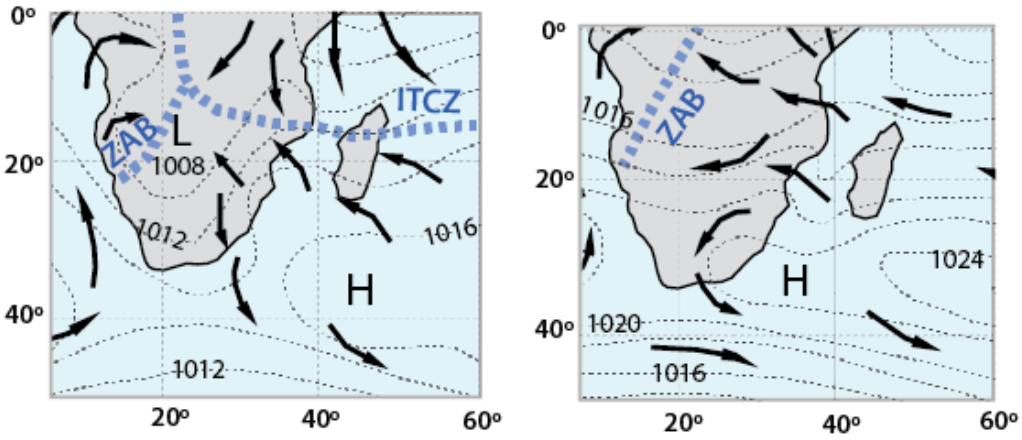


**Figure B3**: Schematic illustration of the mean wind convergence and positions of the ITCZ relative to Madagascar during mid-summer (January, left) and mid-winter (July, right), ZAB is the Zaire Air Boundary, another type of convergence identified in southern Africa. This illustration is a section modified from Fig. 2.3 of Lindesay (1998).

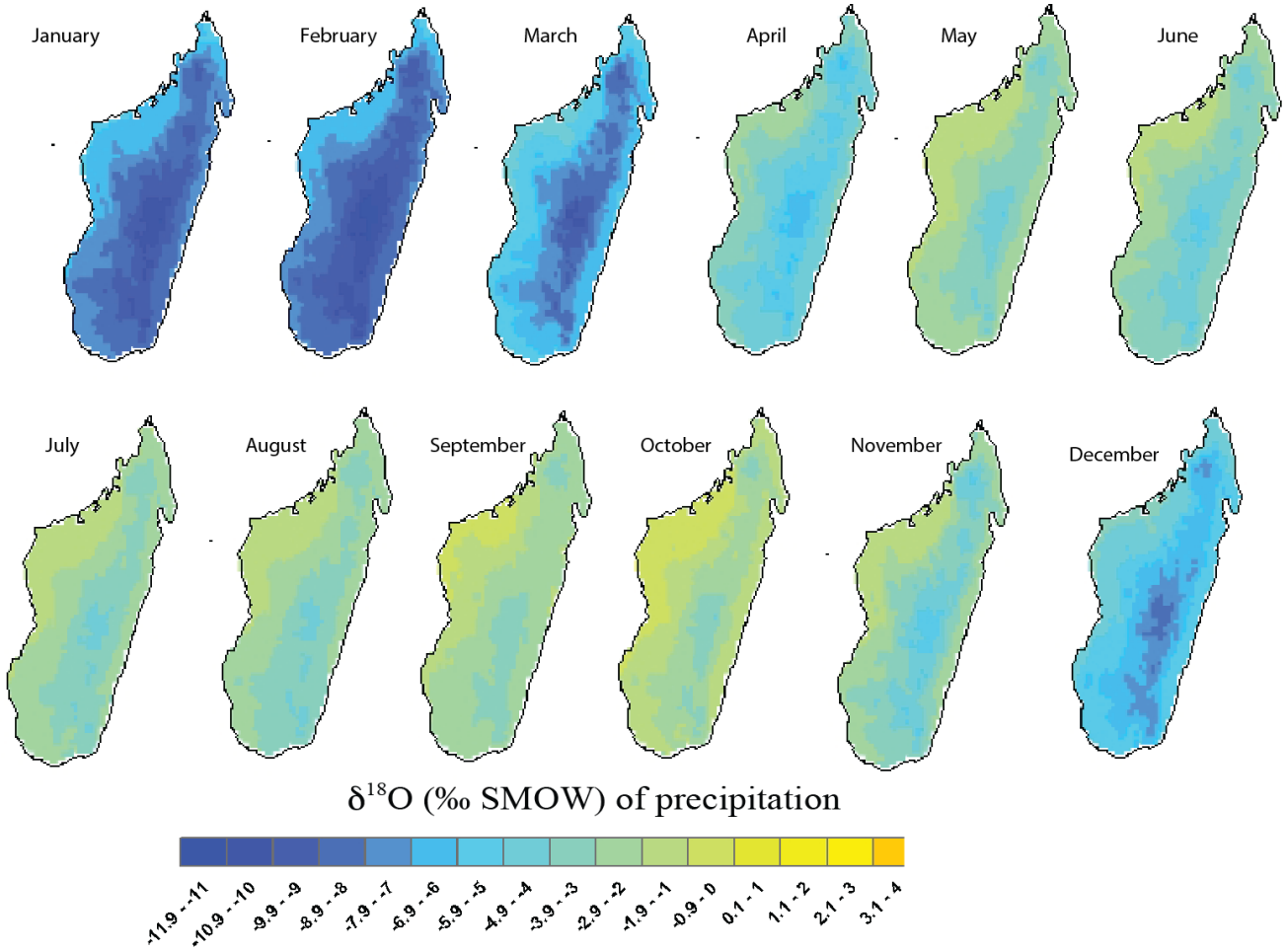
January
February
March
April
May
June
July
August
September
October
November
December
δ18O (‰ SMOW) of precipitation
-11.9 - -11
-10.9 - -10
-9.9 - -9
-8.9 - -8
-7.9 - -7
-6.9 - -6
-5.9 - -5
-4.9 - -4
-3.9 - -3
-2.9 - -2
-1.9 - -1
-0.9 - 0
0.1 - 1
1.1 - 2
2.1 - 3
3.1 - 4

**Figure B4**: Seasonal variability of $\delta^{18}O$ of rainfall in Madagascar from the extrapolation model of Bowen (2013). This series of maps suggests that (1) the rainiest region in Madagascar (eastern) has more negative $\delta^{18}O$ and (2) summer months are characterized by more negative $\delta^{18}O$ in all regions of Madagascar.

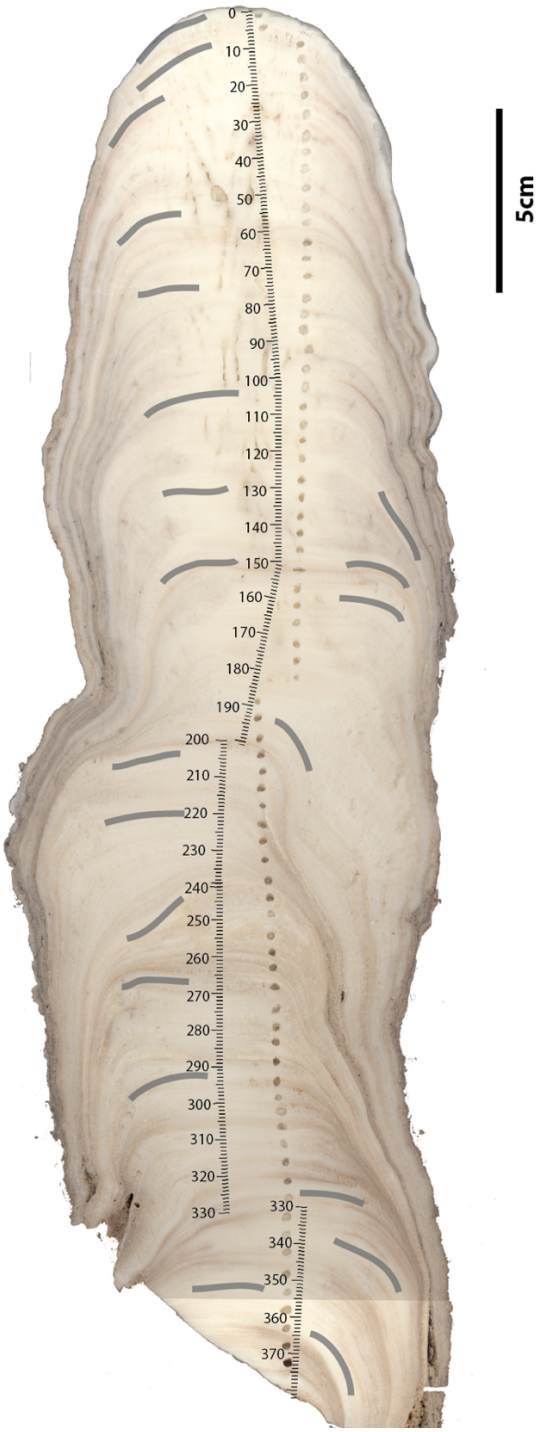


Figure B5: Indexed photograph of Stalagmite MA3, showing the trenches for radiometric analysis and the trenches for isotopic analysis.

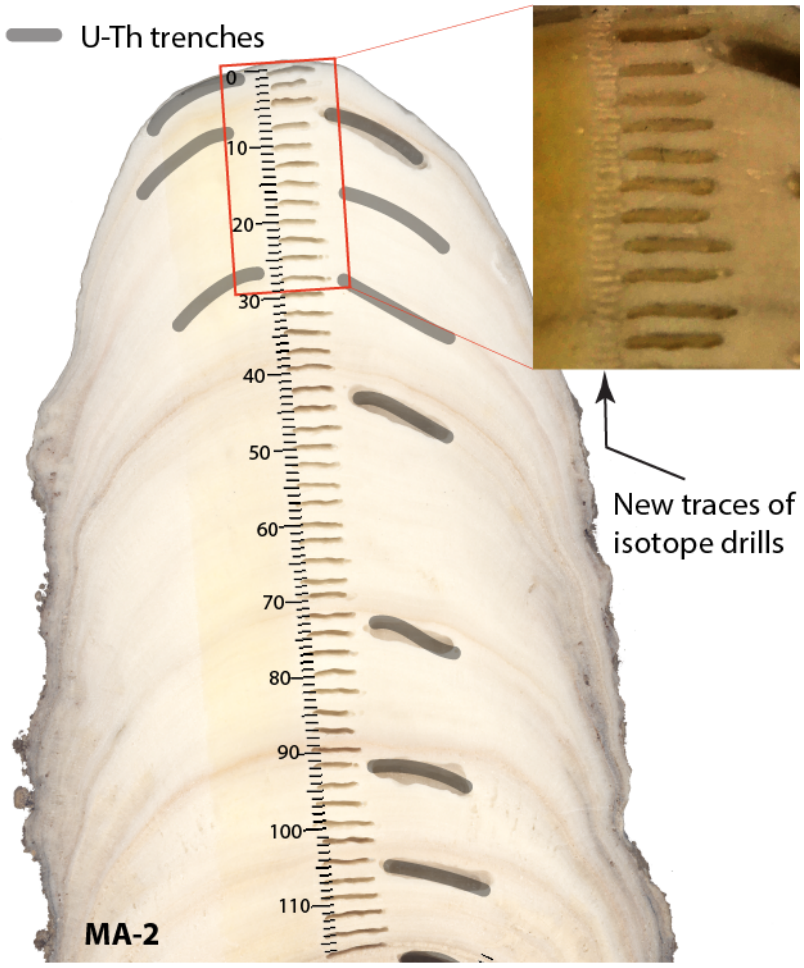


Figure B6: Indexed photograph of Stalagmite MA2, showing the trenches for radiometric analysis and the trenches for isotopic analysis. A close-up of the section highlighted in red square is shown to the right to highlight the new millimeter interval sampling of stable isotopes.

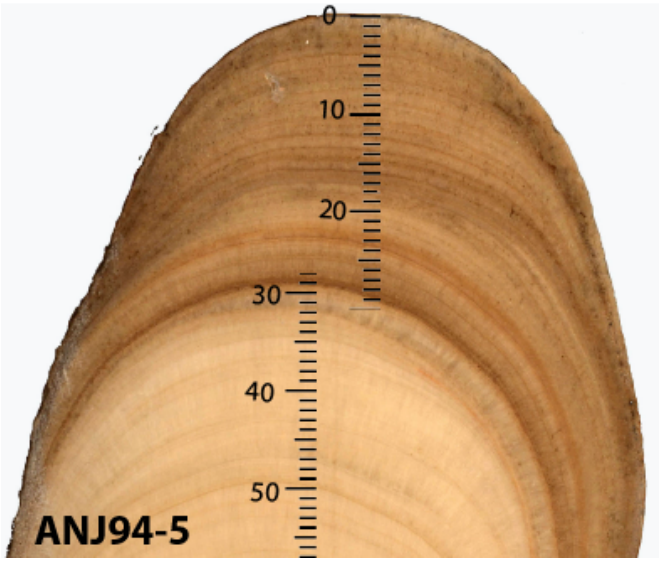


**Figure B7:** Indexed photograph of the upper 57 mm of Stalagmite ANJ94-5. This image was the half of the stalagmite kept for reference. Sample powders for U-series dating and stable isotopes were taken from the quarter of the other half of the stalagmite. This upper 57 mm of Stalagmite ANJ94-5 is composed of aragonite.

**Table B1**: $^{230}$Th dating results, with 2σ error. Samples indicated by √ are considered in the age model (see Section 3.4.2 for explanation)

| mm | Sample No. | 238U (ppb) | | 232Th (ppt) | | 230Th / 232Th (atomic x10-6) | | d234U* (measured) | | 230Th / 238U (activity) | | 230Th Age (year) (uncorrected) | | 230Th Age (year) (corrected) | | d234UInitial** (corrected) | | 230Th Age (year BP) *** (corrected) | | |
|---|---|---|---|---|---|---|---|---|---|---|---|---|---|---|---|---|---|---|---|---|
| 0 | MA3-U1 | 424.2 | ±0.7 | 3735 | ±75 | 12 | ±1 | 10.1 | ±2.3 | 0.0065 | ±0.0006 | 704 | ±66 | 450 | ±191 | 10 | ±2 | 388 | ±191 | |
| 8 | MA-3-U008 | 89 | ±0 | 292 | ±6 | 48 | ±7 | 3.9 | ±1.6 | 0.0096 | ±0.0014 | 1048 | ±155 | 952 | ±169 | 4 | ±2 | 888 | ±169 | |
| 12 | MA3-U2 | 94.4 | ±0.1 | 2354 | ±47 | 14 | ±1 | 6.3 | ±2.1 | 0.0216 | ±0.0006 | 2363 | ±69 | 1640 | ±516 | 6 | ±2 | 1578 | ±516 | |
| 53 | MA3-U3 | 105.3 | ±0.2 | 1957 | ±39 | 17 | ±1 | 6.3 | ±2.2 | 0.0192 | ±0.0006 | 2101 | ±66 | 1562 | ±387 | 6 | ±2 | 1500 | ±387 | |
| 75 | MA-3-U075 | 102 | ±0 | 372 | ±8 | 41 | ±2 | 4.7 | ±1.6 | 0.0090 | ±0.0005 | 980 | ±55 | 874 | ±93 | 5 | ±2 | 810 | ±93 | √ |
| 102 | MA3-U4 | 107.3 | ±0.2 | 667 | ±13 | 31 | ±2 | 3.5 | ±2.3 | 0.0117 | ±0.0005 | 1282 | ±57 | 1102 | ±140 | 3 | ±2 | 1040 | ±140 | |
| 121 | MA3-U5 | 111.3 | ±0.2 | 1325 | ±27 | 24 | ±1 | 5.0 | ±2.2 | 0.0176 | ±0.0005 | 1932 | ±56 | 1587 | ±250 | 5 | ±2 | 1525 | ±250 | |
| 127 | MA-3-U127 | 111 | ±0 | 130 | ±3 | 118 | ±6 | 5.1 | ±2.0 | 0.0084 | ±0.0004 | 912 | ±42 | 878 | ±48 | 5 | ±2 | 814 | ±48 | √ |
| 148.6 | MA3-U6 | 113.0 | ±0.2 | 1070 | ±22 | 29 | ±1 | 5.2 | ±2.3 | 0.0169 | ±0.0005 | 1852 | ±58 | 1578 | ±203 | 5 | ±2 | 1516 | ±203 | |
| 150 | MA-3-U150 | 110 | ±0 | 177 | ±4 | 104 | ±5 | 4.6 | ±1.7 | 0.0101 | ±0.0004 | 1101 | ±49 | 1054 | ±59 | 5 | ±2 | 990 | ±59 | √ |
| 160 | MA-3-U160 | 108 | ±0 | 328 | ±7 | 61 | ±3 | 5.8 | ±2.9 | 0.0113 | ±0.0004 | 1228 | ±49 | 1140 | ±79 | 6 | ±3 | 1076 | ±79 | √ |
| 193 | MA3-U7 | 119.3 | ±0.2 | 254 | ±5 | 80 | ±4 | 2.4 | ±2.3 | 0.0103 | ±0.0005 | 1127 | ±50 | 1065 | ±67 | 2 | ±2 | 1003 | ±67 | √ |
| 201 | MA3-U8 | 119.8 | ±0.2 | 841 | ±17 | 29 | ±1 | 5.2 | ±2.3 | 0.0124 | ±0.0004 | 1355 | ±50 | 1152 | ±152 | 5 | ±2 | 1090 | ±152 | √ |
| 220 | MA-3-U220 | 104 | ±0 | 215 | ±4 | 100 | ±4 | 4.3 | ±2.7 | 0.0125 | ±0.0005 | 1367 | ±51 | 1307 | ±66 | 4 | ±3 | 1243 | ±66 | √ |
| 235.7 | MA3-U9 | 159.0 | ±0.3 | 1163 | ±23 | 30 | ±1 | 6.0 | ±2.6 | 0.0133 | ±0.0003 | 1457 | ±38 | 1245 | ±155 | 6 | ±3 | 1183 | ±155 | |
| 266 | MA3-U10 | 536.4 | ±1.4 | 3131 | ±63 | 37 | ±1 | 2.3 | ±2.1 | 0.0129 | ±0.0001 | 1417 | ±14 | 1248 | ±121 | 2 | ±2 | 1186 | ±121 | |
| 290 | MA3-U11 | 190.6 | ±0.3 | 1418 | ±28 | 31 | ±1 | 7.0 | ±2.0 | 0.0141 | ±0.0003 | 1540 | ±35 | 1325 | ±156 | 7 | ±2 | 1263 | ±156 | √ |
| 324 | MA3-U12 | 130.8 | ±0.2 | 1537 | ±31 | 24 | ±1 | 4.1 | ±2.0 | 0.0169 | ±0.0005 | 1856 | ±57 | 1515 | ±248 | 4 | ±2 | 1453 | ±248 | √ |
| 336 | MA-3-U336 | 140 | ±0 | 3900 | ±78 | 15 | ±0 | 4.8 | ±2.6 | 0.0260 | ±0.0004 | 2859 | ±47 | 2050 | ±574 | 5 | ±3 | 1986 | ±574 | |
| 354 | MA3-U354 | 150 | ±0 | 798 | ±16 | 49 | ±2 | 5.5 | ±1.5 | 0.0157 | ±0.0007 | 1715 | ±78 | 1561 | ±133 | 6 | ±2 | 1497 | ±133 | √ |
| 364 | MA3-U13 | 179.3 | ±0.3 | 10907 | ±219 | 21 | ±0 | 6.4 | ±1.8 | 0.0775 | ±0.0005 | 8738 | ±57 | 6965 | ±1255 | 6 | ±2 | 6903 | ±1255 | |

U decay constants: $\lambda_{238}$ = 1.55125x10$^{-10}$ (Jaffey et al., 1971) and $\lambda_{234}$ = 2.82206x10$^{-6}$ (Cheng et al., 2013). Th decay constant: $\lambda_{230}$ = 9.1705x10$^{-6}$ (Cheng et al., 2013).

*$\delta^{234}U$ = ([$^{234}U/^{238}U$] activity – 1) x1000.

** $\delta^{234}U_{initial}$ was calculated based on $^{230}Th$ age (T), i.e., $\delta^{234}U_{initial} = \delta^{234}U_{measured}$ x e$\lambda^{234xT}$.

Corrected $^{230}Th$ ages assume the initial $^{230}Th/^{232}Th$ atomic ratio of 4.4 ±2.2 x10-6. Those are the values for a material at secular equilibrium, with the bulk earth $^{232}Th/^{238}U$ value of 3.8. The errors are arbitrarily assumed to be 50%.

***B.P. stands for “Before Present” where the “Present” is defined as the year 1950 A.D.

**Table B2:** $^{230}$Th dating results of ANJ94-5, with 2σ error. Samples indicated by √ are considered in the age model

| | | Distance from top (mm) | Sample no. | $^{238}$U (ppb) | | $^{232}$Th (ppt) | | $^{230}$Th / $^{232}$Th (atomic x10$^{-6}$)[1] | | δ$^{234}$U (measured)[2] | | $^{230}$Th / $^{238}$U (activity) | | $^{230}$Th Age (yr) (uncorrected) | | $^{230}$Th Age (yr) (corrected)[3] | | δ$^{234}$U$_{initial}$ (corrected)[4] | | $^{230}$Th Age (yr BP) (corrected)[5] | |
|---|---|---|---|---|---|---|---|---|---|---|---|---|---|---|---|---|---|---|---|---|---|
| | ** | 3 | ANJ94-5-U010 | 1098.9 | ±1.6 | 392 | ±8 | 507 | ±13 | 5.0 | ±1.4 | 0.0110 | ±0.0001 | 1197 | ±16 | 1187 | ±17 | 5 | ±1 | 1125 | ±17 |
| √ | * | 10 | ANJ94-5-W1 | 702 | ±3 | 762 | ±15 | 154.2 | ±3.9 | 9.6 | ±2.8 | 0.0102 | ±0.0002 | 1103 | ±18 | 1071 | ±28 | 9.6 | ±3 | 1009 | ±28 |
| √ | ** | 22 | ANJ94-5-U050 | 1766.4 | ±4.3 | 5134 | ±104 | 68 | ±1 | 4.7 | ±1.9 | 0.0119 | ±0.0001 | 1301 | ±12 | 1217 | ±61 | 5 | ±2 | 1155 | ±61 |
| √ | ** | 31 | ANJ94-5-U078 | 1600.9 | ±3.0 | 731 | ±15 | 432 | ±10 | 3.8 | ±1.6 | 0.0120 | ±0.0001 | 1308 | ±11 | 1295 | ±15 | 4 | ±2 | 1233 | ±15 |
| √ | * | 35 | ANJ94-5-W2 | 603 | ±2 | 469 | ±10 | 267.6 | ±7.3 | 7.0 | ±2.8 | 0.0126 | ±0.0002 | 1375 | ±25 | 1352 | ±30 | 7.0 | ±3 | 1290 | ±30 |
| √ | ** | 44 | ANJ94-5-U110 | 1666.0 | ±3.0 | 392 | ±8 | 887 | ±19 | 5.1 | ±1.4 | 0.0127 | ±0.0001 | 1382 | ±9 | 1375 | ±10 | 5 | ±1 | 1313 | ±10 |

* Decay constants are 9.1577 x 10-6 yr -1 for $^{230}$Th, 2.8263 x $10^{-6}$ yr $^{-1}$ for $^{234}$U and 1.55125 x $10^{-10}$ yr $^{-1}$ for $^{238}$U (Cheng et al., 2000).

**U decay constants: $\lambda_{238}$ = 1.55125x$10^{-10}$ (Jaffey et al., 1971) and $\lambda_{234}$ = 2.82206x$10^{-6}$ (Cheng et al., 2013). Th decay constant: $\lambda_{230}$ = 9.1705x$10^{-6}$ (Cheng et al., 2013).

[1] The degree of detrital $^{230}$Th contamination is indicated by the [$^{230}$Th/$^{232}$Th] atomic ratio instead of the activity ratio.

[2] δ$^{234}$U = ([$^{234}$U/$^{238}$U] activity – 1) x 1000.

[3] Corrected $^{230}$Th ages assume the initial $^{230}$Th/$^{232}$Th atomic ratio of 4.4 ±2.2 x$10^{-6}$. Those are the values for a material at secular equilibrium, with the bulk earth $^{232}$Th/$^{238}$U value of 3.8. The errors are arbitrarily assumed to be 50%.

[4] δ$^{234}$U$_{initial}$ was calculated based on $^{230}$Th age (T), i.e., d$^{234}$U$_{initial}$ = d$^{234}$U$_{measured}$ x e$^{l234xT}$.

[5] B.P. stands for "Before Present" where the "Present" is defined as the year 1950 A.D.

**Table B3**: $^{230}$Th dating results of MA2, with 2σ error. Samples indicated by √ are considered in the age model

| Distance from top (mm) | | Sample no. | $^{238}$U (ppb) | $^{232}$Th (ppt) | $^{230}$Th / $^{232}$Th (atomic x10$^{-6}$)[1] | $\delta^{234}$U (measured)[2] | | $^{230}$Th / $^{238}$U (activity) | $^{230}$Th Age (yr) (uncorrected) | $^{230}$Th Age (yr) (corrected)[3] | $\delta^{234}U_{Initial}$ (corrected)[4] | $^{230}$Th Age (yr BP) (corrected)[5] |
|---|---|---|---|---|---|---|---|---|---|---|---|---|
| √ | ** | 1 | MA2-U001 | 83±0 | 358±8 | 17±12 | 10.2±2.9 | 0.0044±0.0032 | 479±350 | 355±361 | 10±3 | 291±361 |
| √ | * | 6 | MA2-1 | 75.5±0.1 | 208±5 | 3.9±6.3 | 6.2±6.8 | 0.00183±0.00294 | 198.7±319.6 | -26±338.1 | 6.2±6.8 | -84±338.1 |
| | ** | 8 | MA2-U008 | 89±0 | 1279±26 | 16±1 | 6.5±1.5 | 0.0136±0.0004 | 1484±42 | 1068±297 | 6±1 | 1004±297 |
| √ | * | 15 | MA2-015 | 88.7±0.1 | 371±8 | 27±2 | 3.3±2.4 | 0.0080±0.0007 | 875±77 | 732±127 | 3±2 | 670±127 |
| | ** | 26 | MA2-U026 | 87±0 | 893±18 | 45±1 | 3.4±2.3 | 0.0281±0.0005 | 3097±57 | 2797±219 | 3±2 | 2733±219 |
| √ | * | 30 | MA2-030 | 27±0 | 266±5 | 36±3 | 6.4±2.5 | 0.0066±0.0006 | 719±60 | 632±86 | 6±2 | 570±86 |
| √ | * | 44 | MA2-2 | 26±0 | 342±3 | 10.6±2.5 | 2.4±6.5 | 0.00843±0.00199 | 921.0±218.5 | 541±289.3 | 2.4±6.5 | 483±289.3 |
| √ | * | 75 | MA2-3 | 30±0 | 188±4 | 18.3±6.5 | -5.7±6.8 | 0.00705±0.00249 | 775.7±275.5 | 590±290.3 | -5.7±6.8 | 532±290.3 |
| √ | * | 94 | MA2-4 | 27±0 | 189±4 | 19.2±5.7 | -3.2±6.6 | 0.00805±0.00239 | 884.3±263.8 | 682±282.0 | -3.2±6.6 | 631±282.0 |
| √ | * | 107 | MA2-5 | 27±0 | 223±4 | 17.0±4.4 | 1.0±5.8 | 0.00848±0.00220 | 927.7±241.4 | 689±268.9 | 1.0±5.8 | 649±268.9 |

* Decay constants are 9.1577 x 10-6 yr -1 for $^{230}$Th, 2.8263 x $10^{-6}$ yr $^{-1}$ for $^{234}$U and 1.55125 x $10^{-10}$ yr $^{-1}$ for $^{238}$U (Cheng et al., 2000).

**U decay constants: $\lambda_{238}$ = 1.55125x$10^{-10}$ (Jaffey et al., 1971) and $\lambda_{234}$ = 2.82206x$10^{-6}$ (Cheng et al., 2013). Th decay constant: $\lambda_{230}$ = 9.1705x$10^{-6}$ (Cheng et al., 2013).

[1] The degree of detrital $^{230}$Th contamination is indicated by the [$^{230}$Th/$^{232}$Th] atomic ratio instead of the activity ratio.

[2] $\delta^{234}$U = ([$^{234}$U/$^{238}$U] activity – 1) x 1000.

[3] Corrected $^{230}$Th ages assume the initial $^{230}$Th/$^{232}$Th atomic ratio of 4.4 ±2.2 x$10^{-6}$. Those are the values for a material at secular equilibrium, with the bulk earth $^{232}$Th/$^{238}$U value of 3.8. The errors are arbitrarily assumed to be 50%.

[4] $\delta^{234}U_{initial}$ was calculated based on $^{230}$Th age (T), i.e., $d^{234}U_{initial} = d^{234}U_{measured} \times e^{|234xT}$.

[5] B.P. stands for "Before Present" where the "Present" is defined as the year 1950 A.D.

*Supplementary text 1: Possible controls on speleothem $\delta^{13}C$*

Changes in speleothem $\delta^{13}C$ largely depend on the changes in $\delta^{13}C$ of three reservoirs: the atmosphere, the soil, and the limestone bedrock. Among the reservoir sources, atmospheric $CO_2$ has little influence on speleothem $\delta^{13}C$ because the concentration of carbon dioxide ($CO_2$) in the atmosphere stayed constant between AD 370 and AD 1300, during which Stalagmite MA3 grew. The $CO_2$ concentration in the atmosphere and its change in $\delta^{13}C$ have only become significant since the Industrial Revolution causing the Suess effect (Suess, 1955; Verburg, 2007).

Environmental control of speleothem $\delta^{13}C$ is complex, but $\delta^{13}C$ of the soil is fundamental. It depends on two main factors: the nature of vegetation and the rate of biological activity. On the one hand, the $\delta^{13}C$ of the first speleothem calcite deposited from seepage waters reflects the isotopic signature of the dominant vegetation because plants have different $\delta^{13}C$ signatures depending on their photosynthetic pathway. The $\delta^{13}C$ values of $C_3$ plants range between –32 and –20‰ (average –27‰) (Cerling, 1984; Boutton, 1996) and the first speleothem $\delta^{13}C$ values range between –12 and –8‰ (Talma and Vogel, 1992; Brook et al., 1999, 2015). For $C_4$ plants, the $\delta^{13}C$ values range between –17 and –9‰ (average –13‰) (Cerling, 1984; Button, 1996) and the first speleothem $\delta^{13}C$ values range between –2.3 and –1.5‰ (Talma and Vogel, 1992; Brook et al., 1999, 2015). In this regard, the $\delta^{13}C$ of speleothems can be linked to climate-driven vegetation changes because the isotopic composition of soil organic matter is influenced by changes in plant communities. This climate-vegetation relationship is often reflected in the correlation between $\delta^{13}C$ and $\delta^{18}O$ (Dorale and Liu, 2009; Dorale et al., 1998; Hellstrom et al., 1998; Baldini et al., 2005;

Sletten et al., 2013). On the other hand, more biological activity favors greater input of low-$\delta^{13}C$ $CO_2$ to soil gas via root respiration and/or decay of organic matter (e.g. Hesterberg and Siegenthaler; 1991; Baldini et al., 2005). During wet periods, which is also during warm seasons in northwestern Madagascar, intense root respiration results in high $PCO_2$ that ultimately results in depleted $\delta^{13}C$ in speleothems (Hesterberg and Siegenthaler, 1991; Amundson et al., 1998; Genty et al., 2003; Drysdale et al., 2004). Cerling et al. (1991) concluded that the $\delta^{13}C$ of soil-respired $CO_2$ is much lower (by about 4.4‰) than just $CO_2$ occupying pore space in a soil.

The rate of passage of water through the limestone bedrock can also influence the speleothem $\delta^{13}C$ (Fig. B8). The residence time of water above the cave and the duration of exchange between soil $CO_2$ and $CO_2$ from the seeping water is typically controlled by the presence or absence of vegetation cover above the cave (e.g. Baldini et al., 2005). In an open system, the percolating water always exchanges $CO_2$ with the reservoir gaseous $CO_2$ in the soil. In this case, the isotopic composition of all dissolved carbon species is controlled by and reflects the isotopic composition of the soil $CO_2$, the largest reservoir of carbon for speleothems. Under pure $C_3$ vegetation in an open system, the $\delta^{13}C$ of the calcite ranges between –16.8 and –15.5‰ at $PCO_2$ of $10^{-1.5}$ and $10^{-2.5}$, respectively. Under pure $C_4$ vegetation cover, the $\delta^{13}C$ of the calcite ranges between –2.9 and –1.5‰ under the same conditions (Clark and Fritz, 1997). In a closed system, $CO_2$-exchange between the water and soil is minimal, and thus the influence of the soil $CO_2$ on the $\delta^{13}C$ of the dissolved inorganic carbon (DIC) is negligible. Under pure $C_3$ vegetation cover in a closed system, the $\delta^{13}C$ of the calcite ranges between –12.7 and –12.1‰ at $PCO_2$ of $10^{-1.5}$ and $10^{-2.5}$,

respectively. Under pure $C_4$ vegetation cover, the $\delta^{13}C$ of the calcite ranges between –5.3 and –4.9‰ (Fig. B8; Clark and Fritz, 1997).

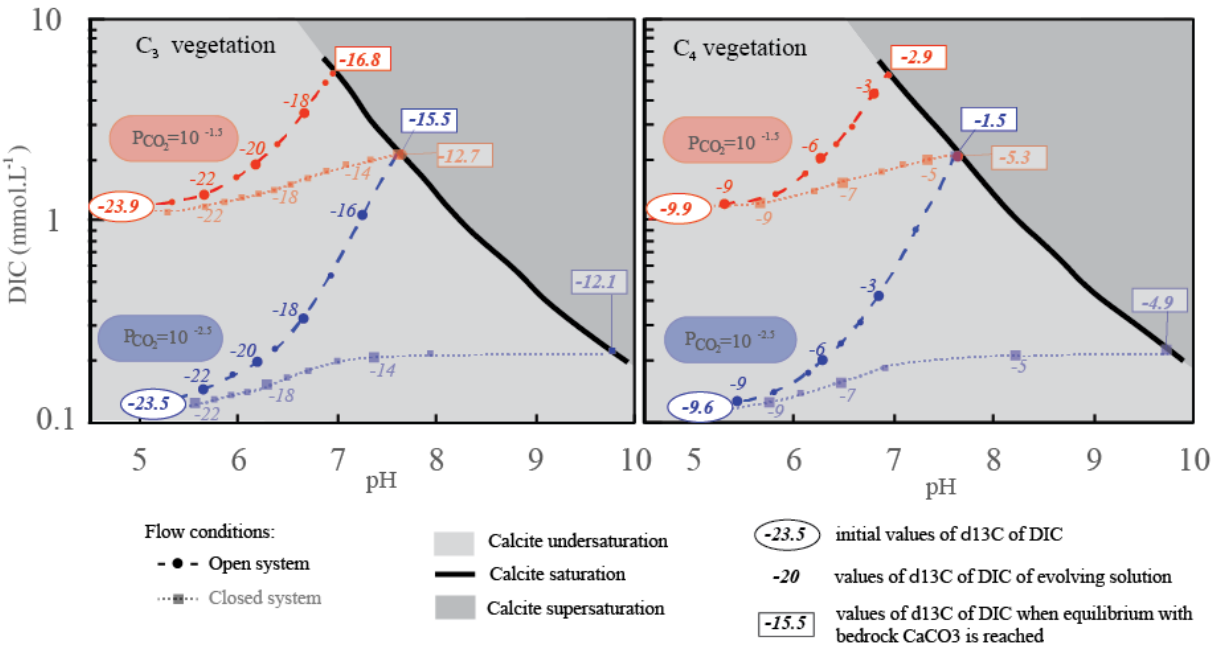


**Figure B8**: Evolution of the $\delta^{13}C$ signature of the dissolved inorganic carbon (DIC) of water during progressive dissolution of $CaCO_3$ where the source of $CO_2$ is from decay of $C_3$ vegetation (left) or $C_4$ vegetation (right). The color code represents conditions at $PCO_2$ of $10^{-2.5}$ (blue) and at $PCO_2$ of $10^{-1.5}$ (red). The $PCO_2$ in Anjohibe cave is close to $10^{-3}$. Open and closed systems are discussed in Section 3.5.2.2 and above. This figure is redrawn and modified from Figure 5.18 of Fairchild and Baker (2012), which was drawn after Figure 5-6 of Clark and Fritz (1997).

Finally, several micro-factors could cause enrichment or depletion of $^{13}C$ of the $CaCO_3$ precipitates, and they must be considered before interpreting carbon isotope records. These include evaporation rate, dripwater rate, degassing rate (and prior carbonate precipitation, PCP), and cave ventilation. All of these factors favor kinetic isotope fractionation. First, under evaporative conditions, non-equilibrium fractionation may cause enrichment in $^{13}C$. This is often expressed in ancient stalagmite layers as widely ranging $\delta^{18}O$ and strong linear correlation between $\delta^{18}O$ and $\delta^{13}C$ (Hendy, 1971; Linge et al., 2001). Second, slower drip rates result in a greater $\delta^{13}C$, and vice versa (e.g. Yadava and Ramesh, 2006). In the cave and with time, there is a progressive $^{13}C$ enrichment as $CaCO_3$ precipitates (Hendy, 1971; Wigley et al 1978; Bar-Matthews et al 1996; Hellstrom et al 1998). Assuming the drip rate is directly proportional to the rainfall in a crude way, this may lead to the dependence of speleothem $\delta^{13}C$ on the amount of rainfall (Baker et al., 1997; Fairchild et al. 2000). Third, degassing and PCP result in an increase in speleothem $\delta^{13}C$ (Dreybrodt and Scholz, 2011; Baker et al., 1997; Fairchild et al., 2000; Johnson et al., 2006; Cruz et al., 2007; Fairchild and Treble, 2009; Oster et al., 2009; 2010). PCP is enhanced by two processes: seasonal decreases in $CO_2$ in the cave air and seasonally low water flows, leading to more extensive penetration of air into the aquifer (Fairchild and McMillan, 2007). Degassing and PCP occur because the $PCO_2$ of the cave air and/or the unsaturated zone above the cave is lower than the dripwater $PCO_2$. The dripwater $PCO_2$ reflects the soil $CO_2$ concentration and thus the rate of biological activity and vegetation cover above the cave. Fourth and finally, ventilation could be another catalyst for degassing and PCP, but it is more seasonal (e.g. James et al., 2015). Enhanced calcite

precipitation occurs during times when the cave is ventilated and cave air $PCO_2$ is reduced (Spötl et al., 2005; Banner et al., 2007; Kowalczk and Froelich, 2010; Mattey et al., 2010; Boch et al., 2011; Frisia et al., 2011; Lambert and Aharon, 2011; Tremaine et al., 2011; Wong et al., 2011).

*Supplementary text 2: Northern Hemisphere records: overview*

The European records are chosen for comparison here because of their high resolution, and the records cover the interval covered by Stalagmite MA3. One might ask if such records could represent the whole Northern Hemisphere or even if they could be used as a reference for global changes in temperature. Four lines of evidence support a positive answer to that question (Fig. B9). First, the negative anomalies identified in the European records, particularly between ca. AD 550-620 and AD 790-900, coincide with the timing of glacial advances in the Swiss Alps (Holzhauser et al., 2005) around AD 500-600 and AD 800-900 respectively, while the intervening periods coincides with the timing of glacial retreat. Second, Alpine glaciers act as sensitive indicators of climatic variability (Denton and Karlen, 1973). This is inferred from the terminal and lateral positions of the Alpine glaciers that fluctuate in response to mass balance adjustments to changing temperature and precipitation regimes (Klok and Oerlemans, 2003). Third, temperature reconstructions from tree rings, ice core $^{18}O$, and ice accumulations from several locations in the world (see Fig. 1 of Mann et al., 1998) that are presented in millennial temperature reconstruction in Figure 3a of Mann and Bradley (1999, data are also available at http://www.ncdc.noaa.gov/paleo/pubs/mann_99.html) present similarity with the

European records (using the data available from http://www.ncdc.noaa.gov/paleo/pubs/buentgen2011/buentgen2011.html), when the data from the latter is smoothed to match with the data from the NH (Fig. B9). Fourth and lastly, the most recent global climate reconstruction of Neukom et al. (2014) presents similarity with the European records (Fig. B9). Neukom et al. (2014) record goes back to AD 1000. It includes several proxies such as tree rings, marine sediments, lake sediments, ice cores, coral $\delta^{18}O$, speleothem $\delta^{18}O$, and documentary data from different parts of the world, with more than 300 individual sites from the Southern Hemisphere.

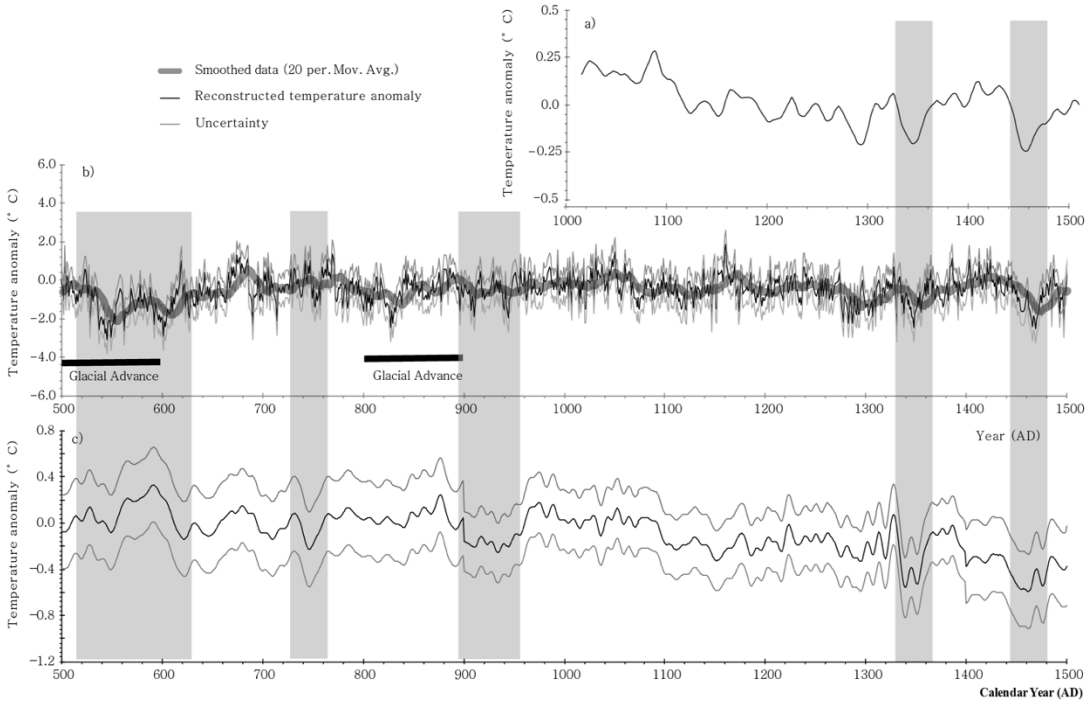


Figure B9: Temperature variability in the northern hemisphere, specifically putting the European records (middle) into perspective. a) 30-year loess filtered ensemble mean temperature reconstruction for the Southern Hemisphere from more than 300 individual sites (Neukom et al., 2014). b) Temperature anomaly reconstruction from tree rings from Europe (Büntgen et al., 2011). Timing for glacial advances recorded in the Swiss Alps (Holzhauser et al., 2005) is indicated in horizontal bars. c) Northern Hemisphere temperature reconstruction based on multiproxy data network and instrumental temperature data (Mann and Bradley., 1999). The gray vertical bars highlight intervals when profiles show similarity.

## REFERENCES


Amundson, R., Stern, L., Baisden, T., Wang, Y., 1998. The isotopic composition of soil and soil-respired $CO_2$: Geoderma 82, 83-114.

Baker, A., Ito, E., Smart, P.L., McEwan, R.F., 1997. Elevated and variable values of C-13 in speleothems in a British cave system. Chem. Geol. 136, 263-270.

Baldini, J.U.L., McDermott, F., Baker, A., Baldini, L.M., Mattey, D.P., Railsback, L.B., 2005. Biomass effects on stalagmite growth and isotope ratios: A 20th century analogue from Wiltshire, England. Earth Planet. Sci. Let. 240, 486-494.

Banner, J.L., Guilfoyle, A., James, E.W., Stern, L.A., Musgrove, M., 2007. Seasonal variations in modern speleothem calcite growth in Central Texas, U.S.A. J Sediment Res 77, 615-622.

Bar-Matthews, M., Ayalon, A., Matthews, A., Sass, E., Halicz, L., 1996. Carbon and oxygen isotope study of the active water-carbonate system in a karstic Mediterranean cave: Implications for paleoclimate research in semiarid regions. Geochim. Cosmochim. Acta 60, 337-347.

Boch, R., Spötl, C., and Frisia, S., 2011. Origin and paleoenvironmental significance of lamination in stalagmites from Katerloch Cave, Austria. Sedimentology 58, 508-531.

Boutton, T.W., 1996. Stable carbon isotope ratios of soil organic matter and their use as indicators of vegetation and climate change. In Boutton, T.W., Yamasaki, S.I. (Eds.), Mass Spectrometry of Soils, pp. 47-82.

Bowen, G., 2013. Gridded maps of the isotopic composition of meteoric waters: Africa/Madagascar. http://www.waterisotopes.org.

Brook, G.A., Rafter, M.A., Railsback, L.B., Sheen, S.W., Lundberg, J., 1999. A high-resolution proxy record of rainfall and ENSO since AD 1550 from layering in stalagmites from Anjohibe Cave, Madagascar. Holocene 9, 695-705.

Brook, G.A., Railsback, L.B., Scott, L., Voarintsoa, N.R.G., Liang, F., 2015. Late Holocene Stalagmite and Tufa Climate Records for Wonderwerk Cave: Relationships Between Archaeology and Climate in Southern Africa. Afr. Arch. Rev. 32, 1-32.

Büntgen, U., Tegel, W., Nicolussi, K., McCormick, M., Frank, D., Trouet, V., Kaplan, J.O., Herzig, F., Heussner, K.U., Wanner, H., Luterbacher, J., Esper, J., 2011. 2500 Years of European Climate Variability and Human Susceptibility. Science 331, 578-582.

Cerling, T.E., 1984. The stable isotopic composition of modern soil carbonate and its relationship to climate. Earth Planet. Sci. Lett. 71, 229–240.

Cerling, T.E., Solomon, D.K., Quade, J., Bowman, J.R., 1991. On the isotopic composition of carbon in soil carbon dioxide. Geochem. Cosmochim. Acta 55, 3403-3405.

Cheng, H., Edwards, R.L., Hoff, J., Gallup, C.D., Richards, D.A., Asmerom, Y., 2000. The half-lives of uranium-234 and thorium-230. Chemical Geology 169, 17–33.

Cheng, H., Edwards, R.L., Shen, C.C., Polyak, V.J., Asmerom, Y., Woodhead, J., Hellstrom, J., Wang, Y.J., Kong, X.G., Spötl, C., Wang, X.F., Alexander, E.C., 2013. Improvements in Th-230 dating, Th-230 and U-234 half-life values, and U-Th isotopic measurements by multi-collector inductively coupled plasma mass spectrometry: Earth Planet. Sci. Lett. 371, 82-91.

Clark, I.D., Fritz, P., 1997. Environmental isotopes in hydrogeology. Lewis Publishers.

Collins, A.S., Windley, B.F., 2002. The tectonic evolution of central and northern Madagascar and its place in the final assembly of Gondwana. J. Geol. 110, 325-339.

Cruz, F., Burns, S., Jercinovic, M., Karmann, I., Sharp, W., Vuille, M., 2007. Evidence of rainfall variations in Southern Brazil from trace element ratios (Mg/Ca and Sr/Ca) in a Late Pliestocene stalagmite. Geochim. Cosmochim. Acta 71, 2250– 2263.

Denton, G.H., Karlen, W., 1977. Holocene glacial and treeline variations in the White River valley and Skolai Pass, Alaska and Yukon Territory. Quat. Res. 7, 63–111.

Dorale, J.A., Liu, Z.H., 2009. Limitations of Hendy Test Criteria in Judging the Paleoclimatic Suitability of Speleothems and the Need for Replication. J. Cave Karst Studies 71, 73-80.

Dorale, J.A., Edwards, R.L., Ito, E., Gonzalez, L.A., 1998. Climate and vegetation history of the midcontinent from 75 to 25 ka: A speleothem record from Crevice Cave, Missouri, USA. Science 282, 1871–1874.

DuPuy, D.J., Moat, J., 1996. A refined classification of the primary vegetation of Madagascar based on the underlying geology: Using GIS to map its distribution and to assess its conservation status. Biogeography and Madagascar, 205-218.

DuPuy, D.J., Moat, J., 2003. Using Geological Substrate to Identify and Map Primary Vegetation Types in Madagascar and the implications for planning biodiversity conservation, in: Goodman, S.M., Benstead, J.P. (Eds.), The Natural History of Madagascar. University of Chicago Press, Chicago, pp. 51-74.

Dreybrodt, W., Scholz, D., 2011. Climatic dependence of stable carbon and oxygen isotope signals recorded in speleothems: from soil water to speleothem calcite. Geochim. Cosmochim. Acta 75, 734–752.

Drysdale, R.N., Zanchetta, G., Hellstrom, J.C., Fallick, A.E., Zhao, J.X., Isola, I., Bruschi, G., 2004. Palaeoclimatic implications of the growth history and stable isotope ($\delta^{18}O$ and $\delta^{13}C$) geochemistry of a Middle to Late Pleistocene stalagmite from central-western Italy. Earth Planet. Sci. Lett. 227, 215–229.

Fairchild, I.J., Baker, A., 2012. Speleothem Science: From Processes to Past Environments, Wiley-Blackwell.

Fairchild, I.J., McMillan, E.A., 2007. Speleothems as indicators of wet and dry periods. Intl. J. Speleol. 36, 9-74.

Fairchild, I.J., Treble, P.C., 2009. Trace elements in speleothems as recorders of environmental change. Quat. Sci. Rev. 28, 449–468.

Fairchild, I.J., Borsato, A., Tooth, A.F., Frisia, S., Hawkesworth, C.J., Huang, Y.M., McDermott, F., Spiro, B., 2000. Controls on trace element (Sr-Mg) compositions of carbonate cave waters: implications for speleothem climatic records. Chem. Geol. 166, 255–269.

Frisia S., Fairchild I.J., Fohlmeister J., Miorandi R., Spötl C., Borsato A., 2011. Carbon mass-balance modelling and carbon isotope exchange processes in dynamic caves. Geochim. Cosmochim. Acta 75, 380–400.

Genty, D., Blamart, D., Ouahdi, R., Gilmour, M., Baker, A., Jouzel, J., Van-Exter, S., 2003. Precise dating of Dansgaard-Oeschger climate oscillations in western Europe from stalagmite data. Nature 421, 833–837.

Hellstrom, J., McCulloch, M., Stone, J., 1998. A detailed 31,000-year record of climate and vegetation change, from the isotope geochemistry of two New Zealand speleothems. Quaternary Res 50, 167-178.

Hendy, C.H., 1971. The isotopic geochemistry of speleothems I: the calculation of the effects of different modes of formation on the isotopic composition of speleothems and their applicability as palaeoclimatic indicators. Geochim. Cosmochim. Acta 35, 801–824.

Hesterberg, R., Siegenthaler, U., 1991. Production and Stable Isotopic Composition of $CO_2$ in a Soil near Bern, Switzerland. Tellus Series B-Chem. Phys. Met. 43, 197-205.

Holzhauser, H., Magny, M., Zumbuhl, H.J., 2005. Glacier and lake-level variations in west-central Europe over the last 3500 years. Holocene 15, 789-801.

Jaffey, A.H., Flynn, K.F., Glendenin, L.E., Bentley, W.C., Essling, A.M., 1971. Precision measurement of half-lives and specific activities of $^{235}U$ and $^{238}U$. Phys. Rev. 4, 1889–1906.

James, E.W., Banner, J.L., Hardt, B., 2015. A global model for cave ventilation and seasonal bias in speleothem paleoclimate records. Geochem. Geophys. Geosys. 16, 1044–1051. doi:10.1002/2014GC005658.

Johnson, K.R., Hu, C.Y., Belshaw, N.S., Henderson, G.M., 2006. Seasonal trace-element and stable-isotope variations in a Chinese speleothem: the potential for high-resolution paleomonsoon reconstruction. Earth Planet Sci. Lett. 244, 394–407.

Klok, E.J., Oerlemans, J., 2003. Deriving historical equilibrium-line altitudes from a glacier length record by linear inverse modeling. The Holocene 13, 343–351.

Kowalczk, A., Froelich, P., 2010. Cave air ventilation and $CO_2$ outgassing by radon-222 modeling: how fast do caves breathe? Earth Planet. Sci. Lett. 289, 209–219.

Lambert W.J., Aharon, P., 2011. Controls on dissolved inorganic carbon and $\delta^{13}C$ in cave waters from DeSoto Caverns: implications for speleothem $\delta^{13}C$ assessments. Geochim. Cosmochim. Acta 75, 753–768.

Lindesay, J. A., 1998. Present Climates of Southern Africa. In Hobbs, J.E., Lindesay, J.A., Bridgman, H.A. (Eds.), Climates of the Southern Continents: Present, Past and Future. John Wiley & Sons Ltd., England, pp. 5-62.

Linge, H., Lauritzen, S.E., Lundberg, J., Berstad, I.M., 2001. Stable isotope stratigraphy of Holocene speleothems: examples from a cave system in Rana, northern Norway. Palaeogeogr. Palaeoclimatol. Palaeoecol., v. 167, no. 3-4, p. 209-224.

Mann, M.E., Bradley R.S., Hughes, M.K., 1998. Global-Scale Temperature Patterns and Climate Forcing Over the Past Six Centuries. Nature 392, 779-787.

Mann, M.E., Bradley R.S., 1999. Northern Hemisphere Temperature During the Past Millenium: Inferences, Uncertainties, and Limitations. Geophys. Res. Lett. 26, 759-762.

Mattey, D.P., Fairchild, I.J., Atkinson, T.C., Latin, J.-P., Ainsworth, M., Durell, R., 2010. Seasonal microclimate control of calcite fabrics, stable isotopes and trace elements in modern speleothem from St Michaels Cave, Gibraltar. Geol. Soc. Lond. Spec. Publ. 336, 323–344.

Neukom, R., Gergis, J., Karoly, D.J., Wanner, H., Curran, M., Elbert, J., Gonzalez-Rouco, F., Linsley, B.K., Moy, A.D., Mundo, I., Raible, C.C., Steig, E.J., van Ommen, T., Vance, T., Villalba, R., Zinke, J., Frank, D., 2014. Inter-hemispheric temperature variability over the past millennium. Nat. Clim. Ch. 4, 362-367.

Oster, J.L., Montanez, I.P., Sharp, W.D., Cooper, K.M., 2009. Late Pleistocene California droughts during deglaciation and Arctic warming. Earth Planet. Sci. Lett., v. 288, no. 3-4, p. 434-443.

Sletten, H.R., Railsback, L.B., Liang, F.Y., Brook, G.A., Marais, E., Hardt, B.F., Cheng, H., Edwards, R.L., 2013. A petrographic and geochemical record of climate change over the last 4600 years from a northern Namibia stalagmite, with evidence of abruptly wetter climate at the beginning of southern Africa's Iron Age. Palaeogeogr. Palaeoclimatol. Palaeoecol. 376, 149-162.

Spötl, C., Fairchild, I. J., and Tooth, A. F., 2005, Cave air control on dripwater geochemistry, Obir Caves (Austria): Implications for speleothem deposition in dynamically ventilated caves: Geochem. Cosmochim. Acta, v. 69, no. 10, p. 2451-2468.

Suess, H.E., 1955. Radiocarbon concentration in modern wood. Science 122, 415–417.

Talma, A.S., Vogel, J.C., 1992. Late Quaternary palaeotemperatures derived from a speleothem from Cango Caves, Cape Province, South Africa. Quat. Res. 37, 203–213.

Tremaine, D.M., Froelich, P.N., Wang, Y., 2011. Speleothem calcite farmed in situ: modern calibration of $\delta^{18}O$ and $\delta^{13}C$ paleoclimate proxies in a continuously- monitored natural cave system. Geochim. Cosmochim. Acta 75, 4929–4950. http://dx.doi.org/10.1016/j.gca.2011.06.005.

Verburg, P., 2007. The need to correct for the Suess effect in the application of $\delta^{13}C$ in sediment in autotrophic Lake Tanganyika, as a productivity proxy in the anthropocene. J. Paleolimnol. 37, 591–602.

Wigley, T.M.L., Plummer, L.N., Parson, Jr., F.J., 1978. Mass transfer and carbon isotope evolution in natural water systems. Geochim. Cosmochim. Acta 42, 1117–l139.

Wong, C., Banner, J.L., Musgrove, M.L., 2011. Seasonal dripwater Mg/Ca and Sr/Ca variations driven by cave ventilation: implications for and modeling of speleothem paleoclimate records. Geochim. Cosmochim. Acta 75, 3514–3529. http://dx.doi.org/10.1016/j.gca.2011.03.025.

Yadava, M.G., Ramesh, R., 2006. Stable oxygen and carbon isotope variations as monsoon proxies: A comparative study of speleothems from four different locations in India. J. Geol. Soc. India 68, 461-475.

APPENDIX C

SUPPLEMENTARY MATERIALS FOR CHAPTER 4

"THREE DISTINCT HOLOCENE INTERVALS REVEALED IN NW MADAGASCAR: EVIDENCE FROM TWO STALAGMITES IN TWO CAVES, AND IMPLICATIONS FOR ITCZ DYNAMICS"

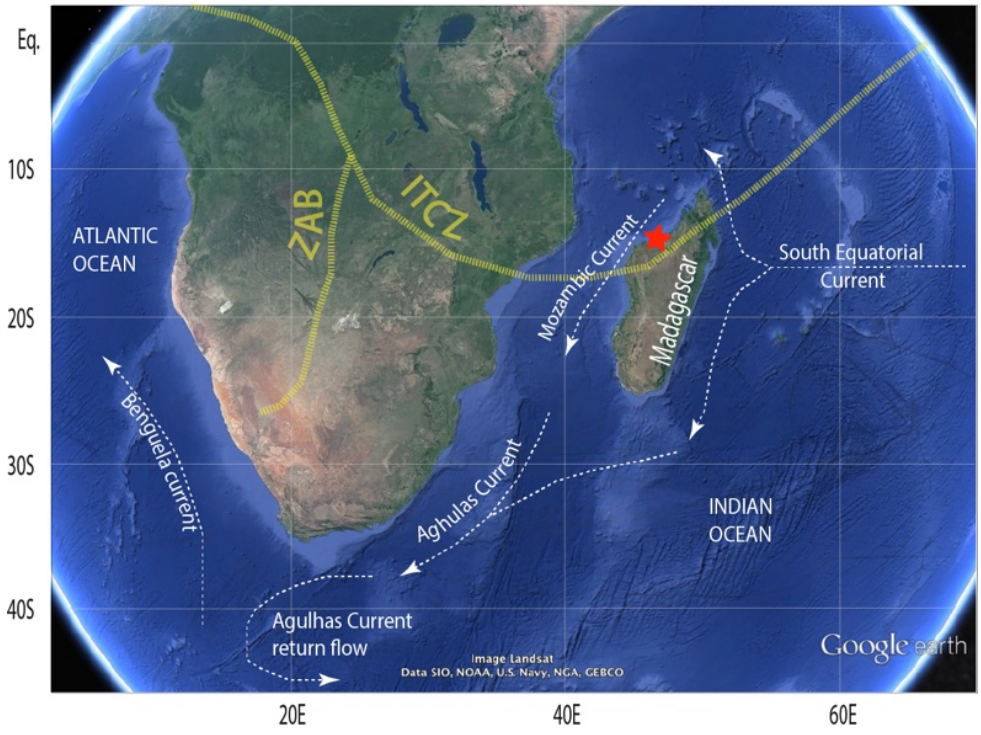


**Figure C1**: Google Earth image putting Madagascar into perspective with regard to oceanic currents and convergence zones (ITCZ and ZAB, Zaire Aire Boundary). The map of the currents was obtained from Lindesay, 1998 and Schott and McCreary (2001). The

map of the ITCZ and ZAB was adopted from Gasse (2000). The red star indicates the study location.

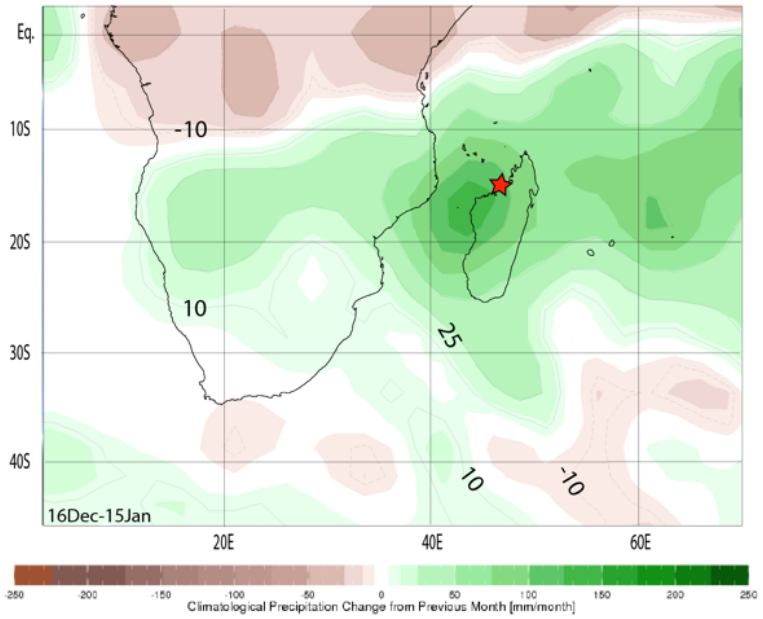


**Figure C2:** Climate setting. Map of summer precipitation between December 16 and January 15 (the wettest months) in Madagascar. Red star indicates the study area. Source: http://iridl.ldeo.columbia.edu/ (accessed August 31, 2016)


**Figure C3:** Cave locations. Google Earth image showing the location of the two caves Anjohibe (ANJB) and Anjokipoty (ANJK) Caves and the current extent of vegetation cover in northwestern Madagascar.

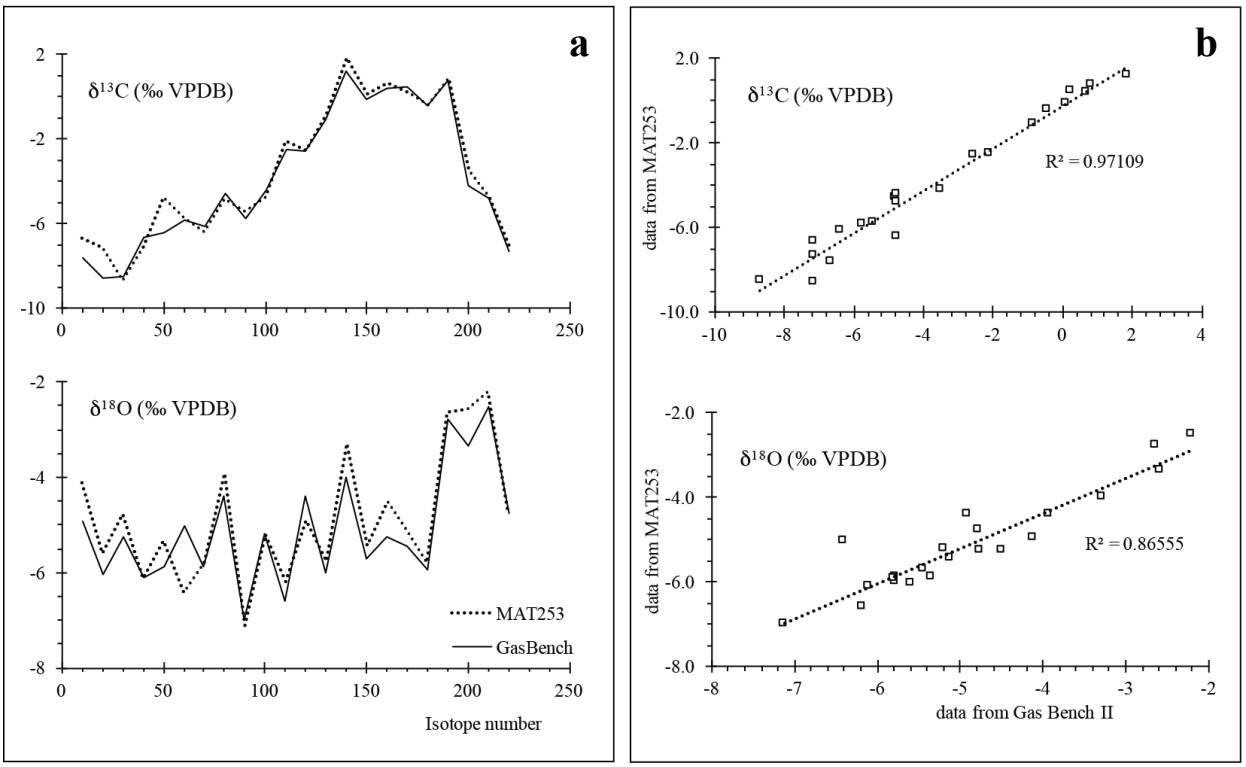


**Figure C4**: Comparison between MAT 253 and Gas Bench II stable isotope results on Stalagmite MAJ-5, showing similarity in the results. a) Depth series of $\delta^{13}C$ and $\delta^{18}O$. b) Scatterplots of $\delta^{13}C$ and $\delta^{18}O$.

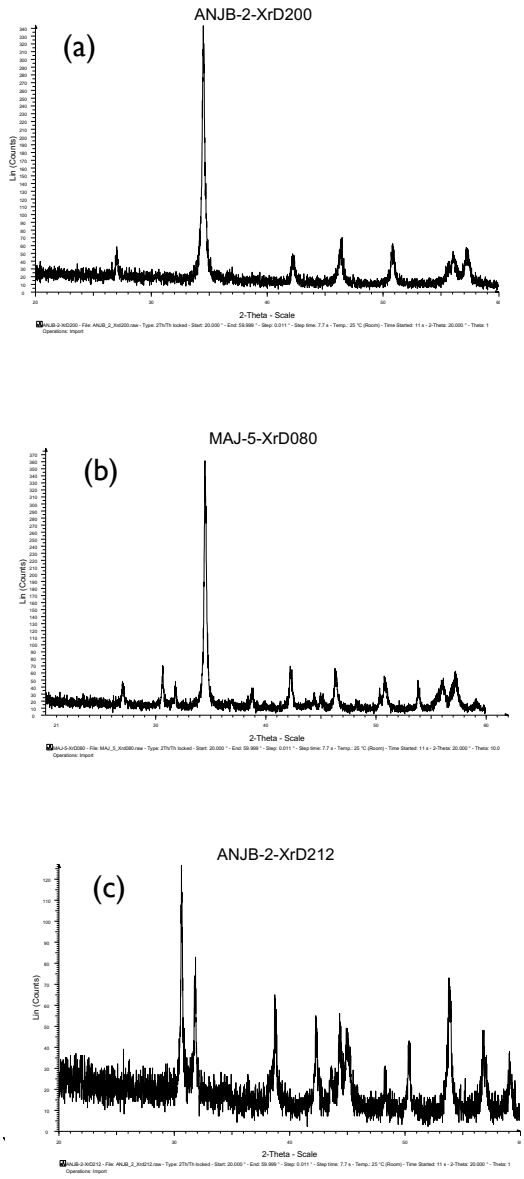


**Figure C5**: Selected X-ray diffraction spectra of the three types of mineralogy identified in Stalagmite ANJB-2 and MAJ-5. (a) 100% calcite. (b) 50% calcite-50% aragonite. (c) 100% aragonite.

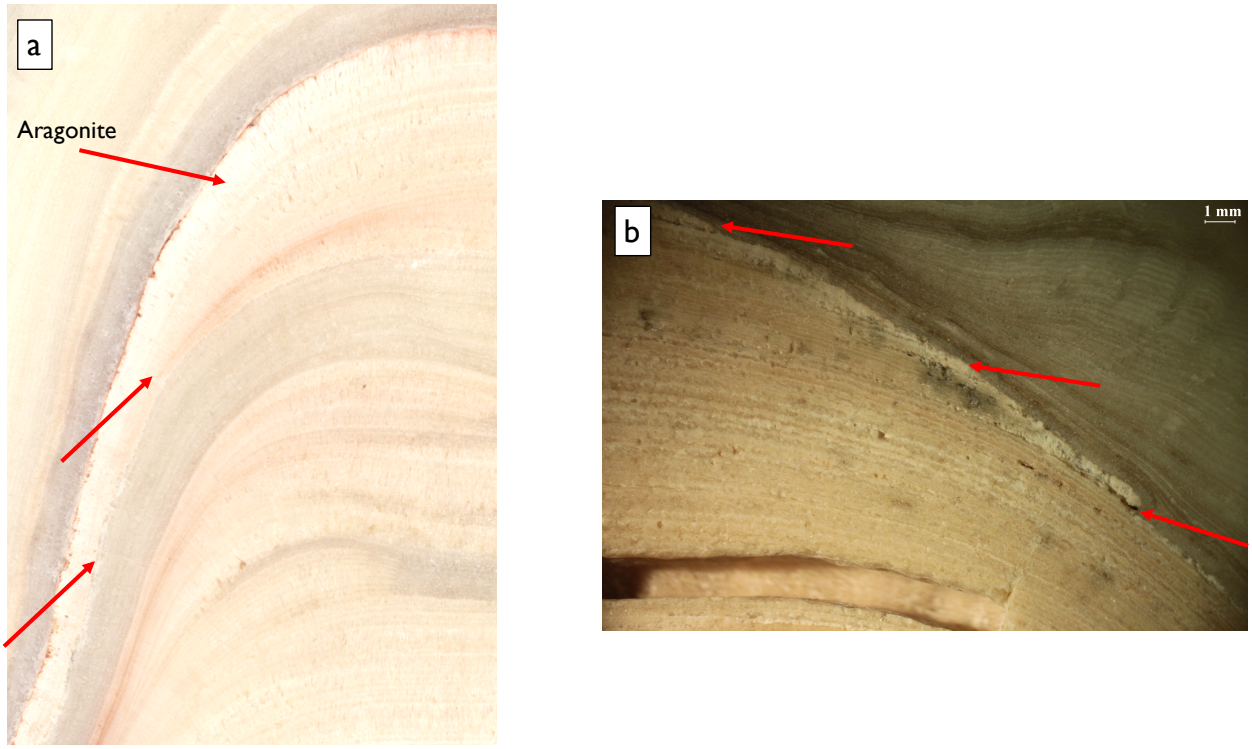


**Figure C6:** Photographs illustrating the mid-Holocene hiatus. Photographs showing the Type L layer-bounding surfaces in Stalagmite ANJB-2 (a) and in Stalagmite MAJ-5 (b). Pinching of layers toward the flank are indicated with arrows. Also, note the white and porous layer of aragonite in Stalagmite ANB-2 that is capped with a very thin brown layer.

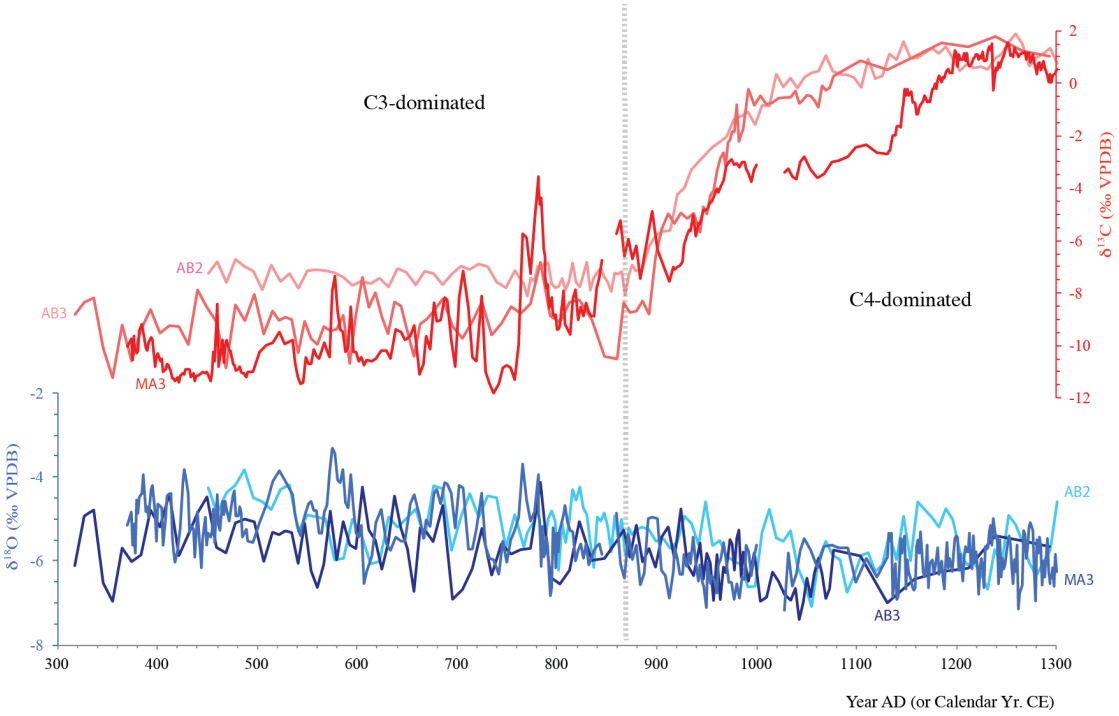


**Figure C7**: Stable isotope profile of $\delta^{18}O$ and $\delta^{13}C$ of the late Holocene in Madagascar from Anjohibe Cave's stalagmites showing the $\delta^{13}C$ from $C_3$-dominated to $C_4$-dominated vegetation (Burns et al., 2016; Voarintsoa et al., accepted). Note that the age scale is in year AD.

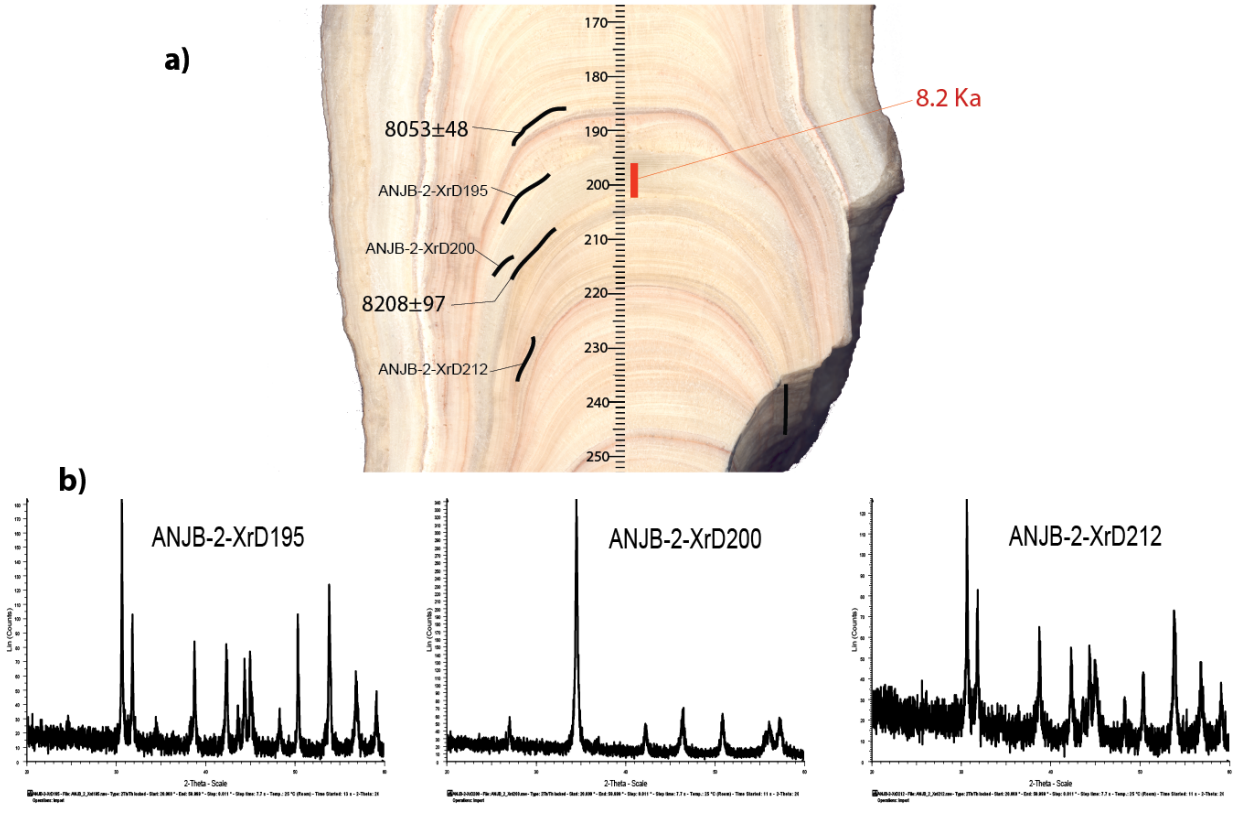


**Figure C8**: The 8.2 ka event identified in Stalagmite ANJB-2. a) Scanned image of a portion of Stalagmite ANJB-2 showing the 8.2 ka event and the corresponding trenches for radiometric dating and X-ray diffraction analyses. b) X-ray diffraction spectra of the stalagmite layers at 195, 200, and 212 mm from the top of the stalagmite.

*Supplementary text 1: Possible climatic response of the latitudinal migration of the ITCZ*

The ITCZ migrates southward in austral summer and northward in boreal summer in response to seasonal insolation. Climate simulations have also reported long-term migration of the ITCZ, the causes of which have been ascribed to changes in insolation and difference in temperature between the Northern and the Southern Hemisphere (e.g. Chiang and Bitz, 2005; Broccolli et al., 2006; Braconnot et al., 2007). The climatic responses to the ITCZ dynamics can vary from region to region and from one time interval to another. Here, we attempt to provide different conceptualized models to understand the climatic regime in Madagascar during the early, the middle, and the late Holocene (as proposed in Sect. 4.5.2. of the manuscript).

Dry conditions in Madagascar could be conceptualized as dry years, such as modeled in case 1 (Fig. C9). In that model, austral summer months receive less rainfall and austral winter months could receive no rainfall. This model could be used to conceptualize the climatic response in Madagascar when the ITCZ moves north, such as during the mid-Holocene.

Wet conditions in Madagascar could be conceptualized as wet years, such as modeled in case 2 and case 3 (Fig. C9). Case 2 suggests that austral summer months receive rain as well as austral winter months, thus it suggests less seasonality. Although the amount of rainfall received during winter months cannot be easily estimated, this model could be used to understand the climatic response in Madagascar during the early Holocene when the southern hemisphere winter insolation was relatively greater than the northen Hemisphere winter insolation (Fig. 4.5a). The ITCZ was already moved southward

due to the globally cold conditions (Figs. 4.6a, c), and because of the higher winter insolation in the SH, heating of land would bring additional precipitation during austral winter. Case 3 suggests that austral summers receive more rainfall than normal years, but austral winters stay dry or with little precipitation, thus seasonality must have been stronger. This scenario could be used to understand the climatic response in Madagascar during the late Holocene when the southern hemisphere summer insolation was greater than the northern hemisphere summer insolation (Fig. 4.5a). Globally cooler conditions (Figs. 4.6a, b) already suggest a southward migration of the ITCZ, and the greater SH summer insolation could have intensified the monsoonal rainfall in northwestern Madagascar during austral summers.

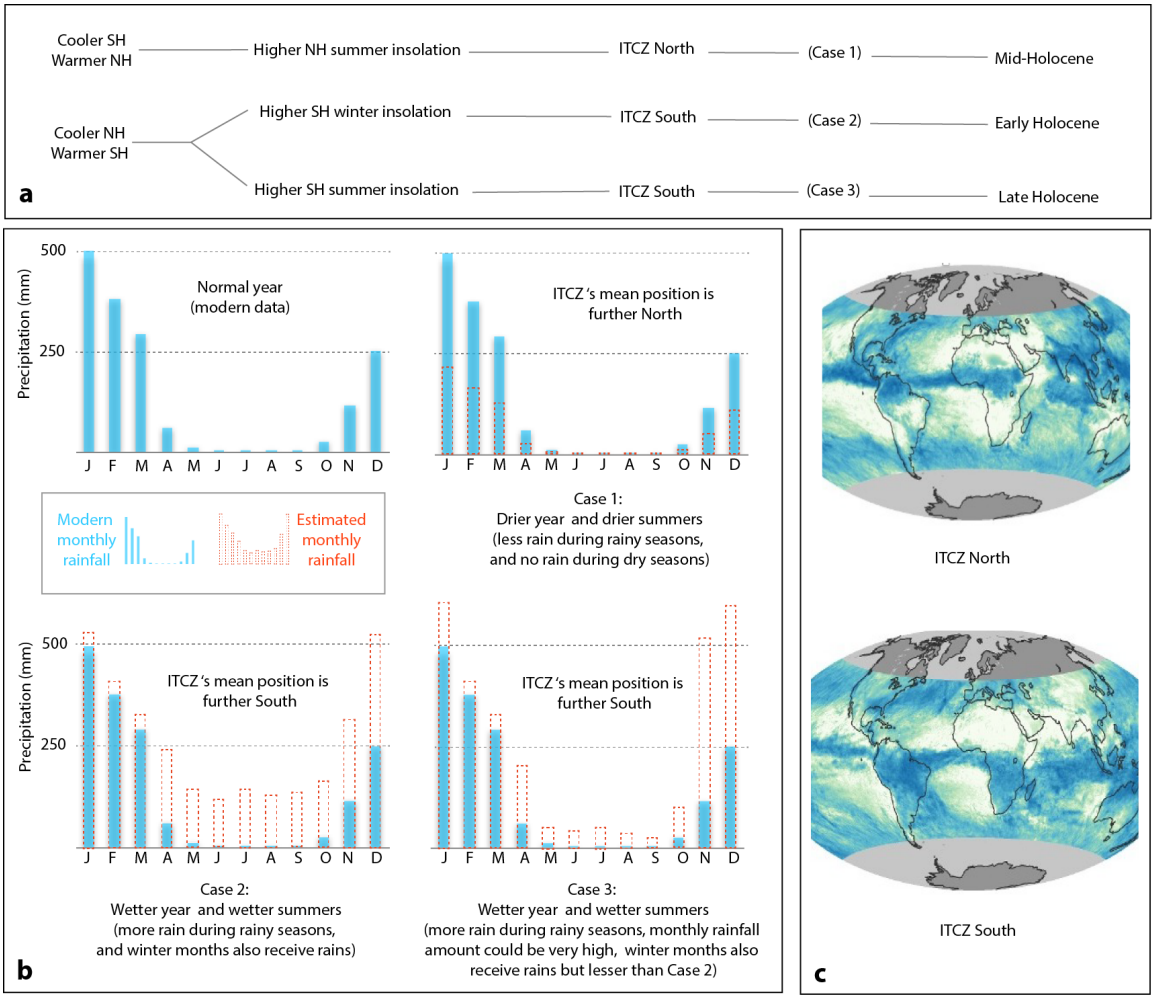
Cooler SH
Warmer NH
Higher NH summer insolation
ITCZ North
(Case 1)
Mid-Holocene
Cooler NH
Warmer SH
Higher SH winter insolation
ITCZ South
(Case 2)
Early Holocene
Higher SH summer insolation
ITCZ South
(Case 3)
Late Holocene
a
Precipitation (mm)
500
250
J F M A M J J A S O N D
Normal year
(modern data)
ITCZ 's mean position is
further North
Case 1:
Drier year and drier summers
(less rain during rainy seasons,
and no rain during dry seasons)
Modern
monthly
rainfall
Estimated
monthly
rainfall
ITCZ 's mean position is
further South
Case 2:
Wetter year and wetter summers
(more rain during rainy seasons,
and winter months also receive rains)
ITCZ 's mean position is
further South
Case 3:
Wetter year and wetter summers
(more rain during rainy seasons, monthly rainfall
amount could be very high, winter months also
receive rains but lesser than Case 2)
b
ITCZ North
ITCZ South
c

Figure C9: Conceptualizing the different possible outcomes of the long-term latitudinal migration of the ITCZ. a) Highlighting the three possible scenarios of the Holocene. b) Barplots of monthly rainfall in northwestern Madagascar, using the modern data as a reference to estimating the region's paleoclimate during drier and wetter conditions. c) Global rainfall maps from NASA (same source as Fig. 4.1 in the manuscript). These maps are modern, but they are only shown here to give a better perspective of the position of Madagascar when the ITCZ is relatively north or south.

**Table C1**: $^{230}$Th dating results for Stalagmite ANJB-2. The error is 2 σ error. Dft= distance from the top of the stalagmite.

| Dft (mm) | Sample no. | $^{238}$U (ppb) | | $^{232}$Th (ppt) | | $^{230}$Th / $^{232}$Th (atomic x10$^{-6}$) | | d$^{234}$U* (measured) | | $^{230}$Th / $^{238}$U (activity) | | $^{230}$Th Age (yr) (uncorrected) | | $^{230}$Th Age (yr) (corrected) | | d$^{234}$U$_{initial}$** (corrected) | | $^{230}$Th Age (yr BP)*** (corrected ) | |
|---|---|---|---|---|---|---|---|---|---|---|---|---|---|---|---|---|---|---|---|
| 3 | ANJB-2-U003 | 3371 | ±11 | 39850 | ±809 | 10 | ±0 | 5.2 | ±2.0 | 0.0070 | ±0.0001 | 761 | ±7 | 419 | ±243 | 5 | ±2 | 355 | ±243 |
| 8 | ANJB-2-008 | 194.6 | ±0.3 | 410 | ±8 | 20 | ±3 | 3.6 | ±1.7 | 0.0026 | ±0.0004 | 284 | ±47 | 223 | ±64 | 4 | ±2 | 161 | ±64 |
| 25 | ANJB-2-025 | 4646.6 | ±6.6 | 1594 | ±32 | 216 | ±5 | 3.4 | ±1.4 | 0.0045 | ±0.0001 | 489 | ±7 | 479 | ±10 | 3 | ±1 | 417 | ±10 |
| 47 | ANJ-B-2-U047 | 64 | ±0 | 634 | ±15 | 31 | ±12 | 3.0 | ±4.3 | 0.0187 | ±0.0074 | 2052 | ±822 | 1762 | ±845 | 3 | ±4 | 1697 | ±845 |
| 53 | ANJ-B-2-U053R | 134 | ±0 | 2325 | ±47 | 20 | ±4 | 4.6 | ±2.0 | 0.0211 | ±0.0037 | 2313 | ±416 | 1808 | ±547 | 5 | ±2 | 1743 | ±547 |
| 72 | ANJB-2-072 | 67.8 | ±0.1 | 382 | ±8 | 48 | ±3 | 8.5 | ±2.4 | 0.0163 | ±0.0008 | 1778 | ±93 | 1615 | ±147 | 9 | ±2 | 1553 | ±147 |
| 92 | ANJ-B-2-U092 | 78 | ±0 | 180 | ±8 | 92 | ±40 | 5.1 | ±3.5 | 0.0129 | ±0.0056 | 1408 | ±610 | 1341 | ±612 | 5 | ±4 | 1276 | ±612 |
| 105 | ANJ-B-2-U105 | 117 | ±0 | 229 | ±9 | 113 | ±34 | 13.5 | ±2.9 | 0.0134 | ±0.0040 | 1450 | ±432 | 1393 | ±434 | 14 | ±3 | 1329 | ±434 |
| 112 | ANJ-B-2-U112 | 1322 | ±2 | 7456 | ±150 | 42 | ±2 | 8.5 | ±2.0 | 0.0145 | ±0.0005 | 1576 | ±50 | 1413 | ±125 | 9 | ±2 | 1348 | ±125 |
| 116 | AB-1a | 130.9 | ±0.2 | 530 | ±14 | 136.7 | ±16.7 | 27.0 | ±3.0 | 0.033539275 | ±0.00400 | 3620 | ±439 | 3506 | ±446 | 27.2 | ±3.0 | 3444 | ±446 |
| 118 | AB-2a | 2569.8 | ±2.9 | 5266 | ±106 | 580.4 | ±11.9 | 7.5 | ±1.6 | 0.072126026 | ±0.00032 | 8100 | ±40 | 8040 | ±58 | 7.6 | ±1.6 | 7978 | ±58 |
| 120 | ANJB-2-U120 | 1710 | ±4 | 20753 | ±418 | 108 | ±2 | 9.1 | ±2.3 | 0.0796 | ±0.0004 | 8955 | ±48 | 8605 | ±252 | 9 | ±2 | 8541 | ±252 |
| 120 | ANJB-2-U120R | 2075 | ±3 | 13340 | ±268 | 197 | ±4 | 6.3 | ±1.5 | 0.0767 | ±0.0003 | 8640 | ±38 | 8454 | ±137 | 6 | ±2 | 8389 | ±137 |
| 130 | ANJB-2-130 | 3042.4 | ±3.8 | 7448 | ±149 | 477 | ±10 | 6.2 | ±1.5 | 0.0709 | ±0.0002 | 7966 | ±26 | 7895 | ±57 | 6 | ±2 | 7833 | ±57 |
| 160 | ANJB-2-160 | 2994.8 | ±4.1 | 2484 | ±50 | 1416 | ±29 | 4.3 | ±1.5 | 0.0712 | ±0.0002 | 8021 | ±30 | 7997 | ±35 | 4 | ±2 | 7935 | ±35 |
| 185 | ANJB-2-U185 | 3490 | ±5 | 6040 | ±122 | 690 | ±14 | 3.6 | ±1.7 | 0.0724 | ±0.0003 | 8167 | ±33 | 8117 | ±48 | 4 | ±2 | 8053 | ±48 |
| 201 | ANJB-2-U205 | 574 | ±1 | 1881 | ±38 | 374 | ±8 | 5.7 | ±1.8 | 0.0743 | ±0.0006 | 8367 | ±70 | 8272 | ±97 | 6 | ±2 | 8208 | ±97 |
| 215 | ANJB-2-U215 | 3146 | ±4 | 5418 | ±109 | 713 | ±15 | 7.0 | ±1.5 | 0.0745 | ±0.0003 | 8379 | ±33 | 8329 | ±48 | 7 | ±2 | 8265 | ±48 |
| 251 | ANJB-2-U251 | 4246 | ±5 | 7290 | ±147 | 745 | ±15 | 6.3 | ±1.3 | 0.0776 | ±0.0002 | 8750 | ±27 | 8700 | ±44 | 6 | ±1 | 8636 | ±44 |
| 275 | ANJB-2-U275 | 6077 | ±9 | 9132 | ±184 | 861 | ±17 | 4.5 | ±1.5 | 0.0785 | ±0.0002 | 8867 | ±32 | 8823 | ±44 | 5 | ±2 | 8759 | ±44 |
| 280 | ANJB-2-U280 | 5721 | ±18 | 5408 | ±110 | 1360 | ±28 | 2.4 | ±1.6 | 0.0780 | ±0.0003 | 8828 | ±36 | 8801 | ±41 | 2 | ±2 | 8737 | ±41 |
| 302 | ANJB-2-U302 | 9833 | ±44 | 1617 | ±33 | 8024 | ±166 | 5.2 | ±1.9 | 0.0800 | ±0.0004 | 9045 | ±50 | 9041 | ±50 | 5 | ±2 | 8977 | ±50 |

U decay constants: $\lambda_{238}$ = 1.55125x10$^{-10}$ (Jaffey et al., 1971) and $\lambda_{234}$ = 2.82206x10$^{-6}$ (Cheng et al., 2013). Th decay constant: $\lambda_{230}$ = 9.1705x10$^{-6}$ (Cheng et al., 2013).

*$\delta^{234}U = ([^{234}U/^{238}U]_{activity} - 1)x1000$. ** $\delta^{234}U_{initial}$ was calculated based on $^{230}$Th age (T), i.e., $\delta^{234}U_{initial} = \delta^{234}U_{measured} \times e\lambda^{234xT}$. Corrected $^{230}$Th ages assume the initial $^{230}Th/^{232}Th$ atomic ratio of 4.4 ±2.2 x10$^{-6}$. Those are the values for a material at secular equilibrium, with the bulk earth $^{232}Th/^{238}U$ value of 3.8. The errors are arbitrarily assumed to be 50%.

***B.P. stands for "Before Present" where the "Present" is defined as the year 1950 A.D.

Table S2: $^{230}$Th dating results for Stalagmite MAJ-5. The error is 2 σ error. Dft= distance from the top of the stalagmite.

| Dft (mm) | Sample no. | $^{238}$U (ppb) | | $^{232}$Th (ppt) | | $^{230}$Th / $^{232}$Th (atomic x10$^{-6}$) | | d$^{234}$U* (measured) | | $^{230}$Th / $^{238}$U (activity) | | $^{230}$Th Age (yr) (uncorrected) | | $^{230}$Th Age (yr) (corrected) | | d$^{234}$U$_{Initial}$** (corrected) | | $^{230}$Th Age (yr BP)*** (corrected ) | |
|---|---|---|---|---|---|---|---|---|---|---|---|---|---|---|---|---|---|---|---|
| 1 | MAJ-5-U001 | 2734 | ±15 | 3044 | ±63 | 33 | ±1 | -3.2 | ±2.7 | 0.0023 | ±0.0000 | 246 | ±5 | 214 | ±24 | -3 | ±3 | 150 | ±24 |
| 10 | MAJ-5-U010 | 6691 | ±38 | 22757 | ±474 | 27 | ±1 | -3.1 | ±3.6 | 0.0056 | ±0.0001 | 609 | ±7 | 510 | ±71 | -3 | ±4 | 446 | ±71 |
| 22 | MAJ-5-U022 | 3292 | ±4 | 11633 | ±234 | 31 | ±1 | -3.0 | ±1.5 | 0.0067 | ±0.0001 | 736 | ±14 | 633 | ±74 | -3 | ±1 | 569 | ±74 |
| 41 | MAJ-5-U041 | 1380 | ±3 | 10604 | ±213 | 32 | ±1 | -1.1 | ±2.1 | 0.0147 | ±0.0001 | 1617 | ±15 | 1393 | ±159 | -1 | ±2 | 1329 | ±159 |
| 50 | MAJ-5-U050 | 1224 | ±4 | 4144 | ±84 | 40 | ±1 | -2.9 | ±2.4 | 0.0082 | ±0.0001 | 898 | ±15 | 799 | ±71 | -3 | ±2 | 735 | ±71 |
| 60 | MAJ-5-U060 | 1578 | ±3 | 14591 | ±293 | 31 | ±1 | -0.9 | ±2.6 | 0.0173 | ±0.0005 | 1901 | ±56 | 1631 | ±199 | -1 | ±3 | 1567 | ±199 |
| 66 | MAJ-5-U066 | 12609 | ±83 | 38990 | ±842 | 461 | ±10 | -4.6 | ±2.9 | 0.0865 | ±0.0006 | 9912 | ±81 | 9821 | ±103 | -5 | ±3 | 9757 | ±103 |
| 80 | MAJ-5-U080 | 11684 | ±16 | 27838 | ±559 | 598 | ±12 | -2.6 | ±1.2 | 0.0864 | ±0.0002 | 9882 | ±24 | 9813 | ±55 | -3 | ±1 | 9749 | ±55 |
| 89 | MAJ-5-U089 | 10930 | ±12 | 30247 | ±606 | 519 | ±10 | -1.2 | ±1.3 | 0.0870 | ±0.0002 | 9941 | ±29 | 9860 | ±64 | -1 | ±1 | 9796 | ±64 |

U decay constants: $\lambda_{238}$ = 1.55125x10$^{-10}$ (Jaffey et al., 1971) and $\lambda_{234}$ = 2.82206x10$^{-6}$ (Cheng et al., 2013). Th decay constant: $\lambda_{230}$ = 9.1705x10$^{-6}$ (Cheng et al., 2013).

*$\delta^{234}U = ([^{234}U/^{238}U]_{activity} - 1)x1000$. ** $\delta^{234}U_{initial}$ was calculated based on $^{230}$Th age (T), i.e., $\delta^{234}U_{initial} = \delta^{234}U_{measured} \times e\lambda^{234xT}$.

Corrected $^{230}$Th ages assume the initial $^{230}$Th/$^{232}$Th atomic ratio of 4.4 ±2.2 x10$^{-6}$. Those are the values for a material at secular equilibrium, with the bulk earth $^{232}$Th/$^{238}$U value of 3.8. The errors are arbitrarily assumed to be 50%.

***B.P. stands for "Before Present" where the "Present" is defined as the year 1950 A.D.

## REFERENCES

Braconnot, P., Otto-Bliesner, B., Harrison, S., Joussaume, S., Peterchmitt, J. Y., Abe-Ouchi, A., Crucifix, M., Driesschaert, E., Fichefet, T., Hewitt, C. D., Kageyama, M., Kitoh, A., Laine, A., Loutre, M. F., Marti, O., Merkel, U., Ramstein, G., Valdes, P., Weber, S. L., Yu, Y., and Zhao, Y.: Results of PMIP2 coupled simulations of the Mid-Holocene and Last Glacial Maximum - Part 1: experiments and large-scale features, Clim Past, 3, 261-277, 2007.

Broccoli, A. J., Dahl, K. A., and Stouffer, R. J.: Response of the ITCZ to Northern Hemisphere cooling, Geophys Res Lett, 33, 10.1029/2005gl024546, 2006.

Burns, S. J., Godfrey, L. R., Faina, P., McGee, D., Hardt, B., Ranivoharimanana, L., and Randrianasy, J.: Rapid human-induced landscape transformation in Madagascar at the end of the first millennium of the Common Era, Quaternary Sci Rev, 134, 92-99, 10.1016/j.quascirev.2016.01.007, 2016.

Cheng, H., Edwards, R. L., Shen, C. C., Polyak, V. J., Asmerom, Y., Woodhead, J., Hellstrom, J., Wang, Y. J., Kong, X. G., Spotl, C., Wang, X. F., and Alexander, E. C.: Improvements in Th-230 dating, Th-230 and U-234 half-life values, and U-Th isotopic measurements by multi-collector inductively coupled plasma mass spectrometry, Earth Planet Sc Lett, 371, 82-91, Doi 10.1016/J.Epsl.2013.04.006, 2013.

Chiang, J. C. H., and Bitz, C. M.: Influence of high latitude ice cover on the marine Intertropical Convergence Zone, Clim Dynam, 25, 477-496, 10.1007/s00382-005-0040-5, 2005.

Gasse, F.: Hydrological changes in the African tropics since the Last Glacial Maximum, Quaternary Sci Rev, 19, 189-211, Doi 10.1016/S0277-3791(99)00061-X, 2000.

Jaffey, A. H., Flynn, K. F., Glendenin, L. E., Bentley, W. C., and Essling, A. M.: Precision measurement of half-lives and specific activities of U-235 and U-238, Phys Rev C, 4, 1889-1906, DOI 10.1103/PhysRevC.4.1889, 1971.

Lindesay, J. A.: Present Climates of Southern Africa, in: Climates of the Southern Continents: Present, Past and Future, edited by: Hobbs, J. E., Lindesay, J. A., and Bridgman, H. A., John Wiley & Sons Ltd., England, 5-62, 1998.

Schott, F. A., and McCreary, J. P.: The monsoon circulation of the Indian Ocean, Prog Oceanogr, 51, 1-123, Doi 10.1016/S0079-6611(01)00083-0, 2001.

Voarintsoa, N. R. G., Wang, L., Bruce Railsback, L., Brook, G. A., Liang, F., Cheng, H., and Lawrence Edwards, R., 2017, Multiple proxy analyses of a U/Th-dated stalagmite to reconstruct paleoenvironmental changes in northwestern Madagascar between 370 CE and 1300 CE: Palaeogeography, Palaeoclimatology, Palaeoecology, v. 469, p. 138-155.